Thèse n° 10 337

Activation of small molecules promoted by multimetallic complexes supported by redox active ligands

Présentée le 23 octobre 2020

à la Faculté des sciences de base
Groupe SCI SB MM
Programme doctoral en chimie et génie chimique

pour l'obtention du grade de Docteur ès Sciences

par

Davide TONIOLO

Acceptée sur proposition du jury

Prof. S. Gerber, présidente du jury
Prof. M. Mazzanti, directrice de thèse
Prof. V. Mougel, rapporteur
Prof. E. Hevia, rapporteuse
Prof. K. Severin, rapporteur

École
polytechnique
fédérale
de Lausanne

2020

Acknowledgements

I would like to first thank all the committee members for accepting to review the present thesis.

I would like to thank my supervisor for helping me with my personal growth over these years and for teaching me how to properly work in a chemical lab.

My greatest thanks goes to my family that have always helped me morally and financially during these years. They are by far the people that support me the most in every situation and I have always considered them my “rock” in good and bad times.
My parents were always available to speak and to give advice. They were always taking the time to come and visit me, bringing food and giving me the energy I needed to continue. In particular I thank my mom that supported me during a heartbroken time.
I thank my sister that was preparing cakes and giving me gifts. She is secretly one of the biggest sources of motivation and one of the people I appreciate the most.
I thank my grandmothers that always think about me and take care of me, making me laugh and giving me food.

I thank my colleagues and ex-colleagues for the time I spent with them. I thank Marta and Rory because they introduced me to the lab and they were a great company at the beginning of my PhD. I thank Luciano because it was always nice to discuss chemistry with him and because he made me see science from a different perspective. I thank Nadir because I had a nice time with him, despite the little incident with liquid nitrogen…
Between my colleagues, a special thanks is given to Rada that ended up being a great friend during these years and supported me many times.

I thank Euro, Rosario and Farzaneh, Anne Sophie and Nadia for the great job they have done during these years.

I thank all of the friends that I found in Lausanne because it was thanks to them that I stayed sane.

I also thank Matteo, Maria and Carmelo because they have always supported me during university and they had a big impact on my growth, and despite the long distance they are great friends of mine.

I thank Gioia because she is a source of fun and advice.

I thank Gwenn, because despite the bad ending I really appreciate the time we spent together and she is one of the most important people in my life.

Also, thanks to Alexandra for reviewing this particular page.

Abstract

The activation of small molecule is a topic of high current interest. A variety of homogeneous end heterogeneous catalysts have been studied to be able to promote chemical transformation of industrial relevance under mild condition and therefore decrease the costs. Often the most performant catalysts are composed by rare and precious metals such as Pd, Pt, Rh, Ir, making the catalyst expensive and not suitable for large scale reactions. Lots of effort is put in researching ways to substitute precious and rare metal while keeping catalytic efficiency and selectivity. F-elements have shown to be able to perform many chemical transformations that are common to d-metals, promoting also in some cases unusual chemical reactivity. Differently from transition metals, f-elements present a unique coordination chemistry, governed by electrostatic interaction with the ligand environment and steric constrain. During my PhD I focused my attention on the synthesis of highly reactive, low valent metal complexes based of f-elements for the activation of small molecules.

In particular, two main pathways have been followed to promote the multi-electrons transfer necessary for the transformation of the substrate:

The first approach consists in the use of redox active ligands to support the metal centre and act as electron reservoir in order to increase the number of electrons exchanged during the reaction. This method has been used for d-, f- and d- mixed f-elements complexes, resulting to be an elegant way for the preparation of multimetallic compounds capable of promoting multi-electron transfer reaction.

In the second approach, divalent classic lanthanides have been stabilized thanks to the bulky tris(*tert*-butoxide)siloxide ligand that resulted a to be a useful tool for the formation of highly reactive bimetallic complexes.

The reactivity of the synthetized complexes towards small molecules such as CO_2, CS_2 and arenes has been tested, proving the ability of those compounds to act as multielectron reducing reagents. Moreover, we proved that multidentate Schiff base ligands are capable of stabilizing low valent d-metal complexes allowing the formation bonding interaction between different metals with the enhancement of the magnetic properties.

Contents

Acknowledgements ..... **iii**

Chapter 1. Introduction **11**

- **The f-elements** 11
  - **Lanthanides** 11
  - **Uranium** 14
- **Small molecules activation** 15
  - **CO_2 activation** 15
  - **CS_2 activation** 22
  - **Arene activation** 25
  - **N_2 activation** 26
- **Implementing Multi-electrons transfer for Small Molecules Activation** 27
  - **Multimetallic compounds** 29
  - **Redox active ligands** 32
  - **Schiff base as redox active ligands** 34
- **Purposes and objectives of the projects** 36

References **38**

Chapter 2. A versatile route to homo- and hetero-bimetallic 5f–5f and 3d–5f complexes supported by a redox active ligand framework **45**

- **Introduction** 45
- **Results and Discussion** 46
- **Experimental** 54
- **References** 61

Chapter 3. Multimetallic assembly of iron Schiff base complexes **65**

- **Introduction** 65
- **Results and discussion** 66
- **Conclusion** 87
- **Experimental** 87
- **References** 93

Chapter 4 Carbon dioxide reduction by lanthanide(III) complexes supported by redox-active Schiff base ligands. **97**

- **Introduction** 97
- **Results and discussion** 99
- **Conclusion** 108
- **Experimental** 109
- **References** 113

Chapter 5. A Tetranuclear Samarium(II) Inverse Sandwich from Direct Reduction of Toluene by a Samarium(II) Siloxide **117**

- **Introduction** 117

Results and Discussion 118
Experimental 123
References 127
Chapter 6. CS_2 Reductive Coupling to Acetylenedithiolate by a Dinuclear Ytterbium(II) Complex 131
Introduction 131
Results and Discussion 132
Experimental 137
References 142
Chapter 7. Carbon Dioxide Reduction by Dinuclear Yb(II) and Sm(II) Complexes Supported by Siloxide Ligands 145
Introduction 145
Results and Discussion 146
Conclusion 159
Experimental 159
References 165
Chapter 8. Anhydrous conditions enable the catalyst-free carboxylation of aromatic alkynes with CO2 under mild conditions. 169
Introduction 169
Results and Discussion 171
Conclusion 178
Experimental 178
References 182
Conclusions and Perspectives 185
Appendix chapter 2 189
Appendix chapter 3 199
Appendix chapter 4 213
Appendix chapter 5 221
Appendix chapter 6 241
Appendix chapter 7 254
Appendix chapter 8 269
Curriculum Vitae 274

Chapter 1. Introduction

The f-elements

The f-elements are a family of elements in which the valence electrons gradually fill the f-orbitals along the series. Normally, they are divided into two families: the lanthanides, which contain 4f electrons, and the actinides in which the electrons are present in the 5f orbitals. Lanthanum, Actinium and Thorium with an electronic configuration of $[Xe]5d^16s^2$, $[Rn]6d^17s^2$ and $[Rn]6d^27s^2$, respectively are included by extension (Figure 1).

57 La	58 Ce	59 Pr	60 Nd	61 Pm	62 Sm	63 Eu	64 Gd	65 Tb	66 Dy	67 Ho	68 Er	69 Tm	70 Yb	71 Lu
89 Ac	90 Th	91 Pa	92 U	93 Np	94 Pu	95 Am	96 Cm	97 Bk	98 Cf	99 Es	100 Fm	101 Mb	102 No	103 Lr

Figure 1. f-elements. First row: lanthanides. Second row: actinides.

These elements were discovered in Sweden in the late 1700's and nowadays, they are widely used in many technological applications such as magnets in computer hard disks, lasers, phosphors for displays, MRI contrast agents and luminescent probes for bio-imaging. Consequently, the demand for f-elements is constantly increasing, and access to these metals is an economic and geopolitical interest. From a chemical point of view, f-elements differ considerably from d-metals. The lanthanides and actinides tend to feature considerably larger ionic radii than the d-block metals, resulting in high coordination numbers (normally between 6 and 12), and due to the low contribution of crystal field, they present unusual coordination geometry that is dictated by electrostatic repulsions of the coordinated molecules. The f-elements cations are hard Lewis acids and as such they preferentially bind hard Lewis bases, in particular oxo and fluoride ligands. The aqua ions tend to hydrolyse unless they are protected by multidentate ligands.

Lanthanides

The characteristic oxidation state for the lanthanides is +3. Despite this tendency to form stable trivalent cations, the lanthanides do not resemble transition metals such as Cr, Fe or Co; metallic lanthanides are more reactive than the d-block elements, and in this respect, they are more similar the alkaline earth metals. As a consequence of the poor shielding effect of the 5s and 5p sub cells by the 4f orbitals, there is a steady increase in the effective nuclear charge and concomitant reduction in the size of the ions along the series, and this effect is called the “lanthanide contraction”. Together with the poor shielding of the f orbitals, another phenomenon that contributes to the contraction is the relativistic effect. Besides being more predominant for heavy elements such as gold or mercury, it has been calculated that the contraction due to the relativistic effect is about 10 %.[1] This effect explains the tendency of the early lanthanides to have higher coordination numbers than the latter, and this allows for finetuning of the sterics around the metal centre by not only changing the ligand, but also by choosing ions with a specific size.

The electronic configuration of elemental lanthanides takes the general form [Xe]4f^{n+1}6s^{2}, with the only four exceptions being lanthanum, cerium, gadolinium and lutetium, which present a [Xe]4f^{n}5d^{1}6s^{2} electronic configuration. With the exception of La and Lu, which have closed-shell electronic configurations, lanthanide cations in the +3 oxidation state possess at least one unpaired 4f electron, making those ions paramagnetic (Table 1).

Table 1. Electronic configuration and ionic radii for trivalent lanthanide

Elements	Ln(0)	Ln(II)	Ln(III)
La	[Xe]5d^{1}6s^{2}	[Xe]5d^{1}	[Xe]
Ce	[Xe]4f^{1}5d^{1}6s^{2}	[Xe]4f^{1}5d^{1}	[Xe]4f^{1}
Pr	[Xe]4f^{3}6s^{2}	[Xe]4f^{2}d^{1}	[Xe]4f^{2}
Nd	[Xe]4f^{4}6s^{2}	[Xe]4f^{4}/4f^{3}5d^{1}	[Xe]4f^{3}
Pm	[Xe]4f^{5}6s^{2}	-	[Xe]4f^{4}
Sm	[Xe]4f^{6}6s^{2}	[Xe]4f^{6}	[Xe]4f^{5}
Eu	[Xe]4f^{7}6s^{2}	[Xe]4f^{7}	[Xe]4f^{6}
Gd	[Xe]4f^{7}5d^{1}6s^{2}	[Xe]4f^{7}5d^{1}	[Xe]4f^{7}
Tb	[Xe]4f^{9}6s^{2}	[Xe]4f^{8}5d^{1}	[Xe]4f^{8}
Dy	[Xe]4f^{10}6s^{2}	[Xe]4f^{10}/4f^{9}5d^{1}	[Xe]4f^{9}
Ho	[Xe]4f^{11}6s^{2}	[Xe]4f^{10}6d^{1}	[Xe]4f^{10}
Er	[Xe]4f^{12}6s^{2}	[Xe] 4f^{11}6d^{1}	[Xe]4f^{11}
Tm	[Xe]4f^{13}6s^{2}	[Xe]4f^{13}	[Xe]4f^{12}

Yb	[Xe]$4f^{14}6s^2$	[Xe]$4f^{14}$	[Xe]$4f^{13}$
Lu	[Xe]$4f^{14}5d^16s^2$	[Xe]$4f^{14}5d^1$	[Xe]$4f^{14}$

Despite +3 being the most stable oxidation state, other oxidation states are possible. Eu, Yb and Sm are normally called “classical divalent lanthanides” because they are the elements that show the most stable +2 oxidation state of the series (Table 2). However, recently Evans and co-workers successfully characterized the divalent complexes [K(cryptand)][$LnCp'_3$] for all the lanthanides except Pm.[2,3] This work allowed the division of the divalent lanthanide cations in three groups, based on the electronic configuration of the atoms. In this environment, Eu, Yb, Sm and Tm present a [Xe]$4f^{n+1}$ electronic configuration, while La, Ce, Pr, Gd, Tb, Ho, Er and Lu present a [Xe]$4f^n5d^1$ configuration. The remaining Dy and Nd can cross over between the two configurations depending on the ligand environment. However, lanthanides in their +2 oxidation state are strong reducing agents, rendering those ions suitable candidates for the activation of small molecules.

Table 1. Reduction potential calculated for Ln^{III}/Ln^{II} couple.

Ln	E^0 (V vs NHE)	Ln	E^0 (V vs NHE)
Eu	-0.35	Pr	-2.7
Yb	-1.15	Ho	-2.9
Sm	-1.55	Er	-3.1
Tm	-2.3	La	-3.1
Dy	-2.6	Ce	-3.2
Nd	-2.6	Tb	-3.7
Pm	-2.6	Gd	-3.9

Other than the +2 and the +3 oxidation states, tetravalent lanthanides are also possible. Ce is the only atom of the series that has a readily accessible +4 oxidation state. However, Ceria (CeO_2) is an oxidizing agent and is indeed widely used as catalyst or support for oxidation reactions.[4] Other Ln(IV) were known only in solid state,[5,6] but recently our group and La Pierre and co-workers, reported two other examples of molecular tetravalent lanthanides. [7,8,9,10]

Uranium

Uranium is one of the heaviest elements found in nature and is known since the 18th century. Uranium occurs in nature with a proportion of about 99.7 % ^{238}U and 0.7 % ^{235}U and both isotopes are radioactive. Uranium is known mostly by the public opinion for producing energy in nuclear plants, or more sadly for nuclear weapons. However, uranium presents a fascinating and unique chemistry; our understanding of it is still in its infancy, and the potential of this element is only starting to be appreciated. The massive stock of uranium and its unique properties make it a desirable tool to promote new type of reactivity and catalysis.

From a chemical point of view, while the 4f orbitals of the lanthanides are buried deeply enough to be almost unaffected from the ligand environment, the 5f orbitals of uranium are more external and more available for bonding interaction, imparting to the atom a rich redox chemistry with many known oxidation states (from 2+ to 6+). Among all, the most stable oxidation state under aerobic conditions or in aqueous solution is U(VI), mostly found in the form of the uranyl cation, UO_2^{2+}. The uranyl ion is very stable and it forms a variety of mono- and polynuclear complexes both in aqueous and organic media[11], and in contrast, examples of non-uranyl U(VI) are limited just because of the stability of the uranyl moiety.

U(V) systems are relatively rare. This is mostly due to their tendency to disproportionate to more stable species U(IV) and U(VI). Moreover, traces of oxygen water can easily oxidize the U(V) making those complexes stable exclusively in organic media, most of the time in the form of pentavalent uranyl.[12] However, recently in our group, pentavalent uranium has been stabilized in an aqueous environment thanks to the use of multidentate ligand that prevent the disproportionation.[13,14]

Complexes containing tetravalent uranium are numerous in non-aqueous solution and have been reported as stable species with a variety of ligands. Tetravalent uranium species such as [UCl_4] or [UI_4] are common, stable starting material widely used for the synthesis of uranium complexes.

In the +3 oxidation state, uranium is a strong reducing agent, with a reducing potential between -1.5 V and -2.9 V depending on the conditions, and it present a large Van der Waals radius (1.86 Å). Many complexes of trivalent uranium have been synthetized, and it has been proved that this oxidation state can be stabilized by a variety of different ligands, such as aryloxide, amides, silylamides, and many other ancillary ligands. Uranium 3+ typically undergoes only stoichiometric reactions, but recently Meyer and co-workers showed that U(III) can be electrochemically generated and demonstrated that the element has great potential to be used as an electrocatalyst for hydrogen evolution.

The +2 state is also known, but four examples of complexes featuring U(II) are reported, making those systems almost unique and essentially unexplored.[15,16]

Small molecules activation

The development of processes and technologies for the capture and selective transformation of small molecules is one of the largest research fields in modern chemistry and chemical engineering. Small molecules such as CO_2, CO, N_2, H_2, C_2H_4, O_2 and others represent a cheap and abundant source of carbon, nitrogen, hydrogen and oxygen and they are widely used in chemical industry as starting materials to produce fuels, fertilizer and other commodity chemicals.

For example, the continuous increasing demand for energy lead to an increase of the emissions of carbon dioxide and other pollutants homogenously dispersed in the atmosphere that now must be somehow removed. The recycling of carbon dioxide, together with a sustainable process capable of transforming it, may contribute to the decrease of carbon emission while providing a cheap carbon source for chemical industry. Another important process that involves the use of small molecules is ammonia synthesis. The energy spent annually for the production of this important chemical is a significant fraction of the global energy production because of the drastic reaction conditions that are necessary to obtain the product in a reasonable time, and therefore reducing the cost would be a great achievement.

However, these molecules are normally characterized by kinetic and or thermodynamic stability, and the promotion of selective reaction focused on obtaining certain products is normally considered a challenge. While the long-term goal is to develop an efficient system capable of transforming small molecule into more valuable products under mild conditions, the fundamental understanding of the chemistry related to this topic is nevertheless important for the rational design of the systems; it is only through increased knowledge in this topic that a sustainable solution can be found.

CO_2 activation

In a world increasingly affected by climate change, CO_2 production and emissions are likely to become more restricted. Research and technology concerning carbon capture, storage and recycling has increased enormously in the last few decades, particularly the use of carbon dioxide as cheap carbon source to build up higher valuable organic molecules.

However, this represents a scientific and technological challenge due to its thermodynamic and kinetic stability. Carbon dioxide has a relatively high LUMO, thus being a poor candidate for direct electron injection. Indeed, many reactions that involve carbon dioxide are characterized by high activation energy barrier and for this reason, they require high temperature and pressure.[17] Nowadays, about 0.1 % of the total amount of the manmade CO_2 is being used in chemical industries,[18] and most of it is utilized for the synthesis of bulk chemicals such as urea, cyclic carbonates and polypropylene carbonate (Scheme 1). The direct reduction of carbon dioxide to formic acid, methanol and methane is less common due to the unfavourable thermodynamics and kinetics of these reactions, but ongoing research is aiming to make these processes competitive with the current methods.

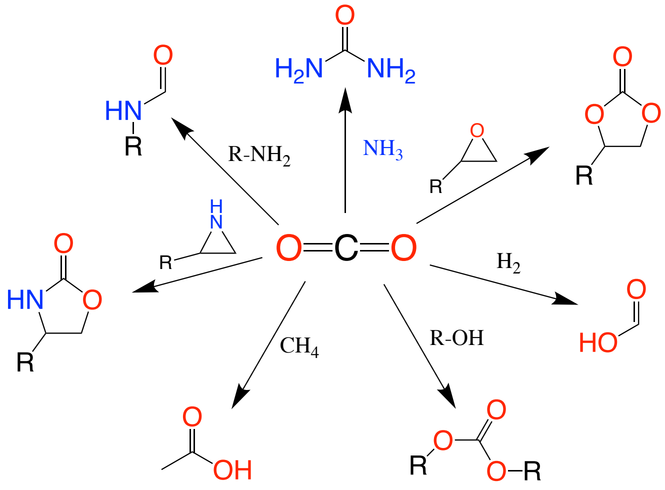

Scheme 1. Examples of how carbon dioxide is used in industry.

However, it is possible to overcome the intrinsic low reactivity of carbon dioxide by designing highly reactive metal complexes capable of binding the molecule and transferring electrons that transform it into more desirable products. Indeed, carbon dioxide can be directly reduced to many valuable molecules such as carbon monoxide, oxalic acid, citric acid, formic acid and so on, but these reactions require strong reducing agents and multiple electrons. (Table 1).

Table 3. Standard potential for the reduction of carbon dioxide (water, 298 K, $P_{CO2} = 1$ atm).

Reaction	E^0 (V vs NHE)
$CO_2 + e^- \rightarrow CO_2^{\cdot-}$	-1.90
$CO_2 + 2\ H^+ + 2\ e^- \rightarrow CO + H_2O$	-0.73
$CO_2 + 2\ H^+ + 2\ e^- \rightarrow HCO_2H$	-0.61
$CO_2 + 4\ H^+ + 4\ e^- \rightarrow CH_2O + H_2O$	-0.48
$CO_2 + 6\ H^+ + 6\ e^- \rightarrow CH_3OH + H_2O$	-0.38
$CO_2 + 8\ H^+ + 8\ e^- \rightarrow CH_4 + 2\ H_2O$	-0.24

In the last 20 years, a plethora of homogeneous and heterogeneous metal catalysts has been characterized, and the coordination and reactivity of carbon dioxide has been summarized in several reviews and textbooks.[19,20,21,22,23] Below, some examples of metal complexes capable of binding and transforming carbon dioxide are considered: the focus is mainly on f-element and multimetallic complexes since they are at the heart of this thesis.

The formation of $CO_2^{\cdot -}$ is probably the rarest event with only a few examples reported in literature. Indeed, $CO_2^{\cdot -}$ is postulated to be the first and most reactive species in the reduction of carbon dioxide and it normally undergoes further transformations.[24] In 2004 by Mayer et al. were able to isolate a U(IV) complex containing a $CO_2^{\cdot -}$ moiety coordinated to the metal centre. The trivalent uranium complex [U((Ad,^{t}BuArO)$_3$)tacn] reacts at room temperature with carbon dioxide affording the unprecedented [U(CO$_2$){(Ad,^{t}BuArO)$_3$)tacn}], featuring a linear $CO_2^{\cdot -}$ ligand (Scheme 2).[25] The authors postulated that the linearity of the radical anion is imposed by the steric hindrance of the ligand scaffold, precluding the molecule from bending and reacting further.

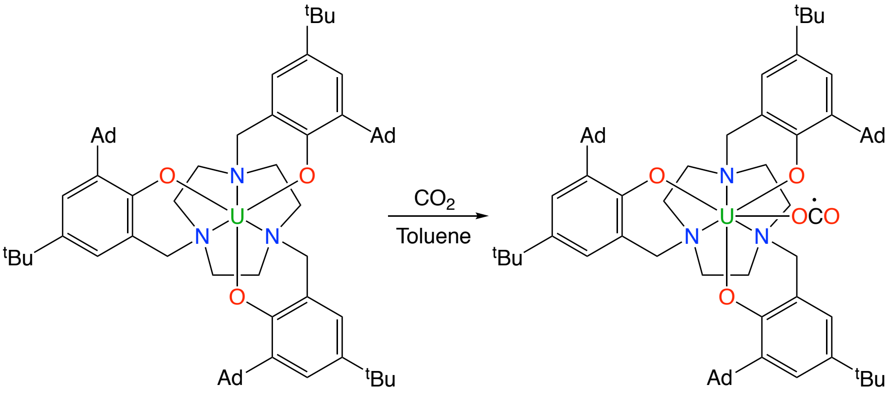

Scheme 2. Mono electron reduction of carbon dioxide promoted by a U(III) complex.

The other example of complex capable of forming the $CO_2^{\cdot -}$ species with an yttrium centre is reported by Evans et al. The reduction of the trivalent [Y(HMDS)$_3$] by metallic potassium in the presence of 18-crown-6 afforded an Y(II) species, which was not isolated, capable of reacting with carbon dioxide, forming a polymeric structure featuring the carbon dioxide radical anion moiety.[26] However, the result must be treated with some caution, considering the possibility of forming isocyanate as reported in related systems.[27] Moreover, the higher nitrogen percentage in the elemental analysis results suggest the presence of isocyanate.

Examples of molecular compounds containing the $CO_2^{\cdot -}$ moiety are rare because it normally undergoes coupling reaction to form oxalate. Evans and coworkers reported in 1998 the reaction between the divalent samarium compound [Sm(C$_5$Me$_5$)(THF)$_2$] and carbon dioxide at room temperature.[24] This reaction resulted in the selective formation of oxalate anion from CO$_2$ together with the formation of the trivalent samarium species (Scheme 3). Similar reactivity was also found for similar ligands and for other lanthanide cations. [28,29]

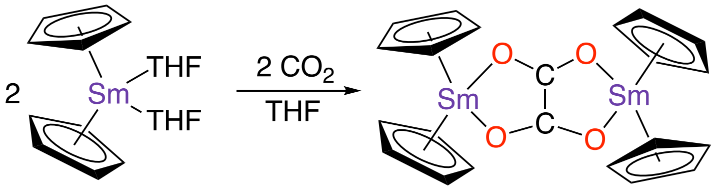

Scheme 3. Reduction of carbon dioxide to oxalate promoted by a divalent samarium complex.

The authors state that the pathway followed by the reaction proceed through the formation of $CO_2^{\cdot -}$ that undergoes coupling reaction forming the oxalate. However, this mechanism shares a common intermediate with the reductive disproportionation of CO_2 that forms CO and carbonate, and those products are sometimes found together in the reaction mixture.

The reductive disproportionation of carbon dioxide is very attractive due to the importance of CO in chemical industries. Several example of this kind of reactivity have been reported in the literature, and most of them involve d-metal complexes as electrocatalysts. [30,31,32] F-elements also show the ability to perform the reductive disproportionation of CO_2. In 2006 Gardiner and coworkers showed that the divalent samarium supported by a porphyrinogen ligand performs the reduction of CO_2 forming CO and a bridging carbonate anion.[33] Another and more recent example was reported by Mazzanti and co-workers. The divalent “ate” ytterbium complex supported by tris(*tert*-butoxy)siloxide ($[K_2Yb(siloxide)_4]$) react with carbon dioxide in toluene solution affording a mixture of carbonate, oxalate and CO, together with the trivalent ytterbium species (Scheme 4).[34]

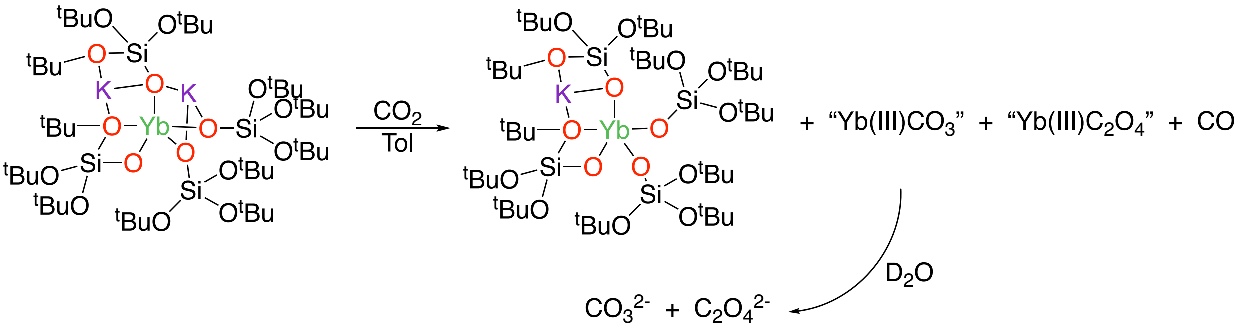
CO$_2$
Tol
+ “Yb(III)CO$_3$” + “Yb(III)C$_2$O$_4$” + CO
D$_2$O
CO$_3^{2-}$ + C$_2$O$_4^{2-}$

Scheme 4. Reaction between the divalent $[K_2Yb(siloxide)_4]$ and CO_2.

Uranium based complexes also showed similar reactivity. The mixed sandwich complex $[U(COT^{R})(Cp^{*R'})]$ was proven to be able to promote the disproportionation of carbon dioxide, together with the formation of other reduced products such as oxalate or CO. The use of supercritical CO_2 was necessary to obtain a “clean” reaction in the case where R = $SiMe_3$ and R’ = Et, ^{i}Pr and ^{t}Bu.

The use of stoichiometric amount of CO_2 lead to a mixture of compounds such es carbonate, oxalate and oxo uranium species.[35]

In 2010 Meyer et al. observed the disproportionation promoted by [U(III)(($^{R,R'}$ArO)tacn)]. It was noticed that depending on the nature of the substituents the complex can undergoes different reactivity such as the formation of bridging oxo, bridging carbonate or binding of linear $CO_2^{\cdot -}$ as previously shown in Scheme 2.[36,37,38] Interestingly, the reduction of the obtained carbonate complex [U((^{nP,Me}ArO)$_3$tacn)(μ-CO_3)] by potassium graphite forms again the starting U(III) complex with concomitant elimination of K_2CO_3 making it theoretically possible to use this complex as electrocatalyst.

Again, our group reported two interesting examples of reductive disproportionation of CO_2 promoted by the bimetallic U(III) complex [U_2(OSi(O^{t}Bu)$_3$)$_6$] and the monometallic "ate" analogue [KU(OSi(O^{t}Bu)$_3$)$_4$)]. The dimeric homoleptic [U_2(OSi(O^{t}Bu)$_3$)$_6$] reacts with two equivalents of CO_2 affording CO and a U(IV)-U(IV) carbonate bridging species (Scheme 5a). However, the carbonate complex was unstable in the given reaction conditions and underwent scrambling reactions affording the mononuclear U(IV) [U(OSi(O^{t}Bu)$_3$)$_4$] and other unidentified U(IV) complexes.[39] DFT calculation showed that the reaction proceeds through the formation of a dinuclear U(IV) binding a CO_2^{2-} moiety, and then a nucleophilic attack from another CO_2 molecule. Alternatively, oxo bridging dimeric U(IV) complexes could be formed with concomitant formation of carbon monoxide. The oxo complex can then insert CO_2 forming again the carbonate adduct.

The reactivity of the "ate" complex [KU(OSi(O^{t}Bu)$_3$)$_4$)] resulted different. The reaction of this specie with CO_2 performed in toluene afforded the U(V) terminal oxo [KUO(OSi(O^{t}Bu)$_3$)$_4$] instead of the expected carbonate anion (Scheme 5b). This reaction is particularly interesting because it underlines the importance of the cooperation between uranium and potassium in the transformation of CO_2. DFT studies confirmed that potassium has an active role in binding the substrate and promoting the release of CO. The removal of the counterion resulted by the addition of 18C6 changed the outcome of the reaction which formed CO and a mixture of [U(OSi(O^{t}Bu)$_3$)$_4$)] and [K(18C6)][KU(CO_3)(OSi(O^{t}Bu)$_3$)$_4$)] (Scheme 5c) in approximately 1 : 1 ratio.

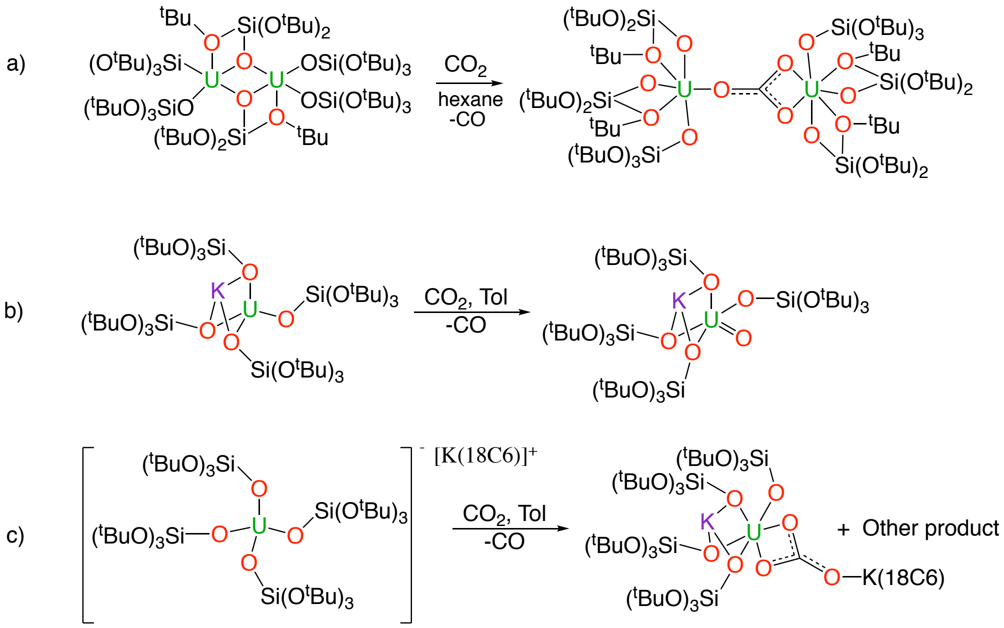

Scheme 5. Reaction of trivalent uranium complexes with carbon dioxide.

It is interesting to notice that the formation of CO and carbonate is always unfavoured compared to the formation of oxalate[36,40,41]. DFT studies have also indicated that the two reactions have a common intermediate that involves the transfer of one electron to the carbon dioxide, forming the $CO_2^{\cdot -}$ species discussed before. However, due to kinetic reasons, the formation of CO and carbonate is observed most of the time, rendering oxalate formation rarer that the CO formation.

Beside carbon monoxide, formic acid is another interesting product derived from two electron reduction of CO_2. The interest for formic acid increased during the last few years due to the thermodynamic instability and its tendency to decompose into CO_2 and H_2, characteristics that makes this compound a promising candidate for hydrogen storage. [42,43,44]

There are many reported catalyst and electrocatalysts for the hydrogenation of carbon dioxide into formic acid or formate based on d-metals[45,46,47,48], but only one example of stoichiometric reaction involving an f-element complex.[49]

Another way to obtain useful product from the reduction of carbon dioxide is via reductive insertion reactions. This consists of the incorporation of a CO_2 molecule into the backbone of a pre-existing organic molecule. Being a reduction, only the insertion that involves the formation of a new C-C bond will be taken in consideration. Non-reductive insertion reactions that form cyclic carbonates, formylated amines, esters, and numerous heterocycles are not discussed because these reactions are outside the scope of this thesis.

The idea of using carbon dioxide as a building block in organic synthesis is well established.[18,21,50,51,52,20] There are numerous examples and industrial processes of this, necessitating a brief discussion of cyclometallation and carboxylation reactions.

Cyclometallation reactions feature the insertion of carbon dioxide, or more generally an oxidizing substrate, into a M-C bond. In the past, cyclometallation catalysts involve low valent Ni or Pd complexes that act as reducing agents (Scheme 6).[53]

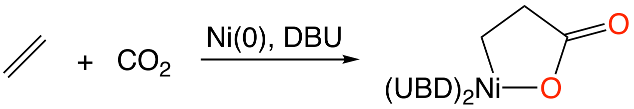

Scheme 6. Cyclometallation reaction between ethylene, carbon dioxide and Ni(0).

These kinds of reactions are normally stoichiometric, so an enormous amount of metal is required for large scale production. However, in 2002 Louie and co-worker discovered a Ni-based complex capable of catalysing the [2+2+2] cycloaddition.[54] Following this result, Behr et al. found that the cyclization products are selectively formed by using [Pd(acac)$_3$] in the presence of P^{i}Pr$_3$ as co-catalyst, resulting in the formation of δ-lactones if butadiene derivatives were used as substrates (Scheme 7).[55]

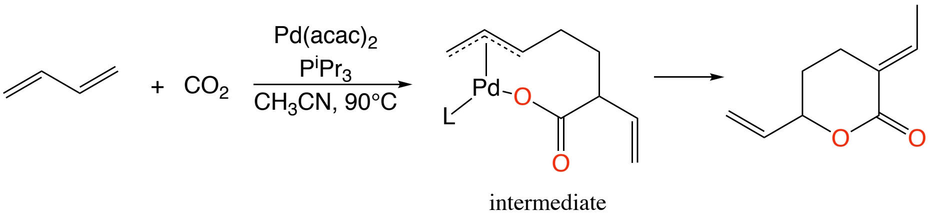

Scheme 7. Synthesis of δ-lactones catalysed by a Pd complex.

Carboxylation reactions are based on the insertion of carbon dioxide into a C-X bond (X = H, BR$_2$, halide etc) with the formation of a carboxylic acid or the equivalent carboxylate salt. Of particular relevance to this thesis is the carboxylation of terminal alkynes. This reaction has been studied by several authors and is normally conducted in the presence of a stoichiometric amount of base and a copper or silver complex, and it represents one of the routes to incorporate carbon dioxide into an organic compound, forming a versatile precursor for further transformation. Propiolic acid derivatives are indeed used as precursors for heterocycles and as starting materials to prepare preservatives and drugs.[56] Lots of research has been carried out to understand the mechanism and find an efficient catalyst that allows the insertion of carbon dioxide into a terminal alkyne C-H bond under mild conditions. DFT studies were carried out in order to decipher the mechanism and develop a new generation of more active catalysts.[57,58,59] The proposed mechanism (Scheme 8) relies on the formation of a metal acetylide complex in which carbon dioxide can undergo an insertion reaction into the M-C bond. Once formed, the metal acetylide can react with the substrate and the base, releasing the propiolic acid and re-forming the starting complex.

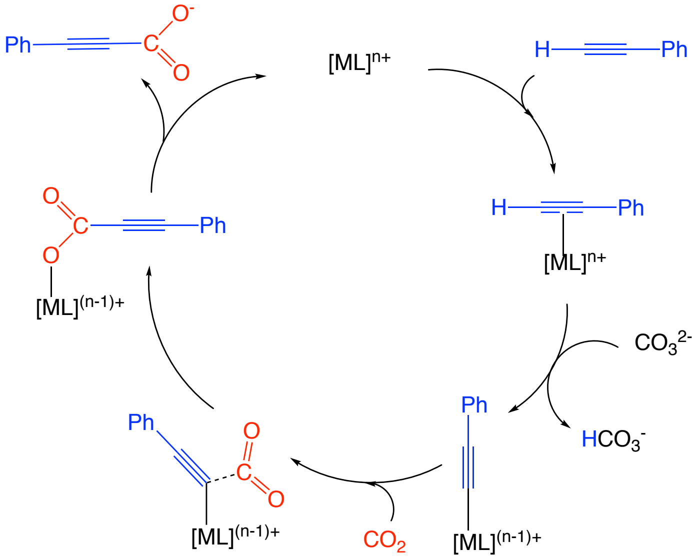

Scheme 8. Proposed mechanism for the metal catalysed carboxylation of terminal alkynes

As shown in Chapter 8, it has been recently found that the reaction proceeds even without a metal catalyst. Indeed, under particular conditions and in the presence of an anhydrous environment, the cesium carbonate is able to deprotonate the terminal alkyne, favouring the insertion of carbon dioxide

CS_2 activation

Carbon disulphide and other sulphur-containing molecules can be found as pollutants in industrial products or by-products that are normally separated or converted into less toxic molecules. Indeed, inefficient removal of sulfurated molecules in fuels leads to the production of toxic sulphur oxides upon fuel combustion, and this is one of the major causes of air pollution. For this reason, the transformation of CS_2 has become more and more important in the petroleum industry and synthetic chemistry, and a variety of metal complexes has been found to be capable of activating the C-S bond.[60] CS_2 is isoelectronic with CO_2, and for this reason it is also commonly used in inorganic chemistry as a more reactive CO_2 model.

The chemical transformation of CS_2 is mostly dominated by transition metal complexes such as Pt, Rh, Ni, Fe, Ru, Re and others.[60,61] Such transformations include the binding of CS_2,[61] breaking the C=S bond,[62] insertion reactions and other types of reactivity. Scheme 9 shows a few examples of the possible coordination mode of CS_2 and products obtained by reduction of CS_2.

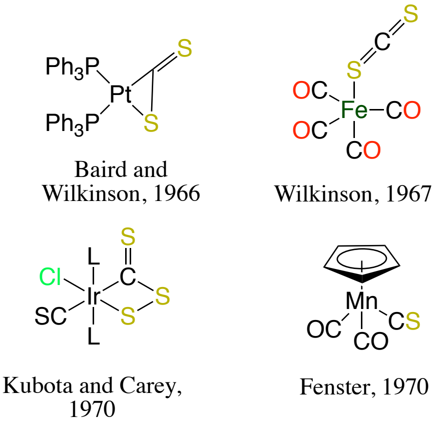
Ph3P
Pt
Ph3P
S
S
S
C
S
OC
Fe
CO
OC
CO
S
L
Cl
C
Ir
S
SC
S
L
Mn
OC
CS
CO

Baird and Wilkinson, 1966

Wilkinson, 1967

Kubota and Carey, 1970

Fenster, 1970

Scheme 9. Examples of d-metal complexes capable of activate and transform carbon disulphide.

Despite the rich chemistry of sulphur and d-metal compounds, examples of reactivity involving CS_2 and lanthanide or actinide complexes are much rarer, and their chemistry remains essentially unexplored.

Regarding uranium chemistry, the reduction of CS_2 is limited to a few examples. In 1986, Andersen and a coworker reported the synthesis of $[\{U(Cp)_3\}_2(\mu\text{-}CS_2)]$ obtained by oxidation of the U(III) complex $[(U(Cp)_3]$ by CS_2. This complex contains the two-electron reduction product of carbon disulphide bridging two uranium centres.

More recently, Meyer and co-workers reported the reduction of CS_2 by a trivalent uranium supported by a multidentate tripodal phenolate ligand $[U(N(^{Ad,\,Me}ArO)_3)(DME)]$ to afford a mixture of thiocarbonate and tetrathiooxalate (Scheme 10).[63,64] The reaction products arise from the competition of two different pathways, one involving the C-C coupling of two $CS_2^{\cdot-}$ radicals formed by one-electron reduction of CS_2, and the cleavage of CS_2^{2-} forming a bridging sulphide and then thiocarbonate.

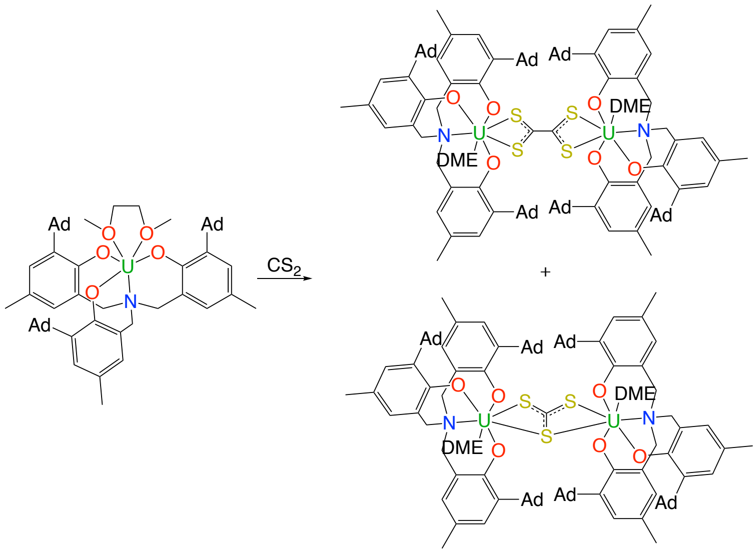
Ad
O
O
Ad
O
O
U
O
N
Ad
CS2
Ad
Ad
Ad
O
DME
O
S
S
N
U
U
N
S
S
DME
O
O
O
O
Ad
Ad
Ad
Ad
+
Ad
Ad
Ad
O
DME
O
S
S
N
U
U
N
S
DME
O
O
O
Ad
Ad
Ad

Scheme 10. Reaction of $[U^{III}(N(^{Ad,\,Me}ArO)_3)(DME)]$ with CS_2, formation of tetrathiooxalate and thiocarbonate.

An example from our group involve again the trivalent binuclear uranium species [$U_2(OSi(O^tBu)_3)_6$].[44] The reaction of this complex with one equiv. of CS_2 afforded a U(IV) complex that features a reduced bridging CS_2^{2-} [$\{U(OSi(O^tBu)_3)_3\}_2\{\mu\text{-}\kappa^2(C,S):\kappa^2(S,S)\text{-}CS_2\}$] (Scheme 11).

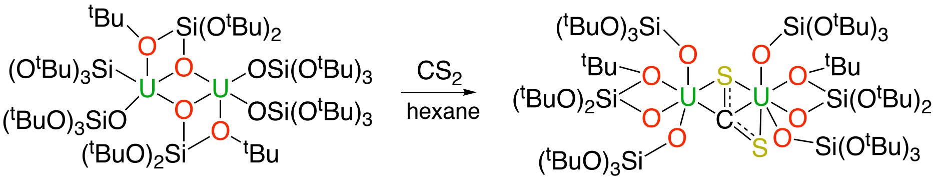

Scheme 11 Two electron reduction of CS_2 promoted by $[U(OSi(O^tBu)_3)_3]_2$

DFT calculations carried out to explain the formation of the complex revealed that the bridging CS_2^{2-} is the most stable product of the reaction because any further transformations to produce thiocarbonate or tetrathiooxalate are either thermodynamically or kinetically unfavourable.

Also recently from our group, the heterometallic [UCo(bis-salophen)(py)$_x$] (x = 2 or 3) has shown activity towards carbon disulphide, being able to release the electrons stored in the ligand scaffold to promote the C-C coupling of two CS_2 molecule to afford tetrathiooxalate (see Chapter 2).

Examples related to lanthanide complexes are rarer. Jones[65] and Junk[66] reported the reactivity of Sm(II) complexes supported by amidinate ligands. In these cases, the reduction of CS_2 resulted in C-S bond coupling, affording a $SCSCS_2^{2-}$ bridging moiety instead of the more common C-C coupling (Scheme 12).

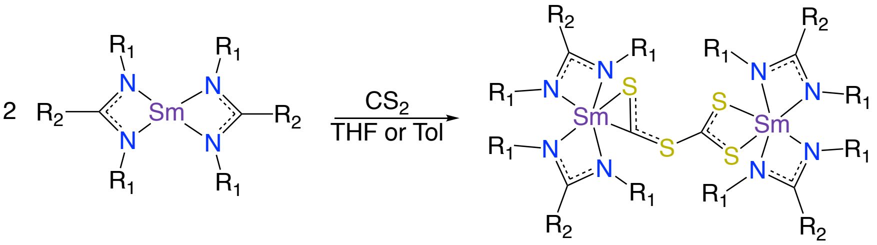

Scheme 12 Reduction of CS_2 to form $SCSCS_2^{2-}$ promoted by divalent samarium complexes.

More recently in our group, Yb(II) and Eu(II) ate complexes supported by tris(*tert*-butoxy)siloxide ligands have shown interesting reactivity with carbon disulphide, producing a mixture of CS_3^{2-}, $C_3S_5^{2-}$ and $C_2S_4^{2-}$ in different ratios depending on the metal centre involved in the reaction, underlining the importance of the number of ligands, the coordination environment and the metal centre on the outcome of the reaction (Scheme 13).[34]

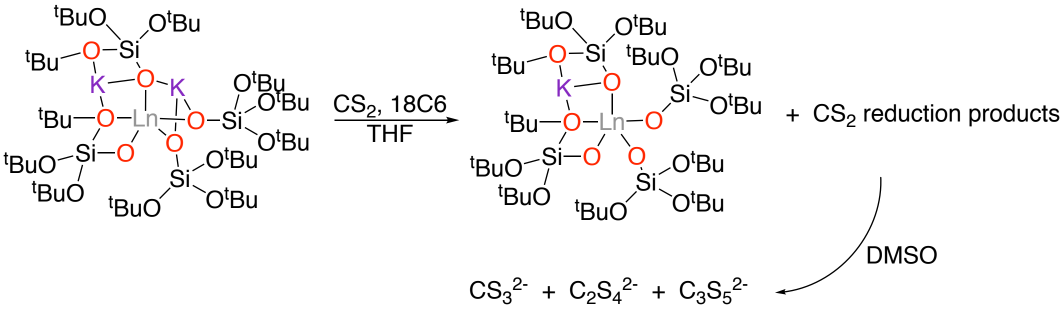

Scheme 13 Reaction of [Ln(siloxide)$_4$K$_2$] with CS$_2$ to form a mixture of CS$_3^{2-}$, C$_2$S$_4^{2-}$ and C$_3$S$_5^{2-}$.

Following the previous work, an Yb(II) complex supported by siloxide ligands has shown interesting reactivity toward carbon disulphide, causing the cleavage of one C-S bond and the coupling of two CS moieties, affording the rare acetylene dithionate anion, which was previously known only for a few transition metal complexes (see Chapter 6).

Arene activation

Extended sandwich structure based on d-metal and main groups elements are well established.[67,68] Differently, the coordination of arenes are rarer in the chemistry of f-element and the example reported are mostly based on Cp and cyclooctatetraenyl (COT) ligands.[69] Evans et al. discovered a novel class of unsolvated triple-decker bent metallocenes of divalent lanthanides.[70] The compounds [(COT){Ln(C$_5$Me$_5$)}$_2$] (Ln = Sm, Eu, Yb) were prepared by desolvation of the corresponding THF solvates. Arene activation has been observed by Arnold and co-worker from the decomposition of [UX$_3$] (X = aryloxide, amide).[71] The trivalent U complex decompose in the arene solution (benzene, toluene or naphtalene) at 90 °C forming inverse sandwich molecules [X$_2$U(μ-h^6:h^6-arene)UX$_2$] and a UX$_4$ by- product. The reduced arene was also active for the silylation and borylation reaction. In our group, the reduction of arenes has been achieved by using the previously presented complex [U$_2$(OSi(O^{t}Bu)$_3$)$_6$].[72] The U(III) compound is capable of reacting with excess toluene in hexane solution forming the inverted sandwich [{U(OSi(O^{t}Bu)$_3$)$_3$(μ-h^6:h^6-toluene)}$_2$] (Scheme 14).

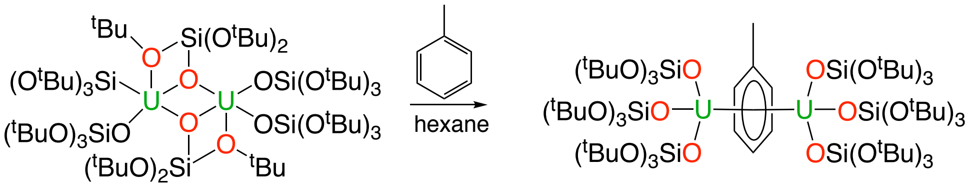

Scheme 14 Reduction of toluene promoted by [U$_2$(OSi(O^{t}Bu)$_3$)$_6$].

More recently, the quadrupole-decker [K(2.2.2-crypt)]$_2$[{(K(OSi(O^{t}Bu)$_3$)$_3$Ce)(μ-h^6:h^6-C$_7$H$_8$)}$_2$Ce] complex was obtained by the reduction of the Ce complex, [KCe(OSi(O^{t}Bu)$_3$)$_4$] with K in toluene/THF, affording an arene bridge multi-decker sandwich of an f-element.[73] Although Ln(II) intermediates are likely to be involved in these reactions, the reduction of toluene or benzene by authenticated Ln complexes was not been confirmed. In Chapter 7 a divalent samarium supported by siloxyde ligands that showed similar reactivity towards arenes, allowing the formation of multideker compounds will be presented.[74]

N_2 activation

The activation of dinitrogen is one of the most difficult challenges in chemistry because of the very strong triple bond in the N_2 molecule and the non-polar nature of the molecule. Despite its similarity with the CO molecule, N_2 is a much weaker sigma donor and a poorer π acceptor, resulting in weak and often reversible binding. Therefore, it is not surprising if the synthesis of ammonia from N_2 and H_2 requires drastic conditions of temperature and pressure even with the use of a catalyst, and represents one of the most important achievements in industrial chemistry.

The chemistry of nitrogen is well developed for d-block metals, and stoichiometric, catalytic or electrocatalytic conversion of N_2 into ammonia are reported (Scheme 15).[75,76,77,78,79,80,81,82, 83]

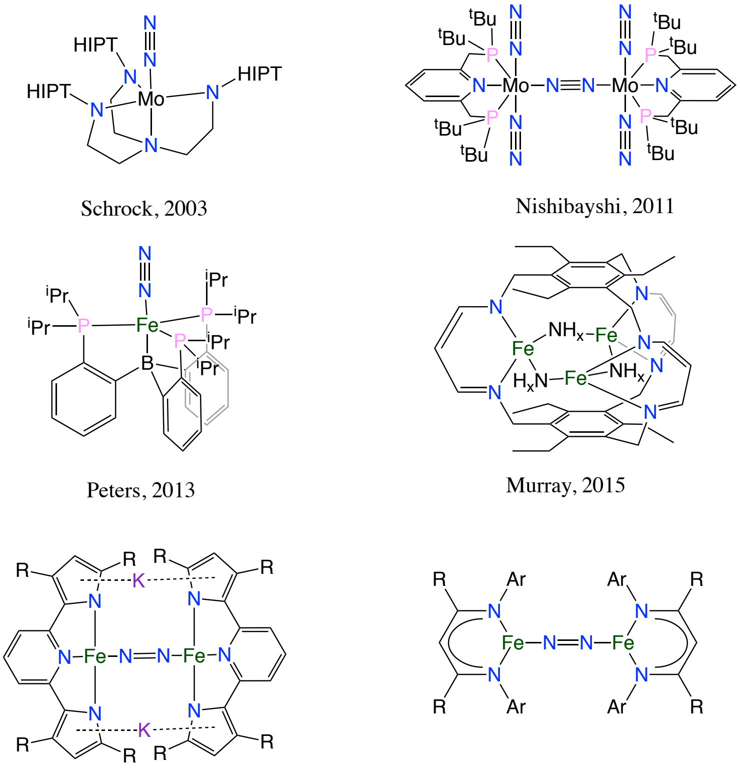
Schrock, 2003
Nishibayshi, 2011
Peters, 2013
Murray, 2015
Meyer, 2020
Holland, 2015

Scheme 15 Examples of d-metal complexes binding and reacting with N_2.

The examples of N_2 activation reported in the literature often rely on d-metals such as Fe[84,85,86,87,88] or Mo,[89,90,91,92,93] and most take advantage of multimetallic centres in order to coordinate the molecule and to release the electrons needed to break the bonds. Also, many examples of f-element based complexes reacting with dinitrogen are reported, proving that these elements are suitable candidates for N_2 activation owing to their generally strong reducing power in low oxidation states.[94] The first example of dinitrogen acting like a ligand was reported by Evans et al. in 1988. [$Sm(C_5Me_5)_2$] reversibly binds and reduce N_2 in toluene solution forming a trivalent samarium complex (Scheme 16).[95] The authors claim that the reversible binding is due to the high reactivity of the complex together with the open coordination environment.

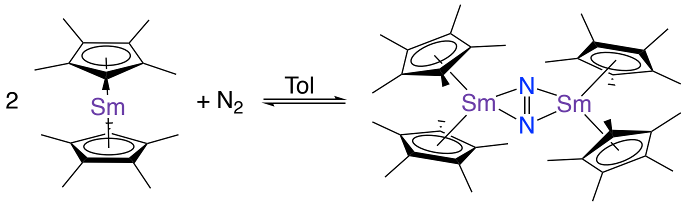

Scheme 16. Reaction of [$Sm(C_5Me_5)_2$] with N_2.

Again, Evans et al. discovered that the reduction of trivalent lanthanides supported by bis(trimethylsilyl) amide (HMDS) generates putative divalent species that are capable of reducing N_2 (Scheme 17).[96,97]

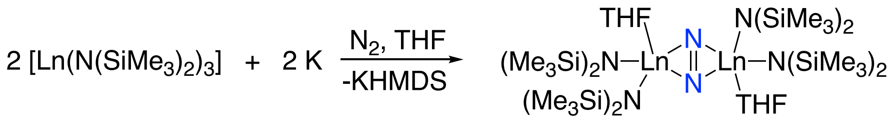

Ln = La, Ce, Pr, Nd, Gd, Tb, Dy, Ho, Er, Y, Tm, Lu

Scheme 17. Examples of f-metal complexes binding and reacting with N_2.

N_2 activation was also found for U(III) complexes. The trivalent [$U(C_5Me_5)_3$] reported again by Evans allows the coordination of dinitrogen in an end on fashion.[98] However, differently from the example previously cited for the lanthanide, the reduction of the substrate is not achieved, and a pressure of more than 5 bar of N_2 have to be applied to stabilize the complex. Arnold et al. reported the two electron reduction of dinitrogen promoted by the trivalent uranium aryloxide[99] and siloxide.[100] Complete cleavage of N_2 is also been observed. Gambarotta et al. reached the cleavage of dinitrogen thanks to a U(III) complex supported by a calixtetrapyrrol ligand in presence of potassium naphthalenide as reducing agent forming a mixed valence U(IV)-U(V) bridging bis-nitride complex.[101] Finally, recently in Mazzanti group a dinuclear "ate" U(III) complex supported by siloxide has been identified to be able to cleave and functionalize N_2.[101,102]

Implementing Multi-electrons transfer for Small Molecules Activation

The activation of small molecules represents one of the biggest challenges in modern chemistry, and the discovery of catalytic systems which allow the use of less drastic conditions would be an economical advantage and would make the processes more environmentally friendly. To be able to activate small molecules, a metal complex has to fulfil some requirements: 1) it has to possess a high reduction potential to overcome the intrinsic thermodynamic and kinetic stability of the substrate, 2) it has to be capable of coordinate the substrate, polarizing the molecule, and 3) it has to be able to participate in a multi-electrons transfer.

It has been described before, low valent f-elements are strong reducing agents and are strong Lewis acids, therefore are good candidates to coordinate and to activate small molecules.

Concerning multi-electron transfer, there are different methods that can be used to achieve this goal. The most obvious, is the use of metals which allow the transfer of more than one electron. As we have already seen, noble metals like Pt, Pd, Rh, Ir, but also non-noble metals like Ni or Cu, are capable of multiple electron transfer. Another possible way is the association of multiple metal centres, forming a so-called multimetallic system.[103,104,105,106] This approach takes inspiration from heterogeneous catalysis, where the coordination of substrates usually involves more than one metal atom. Organometallic chemistry has seen increasing interest in multimetallic systems in the last decades. Indeed, the combination of different metal atoms has often shown a synergetic effect in the activation of small molecules, with an enhancement of the reactivity compared to the monometallic compounds for d-metals and main group elements.[86,103,107,108] The study of multimetallic systems has been probably inspired by the enormous number of biocatalysts containing multiple metal centres. Enzymes such as tyrosinase, FeMoS, superoxide dismutase, methane monooxygenase, ribonucleotide reductase, urease, and many others take advantage of multiple metallic centres to promote very selective reactions under mild conditions. It is therefore obvious that a deep understanding of those systems is not only of fundamental interest but may also allow the creation of more selective catalytic systems, and promote reactivity that is not possible if only one metal is present. Forcing two or more metal centres in close proximity (from 1.5 to 6 Å)[103] is the key to the efficiency and selectivity of enzymatic systems, and confers them the ability to bind substrates on different sides, and consequently increasing the reactivity (Scheme 18). In other words, complexes containing different metals can exhibit synergetic reactivity that is different from compounds containing only one metal. From a mechanistic point of view, one metal acts as a Lewis acid by binding the nucleophilic part of the substrate, while the second metal acts as a Lewis base by binding the electrophilic moiety. This effect is particularly marked when metals with different characteristics, for example early and late transition metals, are coupled together. In those systems, the metals can play different roles, being able to cooperate to bind and transform the substrate.

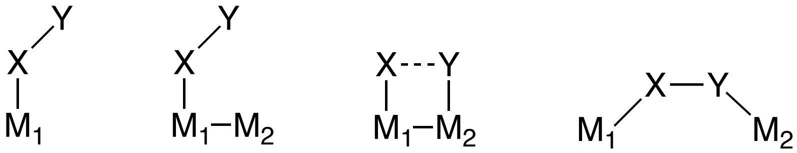

Scheme 18. Different binding mode of a substrate to a metal or multiple metal centres

Another less utilized approach is the use of redox active ligands that can enable redox-type reactions with metal centres that do not possess multiple oxidation states that are easily accessible. Redox active (or non-innocent) are particular kinds of ligands capable of accepting and releasing electrons without necessarily changing the oxidation state of the metal centre (Scheme 19). Like in the case of multi-metallic systems, redox-active ligands have attracted increasing interest in recent years. Many ligands that were considered just spectator ligands are now thought to be non-innocent ligands that play a major role in chemical transformations.

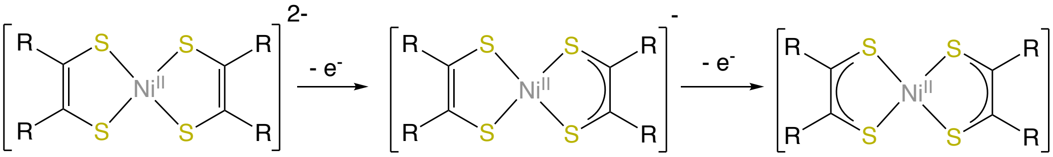

Scheme 19. Example of redox active ligand.

In our group, the strategy chosen for the activation of small molecules is a combination of redox-active ligands with multimetallic compounds. This original idea couples the advantages of both methods, that is the major ability to bind the substrate via interaction with multiple metal centres, and the promotion of multi electron transfer reaction even with the use of metal characterized by mono electron transfer. In the following section, multimetallic systems and redox-active ligand is presented. Again, a particular focus is placed on f-element complexes since they are the main focus of this thesis.

Multimetallic compounds

The importance of multimetallic cooperativity in the binding and the activation of substrates is nowadays recognized. Indeed, lately there has been an explosion of studies regarding the design of architectures for holding two or more metals in close proximity for multi-metallic cooperation for small molecule activation. Many examples have been reported with different kinds of metals, showing several times a synergetic effect of the two metals, with an increase in the properties (catalytic, magnetic, and so on) compared to the monometallic analogues.[109,103,110,109,111,112,113] As we mentioned before, this strategy has probably been inspired by biological systems and seems particularly compelling for the transformation of N_2 into ammonia and derivatives. Nitrogenase, the enzyme that performs the natural N_2 reduction, take advantage of a multi-iron coordination: the active site consists of a cluster containing seven Fe atoms and one molybdenum in a cage and is capable of transforming dinitrogen under ambient conditions.[77] However, dinitrogen is not the only small molecule for which the action of multiple metals is required. As we have seen before, also for the reduction of carbon dioxide multiple electron transfer is necessary, and this may be achieved by using multiple metal centre releasing one electron each. Moreover, since carbon dioxide is a polar molecule, the action of metals with different characteristic may facilitate the coordination of the molecule. In this respect, early transition metal and f-elements are normally able to coordinate the nucleophilic oxygens of carbon dioxide, while the late transition metal often coordinate the electrophilic part in different modes.[114] It is therefore clear that complexes containing more than one metal centre possess a clear advantage compared to the monometallic ones. However, their chemistry is challenging, probably because of the difficulties associated with the synthesis of these compounds, that in many cases relies on a random or unexpected self-assembly more than a rationalized method. Indeed, in the absence of a protein bulk, the goal is to generate a ligand scaffold that could accommodate multiple transition metal ions in the same proximal space, allowing us to explore the reaction chemistry of clusters as molecular units. An ideal ligand platform would permit control over the coordination environment of the individual metal sites within a mutimetallic assembly, while directing the open coordination sites to allows the metal to interact and cooperate. Some examples of these kinds of complexes will follow. The binuclear $[Cu(m\text{-xpt})_2X_2][PF_6]_2$ ($X = NO_3^-$ or Cl^-) reported by Pokharel et al.[115] represents an interesting case of a complex displaying an empty cavity spacing two Cu(II) centres with a long metal-metal distance (> 5 Å) (Scheme 20). The complex can be reduced to the analogue Cu(I) compound by the action of sodium ascorbate or via electrochemical way, and in its reduced forms it reacts with carbon dioxide reducing it to oxalate bridging the two copper cations.

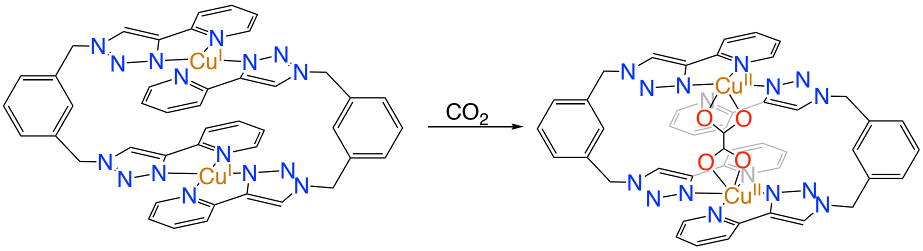

Scheme 20. Selective reduction of carbon dioxide to oxalate promoted by a dinuclear Cu(I).

Interestingly, the complexes perform the reduction of carbon dioxide selectively over O_2. Indeed, the reaction can be carried out under air and oxalate results the only product of the reaction. The author claim that this selectivity is due to the special environment in which the copper atoms are placed, reinforcing the idea that the geometric and steric characteristic of the complex, together with the bimetallic cooperativity, plays a key role in the outcome of a chemical reaction.

Another case reported by Murray, involves a tris(β-diketiminate) cyclophane ligand capable of hosting three metal cations in its internal pocket. Trimetallic iron(II), cobalt(II) and zinc(II) complexes have been synthetized and characterized. These complexes have shown interesting reactivity towards carbon dioxide being able to selectively promote hydride transfer to carbon dioxide forming formate bridging species.[116] In particular, the trinuclear zinc bridging hydride showed unusual stability in air and water, reacting selectively with CO_2 and showing no reaction towards nitriles, aldehydes and even CS_2.[117] Finally, upon reduction with alkali metals, the trinuclear complex promoted the cleavage of dinitrogen with the formation of bridging nitrides or amides then can act as catalysts for silylation reactions.[84,85,118] The unique reactivity of those systems compared to the monometallic analogues is due to the particular geometry in which the metal centres are forced, reinforcing the idea of multimetallic cooperation.

A series of trimetallic complexes were also reported by Betley and co-workers. The particular ligand used in that study (Scheme 21) forced the metallic centres in close proximity, with a distance within the range of Fe-Fe bond.[119]

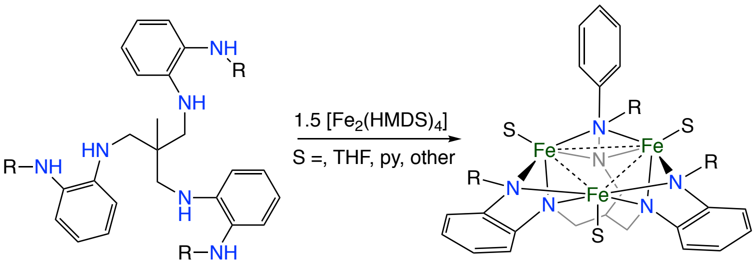

Scheme 21. Formation of a trimetallic Fe(II) complex

Those complexes showed a series of interesting reactivity towards azobenzene derivatives[120] and azides[121], and the interaction of the iron centres give rise to an unprecedent magnetic coupling that is retained at room temperature.[110]

Regarding the f-metals or mixed d-f- metal complexes, interesting examples are found in literature. In 2014 Arnold, Love and co-workers reported the synthesis and characterization of a dinuclear uranium complex supported by a polypyrrolic macrocycle (commonly known as Pacman ligand).[122] This macrocyclic ligand has been used to synthetize several bimetallic complexes showing the ability of forcing them into close proximity (3.5 - 7.8 Å, depending on the metal centre and coordinated anions).[123]

Again Arnold et al. documented the synthesis of a series of U(IV) and d-metal complexes held together by a diphenylphosphino phenolate ligand. [124,125] The main characteristic of this ligand is the

presence of two distinct coordination site capable of binding both oxophilic, hard metals such as lanthanide, actinides or early transition metals and softer metals such as late transition metals.
Lu et al. used a similar ligand reporting the synthesis of hetero-bimetallic complexes (Scheme 22) featuring short metal-metal distances (1.9 – 2.6 Å depending on the metal centres).[126,127] Those compounds resulted are also active catalysts for hydrogenation or isomerization reactions, underlining the utility of rare earth metal ions as promoters, being able to influence the electronics of the second metal centre.[128]

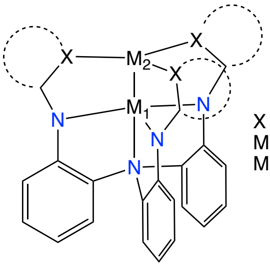

X = N, P
M$_1$ = RE, d-metal
M$_2$ = d-metal

Scheme 22. Hetero- bimetallic complexes featuring short M$_1$-M$_2$ distances.

However, the examples reported take advantage of a preorganized organic ligand specifically designed to hold the metal centres in close proximity. Simpler ligands can also be used to promote the formation of multimetallic systems. In this respect, the ancillary ligand tris(tert-butoxy)siloxide represents a good candidate thanks to its flexible coordination modes, being able to act as a mono- or multi-dentate ligand. The tris(tert-butoxy)siloxide ligand, like alkoxides and aryloxide, can act as σ and π donor. Being a hard donor, the metal oxygen bond that this ligand form with f-elements is strong, mainly due to electrostatic interactions. Moreover, this ligand is reasonably bulky (Tolman's angle of about 125 °) and is therefore appropriate for forming low coordinated reactive metal centres, also thanks to the possibility of coordinate the metals in a multidentate mode. Binuclear complexes of trivalent lanthanides supported by siloxide ligands have already been reported, proving the ability of this ligand to promote the formation of systems with metals in proximity to each other.[129] Moreover, in the past the use of this type of ligands has been limited in f-element chemistry, with only two examples reported for divalent lanthanides, making this chemistry almost unexplored.[130,131]

Redox active ligands

The vast majority of homogeneous or heterogeneous catalysts contain one or more metal centres. Generally speaking, catalytic processes can be divided into redox-active (when a change in the oxidation state of the metal centre is involved in the reaction mechanism) or redox-neutral (when the oxidation state of the metals remains unchanged during the reaction). For example, the ability of Pd or Pt to undergo two-electron transfer (Pd/Pd^0, Pt/Pd^{II}, Pt/Pd^{IV}) has been widely used to promote many organic reactions.[132,133] On the contrary, the redox stability of Ti^{IV} or Zr^{IV} makes those metals suitable candidates for alkene polymerization catalysts.[134] However, metals that does not have multiple accessible redox states may instead possess other characteristics that make them ideal candidates for the coordination of the substrate, and consequently the possibility to impart redox ability would be a great achievement.

When a non-redox-active ligand is coordinated to a metal centre, the energy that is required for its oxidation or reduction is generally much larger than the energy required for a change in the oxidation state of the metal. Consequently, the exchange of electrons that are needed for the reaction to proceed occurs at the metal centre. On the contrary, redox-active ligands have more energetically accessible levels for reduction or oxidation, and this translates to their ability to participate in the electron exchange with the possibility of the metal maintaining the same oxidation state during the transformation. However, sometimes the assignment of the oxidation state of the metal can be difficult when it is bound to redox-active ligands. This fact resulted in the classification of these ligands as "non-innocent" because they are "guilty" of hiding the real oxidation state of the metal centre.

For what is discussed above, it is clear that redox active ligands may be powerful tools to confer redox ability to metals which do not readily change oxidation state by accommodating electrons in their scaffold, thereby acting as an electron reservoir. For these reasons, the use of these ligands has become increasingly popular in d-block chemistry for both fundamental understanding of the phenomena, and for the development of molecular batteries[135] and catalysts[136,137] for small molecule activation.

Ligand such as catechol, aminophenol and phenylenediamine derivatives can coordinate to a metal in three different oxidation states.

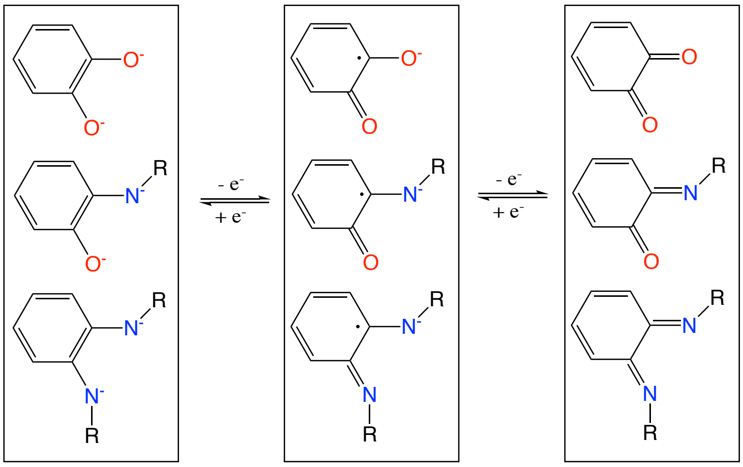

Scheme 23 Examples of redox active ligands.

The coordination behaviour of these ligands in their different oxidation states has been studied in great detail for d-metals.[138]

The use of redox-active ligands has been recently extended to f-elements in order to promote redox reactions to atoms which have only one stable oxidation state. An interesting example was reported by Bart and co-workers, who discovered that a pyridine(diimine) ligand can stabilize a series of highly reduced uranium coordination complexes by storing one, two or three electrons in the ligand, and that they can be released afterwards for the reduction of organic azides (Scheme 24).[139]

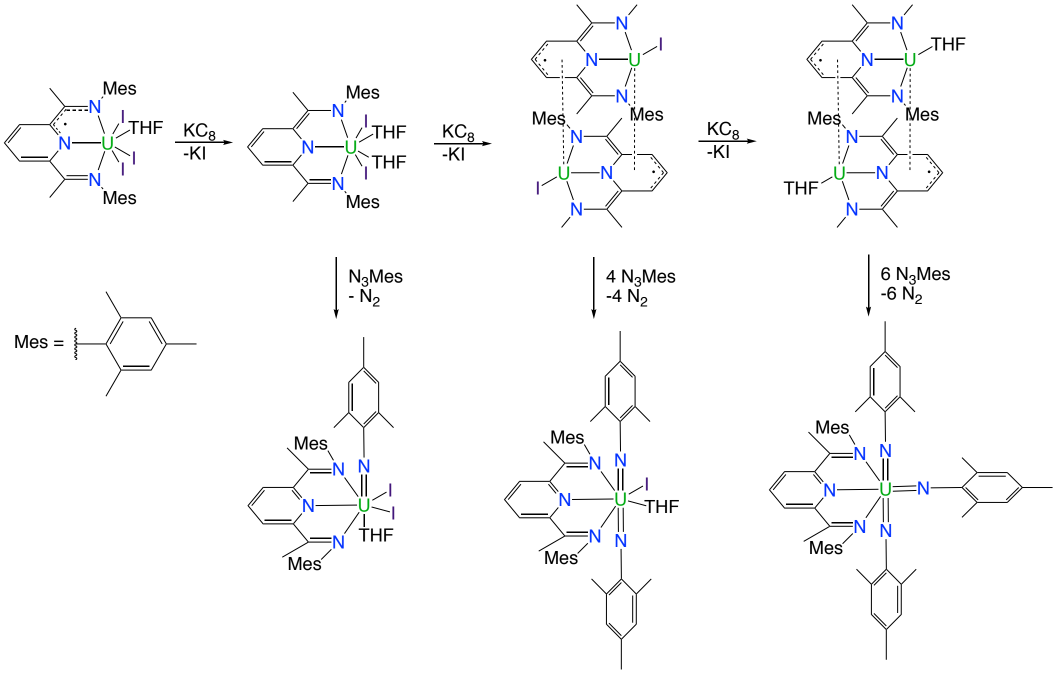

Scheme 24. Multi electron reduction and reactivity towards organic azides of [U(^{Mes}PDI^{Me})].

Spectroscopic and structural characterization of these compounds supports the idea that electrons are stored in the ligand framework and are used in subsequent reactivity.

Schiff base as redox active ligands

Of all the redox-active ligands that can be associated to f-elements to perform redox chemistry, our group has identified polydentate Schiff bases as a very convenient and synthetically versatile choice. Schiff bases contain an imine functionality and are usually obtained from the reaction of an amine and a carbonyl compound. The simple synthesis and the possibility to easily change the steric and electronic properties makes them ideal candidates for our studies and numerous example of multimetallic Schiff base complex have been reported.[109] In the last years, our group has focused on polydentate Schiff bases as supporting ligands for uranium and lanthanides in order to achieve multi-electron reductions. As opposed to the previous mentioned examples in which the electrons were stored as radicals in the ligand scaffold, the reduction of complexes containing Schiff bases often affords the reversible formation of a C-C bond.[140,141,142,143,144]

Previously in our laboratory, uranium complexes supported by the redox-active ligand ^{Me}naphtquinolen[145] and salfen[143] were studied (Scheme 25). The reduction of [U(salfen)$_2$] and [U(^{Me}naphtquinolen)$_2$] did not lead to the formation of a U(III) species, but instead proceeded via a reductive coupling of the imino function of the ligand, leading to a new U(IV) complex with four electrons stored in two C-C bonds.

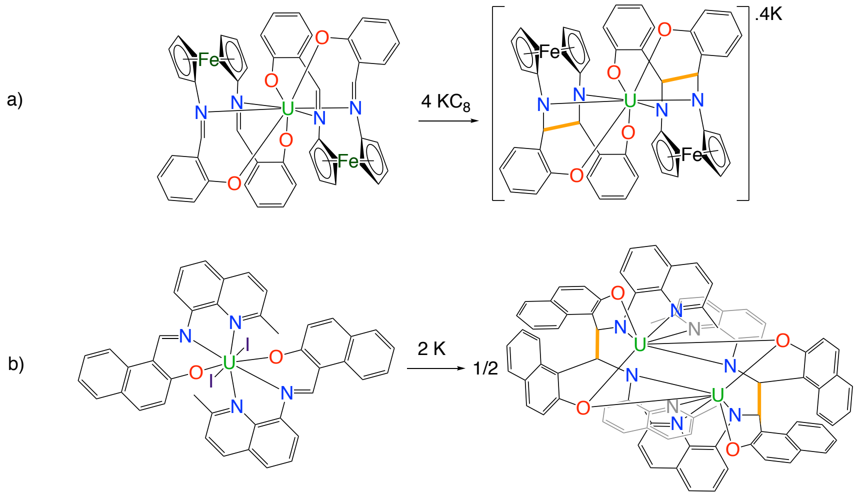

Scheme 25. Reduction of Uranium Schiff base complexes, formation of new C-C bonds for the complexes a) [U(salfen)$_2$] and b) [U(^{Me}naphtquinolen)$_2$].

Also, complexes supported by salophen derivatives have been studied in our group for d-metals,[146] lanthanides[147] and uranium.[144] Differently from the previous examples, those complexes can be reduced under control with two or four electrons, forming macrocyclic ligand in the presence of two imido groups. The new ligand obtained by four electron reduction can host two metal centres closeness, and it has been used in the past by Floriani and co-worker to promote the formation of metal-metal bonds between d-metals.[141] As it will be shown in Chapters 2, 3 and 4, the study of Schiff base supported complexes has been extended for iron, lanthanides and U mixed d-metals.

Purposes and objectives of the projects

The work presented here concern the area of fundamental organometallic chemistry. The main goal of the work was the design of f- and d-elements complexes capable to promote the activation of small molecules, which is an attractive and challenging field in contemporary chemistry. Indeed, beyond the fundamental interest, this research may represent a step towards the development of efficient molecular catalysts or electrocatalysts that convert cheap and abundant molecules into valuable chemicals.

Being small molecule normally relative inert, their utilization depends on surmounting a significant activation barrier. Moreover, due to their thermodynamic stability, high reducing potentials are generally required for their reduction.

To overcome these problems fundamental research is focused on designing compounds that coordinate the substrate and allow them to undergo the addition of multiple electrons that are normally required for their transformation.

Compared to d-metals, few examples of small molecule activation promoted by f-element are reported in literature despite the unique properties these elements possess, such as flexible coordination sphere and the high reducing potential in low oxidation state. However, the redox chemistry of f-elements is mostly dominated by one electron process, while a multielectron transfer is required for the reduction of small molecule.

During my PhD I synthetized and characterized highly reactive d- and f-metal complexes designed to perform multi electron redox reactions that can be exploited in the activation of small molecules. More specifically, two main strategies have been used both directed to implement multi-electron transfer in f-element chemistry: the first involves in the study of Schiff base as supporting redox active ligands capable to store and release electrons during reactivity, and the second consists in the design of compounds bearing multiple metal centres in low valent oxidation state.

For what concerns the first approach, in Chapters 2, 3 and 4 will be presented a series of homo- and hetero- bi and tri-metallic complexes supported by Schiff base ligands and their reactivity towards small molecules. It will be shown how electrons can be stored and released from the ligand scaffold trough the reversible formation of multiple carbon- carbon bonds. An important target of the projects was to study the possibility of tuning the reducing ability of the complexes by changing both the metal centres involved and the ligand. In those studies, the reduction of metal ions supported by the salophen and the trensal ligand was expanded to mixed metal complexes, iron and lanthanides.

In Chapters 5, 6 and 7 will be presented dinuclear systems resulting by using the ligand tris(tert-butoxy)siloxide with 4f-metal complexes. In this case, the use of a spectator ligand was explored with the idea of building multimetallic systems capable of multielectron reactions, that in this case were stored in the metal centres.

Finally, in Chapter 8, the insertion of carbon dioxide into the C-H bond of terminal alkynes is presented. Despite the reaction was conducted in presence of metal catalysts, it will be shown that under specific conditions the catalytic specie is not required.

References

1 P. Pyykko, *Chem. Rev.*, 1988, **88**, 563–594.

2 M. R. MacDonald, J. E. Bates, M. E. Fieser, J. W. Ziller, F. Furche and W. J. Evans, *J. Am. Chem. Soc.*, 2012, **134**, 8420–8423.

3 M. R. MacDonald, J. E. Bates, J. W. Ziller, F. Furche and W. J. Evans, *J. Am. Chem. Soc.*, 2013, **135**, 9857–9868.

4 S. Liu, X. Wu, D. Weng and R. Ran, *J. Rare Earths*, 2015, **33**, 567–590.

5 M. El-Ghozzi and D. Avignant, *J. Fluor. Chem.*, 2001, 5.

6 S. G. Minasian, E. R. Batista, C. H. Booth, D. L. Clark, J. M. Keith, S. A. Kozimor, W. W. Lukens, R. L. Martin, D. K. Shuh, S. C. E. Stieber, T. Tylisczcak and X. Wen, *J. Am. Chem. Soc.*, 2017, **139**, 18052–18064.

7 A. R. Willauer, C. T. Palumbo, R. Scopelliti, I. Zivkovic, I. Douair, L. Maron and M. Mazzanti, *Angew. Chem.*, 2020, **132**, 3577–3581.

8 A. R. Willauer, C. T. Palumbo, F. Fadaei-Tirani, I. Zivkovic, I. Douair, L. Maron and M. Mazzanti, *J. Am. Chem. Soc.*, 2020, **142**, 5538–5542.

9 C. T. Palumbo, I. Zivkovic, R. Scopelliti and M. Mazzanti, *J. Am. Chem. Soc.*, 2019, **141**, 9827–9831.

10 N. T. Rice, I. A. Popov, D. R. Russo, J. Bacsa, E. R. Batista, P. Yang, J. Telser and H. S. La Pierre, *J. Am. Chem. Soc.*, 2019, **141**, 13222–13233.

11 S. Fortier and T. W. Hayton, *Coord. Chem. Rev.*, 2010, **254**, 197–214.

12 P. L. Arnold, J. B. Love and D. Patel, *Coord. Chem. Rev.*, 2009, **253**, 1973–1978.

13 R. Faizova, R. Scopelliti, A.-S. Chauvin and M. Mazzanti, *J. Am. Chem. Soc.*, 2018, **140**, 13554–13557.

14 R. Faizova, F. Fadaei-Tirani, R. Bernier-Latmani and M. Mazzanti, *Angew. Chem.*, 2020, **132**, 6822–6825.

15 T. F. Jenkins, D. H. Woen, L. N. Mohanam, J. W. Ziller, F. Furche and W. J. Evans, *Organometallics*, 2018, **37**, 3863–3873.

16 M. R. MacDonald, M. E. Fieser, J. E. Bates, J. W. Ziller, F. Furche and W. J. Evans, *J. Am. Chem. Soc.*, 2013, **135**, 13310–13313.

17 B. M. Bhanage and M. Arai, Eds., *Transformation and Utilization of Carbon Dioxide*, Springer Berlin Heidelberg, Berlin, Heidelberg, 2014.

18 M. Cokoja, C. Bruckmeier, B. Rieger, W. A. Herrmann and F. E. Kühn, *Angew. Chem. Int. Ed.*, 2011, **50**, 8510–8537.

19 B. M. Bhanage and M. Arai, Eds., *Transformation and Utilization of Carbon Dioxide*, Springer Berlin Heidelberg, Berlin, Heidelberg, 2014.

20 D. Yu, S. P. Teong and Y. Zhang, *Coord. Chem. Rev.*, 2015, **293–294**, 279–291.

21 G. Yuan, C. Qi, W. Wu and H. Jiang, *Curr. Opin. Green Sustain. Chem.*, 2017, **3**, 22–27.

22 K. A. Grice, *Coord. Chem. Rev.*, 2017, **336**, 78–95.

23 S. Nitopi, E. Bertheussen, S. B. Scott, X. Liu, A. K. Engstfeld, S. Horch, B. Seger, I. E. L. Stephens, K. Chan, C. Hahn, J. K. Nørskov, T. F. Jaramillo and I. Chorkendorff, *Chem. Rev.*, 2019, **119**, 7610–7672.

24 W. J. Evans, C. A. Seibel and J. W. Ziller, *Inorg. Chem.*, 1998, **37**, 770–776.

25 I. Castro-Rodriguez, *Science*, 2004, **305**, 1757–1759.

26 M. Fang, J. H. Farnaby, J. W. Ziller, J. E. Bates, F. Furche and W. J. Evans, *J. Am. Chem. Soc.*, 2012, **134**, 6064–6067.

27 C. Camp, L. Chatelain, C. E. Kefalidis, J. Pécaut, L. Maron and M. Mazzanti, *Chem. Commun.*, 2015, **51**, 15454–15457.

28 W. J. Evans, J. M. Perotti, J. C. Brady and J. W. Ziller, *J. Am. Chem. Soc.*, 2003, **125**, 5204–5212.

29 W. J. Evans, S. E. Lorenz and J. W. Ziller, *Inorg. Chem.*, 2009, **48**, 2001–2009.
30 G. R. Lee, J. M. Maher and N. J. Cooper, *J. Am. Chem. Soc.*, 1987, **109**, 2956–2962.
31 J.-M. Savéant, *Chem. Rev.*, 2008, **108**, 2348–2378.
32 A. Chapovetsky, T. H. Do, R. Haiges, M. K. Takase and S. C. Marinescu, *J. Am. Chem. Soc.*, 2016, **138**, 5765–5768.
33 N. W. Davies, A. S. P. Frey, M. G. Gardiner and J. Wang, *Chem. Commun.*, 2006, 4853.
34 J. Andrez, J. Pécaut, P.-A. Bayle and M. Mazzanti, *Angew. Chem. Int. Ed.*, 2014, **53**, 10448–10452.
35 N. Tsoureas, L. Castro, A. F. R. Kilpatrick, F. G. N. Cloke and L. Maron, *Chem Sci*, 2014, **5**, 3777–3788.
36 L. Castro, S. Labouille, D. R. Kindra, J. W. Ziller, F. Nief, W. J. Evans and L. Maron, *Chem. - Eur. J.*, 2012, **18**, 7886–7895.
37 L. Castro, O. P. Lam, S. C. Bart, K. Meyer and L. Maron, *Organometallics*, 2010, **29**, 5504–5510.
38 A.-C. Schmidt, A. V. Nizovtsev, A. Scheurer, F. W. Heinemann and K. Meyer, *Chem. Commun.*, 2012, **48**, 8634.
39 O. Cooper, C. Camp, J. Pécaut, C. E. Kefalidis, L. Maron, S. Gambarelli and M. Mazzanti, *J. Am. Chem. Soc.*, 2014, **136**, 6716–6723.
40 M. Xémard, V. Goudy, A. Braun, M. Tricoire, M. Cordier, L. Ricard, L. Castro, E. Louyriac, C. E. Kefalidis, C. Clavaguéra, L. Maron and G. Nocton, *Organometallics*, 2017, **36**, 4660–4668.
41 A. R. Willauer, D. Toniolo, F. Fadaei-Tirani, Y. Yang, M. Laurent and M. Mazzanti, *Dalton Trans.*, 2019, **48**, 6100–6110.
42 K. Müller, K. Brooks and T. Autrey, *Energy Fuels*, 2017, **31**, 12603–12611.
43 S. Enthaler, J. von Langermann and T. Schmidt, *Energy Environ. Sci.*, 2010, **3**, 1207.
44 F. Joó, *ChemSusChem*, 2008, **1**, 805–808.
45 C. Costentin, M. Robert and J.-M. Savéant, *Chem. Soc. Rev.*, 2013, **42**, 2423–2436.
46 P. G. Jessop, F. Joó and C.-C. Tai, *Coord. Chem. Rev.*, 2004, **248**, 2425–2442.
47 P. G. Jessop, T. Ikariya and R. Noyori, 14.
48 A. Taheri, E. J. Thompson, J. C. Fettinger and L. A. Berben, *ACS Catal.*, 2015, **5**, 7140–7151.
49 J. A. Higgins, F. G. N. Cloke and S. M. Roe, *Organometallics*, 2013, **32**, 5244–5252.
50 B. Yu and L.-N. He, *ChemSusChem*, 2015, **8**, 52–62.
51 O. Vechorkin, N. Hirt and X. Hu, *Org. Lett.*, 2010, **12**, 3567–3569.
52 F. D. Bobbink, W. Gruszka, M. Hulla, S. Das and P. J. Dyson, *Chem. Commun.*, 2016, **52**, 10787–10790.
53 Q. Liu, L. Wu, R. Jackstell and M. Beller, *Nat. Commun.*, 2015, **6**, 5933.
54 J. Louie, J. E. Gibby, M. V. Farnworth and T. N. Tekavec, *J. Am. Chem. Soc.*, 2002, **124**, 15188–15189.
55 A. Behr and G. Henze, *Green Chem*, 2011, **13**, 25–39.
56 F. Manjolinho, M. Arndt, K. Gooßen and L. J. Gooßen, *ACS Catal.*, 2012, **2**, 2014–2021.
57 J. Jover and F. Maseras, *J. Org. Chem.*, 2014, **79**, 11981–11987.
58 C. Liu, Y. Luo, W. Zhang, J. Qu and X. Lu, *Organometallics*, 2014, **33**, 2984–2989.
59 R. Yuan and Z. Lin, *ACS Catal.*, 2014, **4**, 4466–4473.
60 I. S. Butler and A. E. Fenster, *J. Organomet. Chem.*, 1974, **66**, 161–194.
61 M. C. Baird, G. Hartwell and G. Wilkinson, *Inorg. Phys. Theor.*, 1967, 2037–2040.
62 A. E. Fenster and I. S. Butler, *Inorg. Chem.*, 1974, **13**, 915–920.
63 O. P. Lam, F. W. Heinemann and K. Meyer, *Angew. Chem. Int. Ed.*, 2011, **50**, 5965–5968.
64 O. P. Lam, L. Castro, B. Kosog, F. W. Heinemann, L. Maron and K. Meyer, *Inorg. Chem.*, 2012, **51**, 781–783.
65 D. Heitmann, C. Jones, D. P. Mills and A. Stasch, *Dalton Trans.*, 2010, **39**, 1877.
66 G. B. Deacon, P. C. Junk, J. Wang and D. Werner, *Inorg. Chem.*, 2014, **53**, 12553–12563.
67 V. Beck and D. O'Hare, *J. Organomet. Chem.*, 2004, **689**, 3920–3938.

68 A. H. Cowley, *Chem Commun*, 2004, 2369–2375.

69 F. T. Edelmann, *New J Chem*, 2011, **35**, 517–528.

70 W. J. Evans, M. A. Johnston, M. A. Greci and J. W. Ziller, *Organometallics*, 1999, **18**, 1460–1464.

71 P. L. Arnold, S. M. Mansell, L. Maron and D. McKay, *Nat. Chem.*, 2012, **4**, 668–674.

72 V. Mougel, C. Camp, J. Pécaut, C. Copéret, L. Maron, C. E. Kefalidis and M. Mazzanti, *Angew. Chem. Int. Ed.*, 2012, **51**, 12280–12284.

73 R. P. Kelly, L. Maron, R. Scopelliti and M. Mazzanti, *Angew. Chem. Int. Ed.*, 2017, **56**, 15663–15666.

74 R. P. Kelly, D. Toniolo, F. F. Tirani, L. Maron and M. Mazzanti, *Chem. Commun.*, 2018, **54**, 10268–10271.

75 D. V. Yandulov, *Science*, 2003, **301**, 76–78.

76 M. M. Rodriguez, E. Bill, W. W. Brennessel and P. L. Holland, *Science*, 2011, **334**, 780–783.

77 B. A. MacKay and M. D. Fryzuk, *Chem. Rev.*, 2004, **104**, 385–402.

78 J. S. Anderson, J. Rittle and J. C. Peters, *Nature*, 2013, **501**, 84–87.

79 S. Kuriyama, K. Arashiba, K. Nakajima, Y. Matsuo, H. Tanaka, K. Ishii, K. Yoshizawa and Y. Nishibayashi, *Nat. Commun.*, 2016, **7**, 12181.

80 A. Eizawa, K. Arashiba, H. Tanaka, S. Kuriyama, Y. Matsuo, K. Nakajima, K. Yoshizawa and Y. Nishibayashi, *Nat. Commun.*, 2017, **8**, 14874.

81 C. Tang and S.-Z. Qiao, *Chem. Soc. Rev.*, 2019, **48**, 3166–3180.

82 X. Guo, H. Du, F. Qu and J. Li, *J. Mater. Chem. A*, 2019, **7**, 3531–3543.

83 D. Sorsche, M. E. Miehlich, K. Searles, G. Gouget, E. M. Zolnhofer, S. Fortier, C.-H. Chen, M. Gau, P. J. Carroll, C. B. Murray, K. G. Caulton, M. M. Khusniyarov, K. Meyer and D. J. Mindiola, *J. Am. Chem. Soc.*, 2020, **142**, 8147–8159.

84 D. M. Ermert, J. B. Gordon, K. A. Abboud and L. J. Murray, *Inorg. Chem.*, 2015, **54**, 9282–9289.

85 Y. Lee, F. T. Sloane, G. Blondin, K. A. Abboud, R. García-Serres and L. J. Murray, *Angew. Chem. Int. Ed.*, 2015, **54**, 1499–1503.

86 K. P. Chiang, S. M. Bellows, W. W. Brennessel and P. L. Holland, *Chem. Sci.*, 2013, **5**, 267–274.

87 J. M. Smith, A. R. Sadique, T. R. Cundari, K. R. Rodgers, G. Lukat-Rodgers, R. J. Lachicotte, C. J. Flaschenriem, J. Vela and P. L. Holland, *J. Am. Chem. Soc.*, 2006, **128**, 756–769.

88 D. L. J. Broere, B. Q. Mercado, E. Bill, K. M. Lancaster, S. Sproules and P. L. Holland, *Inorg. Chem.*, 2018, **57**, 9580–9591.

89 D. C. Graham, G. J. O. Beran, M. Head-Gordon, G. Christian, R. Stranger and B. F. Yates, *J. Phys. Chem. A*, 2005, **109**, 6762–6772.

90 Y. Ohki, K. Uchida, M. Tada, R. E. Cramer, T. Ogura and T. Ohta, *Nat. Commun.*, 2018, **9**, 3200.

91 J. A. Hernandez, S. J. George and L. M. Rubio, *Biochemistry*, 2009, **48**, 9711–9721.

92 M. Hidai, *Coord. Chem. Rev.*, 1999, **185–186**, 99–108.

93 C. E. Laplaza, M. J. A. Johnson, J. C. Peters, A. L. Odom, E. Kim, C. C. Cummins, G. N. George and I. J. Pickering, *J. Am. Chem. Soc.*, 1996, **118**, 8623–8638.

94 Z. Turner, *Inorganics*, 2015, **3**, 597–635.

95 W. J. Evans, T. A. Ulibarri and J. W. Ziller, *J. Am. Chem. Soc.*, 1988, **110**, 6877–6879.

96 W. J. Evans, D. S. Lee and J. W. Ziller, *J. Am. Chem. Soc.*, 2004, **126**, 454–455.

97 W. J. Evans, M. Fang, G. Zucchi, F. Furche, J. W. Ziller, R. M. Hoekstra and J. I. Zink, *J. Am. Chem. Soc.*, 2009, **131**, 11195–11202.

98 W. J. Evans, S. A. Kozimor and J. W. Ziller, *J. Am. Chem. Soc.*, 2003, **125**, 14264–14265.

99 S. M. Mansell, N. Kaltsoyannis and P. L. Arnold, *J. Am. Chem. Soc.*, 2011, **133**, 9036–9051.

100 S. M. Mansell, J. H. Farnaby, A. I. Germeroth and P. L. Arnold, *Organometallics*, 2013, **32**, 4214–4222.

101 M. Falcone, L. Chatelain, R. Scopelliti, I. Živković and M. Mazzanti, *Nature*, 2017, **547**, 332–335.

102 M. Falcone, L. Barluzzi, J. Andrez, F. Fadaei Tirani, I. Zivkovic, A. Fabrizio, C. Corminboeuf, K. Severin and M. Mazzanti, *Nat. Chem.*, 2019, **11**, 154–160.
103 B. G. Cooper, J. W. Napoline and C. M. Thomas, *Catal. Rev.*, 2012, **54**, 1–40.
104 V. T. Annibale and D. Song, *RSC Adv.*, 2013, **3**, 11432.
105 J. I. van der Vlugt, *Eur. J. Inorg. Chem.*, 2012, **2012**, 363–375.
106 P. Power, *J. Am. Chem. Soc.*, 2007, **129**, 8396–8396.
107 M. Fairley, L. Davin, A. Hernán-Gómez, J. García-Álvarez, C. T. O'Hara and E. Hevia, *Chem. Sci.*, 2019, **10**, 5821–5831.
108 R. McLellan, M. Uzelac, A. R. Kennedy, E. Hevia and R. E. Mulvey, *Angew. Chem. Int. Ed.*, 2017, **56**, 9566–9570.
109 R. M. Clarke and T. Storr, *Dalton Trans.*, 2014, **43**, 9380.
110 E. V. Eames, T. D. Harris and T. A. Betley, *Chem Sci*, 2012, **3**, 407–415.
111 J. Park and S. Hong, *Chem. Soc. Rev.*, 2012, **41**, 6931.
112 R. Xu, L. Hua, X. Li, Y. Yao, X. Leng and Y. Chen, *Dalton Trans.*, 2019, **48**, 10565–10573.
113 P. Buchwalter, J. Rosé and P. Braunstein, *Chem. Rev.*, 2015, **115**, 28–126.
114 D. H. Gibson, *Coord. Chem. Rev.*, 1999, **185–186**, 335–355.
115 U. R. Pokharel, F. R. Fronczek and A. W. Maverick, *Nat. Commun.*, 2014, **5**, 5883.
116 Y. Lee, K. J. Anderton, F. T. Sloane, D. M. Ermert, K. A. Abboud, R. García-Serres and L. J. Murray, *J. Am. Chem. Soc.*, 2015, **137**, 10610–10617.
117 D. M. Ermert, I. Ghiviriga, V. J. Catalano, J. Shearer and L. J. Murray, *Angew. Chem. Int. Ed.*, 2015, **54**, 7047–7050.
118 R. B. Ferreira, B. J. Cook, B. J. Knight, V. J. Catalano, R. García-Serres and L. J. Murray, *ACS Catal.*, 2018, 7208–7212.
119 Q. Zhao and T. A. Betley, *Angew. Chem. Int. Ed.*, 2011, **50**, 709–712.
120 T. M. Powers and T. A. Betley, *J. Am. Chem. Soc.*, 2013, **135**, 12289–12296.
121 T. M. Powers, A. R. Fout, S.-L. Zheng and T. A. Betley, *J. Am. Chem. Soc.*, 2011, **133**, 3336–3338.
122 P. L. Arnold, C. J. Stevens, J. H. Farnaby, M. G. Gardiner, G. S. Nichol and J. B. Love, *J. Am. Chem. Soc.*, 2014, **136**, 10218–10221.
123 J. B. Love, *Chem. Commun.*, 2009, 3154.
124 J. A. Hlina, J. R. Pankhurst, N. Kaltsoyannis and P. L. Arnold, *J. Am. Chem. Soc.*, 2016, **138**, 3333–3345.
125 J. A. Hlina, J. A. L. Wells, J. R. Pankhurst, J. B. Love and P. L. Arnold, *Dalton Trans*, 2017, **46**, 5540–5545.
126 P. A. Rudd, S. Liu, N. Planas, E. Bill, L. Gagliardi and C. C. Lu, *Angew. Chem. Int. Ed.*, 2013, **52**, 4449–4452.
127 S. J. Tereniak, R. K. Carlson, L. J. Clouston, V. G. Young, E. Bill, R. Maurice, Y.-S. Chen, H. J. Kim, L. Gagliardi and C. C. Lu, *J. Am. Chem. Soc.*, 2014, **136**, 1842–1855.
128 B. L. Ramirez and C. C. Lu, *J. Am. Chem. Soc.*, 2020, **142**, 5396–5407.
129 G. Lapadula, M. P. Conley, C. Copéret and R. A. Andersen, *Organometallics*, 2015, **34**, 2271–2277.
130 D. J. Duncalf, P. B. Hitchcock and G. A. Lawless, 3.
131 M. Nishiura, Z. Hou and Y. Wakatsuki, *Organometallics*, 2004, **23**, 1359–1368.
132 K. C. Nicolaou, P. G. Bulger and D. Sarlah, *Angew. Chem. Int. Ed.*, 2005, **44**, 4442–4489.
133 N. Kambe, T. Iwasaki and J. Terao, *Chem. Soc. Rev.*, 2011, **40**, 4937.
134 D. W. Stephan, *Organometallics*, 2005, **24**, 2548–2560.
135 P. J. Cabrera, X. Yang, J. A. Suttil, K. L. Hawthorne, R. E. M. Brooner, M. S. Sanford and L. T. Thompson, *J. Phys. Chem. C*, 2015, **119**, 15882–15889.
136 V. Lyaskovskyy and B. de Bruin, *ACS Catal.*, 2012, **2**, 270–279.
137 H. Grützmacher, *Angew. Chem. Int. Ed.*, 2008, **47**, 1814–1818.

138 D. L. J. Broere, R. Plessius and J. I. van der Vlugt, *Chem. Soc. Rev.*, 2015, **44**, 6886–6915.
139 N. H. Anderson, S. O. Odoh, Y. Yao, U. J. Williams, B. A. Schaefer, J. J. Kiernicki, A. J. Lewis, M. D. Goshert, P. E. Fanwick, E. J. Schelter, J. R. Walensky, L. Gagliardi and S. C. Bart, *Nat. Chem.*, 2014, **6**, 919–926.
140 S. De Angelis, E. Solari, E. Gallo, C. Floriani, A. Chiesi-Villa and C. Rizzoli, *Inorg. Chem.*, 1996, **35**, 5995–6003.
141 C. Floriani, E. Solari, F. Franceschi, R. Scopelliti, P. Belanzoni and M. Rosi, *Chem. - Eur. J.*, 2001, **7**, 3052–3061.
142 E. Gallo, E. Solari, N. Re, C. Floriani, A. Chiesi-Villa and C. Rizzoli, *J. Am. Chem. Soc.*, 1997, **119**, 5144–5154.
143 C. Camp, L. Chatelain, V. Mougel, J. Pécaut and M. Mazzanti, *Inorg. Chem.*, 2015, **54**, 5774–5783.
144 C. Camp, V. Mougel, P. Horeglad, J. Pécaut and M. Mazzanti, *J. Am. Chem. Soc.*, 2010, **132**, 17374–17377.
145 C. Camp, J. Andrez, J. Pécaut and M. Mazzanti, *Inorg. Chem.*, 2013, **52**, 7078–7086.
146 J. Andrez, V. Guidal, R. Scopelliti, J. Pécaut, S. Gambarelli and M. Mazzanti, *J. Am. Chem. Soc.*, 2017, **139**, 8628–8638.
147 C. Camp, V. Guidal, B. Biswas, J. Pécaut, L. Dubois and M. Mazzanti, *Chem. Sci.*, 2012, **3**, 2433.

Chapter 2. A versatile route to homo- and hetero-bimetallic 5f–5f and 3d–5f complexes supported by a redox active ligand framework*

Introduction

Heterometallic 3d-5f coordination compounds are attracting increasing attention because of their importance in the fundamental understanding of the nature bonding and metal-metal interaction in 5f elements.[1] Moreover, they offer the possibility to combine the distinct characteristics of f and d block elements to obtain new physical properties and to promote novel chemical reactivity.[2] Notably the association of uranium with 3d elements led to the discovery of original uranium-3d polymetallic assemblies with unique magnetic properties.[3] Moreover, the importance of multimetallic cooperativity in the stoichiometric and catalytic transformation of molecules such as CO_2, CO or CS_2 is increasingly recognized,[2,4] but most studies have so far focused of hetero-bimetallic complexes associating early/main group and late d-block metal ions.[2,5]

To date, only a handful examples of heterobimetallic complexes that feature d-block and uranium metal centres in close proximity have been reported and their reactivity remains essentially unexplored.[6] Moreover, the of use redox active ligands[7] in the synthesis and reactivity of 5f-3d complexes is so far limited to ferrocene-based systems.[6c,8]

Recently, we have explored the chemistry of uranium complexes supported by Schiff-base ligands.[8b,9] We found that the reduction of the $[U^{IV}(salophen)_2]$ complex with Na (Scheme 1),[9a] affords a U(IV) complex of the new dinucleating bis-salophen ligand via ligand-based reduction.

---

* Portion of this chapter have been published: C. Camp, D. Toniolo, J. Andrez, J. Pécaut, M. Mazzanti, *Dalton Trans.* 2017, **46**, 11145– 11148

Authors contributions: C.C. and M.M. originated the idea and wrote the manuscript. C.C., J.A. and D.T. performed the synthesis and the characterization of the complexes. In particular DT optimized the synthesis of all compounds beside **2-py** and obtained the crystals of **3**, **4-3py** and **6**. J. P. performed the X-ray single crystal analysis.

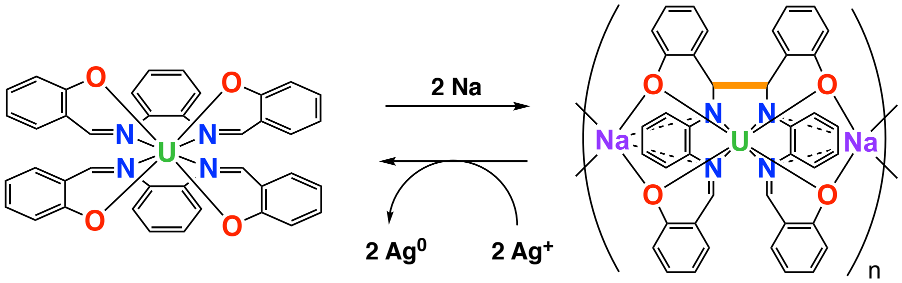

[U(salophen)$_2$] **[Na$_2$U(bis-salophen)]$_n$, 1**

Scheme 1. C-C bond formation/cleavage in U(IV) Schiff base complexes.

Here we show that the hetero-bimetallic complex [Na$_2$U(bis-salophen)]$_n$, **1**, (Scheme 1) provides a versatile precursor for the synthesis of homo-and hetero-bimetallic complexes of the redox-active bis-salophen ligand via salt metathesis reaction.

Results and Discussion

The addition of one equivalent of [UI$_4$(OEt$_2$)$_2$] or UCl$_4$ to a THF solution of [Na$_2$U(bis-salophen)]$_n$, **1** yields the homo-bimetallic complexes [U$_2$(bis-salophen)(S)$_n$]I$_2$ (S= THF, n = 3, **2-THF; S** = Py, n= 6, **2-py)** and [U$_2$(bis-salophen)(THF)$_2$Cl$_2$], **3**, respectively (Scheme 2). ESI/MS spectra of **2-THF** indicate the presence of a binuclear species in THF solution (m/z = 1231.1, corresponding to the {[U$_2$(bis-salophen)]I}$^+$ moiety).

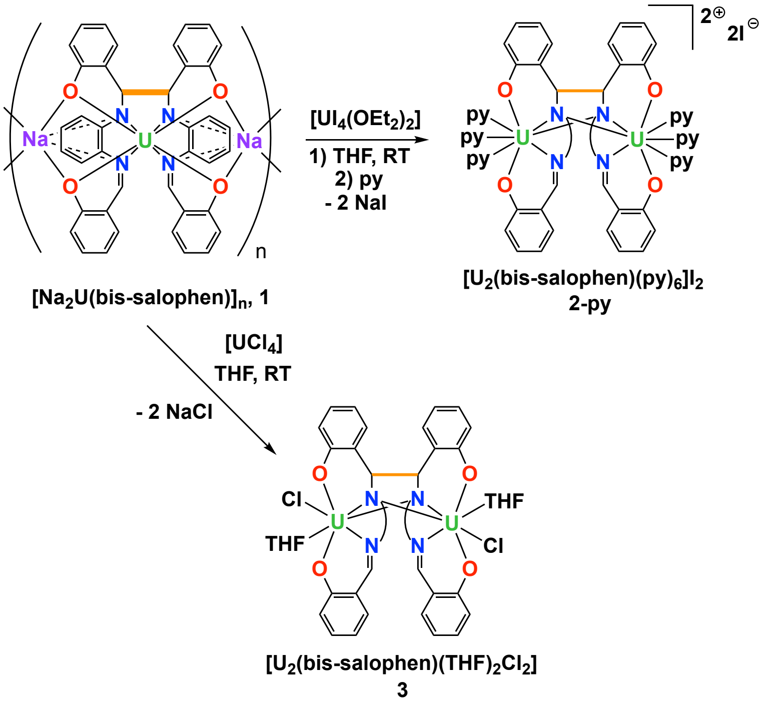

[Na$_2$U(bis-salophen)]$_n$, 1

[U$_2$(bis-salophen)(py)$_6$]I$_2$
2-py

[U$_2$(bis-salophen)(THF)$_2$Cl$_2$]
3

Scheme 2. Synthesis of complexes **2-py** and **3**.

Single crystals of **2-py** were obtained by recrystallization of **2-THF** from a pyridine/hexane solution while crystals of **3** were obtained from slow diffusion of hexane into a THF solution of the compound.

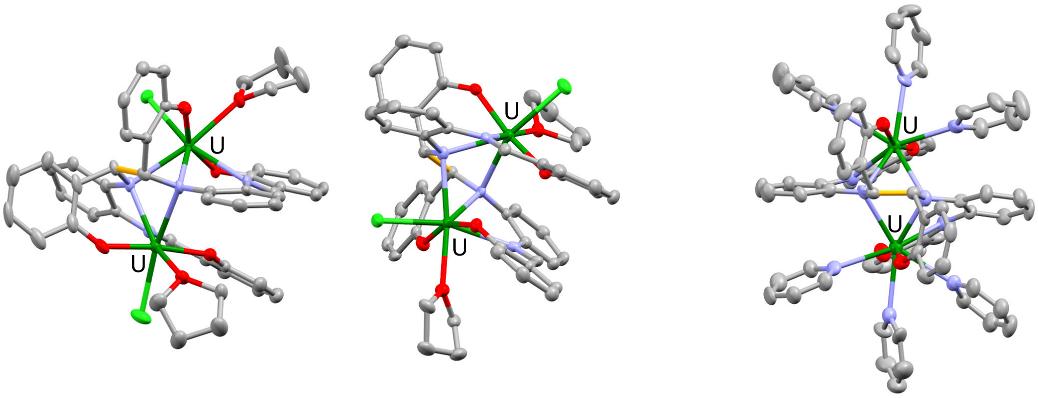

Figure 1. Solid-state structures of the cation [U_2(bis-salophen)$(py)_6$]$^{2+}$ in **2-py** (right) and **3** (left) (50% probability ellipsoids). Hydrogen atoms, outer sphere counter anions and interstitial solvent molecules have been omitted for clarity. C-C bond formed by coupling of imino groups highlighted in yellow.

The crystalline structure of **2-py** consists of isolated ions pairs and the structure of the [U_2(bis-salophen)$(py)_6$]$^{2+}$ cation is presented in Figure 1. The structure of **3** (Figure 1) shows the presence of a neutral complex where a chloride ion binds each uranium cation. In both complexes two U(IV) ions are encapsulated by the octadentate hexaanionic chelating ligand bis-salophen, which adopts a helical structure. It is remarkable that upon substitution of the two sodium ions in **1** by a U(IV) cation the hexaanionic ligand bi-salophen unfolds to accommodate the uranium(IV) ion. These dinuclear complexes present a pseudo-C_2 axis located between the two uranium ions and the two carbon atoms forming the C-C bond (in orange in Scheme 1) connecting the two salophen moieties. Both uranium(IV) centres in **2-py** are eight-coordinated by two phenolate, two amido and one imino moieties from the bis-salophen ligand and three pyridine molecules in a slightly distorted dodecahedral fashion. The two imido moieties of the ligand act as bridging units and are unsymmetrically coordinated to the uranium atoms, the U1-N2 (2.4283(1) Å) and U2-N21 (2.4606(1) Å) bond distances being shorter than those of U1-N21 (2.6603(1) Å) and U2-N2 (2.6643(1) Å), in **2-py** and U1-N2 (2.448(5) Å) and U2-N4 (2.453(5) Å) being shorter than U2-N2 2.610(5) Å) and U1-N4 (2.528(5) Å) in **3**. This results in a 4.0241(2) Å and 3.86(1) Å separation of the two uranium atoms in **2-py** and **3** respectively, which is significantly longer than that (3.54(1) Å) observed in the more sterically constrained complex [U_2(cyclo-salophen)$(THF)_4$].[9a] The U-N_{imino} and the the U-N_{amido} average bond distances in complexes **2-py** and **3** are very similar to those found in complex **1**. Similarly, the values of the C-C bond distance between the two amido groups in the bis-salophen ligand remain unchanged compare to **1**. The ^{1}H NMR spectra of **2-py** and **3** in py-d5 solution, display 13 and 12 shifted paramagnetic resonances respectively in agreement with the symmetry found in the solid state structure.

The two electrons stored in the C-C bond between the two amido groups in **2-py** can become available for the reduction of oxidizing substrates. Notably, treatment of **2-py** with one equivalent of iodine leads to the cleavage of the C-C bond restoring the original Schiff base structure to yield [UI$_2$(salophen)py$_2$] (Scheme 3). However, the homo-bimetallic complexes **2-py** and **3** do not react with less reactive molecules such as CO$_2$ or CS$_2$.

The reduction of **2-py** and **3** by potassium or sodium metal affords the previously reported [U$_2$(cyclo-salophen)(THF)$_4$][9a] complex (Scheme 3). It should be noted that the complex **2-THF** could not be prepared by reduction of [UI$_2$(salophen)(THF)$_2$] with one equivalent of potassium or sodium, a reaction that only leads to the formation of the fully reduced [U$_2$(cyclo-salophen)(THF)$_4$][9a] complex and unreacted precursor.

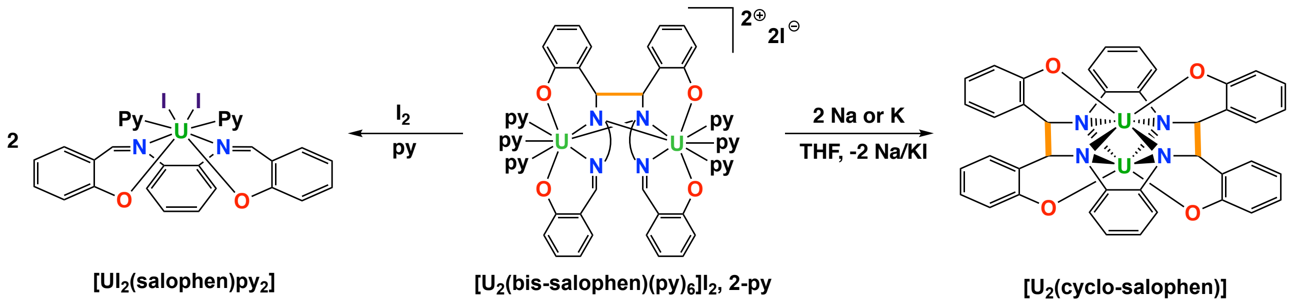

Scheme 3. Ligand-based redox reactivity of complex **2-py**.

We then extended this versatile synthetic route to access original 3d-5f hetero-bimetallic complexes. The reaction of **1** with an equimolar amount of [MX$_2$] (M, X = Co, Cl; Fe, Cl; Ni, I) in THF or in pyridine affords [UCo(bis-salophen)(S)$_x$] (S = THF, x = 2, **4-THF**, S = py, x = 2, **4-2py**, S = py, x = 3, **4-3py**), [UNi(bis-salophen)(THF)$_2$], **5-THF**, and [UFe(bis-salophen)(py)$_3$], **6** in 57-89% yield (Scheme 4). The ^{1}H NMR spectra of complexes **4** and **5** in py-d5 display 24 paramagnetic resonances indicating fully asymmetric species in solution (Figure 2, 3).

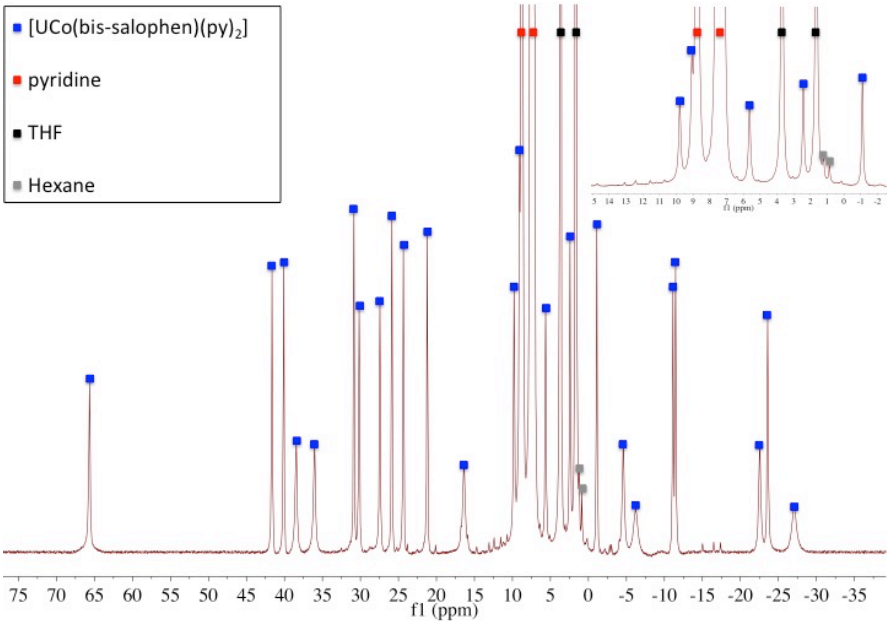

Figure 2 ^{1}H NMR spectrum of **4-2py** (py-d5, 298K, 400 MHz).

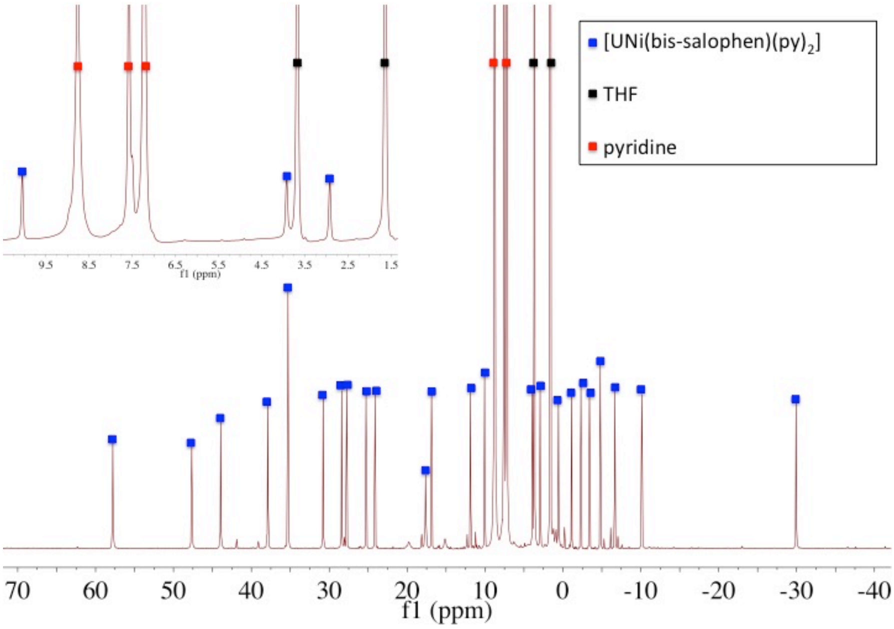

Figure 3 ^{1}H NMR spectrum of **5-py** (py-d5, 298K, 400 MHz).

Interestingly, in order to obtain complexes **4** and **5** as the only reaction products the addition of the Co(II) and Ni((II) salts to **1** should be slow. Fast addition of [MX_2] salts (M = Co, Ni) results in the formation of significant amounts of the oxidation product [U(salophen)$_2$] and Co(0) or Ni(0).

Differently from **4** and **5**, complex **6** resulted unstable in THF and its synthesis could only be performed in pyridine solution. Dissolution of **6**, isolated from pyridine, in THF resulted in the decomposition of the complex in [U(salophen)$_2$], and other minor unidentified product, with concomitant formation of Fe(0). However, the ^{1}H NMR spectrum of **6** in py-d5 displays 27 signals in the paramagnetic range, consistent with a fully asymmetric specie already found for **4** and **5**.

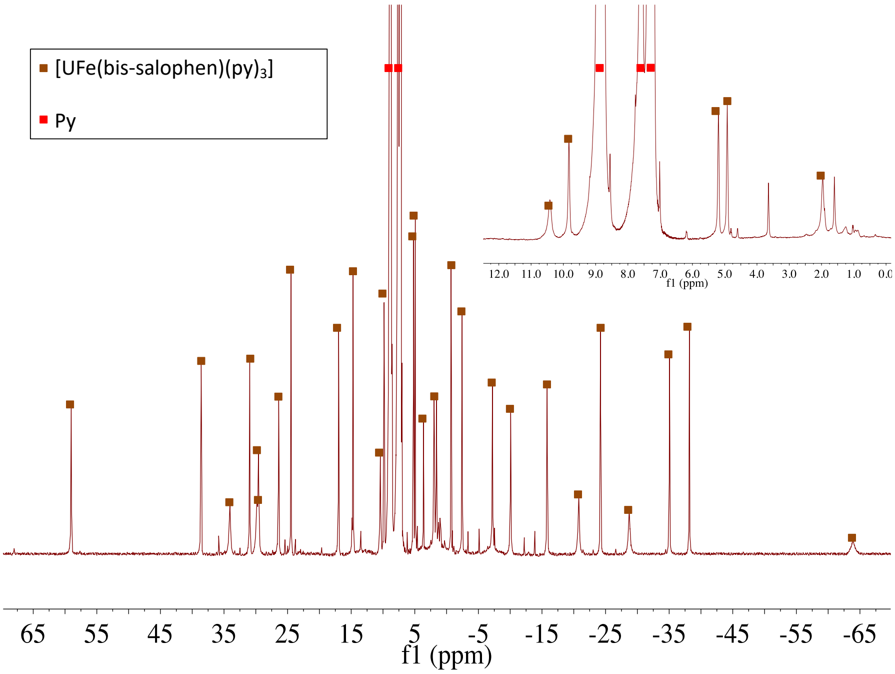

Figure 4 ^{1}H NMR spectrum of **6** (py-d5, 298K, 400 MHz).

Complex **6** resulted less stable that than **4** and **5**, showing traces of decomposition, such as [Fe(salophen)], **2-py** and other unidentified products, in pyridine solution after three days at room temperature.

The reactivity of **1** with PbI_2, does not afford a U-Pb heterobimetallic species but leads quantitatively to the [U(salophen)$_2$] complex (Scheme 4). This shows that in order to prepare heterobimetallic complexes from **1** the redox potential of the metal halide precursor has to be compatible with that of **1** to avoid unwanted ligand-based oxidation.

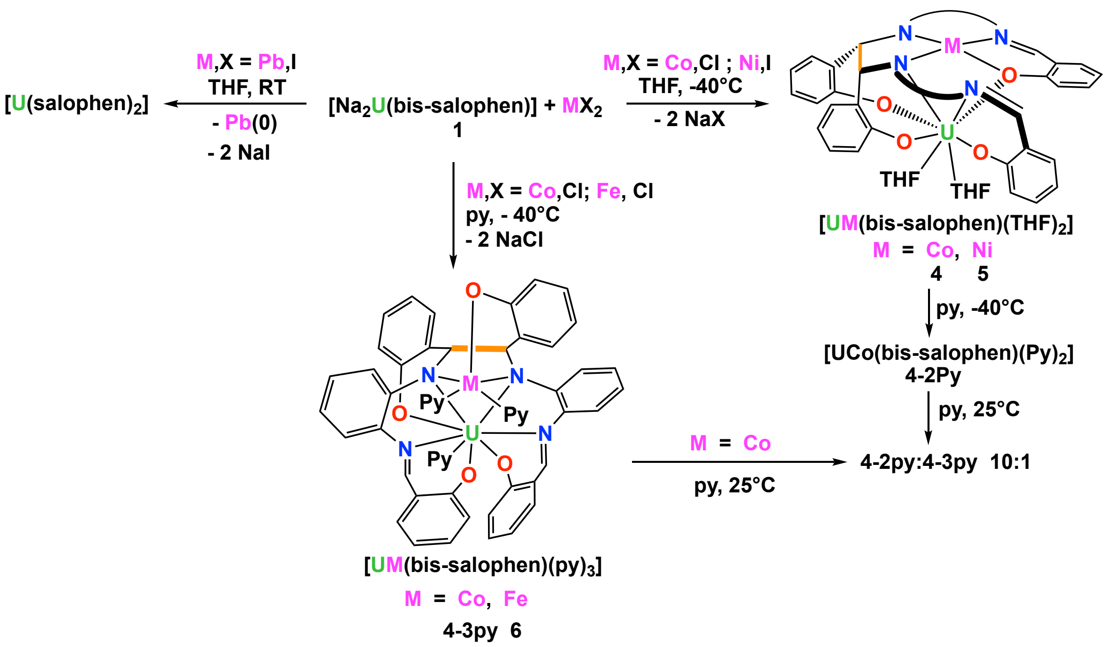
M,X = Pb,I
THF, RT
- Pb(0)
- 2 NaI
[U(salophen)2]
[Na2U(bis-salophen)] + MX2
1
M,X = Co,Cl ; Ni,I
THF, -40°C
- 2 NaX
[UM(bis-salophen)(THF)2]
M = Co, Ni
4 5
M,X = Co,Cl; Fe, Cl
py, - 40°C
- 2 NaCl
py, -40°C
[UCo(bis-salophen)(Py)2]
4-2Py
py, 25°C
M = Co
py, 25°C
4-2py:4-3py 10:1
[UM(bis-salophen)(py)3]
M = Co, Fe
4-3py 6

Scheme 4. Reactivity of **1** with divalent metal halides.

The molecular structures of **4-S (S = THF, 2py, 3py)**, **5-THF** and **6** were determined by X-ray crystallography (Figure 6, 7). Depending on the conditions of crystallization of **4** in pyridine (see experimental part) two different types of compounds were isolated (**4-2py** and **4-3py**). These two compounds both exist in solution and display different proton NMR signals. Dissolution of **4-THF** in pyridine at room temperature affords **4-2py** as a major product. When the reaction of **1** with [$CoCl_2$] is carried out in pyridine at -30° C, **4-3py** is obtained. However, **4-3py** rearranges in pyridine solution at room temperature affording **4-2py** with a final ration between the two compounds of 1:10 respectively, visible by ^{1}H NMR spectroscopy (Figure 5).

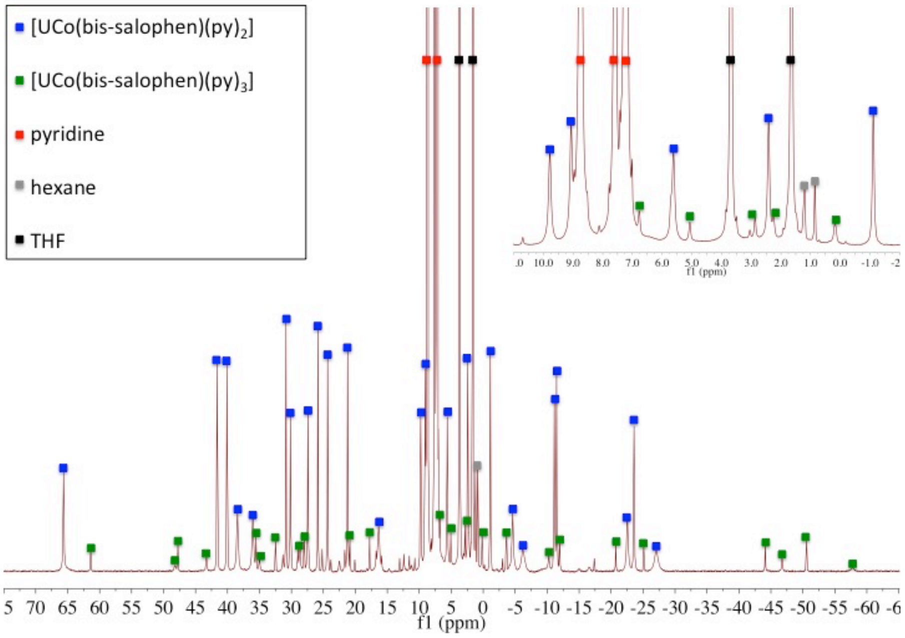

Figure 5 ^{1}H NMR spectrum of **4-3py** after 14 days in pyridine at room temperature (py-d5, 298K, 400 MHz).

The X-ray crystal structures of the THF and pyridine adducts of **4-THF**, **4-2py** and **5-THF** are fairly similar, showing the presence of a four-coordinate square-planar cobalt(II) or nickel(II) ion in a ONNN pocket (Figure 6).

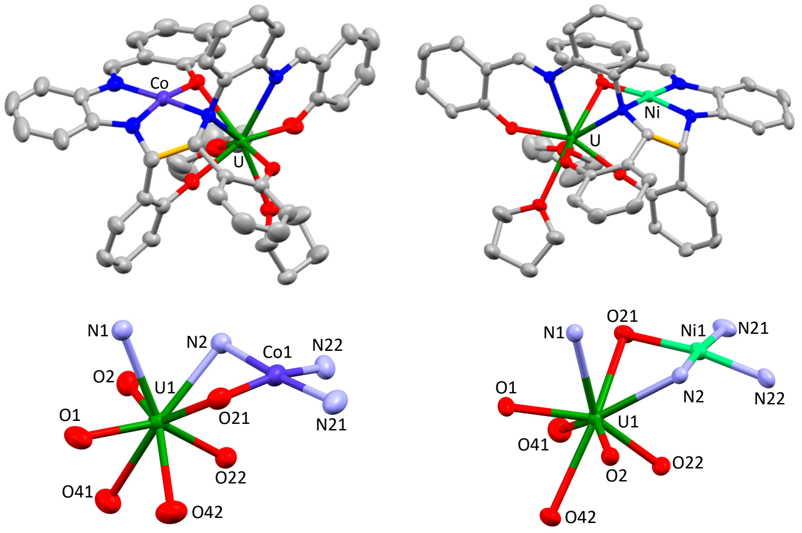
Co
U
Ni
U
N1
N2
Co1
N22
O2
U1
O1
O21
N21
O22
O41
O42
O21
N1
Ni1
N21
O1
N2
N22
U1
O41
O2
O22
O42

Figure 6. Solid-state molecular structures of **4-2py** and its metal coordination sphere (left) and **5-THF** and its metal coordination sphere (right) (50% probability ellipsoids). Hydrogen atoms have been omitted for clarity. C-C bond formed by coupling of imino groups highlighted in yellow.

In contrast, in **4-3py** and **6** the cobalt(II) or the iron(II) ions are pentacoordinated by the one oxygen and two nitrogen atoms from the bis-salophen ligand and two pyridine nitrogen atoms with a square pyramidal geometry (Figure 7).

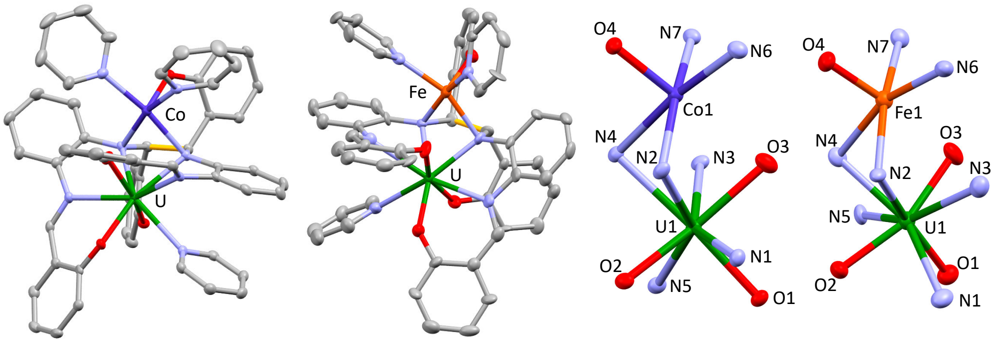

Figure 7. Solid-state molecular structures of **4-3py** and **6** (left) (50% probability ellipsoids) and metals coordination spheres in **4-3py** and **6** (right). Hydrogen atoms and interstitial solvent molecules have been omitted for clarity. C-C bond formed by coupling of imino groups highlighted in yellow

Similarly to what was observed for the formation of the homo-binuclear uranium complexes **2-py** and **3**, the bis-salophen ligand unfolds to accommodate a 3d metallic ion. The overall final structures are asymmetric and the bis-salophen ligand is highly distorted. All five structures present an octadentate dinucleating bis-salophen ligand that coordinates a divalent 3d metal (Co(II), Ni(II) or Fe(II)) and a U(IV) ion. The metrical parameters of the ligand are in agreement with the presence of the hexaanionic amidoiminophenolate bis-salophen. In **4-2py** and **5-THF** the uranium ion is hexacoordinated by the ligand, and its coordination sphere is completed to eight in a distorted square antiprismatic fashion by the coordination of two solvent molecules. The two metallic ions are connected through μ-N$_{amido}$ and μ-O$_{phenolate}$ bridging atoms, and lie in remarkably close proximity (U-M distance: 3.0439(5) Å in **4-2py**, 3.1340(6) Å in **5-THF**). These U-M distances are significantly shorter than those found in trimeric $U^{IV}Co^{II}$ (3.68(2) Å) and $U^{IV}Ni^{II}$ (3.64(1) Å) complexes supported by Schiff bases.[3a,10] Arnold and colleagues recently reported the sole examples of U-Ni bonds featuring significantly shorter intermetallic bond distances (2.556(1)–2.520(1) Å).[6e] The U-Co separation in **4-2py** is larger than the sum of the covalent radii for Co and U (2.81 Å),[11] but is very close to the three examples of U-Co bonds reported in the literature (3.0319(7)-2.874(3) Å) [6d,6h,6j] suggesting the presence of a U-Co interaction. Another unexpected feature of the structure of **4-THF**, **4-2py** and **5-THF** is the configuration inversion of one single carbon atom from $[Na_2U(\text{bis-salophen})]_n$. This suggests that the C-C bridging bond is broken and reformed during the coordination of the Co and Ni cation. This inversion is not observed in complexes **4-3py** or **6**.

In **4-3y** and **6** the uranium ion is eptacoordinated by the ligand, and its coordination sphere is completed to eight in a distorted square antiprismatic fashion by the coordination of a pyridine molecule. The two metallic ions are connected through the two μ-N_{amido} bridging atoms with a U-M distance slightly longer than the one found for **4-2py** and **5-THF** (U-M distance: 3.0439(5) Å in **4-3py**, and 3.3022 Å in **6**).

The geometry adopted by the bis-salophen ligand as a result of the bridging mode of the imido group in the structures of bimetallic the complexes reported here differs significantly from the geometry of the bis-salophen ligand in previously reported homo-bimetallic complexes of Co(II) and Ni(II) where the M(II) metals are bound in independent ONNO pockets of the bis-salophen ligand.[12]

Studies of the reactivity of the U-Co complex **4-3py** with CS_2 show that the presence of the Co(II) ion leads to an increased reactivity compared to the homo-bimetallic complexes **2-py** and **3**. ^{1}H NMR studies show that the reaction of **4-3py** with 2 equiv. of CS_2 leads to cleavage of the C-C bond of the bis-salophen ligand with complete conversion to the [U(salophen)$_2$] complex and concomitant formation of a Co(II) compound identified by EPR spectroscopy (see appendix). ^{13}C NMR of the reaction mixture in py-d5 show a signal at 248 ppm assigned to the $C_2S_4^{2-}$ anion[13] indicating that the two electrons stored on the bis-salophen ligand have become available for CS_2 reduction in the UCo heterobimetallic complex.

In summary, we reported a new versatile route to unusual heterobimetallic 3d-5f complexes supported by a redox non-innocent ligand. The combination of a redox non-innocent ligand together with uranium-transition metal cooperativity provides an attractive platform to enable multi-electron chemical transformations. Notably, preliminary studies show that in the hetero-bimetallic UCo complex the electrons stored in the ligand becomes available for the reduction of CS_2. Future studies will be directed to expand the reported synthetic strategy to other hetero-bimetallic systems and to investigate their reactivity.

Experimental

General Considerations. Unless otherwise noted, all reactions were performed either using standard Schlenk line techniques or in an inert atmosphere glovebox under an atmosphere of purified argon (<1 ppm O_2/H_2O). Glassware was dried overnight at 130°C prior to use. Unless otherwise noted, reagents were acquired from commercial sources and used without further purification. The solvents were purchased from Aldrich or Eurisotop (deuterated solvents) in their anhydrous form, conditioned under argon and vacuum distilled from K/benzophenone or Nadispersion/benzophenone (hexane, diisopropylether, pyridine and THF) and degassed prior to use. Syntheses were performed using glass covered stirring bars. Anhydrous [$CoCl_2$] and [$NiCl_2$] were purchased from Sigma Aldrich and further purified by extraction in THF. The amount of THF present in the resulting [$CoCl_2$(THF)] and [$NiCl_2(THF)_{0.6}$] solvate was determined by NMR titration using naphthalene as internal reference. $UI_4(OEt_2)_2$,[14] UCl_4,[15] and [Na_2U(bis-salophen)]$_n$, **1**,[9] were prepared using literature procedures. NMR experiments were carried out using NMR tubes adapted with J. Young valves. NMR spectra were recorded on Bruker 200 MHz and 400 MHz spectrometers. ^{1}H chemical shifts are reported in ppm and were measured relative to residual solvent peaks, which were assigned relative to an external TMS standard set at 0.00 ppm. EPR spectra of were measured with a Bruker Elexsys E500 spectrometer working at 9.4 GHz frequency with an oxford ESR900 cryostat for 4–300 K operation. Elemental analyses were performed under argon by Analytische Laboratorien GMBH at Lindlar, Germany and by the analytical service at EPFL. Mass spectra were acquired on a LXQ-linear ion trap (Thermo Scientific, San Jose, CA, USA), equipped with an electrospray source. Solutions of the complexes were prepared and filtered on microporous filters in the glove-box and maintained under argon until injection in the mass spectrometer. The experimental isotopic profile was compared in each case to the theoretical one. Experimental details concerning X-ray structural determinations are reported below.

Reaction of [Na_2U(bis-salophen)] with PbI_2.

To a solution of **1** (10.0 mg, 0.011 mmol, 1 equiv) in THF (0.5 mL) was added a suspension of PbI_2 (5.1 mg, 0.011 mmol, 1 equiv.) in THF (0,5 mL). The reaction mixture was stirred 16 hours, affording a dark brown suspension. The mixture was filtered to remove NaI salts and Pb(0) and the brown filtrate was analysed by 1H NMR. The spectrum 2 (200 MHz, THF-d8, 298 K) displayed the characteristic resonances of the isomeric mixture of the previously reported [U(salophen)2] complex.

Synthesis of [U_2(bis-salophen)$(S)_6$]I_2 , 2-THF and 2-py.

A deep purple solution of **1** (98.2 mg, 0.107 mmol, 1 equiv.) in THF (1 mL) was added dropwise to a red solution of [$UI_4(OEt_2)_2$)] (96.2 mg, 0.107 mmol, 1 equiv.) in THF (1 mL). The reaction mixture was stirred for 12 hours at room temperature, affording a deep orange/brown suspension. The reaction mixture was filtered to remove NaI and 2 mL of hexane were added to the brown filtrate. The resulting solid was collected and dried in vacuo to give [U_2(bis-salophen)$I_2(THF)_2$].3.3NaI, **2-THF.3.3NaI** as a brown powder (107.0 mg, 50% yield). Attempts to further purify this solid from NaI impurities were unsuccessful. Anal. Calc. (%) for [U_2(bis-salophen)$(I)_2(THF)_2$].3.3NaI: C, 28.86; H, 2.22; N,

2.80. Found: C, 28.58; H, 2.58; N, 3.00. ESI-MS: m/z = 1231.1 ([U_2(bis-salophen)I]$^+$). ^{1}H NMR (200 MHz, THF-d8, 298 K): δ = 91.2 (brs, 2H), 74.1 (brs, 2H), 70.6 (brs, 2H), 52.2 (brs, 2H), 50.8 (brs, 2H), 39.0 (s, 2H), 36.8 (s, 2H), 35.8 (brs, 2H), 26.6 (s, 2H), 17.9 (brs, 2H), -12.8 (s, 2H), -18.3 (s, 2H), -24.5 (s, 2H), -40.4 (s, 2H). ^{1}H NMR (200 MHz, pyridine-*d*5, 298 K): δ = 86.0 (brs, 4H), 83.6 (s, 2H), 72.7 (s, 2H), 68.6 (s, 2H), 55.0 (s, 2H), 50.0 (s, 2H), 43.4 (s, 2H), 41.1 (s, 2H), 32.1 (s, 2H), -19.6 (s, 2H), -21.3 (s, 2H), -24.0 (s, 2H), -27.6 (s, 2H). Single crystals of [U_2(bis-salophen)(py)$_6$]I_2, **2-py**, suitable for X-ray diffraction where obtained by slow diffusion of hexane into a pyridine solution of the complex.

Synthesis of [U_2(bis-salophen)(THF)$_2$$Cl_2$], 3.

A pale green solution of UCl_4 (17.4 mg, 0.047 mmol, 1 equiv.) in THF (2.5 mL) was added dropwise to a solution of **1** (43.3 mg, 0.047 mmol, 1 equiv.) in THF (1.5 mL). The reaction mixture was stirred for 4 hours at room temperature affording an orange/brown solution. The reaction mixture was filtered in order to remove NaCl. The filtrate was concentrated to 1 mL and 3 mL of hexane were added. Complex [U_2(bis-salophen)(THF)$_2$$Cl_2$], **3**, precipitated out of the solution as an orange powder that was collected and dried under vacuum (31.3 mg, 50% yield). Single crystals of **3** suitable for X-ray diffraction where obtained by slow diffusion of hexane into a THF solution of the complex. ^{1}H NMR (400 MHz, THF-d8, 298 K): δ = 82.9 (s, 2H), 67.0 (s, 2H), 45.6 (s, 4H), 35.6 (s, 2H), 32.8 (s, 4H), 32.0 (s, 2H), 24.3 (s, 2H), 6.7 (s, 2H), -10.2 (s, 2H), -15.2 (s, 2H), -20.6 (s, 2H), -38.2 (s, 2H). Elemental analysis for [U_2(bis-salophen)(THF)$_2$$Cl_2$]: C, 43.68; H, 3.36; N, 4.24. Found: C, 43.37; H, 3.62; N, 3.85.

Reduction of 2-THF with KC_8 yields [U_2(cyclo-salophen)(THF)$_4$].

A deep purple solution of **1** (20.0 mg, 0.022 mmol, 1 equiv.) in THF (1 mL) was added dropwise to a red solution of [UI_4(OEt_2)$_2$)] (19.6 mg, 0.022 mmol, 1 equiv.) in THF (2 mL). The THF volume was adjusted to 4 mL and the reaction mixture was stirred for 12 hours, affording a deep orange/brown suspension of **2-THF**. A potassium chunk (1.7 mg, 0.043 mmol, 2 equiv.) was added to a orange/brown suspension of **2-THF** in THF prepared in situ by reacting a solution of Na_2[U(bis-salophen)] **2** (20.0 mg, 0.022 mmol, 1 equiv.) in THF (1 mL) with a solution of [UI_4(OEt_2))$_2$] (19.6 mg, 0.022 mmol, 1 equiv.) in THF (2 mL). The reaction mixture was stirred for another 12 hours resulting in a dark brown suspension. The reaction mixture was filtered and the resulting dark brown solution was taken to dryness to give the previously reported complex [U_2(cyclo-salophen)(THF)$_4$] as confirmed by ^{1}H NMR spectroscopy

Reduction of 3 with KC_8 yields $[U_2(\text{cyclo-salophen})(THF)_4]$.

2.6 mg of KC_8 (0.019 mmol, 2 equiv.) were added to a solution of **3** (12.8 mg, 0.0097 mmol, 1 equiv.) in THF-d8 (0.5ml). The reaction was stirred at room temperature overnight and then was filtered. ^{1}H NMR spectra of the resulting solution showed a complete conversion to the previously reported complex $[U_2(\text{cyclo-salophen})(THF)_4]$.

Reaction of $[U_2(\text{bis-salophen})(py)_6]I_2$ with I_2.

A solution of **2-py** (10.0 mg, 0.007 mmol, 1 equiv.) in pyridine (0.5 mL) was added onto I_2 (3.7 mg, 0.015 mmol, 2 equiv.). The mixture was stirred at room temperature for 12 hours, affording a red-orange solution. The ^{1}H NMR spectrum (200 MHz, py-d5, 298 K) recorded for the crude reaction mixture showed that complex $[UI_2(\text{salophen})(py)_2]$ was quantitatively formed.

Synthesis of $[UI_2(\text{salophen})(S)_2]$ (S= THF, pyridine).

$[UI_2(\text{salophen})(S)_2]$ (S = THF, pyridine) was prepared independently by reacting the U(IV) precursor $[UI_4(PhCN)_4]$ with one equivalent of the deprotonated form of the Schiff base ligand to ensure its correct identification.

A solution of $[UI_4(PhCN)_4]$ (272.1 mg, 0.235 mmol, 1 equiv.) in acetonitrile (2 mL) was added to a yellow suspension of K2salophen (92.2 mg, 0.235 mmol, 1 equiv.) in 8 mL of acetonitrile. This suspension was stirred at room temperature for 20 min to yield a clear dark red solution. The solution was filtered and the filtrate was layered with 4 mL THF. After 2 days, 174 mg of red-orange crystals of $[UI_2(\text{salophen})(THF)_2]$, were collected by filtration (0.183 mmol, 79% yield). Anal. Calc. (%) for $C_{28}H_{28}I_2N_2O_4U$: C, 35.46; H, 2.98; N, 2.95. Found: C, 35.25; H, 3.13; N, 3.02. ^{1}H NMR (200 MHz, py-d5, 298 K): δ = 80.22 (s, 2H), 46.16 (s, 2H), 45.74 (s, 2H), 42.18 (s, 2H), 30.36 (s, 2H), -6.19 (s, 2H), -8.24 (s, 2H).

Reaction of $[Na_2U(\text{bis-salophen})]$ with $CoCl_2$, synthesis of $[UCo(\text{bis-salophen})(THF)_2]$, 4-THF.

A blue solution of $[CoCl_2(THF)]$ (17.9 mg, 0.089 mmol, 1 eq) in THF (4ml) was slowly added (dropwise) to a stirred deep purple solution of **1** (80.9 mg, 0.089 mmol, 1 eq) in THF (3 ml) kept at -40 °C. The resulting deep brown reaction mixture was stirred at -40°C for 3 hours. The mixture was filtered to remove NaCl; the solvent volume was reduced to 2 ml and 3 ml of hexane were added maintaining the solution at -40 °C. A brown solid formed after one night that was collected (13 mg). Further solvent reduction and hexane addition afforded additional product yielding overall 58 mg of

[UCo(bis-salophen)(THF)2].0.5 NaCl as dark brown powder (60% yield). Re-crystallization at -40 °C of this solid by slow diffusion of DIPE into a THF solution of the complex or slow diffusion of hexane into a pyridine solution of the complex afforded black single crystals suitable for X-ray diffraction of [UCo(bis-salophen)(THF)$_2$], **4-THF** and [UCo(bis-salophen)(py)$_2$], **4-2py** respectively. ES-MS: m/z= 1141.7 [M+THF]$^+$. ^{1}H NMR (200 MHz, THF-d8, 298 K): δ = 64.7 (s, 1H), 59.3 (s, 1H), 43.7 (s, 1H), 43.50 (s, 1H), 40.5 (s, 1H), 37.7 (s, 1H), 31.7 (s, 1H), 27.3 (s, 1H), 26.8 (s, 1H), 26.5 (s, 1H), 22.4 (s, 1H), 20.9 (s, 1H), 11.1 (s, 1H), 8.9 (s, 1H), 7.2 (s, 2H), 3.2 (s, 1H), 2.8 (s, 1H), -0.65 (s, 1H), -0.74 (s, 1H), -2.4 (s, 1H), -13.2 (s, 1H), -13.5 (s, 1H), -14.0 (s, 1H), -14.9 (s, 1H), -21.6 (s, 1H), -28.6 (s, 1H), -37.3 (s, 1H). ^{1}H NMR (200 MHz, py-d5, 298 K): δ = 65.6 (s, 1H), 41.6 (s, 1H), 40.1 (s, 1H), 38.5 (s, 1H), 36.1 (s, 1H), 30.8 (s, 1H), 30.1 (s, 1H), 27.4 (s, 1H), 25.8 (s, 1H), 24.4 (s, 1H), 21.2 (s, 1H), 16.4 (s, 1H), 9.8 (s, 1H), 9.1 (s, 1H), 5.6 (s, 1H), 2.4 (s, 1H), -1.1 (s, 1H), -4.6 (s, 1H), -6.22 (s, 1H), -11.2 (s, 1H), -11.5 (s, 1H), -22.5 (s, 1H), -23.6 (s, 1H), -27.1 (s, 1H).
Attempts to obtain the complex **4-THF** analytically pure by recrystallization from THF/DIPE resulted always in the presence of variable amount of co-crystallized NaCl. Elemental analysis calc. for [UCo(bis-salophen)(THF)$_2$]. 0.5 NaCl: C, 52.45; H, 4.04; N, 5.10. Found: C, 52.36; H, 4.10; N, 4.96. Complex **4-2THF** and **4-2py** are stable in solution at room temperature. However the complex **4-2py**, presenting a tetra-coordinate square planar cobalt, slowly undergoes a rearrangement in solution affording complex [UCo(bis-salophen)(py)$_3$], **4-3py** (see following synthesis) where a penta-coordinate square pyramidal cobalt is formed upon pyridine binding to the cobalt centre. After 14 days an equilibrium is reached showing a ratio **4-2py**:**4-3py** of 10:1.

If [CoCl$_2$(THF)] is rapidly added to the solution of complex Na$_2$[U(bis-salophen)] at room temperature significant amounts of the oxidation products [U(salophen)$_2$] and [U(salophen)Cl$_2$] are formed with concomitant formation of Co(0). This is probably due to the presence of local excess of [CoCl$_2$(THF)] that leads to oxidation of the uranium complex.

Reaction of [Na$_2$U(bis-salophen)] with CoCl$_2$, synthesis of [UCo(bis-salophen)(py)3], 4-3py.

A -40 °C solution of [CoCl$_2$(THF)] (8.9 mg, 0.044 mmol, 1 equiv.) in py (2 ml) was slowly added to a -40 °C solution of **1** (39.6 mg, 0.044 mmol, 1 equiv.) in py (2 ml). The mixture was stirred overnight affording a red/brown solution. The solution was evaporated (0.5 ml), filtered and 6 ml of cold hexane were added at -40 °C. The resulting precipitate of [UCo(bis-salophen)(py)$_3$], **4-3py** (33 mg, 57 %) was collected and conserved at low temperature. Re-crystallization of this solid by slow diffusion of hexane into a pyridine solution of **4-3py** at –40 °C afforded dark red crystals suitable for X-ray diffraction. Elemental analysis for [UCo(bis-salophen)(py)$_3$]: C,56.82; H, 3.73; N, 8.43. Found: C, 56.65; H, 3.55; N, 8.43. ^{1}H NMR (400 MHz, py-d5, 298 K): δ = 61.39 (s, 1H), 48.23 6 (s, 1H), 47.74 (s, 1H), 43.30 (s, 1H), 35.55 (s, 1H), 34.99 (s, 1H), 32.48 (s, 1H), 28.98 (s, 1H), 28.62 (s, 1H), 28.00 (s, 1H), 20.84 (s, 1H), 17.78 (s, 1H), 6.75 (t, 1H), 5.69 (s, 1H), 2.86 (d, 1H), 2,23 (s, 1H), 0.18 (s, 1H), -3.57 (s, 1H) - 3.67 (s, 1H), - 10.28 (s, 1H), -11.98 (s, 1H), -20.76 (s, 1H), -25.13 (s, 1H), - 44.13 (s, 1H), -46.78 (s, 1H), -50.60 (s, 1H), - 57.81 (s, 1H).

The proton NMR of **4-3py** in py-d5 at -30 °C shows only the signals assigned to **4-3py** which remains the only product at -30°C for several days. After 14 days at room temperature a ratio **4-2py**:**4-3py** of 10 : 1 is reached.

Reaction of [Na_2U(bis-salophen)] with $NiCl_2$, synthesis of [UNi(bis-salophen)(S)$_2$], (S= py, 5-py; S=THF, 5-THF).

A cold solution (-40 °C) of [$NiCl_2(THF)_{0.6}$] (8.5 mg, 0.049 mmol, 1 equiv.) in py (3.5 mL) was added dropwise to a stirred cold solution of **1** (44.6 mg, 0.049 mmol, 1 equiv.) in py (1.5 mL). The mixture was let slowly return at room temperature and left stirring overnight to give a yellow/brown solution. The solution was evaporated (0.5 mL), filtered and 6 mL of hexane were added. [UNi(bis-salophen)(py)$_2$], **5-py** precipitated out of the solution immediately as a black solid, that was collected and dried under vacuum (38 mg, 64 %). ^{1}H NMR (400 MHz, py-d5, 298K) δ= 57.8 (s, 1H); 47.7 (s, 1H); 43.9 (s, 1H); 37.9 (s, 1H); 35.3 (s, 2H); 30.8 (s, 2H); 28.4 (s, 1H); 27.9 (s, 1H); 25.3 (s, 1H); 24.1 (s, 1H); 17.6 (s, 1H); 16.8 (s, 1H); 11.90 (s, 1H); 10.10 (s, 1H); 3.9 (s, 1H); 2.9 (s, 1H); 0.6 (s, 1H); -1.1 (s, 1H); -2.3 (s, 1H); -3.4 (s, 1H); -4.8 (s, 1H); -6.7 (s, 2H); -10.1 (s, 1H); -30.0 (s, 1H). Elemental analysis calcd. for [UNi(bis-salophen)(py)$_2$].0.9py: C, 56.70; H, 3,71; N, 8.37. Found: C, 56.66; H, 3.87; N, 8.16. The coordinated py molecules were replaced by THF molecules by dissolving the product in THF and taking it to dryness for 3 time affording complex [UNi(bis- salophen)(THF)$_2$], **5-THF**. Elemental analysis for [UNi(bis-salophen)(THF)$_2$]: C, 53.90; H, 4.15; N, 5.24. Found: C, 53.64; H, 4.14; N, 5.21. ^{1}H NMR (200MHz, THF-d8, 298K) δ= 57.9 (s, 1H); 48.3 (s, 1H); 43.4 (s, 1H); 38.2 (s, 1H); 34.6 (s, 1H); 33.9 (s, 1H); 31.1 (s, 1H); 28.6 (s, 1H); 26.1 (s, 1H); 25.5 (s, 1H); 23.9 (s, 1H); 19.0 (s, 1H); 16.0 (s, 1H); 11.3 (s, 1H); 9.8 (s, 1H); 7.3 (s, 1H); 6.6 (s, 1H); 3.9 (s, 1H); 3.2 (s, 1H); 1.9 (s, 1H); -0.3 (s, 1H); -1.5 (s, 2H); -3.1 (s, 1H); -3.8 (s, 1H); -7.2 (s, 1H); -11.3 (s, 1H); -28.4 (s, 1H).

Dark-green single crystals of **5-THF** suitable for X-ray diffraction analysis were obtained from by slow diffusion of DIPE into a THF solution of **5-THF**.

Reaction of [Na_2U(bis-salophen)] with $FeCl_2$, synthesis of [UFe(bis-salophen)(py)$_3$], 6.

A -40 °C solution of [$FeCl_2$] (14.9 mg, 0.117 mmol, 1 equiv.) in py (2 mL) was slowly added to a -40 °C solution of **1** (120.0 mg, 0.117 mmol, 1 equiv.) in py (2 mL). The mixture was stirred overnight affording a red/brown solution. The solution was evaporated (1 mL), filtered and cold hexane (6 mL) was added at -40 °C. The resulting precipitate of [UFe(bis-salophen)$(py)_3$], **6** (100 mg, 89 %) was collected and conserved at low temperature. Re-crystallization of this solid by slow diffusion of hexane into a pyridine solution of **6** at -40 °C afforded dark brown crystals suitable for X-ray diffraction. Elemental analysis for [UFe(bis-salophen)$(py)_3$]: C,54.58; H, 3.68; N, 8.35. Found: C, 54.50; H, 3.09; N, 8.43. ^{1}H NMR (400 MHz, py-d5, 298 K): δ = 58.98 (s, 1H), 38.55 (s, 1H), 34.02 (s, 1H), 30.92 (s, 1H), 29.77 (s, 1H), 29.54 (s, 1H), 26.36 (s, 1H), 24.41 (s, 1H), 16.94 (s, 1H), 14.66 (s, 1H), 10.37 (s, 1H), 9.79(s, 1H), 5.16 (t, 1H), 4.88 (s, 1H), 1.92 (d, 1H), 1.13 (s, 1H), 0.79 (s, 1H), -0.76 (s, 1H), -2.48 (s, 1H), -7.26 (s, 1H), -10.13 (s, 1H), -15.86 (s, 1H), -20.83 (s, 1H), -24.25 (s, 1H), -28.79 (s, 1H), -25.10 (s, 1H), -38.22 (s, 1H), -63.99 (s, 1H).

Reaction of 4-3py with CS2

$^{13}CS_2$ (5.8 µL, 0.059 mmol, 2 equiv.) was added to a solution of **4-3py** (30.0 mg, 0.0293 mmol, 1 equiv.) in 0.5 ml py-d5. The resulting suspension was stirred for 2 days until complete consumption of **4-3py**. The suspension was centrifuged to remove the formed dark solid. The ^{1}H NMR (200MHz, py-d5, 298K) of the resulting solution shows signals assigned to the [U$(salophen)_2$] complex. The quantitative integration of the signals assigned to the [U$(salophen)_2$] show complete conversion of **4-3py** into [U$(salophen)_2$]. The ^{13}C NMR spectrum of the solution shows a signal at 248 ppm assigned to the presence of $^{13}C_2S_4^{2-}$. The dark solid formed in the reaction is partially soluble in pyridine. The X- band EPR spectrum of the solid formed in the reaction shows the presence of Co(II). The presence of $C_2S_4^{2-}$ in the solid was detected by ^{13}C NMR in agreement with the presence of [$Co(C_2S_4)$]. X-ray photoelectron spectroscopy (XPS) analysis of the solid showed a ratio S/Co of 1.8 suggesting that the solid contains at least an additional sulphur containing Co(II) species. The low solubility of this solid in all organic solvent prevented further analysis.

References

1 S. T. Liddle and D. P. Mills, *J. Chem. Soc.-Dalton Trans.*, 2009, 5592-5605.

2 B. G. Cooper, J. W. Napoline and C. M. Thomas, *Cat. Rev. - Sci. Eng.*, 2012, **54**, 1-40.

3 (a)T. Le Borgne, E. Riviere, J. Marrot, J. J. Girerd and M. Ephritikhine, *Angew. Chem. Int. Ed. Engl.*, 2000, **39**, 1647-1649; (b)L. Chatelain, J. P. S. Walsh, J. Pecaut, F. Tuna and M. Mazzanti, *Angew. Chem. Int. Ed. Engl.*, 2014, **53**, 13434-13438; (c)V. Mougel, L. Chatelain, J. Pecaut, R. Caciuffo, E. Colineau, J. C. Griveau and M. Mazzanti, *Nat. Chem.*, 2012, **4**, 1011-1017; (d)P. L. Arnold, E. Hollis, G. S. Nichol, J. B. Love, J.-C. Griveau, R. Caciuffo, N. Magnani, L. Maron, L. Castro, A. Yahia, S. O. Odoh and G. Schreckenbach, *J. Am. Chem. Soc.*, 2013, **135**, 3841-3854.

4 (a)K. P. Chiang, S. M. Bellows, W. W. Brennessel and P. L. Holland, *Chem. Sci.*, 2014, **5**, 267-274; (b)M. Falcone, C. E. Kefalidis, R. Scopelliti, L. Maron and M. Mazzanti, *Angew. Chem. Int. Ed. Engl.*, 2016, **55**, 12290-12294; (c)S. Gambarotta and J. Scott, *Angew. Chem. Int. Ed. Engl.*, 2004, **43**, 5298-5308; (d)E. E. Benson, C. P. Kubiak, A. J. Sathrum and J. M. Smieja, *Chem. Soc. Rev.*, 2009, **38**, 89-99; (e)J. H. Jeoung and H. Dobbek, *Science*, 2007, **318**, 1461-1464; (f)G. Fachinetti, C. Floriani and P. F. Zanazzi, *J. Am. Chem. Soc.*, 1978, **100**, 7405-7407; (g)S. Gambarotta, F. Arena, C. Floriani and P. F. Zanazzi, *J. Am. Chem. Soc.*, 1982, **104**, 5082-5092; (h)J. P. Krogman, B. M. Foxman and C. M. Thomas, *J. Am. Chem. Soc.*, 2011, **133**, 14582-14585; (i)O. Cooper, C. Camp, J. Pecaut, C. E. Kefalidis, L. Maron, S. Gambarelli and M. Mazzanti, *J. Am. Chem. Soc.*, 2014, **136**, 6716-6723.

5 L. H. Gade, *Angew. Chem. Int. Ed. Engl.*, 2000, **39**, 2658-2678.

6 (a)R. S. Sternal and T. J. Marks, *Organometallics*, 1987, **6**, 2621-2623; (b)M. J. Monreal and P. L. Diaconescu, *Organometallics*, 2008, **27**, 1702-1706; (c)M. J. Monreal, C. T. Carver and P. L. Diaconescu, *Inorg. Chem.*, 2007, **46**, 7226-7228; (d)A. L. Ward, W. W. Lukens, C. C. Lu and J. Arnold, *J. Am. Chem. Soc.*, 2014, **136**, 3647-3654; (e)J. A. Hlina, J. R. Pankhurst, N. Kaltsoyannis and P. L. Arnold, *J. Am. Chem. Soc.*, 2016, **138**, 3333-3345; (f)D. Patel, D. M. King, B. M. Gardner, J. McMaster, W. Lewis, A. J. Blake and S. T. Liddle, *Chem. Commun.*, 2011, **47**, 295-297; (g)B. M. Gardner, D. Patel, A. D. Cornish, J. McMaster, W. Lewis, A. J. Blake and S. T. Liddle, *Chem. Eur. J.*, 2011, **17**, 11266-11273; (h)D. Patel, F. Moro, J. McMaster, W. Lewis, A. J. Blake and S. T. Liddle, *Angew. Chem. Int. Ed. Engl.*, 2011, **50**, 10388-10392; (i)B. M. Gardner, J. McMaster, W. Lewis and S. T. Liddle, *Chem. Commun.*, 2009, 2851-2853; (j)J. W. Napoline, S. J. Kraft, E. M. Matson, P. E. Fanwick, S. C. Bart and C. M. Thomas, *Inorg. Chem.*, 2013, **52**, 12170-12177; (k)S. Fortier, J. R. Walensky, G. Wu and T. W. Hayton, *J. Am. Chem. Soc.*, 2011, **133**, 11732-11743.

7 N. H. Anderson, S. O. Odoh, Y. Y. Yao, U. J. Williams, B. A. Schaefer, J. J. Kiernicki, A. J. Lewis, M. D. Goshert, P. E. Fanwick, E. J. Schelter, J. R. Walensky, L. Gagliardi and S. C. Bart, *Nat. Chem.*, 2014, **6**, 919-926.

8 (a)M. J. Monreal and P. L. Diaconescu, *J. Am. Chem. Soc.*, 2010, **132**, 7676-7683; (b)C. Camp, L. Chatelain, V. Mougel, J. Pecaut and M. Mazzanti, *Inorg. Chem.*, 2015, **54**, 5774-5783.

9 (a)C. Camp, V. Mougel, P. Horeglad, J. Pecaut and M. Mazzanti, *J. Am. Chem. Soc.*, 2010, **132**, 17374-17377; (b)C. Camp, J. Andrez, J. Pecaut and M. Mazzanti, *Inorg. Chem.*, 2013, **52**, 7078-7086.

10 T. Le Borgne, E. Riviere, J. Marrot, P. Thuery, J. J. Girerd and M. Ephritikhine, *Chem. Eur. J.*, 2002, **8**, 774-783.

11 P. Pyykko and M. Atsumi, *Chem. Eur. J.*, 2009, **15**, 186-197.

12 (a)S. Gambarotta, F. Urso, C. Floriani, A. Chiesivilla and C. Guastini, *Inorg. Chem.*, 1983, **22**, 3966-3972; (b)S. DeAngelis, E. Solari, E. Gallo, C. Floriani, A. ChiesiVilla and C. Rizzoli, *Inorg. Chem.*, 1996, **35**, 5995-6003.

13 C. Camp, O. Cooper, J. Andrez, J. Pecaut and M. Mazzanti, *J. Chem. Soc.-Dalton Trans.*, 2015, **44**, 2650-2656.

---

14 C. D. Carmichael, N. A. Jones and P. L. Arnold, *Inorg. Chem.*, 2008, **47**, 8577-8579

15 (a)J. A. Hermann and J. F. Suttle, *Inorg. Synth.*, 1957, **5**, 143-145; (b)J. L. Kiplinger, D. E. Morris, B. L. Scott and C. J. Burns, *Organometallics*, 2002, **21**, 5978-5982

Chapter 3. Multimetallic assembly of iron Schiff base complexes†

Introduction

Polynuclear complexes of iron compounds continue to attract large interest because of their potential application in the catalytic conversion of dinitrogen and because they provide pertinent models for iron catalysed enzymatic transformations.[1,2,3] Notably, the reactivity of multimetallic cofactors in enzymes is proposed to rely on cooperative pathway where oxidation state changes occur simultaneously at several coupled metal centres and result in multielectron transfer to the substrate.[4,5,6] Also, the multielectron processes required for the biological transformation of small molecules often rely on redox-active supporting ligands incorporated into enzymatic active sites.[7,8,9] Redox-active ligands allow to store and release electrons during substrate transformation, with or without a change in the metal oxidation state, thus providing access to novel reactivity.

The storage of the electrons can sometimes be accompanied by the formation of a new C-C bond that in many cases results reversible, being broken when the electrons are released.[10,11,12,13]

Tetradentate Schiff bases has been proven to act as redox-active ligands[14,15] in complexes of d-metals such as Co,[16] Ni,[17] V,[18] Ti,[14] Zr,[19] and Mn,[20] and f-metals,[21,22,23,24,25] leading to intramolecular or intermolecular C-C bond formation. Thanks to the formation of new bonds, Schiff bases offer the possibility to build multi-metallic complexes via in situ formation of more elaborated ligands. For example, the one electron reduction of M-salophen complexes leads to one C-C bond and formation of the bis-salophen complexes where the new octadentate ligand can bind two ions in the two pockets of the ligand (Co, Ni) [16,17] (Scheme 1) or one single ion in the case of large f block ions (Ln^{3+} or U^{4+}).[22,24]

---

† Part of this chapter have been published: D. Toniolo, R. Scopelliti, I. Zivkovic, and M. Mazzanti, *J. Am. Chem. Soc.*, 2020, **142**, 7301−7305
Author contributions: D.T. performed the synthesis and the characterizations of the compounds, R.S. performed the X ray analysis, I.Z. performed the magnetic characterizations and M.M. originated the central idea and coordinated the work.

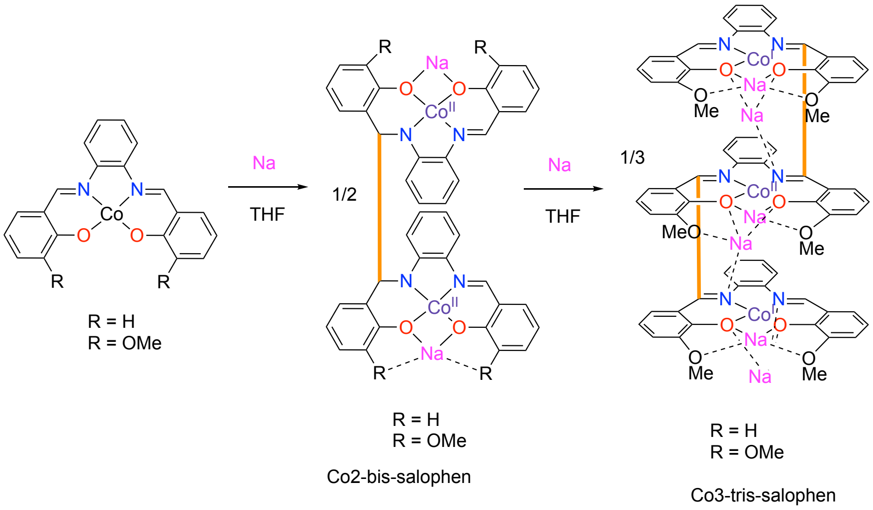

Scheme 1 Reduction of Co(salophen) complexes.

The two electron reduction of M-salophen complexes has shown to lead to the macrocyclic amidophenolate cyclo-salophen ligand that hold two ions in close proximity (Nd, U, Zr, Mn)[19,20,21,22] and in some cases leads to direct metal-metal interaction with a single bond character for Ti[14] at 2.518(1) Å, and double bond character in the V-V complex[18] and at 2.393(1) Å . So far, only the two-electron reduction of [Co(salophen)] resulted in the formation of an additional intermolecular C-C bond to afford a trinuclear complex of the linear tris-salophen ligand (Scheme 1).[26]

Here we extend the study of d-metal supported by salophen ligand to divalent iron. We show that the reduction of an easily prepared mononuclear Fe(II) Schiff base complex provides a facile route to the synthesis of polynuclear complexes that exhibit iron in different oxidation states and capable of storing up to six electrons. In particular, a trinuclear Fe(II) complexes has been synthetized, providing a rare example[27] of trinuclear clusters featuring Fe-Fe interactions that produce a high spin state persistent at room temperature.

Results and discussion

Reduction of [Fe(salophen)(THF)] with 1 equiv. of Na

The reduction of the Fe(II) complex [Fe(salophen)(THF)] with one equivalent of sodium metal in THF affords the polymeric complex $[Na_2Fe_2(\text{bis-salophen})(THF)_4]_n$, 1-THF (Scheme 2).

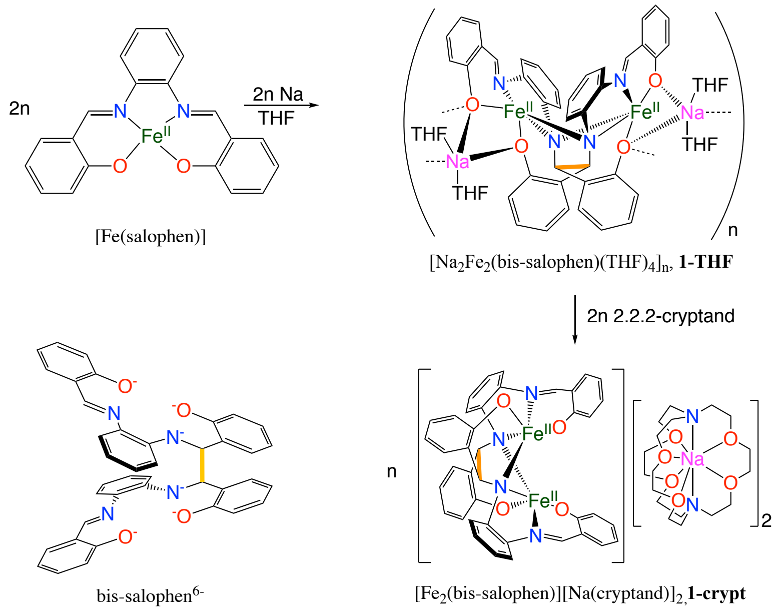
2n
Fe^II
[Fe(salophen)]
2n Na
THF
THF
Na
THF
Fe^II
Fe^II
Na
THF
THF
n
[Na2Fe2(bis-salophen)(THF)4]n, 1-THF
2n 2.2.2-cryptand
bis-salophen6-
n
Fe^II
Fe^II
Na
2
[Fe2(bis-salophen)][Na(cryptand)]2, 1-crypt

Scheme 2. Reduction of [Fe(salophen)] with 1 equivalent of sodium metal, synthesis of **1-THF** and **1-crypt**.

The solid-state structure of $[Na_2Fe_2(\text{bis-salophen})(THF)_4]_n$ (Figure 1) determined by X-ray diffraction shows the presence of a heterobimetallic Fe-Na polymer composed by $[Fe_2(\text{bis-salophen})]^{2-}$ units connected together by sodium cations.

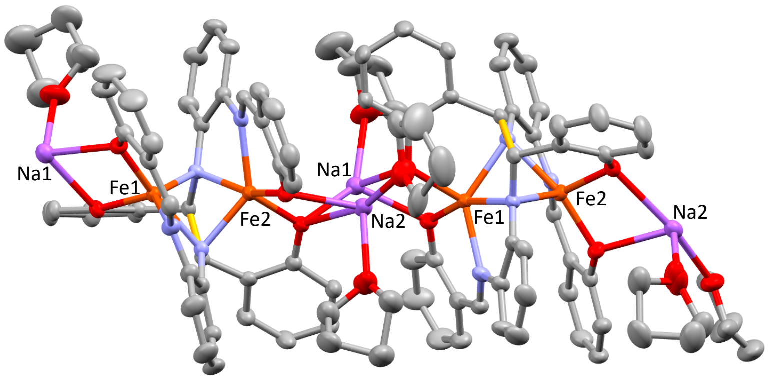
Na1
Fe1
Fe2
Na1
Na2
Fe1
Fe2
Na2

Figure 1. Solid-state structure of two asymmetric units in **1-THF** (50 % probability ellipsoids). The C-C bonds formed by reduction of salophen^{2-} are highlighted in yellow. Hydrogen atoms have been omitted for clarity.

The structure shows that the reduction does not occur on the metal centre but yields the hexa-anionic bis-salophen ligand arising from the formation of a C-C bond (1.600(5) Å) between two reduced imino carbons of two different salophen units. The arrangement of the bis-salophen ligand around the metal centre differs from those found in dinuclear Co(II)[16,26] and Ni(II)[17] complexes, in which the metal centres are coordinated by independent [N,O,O,N] pockets of the ligand with a large separation of the metal ions (6.372 for Co(II) and 6.367 Å for Ni(II)). The arrangement of the bis-salophen ligand around the two metal centres is similar to that found in dinuclear complexes of U(IV) where the two U(IV) ions are 4.0241(2) Å and 3.86(1) Å apart.[24] Such difference is likely to be due to the preferred square-planar geometry of Co and Ni. In **1-THF** each iron centre is bound by the two amido nitrogen atoms, one imino nitrogen and two oxygen atoms of the bis-salophen ligand. Each iron centre lies in a distorted five-coordinate geometry (geometry index τ_5 = 0.48). The mean Fe–O (1.992(5) Å) and Fe–N (2.12(1) Å) distances are comparable with those found in the parent [Fe(salophen)EtOH] complex and its derivatives[28] and Fe-N = 2.099(3) Å). The ligand brings the iron atoms in close proximity with an Fe–Fe distance of 2.7108(7) Å within range of weak Fe-Fe bonding interactions.[29,30] Bond valence sum (BVS) analysis was performed for complex **1-THF** and indicates an average oxidation state of 2.06 for each iron centre, which is consistent with the presence of a bis-salophen ligand and with the structural parameters. Recrystallization of **1-THF** from pyridine afforded the analogous pyridine solvate polymeric Fe(II) complex $[Na_2Fe_2(\text{bis-salophen})(py)_4]_n$, **1-py**.

The ^{1}H NMR spectra of **1-THF** and **1-py** (Figure 2) recorded at 298 K in the respective deuterated solvents show the presence of only one set of ten paramagnetically shifted resonances, in agreement with the presence of a high Fe(II) bis-salophen complex.

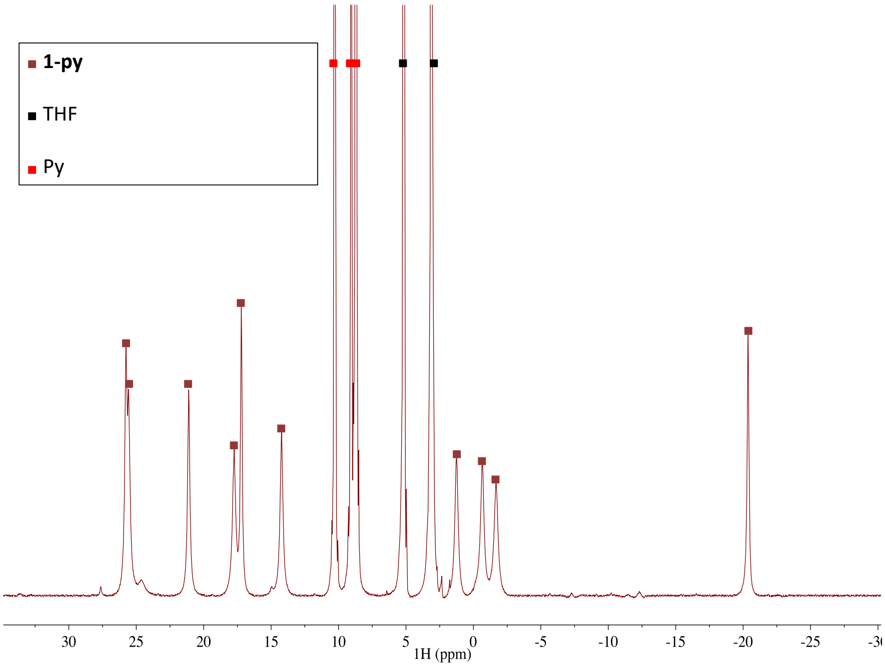

Figure 2.^{1}H NMR spectrum of $[Na_2Fe_2(\text{bis-salophen})(py)_4]$, **1-py** (py-d5, 400 MHz, 298 K).

However, in pyridine solution two sets of signals are present at lower temperatures that indicate the presence of two solution species. Variable temperature ^{1}H NMR experiments performed between 233 and 298 K showed the presence of an equilibrium between the two species that is shifted with the temperature. At room temperature, the resonances assigned **1-py** are observed between ±25 ppm and it represent the major solution species. On progressively lowering the temperature, the seven signals assigned to a second species steadily increase in intensity whilst the resonances of **1-py** decrease (Figure 3). The shift of the equilibrium towards the formation of the second specie is also accompanied by a colour change of the solution from dark brown to dark blue.

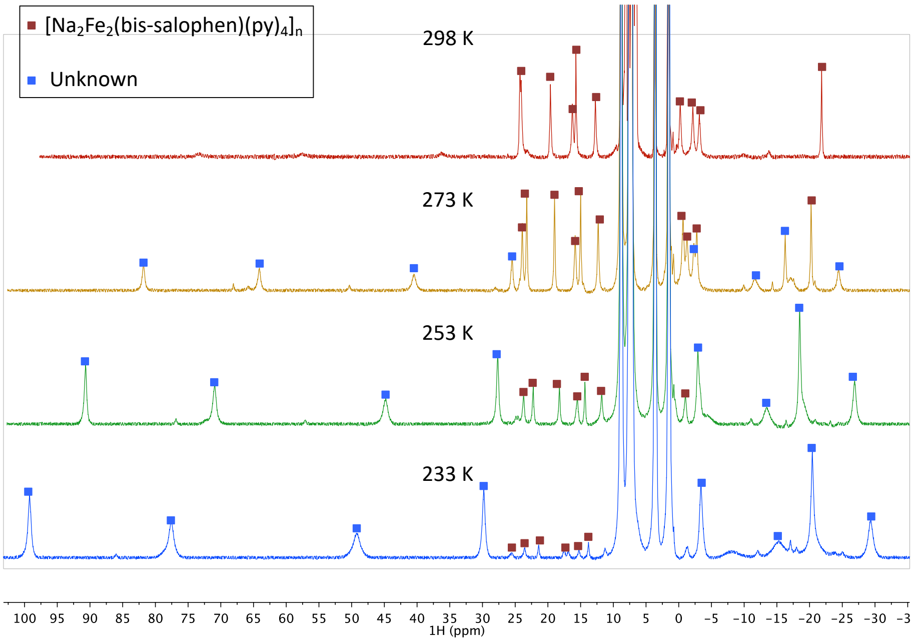

Figure 3. ^{1}H NMR spectra of **1-py** in py-d5 at variable temperature.

The thermodynamic parameters of the equilibrium were determined from the NMR data, giving $\Delta H = -15.7$ kJ mol^{-1} and $\Delta S = -55.9$ J K^{-1} mol^{-1}. These values rules out a dimer-monomer equilibrium such as that reported for the $[Co^{II}_2(\text{bis-salophen})M_2]$ (M =Li, Na)[26] because a dimerization reaction should be accompanied by an increase of the entropy and is shifted toward the monomer when the temperature increases.

Moreover, the significant difference in paramagnetic shift of the two complexes are more indicative of a change in oxidation state of the metal centres. Therefore a more plausible explanation involves a metal to ligand electron transfer resulting in the formation of a Fe(III) dimer (Scheme 3).

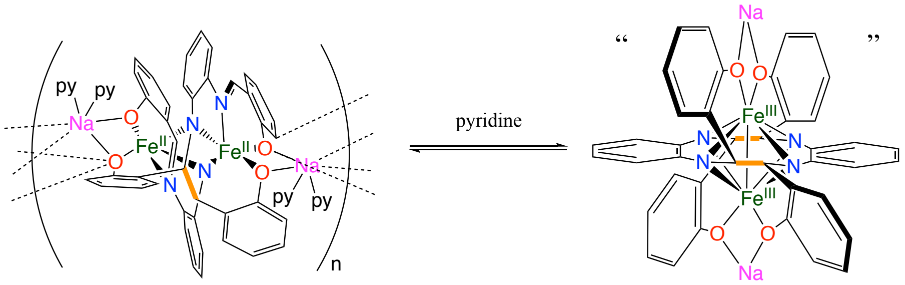

[Na_2Fe_2(bis-salophen)$(THF)_4$]$_n$, **1-py**

“[Na_2Fe_2(cyclo-salophen)]”,**1-blu**

Scheme 3. Supposed species involved in the equilibrium of **1-py**.

An important effect of cation binding on the electron localization was reported for cobalt salophen complexes, which resulted in ligand based ([Co^{II}_2(bis-salophen)M_2] (M =Li, Na) versus metal based reduction products ([Co^{I}(salophen)K]).[26] In order to elucidate the effect of the cation binding on the structure of the reduced Fe salophen complexes, the reaction between **1-THF** and 2.2.2-crytand was performed. The addition of 2 eq of 2.2.2-cyptand to a solution on **1-THF** results in the removal of the sodium counterions from the inner coordination sphere, leading to the cleavage of the polymeric structure and the formation of the dinuclear complex [Fe_2(bis-salophen)][Na(cryptand)]$_2$, **1-crypt** (Scheme 2). Interestingly, the solid state structure of **1-crypt** shows that the coordination environment of the Fe(II) centres remains similar to that in **1-THF** and **1-py**, with comparable Fe–Fe, and mean Fe-N and Fe-O distances (Table 1).

The ^{1}H NMR spectrum of **1-crypt** in py-d5 measured between 298 and 233 K shows the presence of only one set of 14 signals in the paramagnetic range, in agreement with the presence of the non-symmetric Fe(II) complex of the bis-salophen^{2-} ligand as the only solution species in the studied temperature range.

Table 2. Fe-Fe distances and mean values of Fe-N, Fe-O and C-C bond lengths (Å) for the reduced [Fe(salophen)] complexes.

	[Fe(Slp)]	**1-THF**	**1-py**	**1-crypt**	**2-THF**	**2-py**	**3-crypt**
Fe-Fe	-	2.7108(7)	2.7401(18)	2.7314(4)	2.410(1)	2.3971(14)	-
Fe-N	2.099(3)	2.12(1)	2.11(1)	2.124(5)	2.1(1)	2.12(8)	1.87(15)
Fe-O	1.953(3)	1.992(5)	1.993(7)	1.969(5)	2.02(2)	2.026(9)	1.88(13)
C-C	-	1.600(5)	1.600(10)	1.592(2)	1.60(15)	1.60(2)	-

Reduction of [Fe(salophen)(THF)] with 1.5 equiv. of Na

The reduction of [Fe(salophen)(THF)] with 1.5 equivalents of Na metal in THF at room temperature led to the isolation of the tetranuclear dimer [Na_3Fe_2(cyclo-salophen)$(THF)_5]_2$, **2-THF**, in 64% yield. Recrystallization of **2-THF** in pyridine afforded the dinuclear complex [Na_3Fe_2(cyclo-salophen)$(py)_8$], **2-py** (Scheme 4).

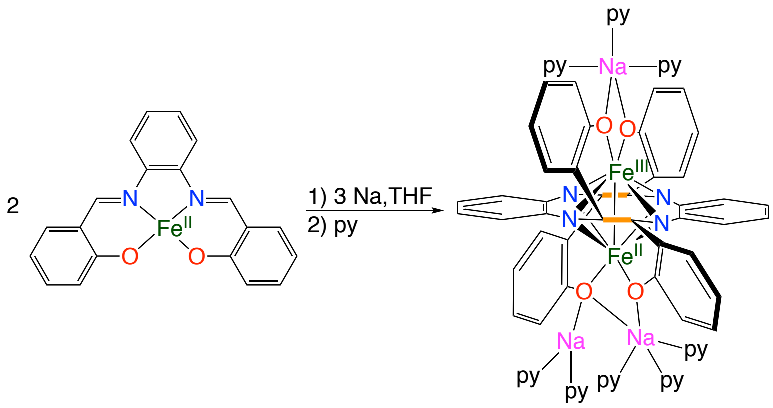

[Fe(salophen)]

[Na_3Fe_2(cyclo-salophen)$(py)_8$], **2-py**

Scheme 4. Reduction of [Fe(salophen)] with 1.5 equivalents of sodium metal, synthesis of **2-py**.

The solid state structure of **2-THF** shows a tetranuclear moieties where two [Na_3Fe_2(cyclo-salophen)$(THF)_5$] moieties are bridged to yield a dimer through the binding of the sodium cations (Na1) to the phenolate oxygen atoms from a second moiety. An inversion centre located between the two Na1 cations relates the two crystallographically equivalent [Na_3Fe_2(cyclo-salophen)$(THF)_5$] moieties. Four sodium cations are found on the periphery of the tetranuclear complex and are penta-coordinated by two oxygen atoms from the cyclo-salophen ligand, one bridging and two terminal THF molecules. In the structure of the complex **2-Py** (Figure 4) three molecules of pyridine solvent bind the sodium cations disrupting the Na-$O_{phenolate}$ bridges and cleaving the dimeric structure found in **2-THF**.

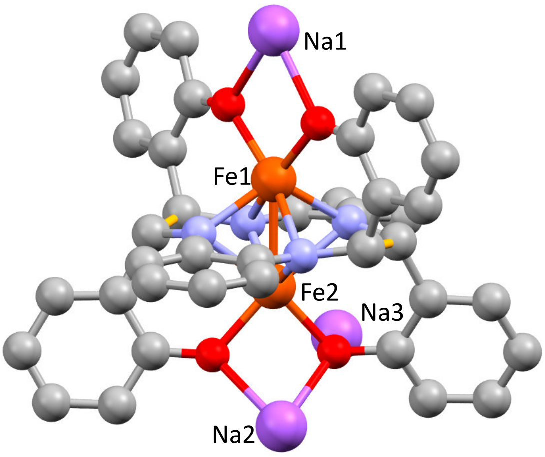

Figure 4. Solid state structure of **2-py**. The C-C bonds formed by reduction of salophen^{2-} are highlighted in yellow. Hydrogen atoms and coordinated solvent molecules have been omitted for clarity.

Both complexes **2-THF** and **2-py** show the presence of a dinuclear moiety [Na_3Fe_2(cyclo-salophen)$(S)_x$] where the two iron ions are found in a similar coordination environment. The two iron cations are coordinated by the octadentate octaanionic amidophenolate macrocyclic ligand cyclo-salophen, resulting from the double reductive C–C coupling of the imine moieties of two salophen ligands (C-C = 1.588(9) Å and 1.618(9) Å). Each iron ion is coordinated by the four amido nitrogen atoms and two oxygen atoms of the cyclo-salophen ligand in a distorted trigonal prismatic geometry. Similar dinuclear complexes of the cyclo-salophen macrocycles were previously obtained from the two-electron reduction of M-salophen complexes.[14,17,19-22] In all these examples the oxidation state of the metal centre remained unchanged and the two-electrons transfer resulted in the reduction of the salophen ligand. In contrast the reduction of [Fe(salophen)] proceeds towards the formation of the diiron complex of cyclo-salophen when less than two equivalents of reducing agents are used. Overall the reduction of [Fe(salophen)] to the **2-py** and **2-THF** results in a one electron oxidation of one of the two metal centres of the [Na_3Fe_2(cyclo-salophen)$(S)_x$] moiety affording a Fe(II)/ Fe(III) complex. This suggests that one of iron ion, instead of being reduced by the addition of sodium metal, contributes to the ligand reduction by transferring one electron to the ligand to yield the cyclo-salophen. This is probably the result of a high stability of the mixed valent complexes **2-py** and **2-THF.** The Fe-Fe distances in **2-THF** and **2-py** (2.410(1) Å and 2.3971(14) Å respectively) are significantly shortened compared to those found in **1-THF** or **1-py**. The values of the Fe–O (2.02(2) Å and 2.026(9) Å) and Fe–N (2.1(1) Å and 2.12(8) Å) distances are comparable in the two complexes (Table 1). BVS analysis was performed for **2-THF** and **2-py**, resulting in an average oxidation state for the iron ions of about 2.50, which is in agreement with a mixed valent Fe(II)/ Fe(III) in the structure. The metrical parameters are very similar for both Fe ions suggesting the presence of a fully delocalized valence.

The EPR analysis performed on a frozen solution of **2-THF** in a mixture THF-Tol (1:1) at 10 K shows a signal assigned to Fe(III) (Figure 5).[31]

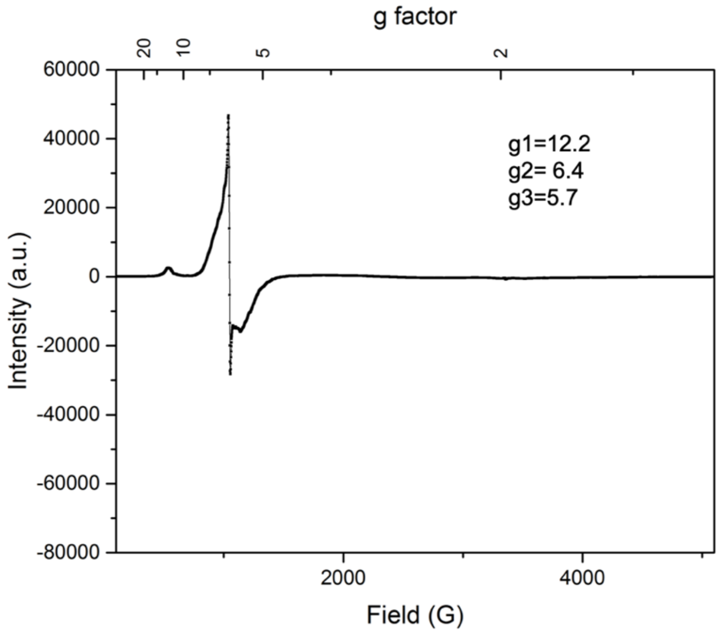

Figure 5. EPR spectrum of **2-THF**.

Reduction of [Fe(salophen)(THF)] with 2 equiv. of Na

The reduction of [Fe(salophen)(THF)] with two equivalents of sodium metal in THF at room temperature (Scheme 5) affords an orange solid that could be recrystallized both from THF and pyridine, upon slow dissolution, to yield crystals of the hexanuclear heterometallic compound [$Na_{12}Fe_6$(tris-cyclo-salophen)$_2$(THF)$_{14}$], **3-THF**, in 84 % yield and the trinuclear complex [Na_6Fe_3(tris-cyclo-salophen)(py)$_9$], **3-py** in 72 % yield.

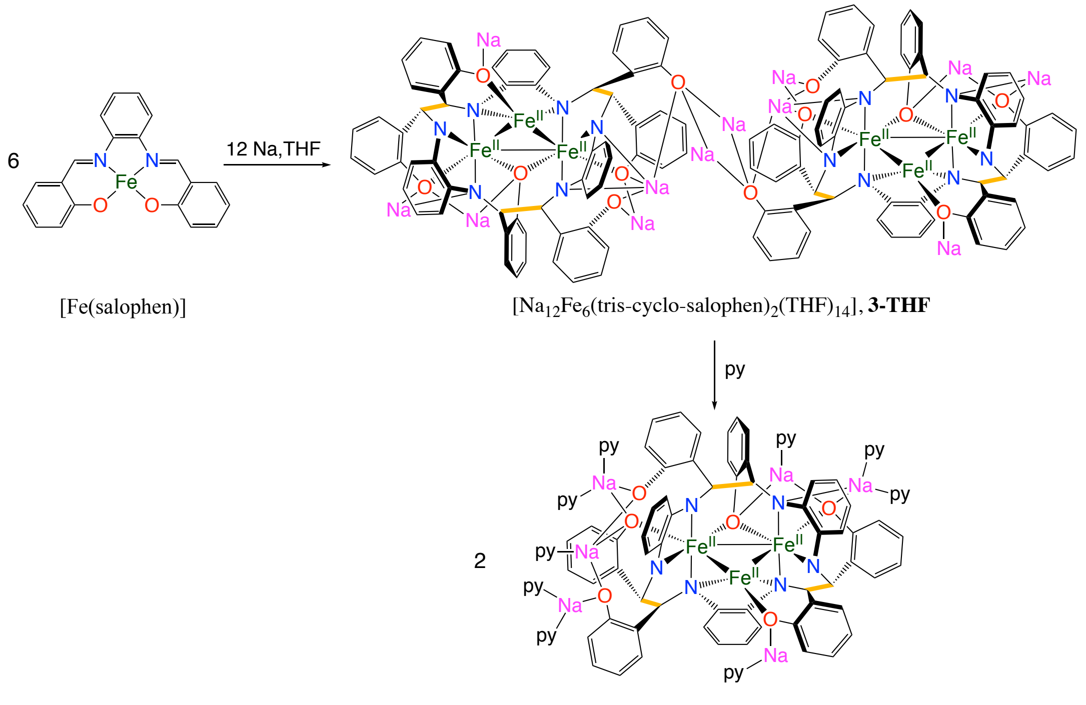

[Fe(salophen)]

$[Na_{12}Fe_6(\text{tris-cyclo-salophen})_2(THF)_{14}]$, **3-THF**

$[Na_6Fe_3(\text{tris-cyclo-salophen})(py)_9]$, **3-py**

Scheme 5. Reduction of [Fe(salophen)] to yield **3-THF** and **3-py** (THF molecule coordinated to **3-THF** have been omitted for clarity).

After slow dissolution of the orange powder formed in the reduction of [Fe(salophen)(THF)] (see experimental part), the isolated **3-THF** and **3-py** turned out to be highly soluble in pyridine or THF. However, no signal could be detected in the ^{1}H NMR spectrum in THF-d8 or in py-d5, from -40 °C to room temperature, probably as a result of the high magnetic moment of the complex, ($\chi_M T = 14.6$ emu K/mol and $\mu_{eff} = 10.80\ \mu_B$ for **3-py,** and $\chi_M T = 15.7$ emu K/mol and $\mu_{eff} = 11.20\ \mu_B$ for **3-THF** as measured by Evan's method at 298 K).

Complex **3-THF** crystallizes in the *P2₁/c* space group with half a molecule per asymmetric unit while **3-py** crystallizes in the *P1* space group with one molecule per asymmetric unit. The overall structure of **3-THF** (see appendix) is comprised of two identical trinuclear $[Na_6Fe_3(\text{tris-cyclo-salophen})(THF)_7]$ moieties which are held together by two sodium–aryloxide bonds. The structure of each trinuclear moiety is very similar to the structure of the trinuclear complex **3-py.** (Figure 5 and 6) The trinuclear moiety in **3-THF** and **3-py** consists of a triangular core of Fe(II) ions held together by the hexa-amide, hexa-phenolate macrocyclic ligand *tris-cyclo-salophen*$^{12-}$ (Scheme 5). The macrocyclic ligand *tris-cyclo-salophen*$^{12-}$ is generated by the reductive coupling of the imino groups of three distinct salophen ligands resulting in three new C–C bonds (average C-C distance: 1.564(6) Å for **3-THF** and 1.567(5) Å for **3-py**). Six inner sphere sodium counterions bind each trimeric unit in both structures.

In the trinuclear complex **3-py** (Figure 6) each Fe(II) ion presents a unique coordination environment (two iron ions present a distorted square pyramidal geometry and one iron ion present a distorted square planar geometry). The values of the Fe-N bond distances range from 2.289(3) Å to 1.961(3) Å and the values of the Fe-O distance range from 1.944(3) to 2.131(3) Å (2.05(6) Å average) with the longer distances found for an aryloxide binding two sodium cations. These values are in the range of those reported for Fe(II) amido[27] and phenolate[32] complexes. The C-N bond distances in **3-py** (1.450(5)-1.474(5) Å) are significantly longer compared to those reported for the [Fe(salophen)(EtOH)] complex (1.299(4) Å) which clearly indicates imine reduction.[28] The values of the Fe-Fe distances range from 2.4405(7) Å, 2.5054(9) Å and 2.7942(7) Å) with a longer Fe(3)-Fe(1) distance, indicative of a weaker bonding interaction. These values are within range of bonding interactions and are similar to the Fe(II)-Fe(II) distances found in trinuclear complexes showing magnetic coupling arising from direct orbital overlap. [27,29,30,33,34,35,36]

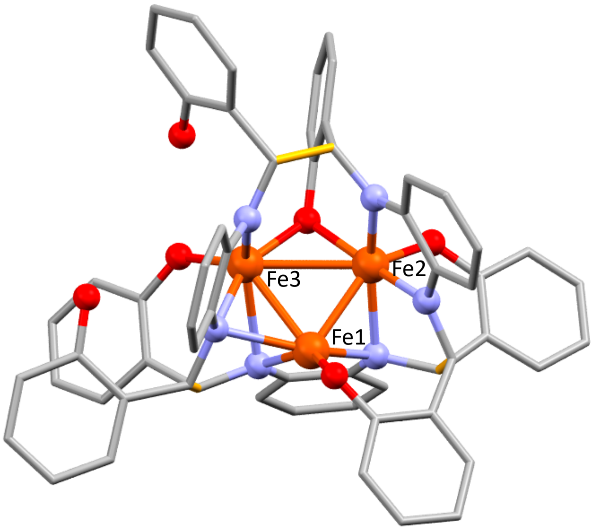

Figure 6. Mercury diagram of the structure of **3-py**. The three C-C bonds formed by reduction of salophen^{2-} are shown in yellow. Hydrogen atoms, sodium cations and Na-bound pyridine molecules have been omitted for clarity.

Two distinct coordination environments are found in the trinuclear moiety of **3-THF** (Figure 7) for the Fe(II) ions with Fe-N and Fe-O bond distances comparable to those found in **3-py**. The values of the Fe-Fe bond distances in **3-THF** (2.403(1) Å, 2.438(1) Å, and 2.703(1) Å) are shorter than those found in **3-py** and therefore within the range of bonding interactions.

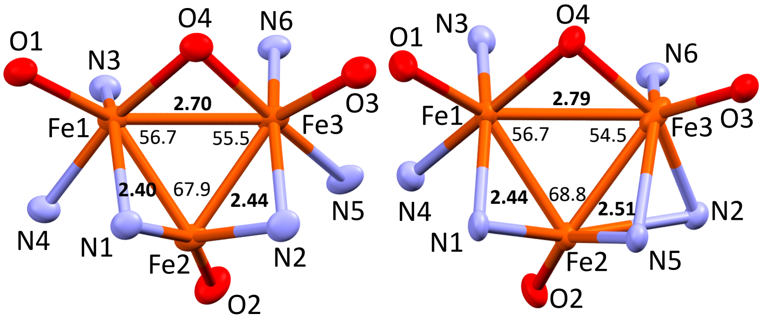

Figure 7. Mercury diagram of the trinuclear core in the structures of **3-THF** (left) and **3-py** (right) with Fe-Fe distances in Å (bold), Fe-Fe-Fe angles in degrees (normal) (50% probability ellipsoids).

As mentioned before, the nature of the cation can have a significant impact on the stability of these reduced complexes. In the case of **3-THF**, the addition of 2.2.2-cryptand to a solution of **3-THF** resulted in the formation of a crystalline precipitate of the binuclear Fe(I) complex [Na(Fe(salophen))$_2$][Na(cryptand)]$_3$, **3-crypt** (Scheme 6).

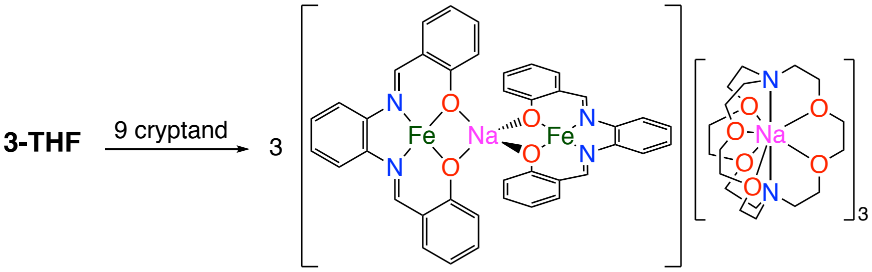

[Na(Fe(salophen))$_2$][Na(cryptand)], **3-crypt**

Scheme 6. Cleavage of the C–C bonds promoted by 2.2.2-cryptand, synthesis of **3-crypt**.

The structure of **3-crypt** (Figure 8) shows the presence of a trianionic, dimeric iron species and three [Na(cryptand)] cations. The [Na(Fe(salophen))$_2$]$^{3-}$ shows two [Fe(salophen)] units connected to each other through a sodium cation binding the oxygen atoms of the two salophen ligands in a quasi-perpendicular fashion (65.09 ° between the plane define by N2O2 sites of the ligands). The iron atoms are tetracoordinated in a square planar geometry with average Fe-O and Fe-N distances of 1.88(13) Å and 1.87(15) Å, significantly shorter than the distances found in [Fe(salophen)] (1.99 Å and 2.11 Å respectively).

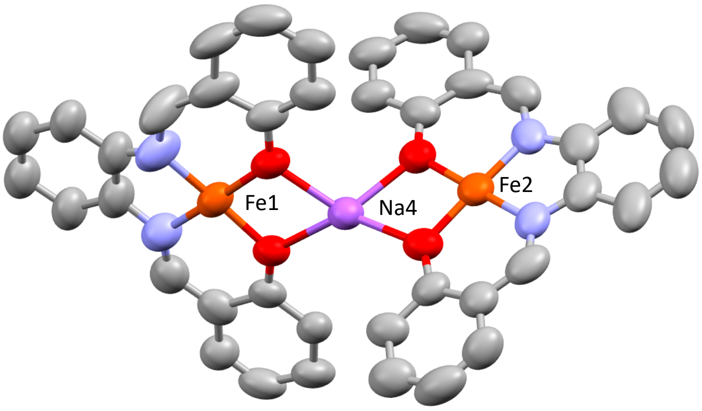

Figure 8. Solid state structure of $[Na(Fe(salophen))_2]^{3-}$ anion in **3-crypt** (50% probability ellipsoids). Hydrogen atoms have been omitted for clarity.

3-crypt resulted insoluble in THF but soluble in pyridine, and it did not show sign of decomposition after one week. However, the ^1H NMR spectrum of **3-crypt** in py-d5 shows only two broad signals in the diamagnetic range assigned to the [Na(cryptand)] cations. The remarkable structural change resulting by addition of 2.2.2-cryptand underline the important role of the cation in the stabilization of the structure and proves that the electrons can be easily redistributed between the ligand and the metal centre. To further characterize the complex, the EPR spectrum was measured. The EPR spectrum of a solution of **3-crypt** in pyridine solution (Figure 9) showed the presence of two sets of signals with similar g factor (i: g1 = 2.88, g2 = 2.15, g3= 1.99; ii: g1 = 2.74, g2 = 2.17, g3= 1.98), both assigned to Fe(I) species, in agreement with examples previously reported in literature.[37]

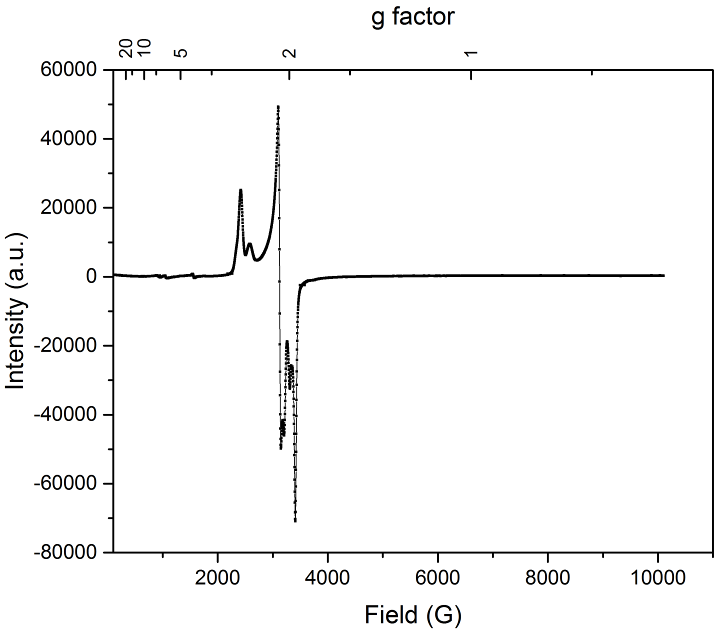

Figure 9. EPR spectrum of **3-crypt** in pyridine.

Magnetic characterization

The presence of potential magnetic Fe-Fe interactions was investigated by measuring variable temperature (5-300 K) magnetic susceptibility data for **1**, **2** and **3** under an applied magnetic field of 1 T. The χ_MT vs T plot for **1-THF** (Figure 10) shows an unusual behaviour with the values of χ_MT increasing with the temperature in a quadratic way. The χ_MT *vs.* T plot for **1-py** resulted superimposable with **1-THF**.

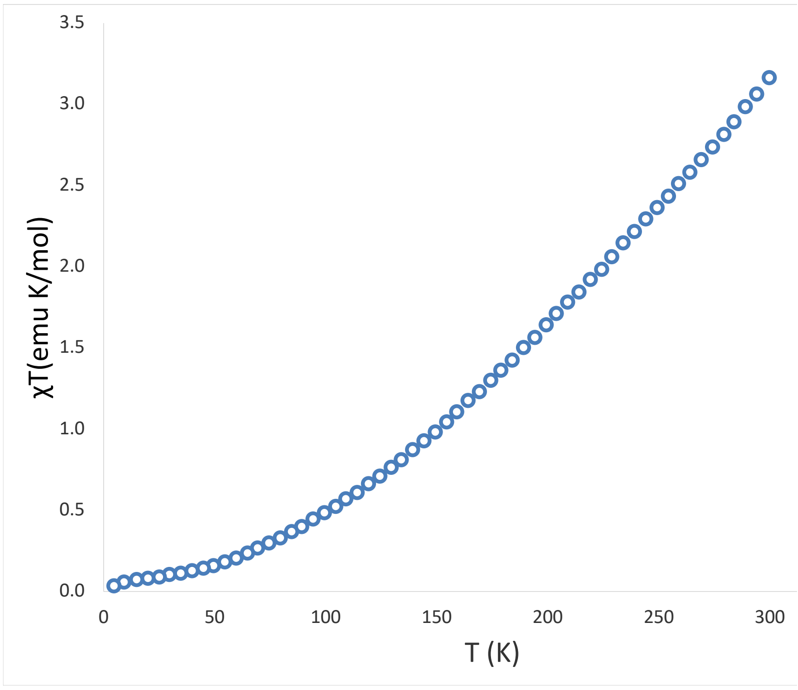

Figure 10. χ_MT vs. T graphic for **1-THF** (10^3 Oe, 300-5 K).

Similar behaviour was also found after the cleavage of the polymeric structure by addition of cryptand (Figure 11). The χ_MT *vs.* T plot for **1-crypt** shows a decrease of the values while decreasing the temperature, reaching a χ_MT of about 0.5 emuK/mol ($\mu = 2\ \mu_B$) at 5 K. This result excludes the possibility that the non-common behaviour of **1-THF** was due to the polymeric nature of the complex.

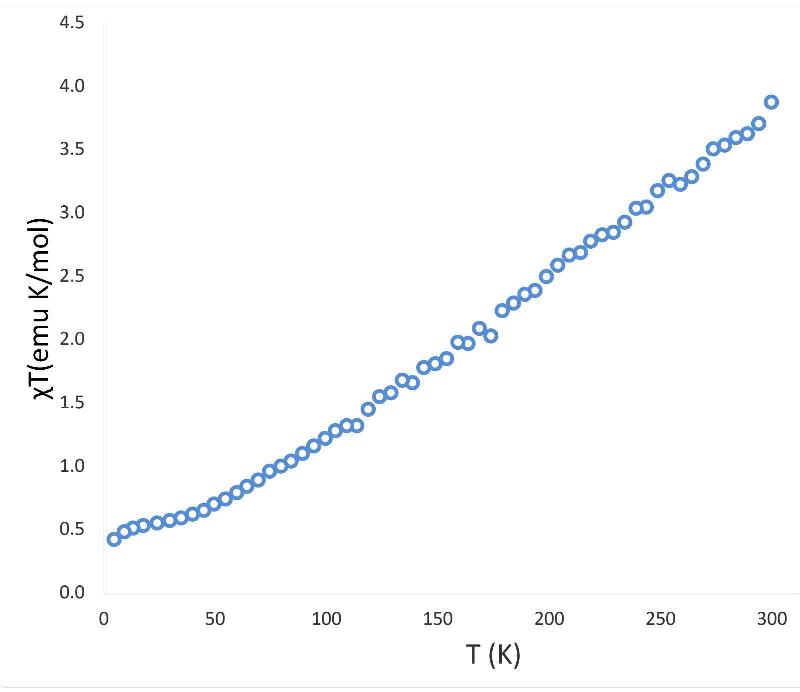

Figure 11. $\chi_M T$ vs. T graphic for **1-crypt** (10^3 Oe, 300-5 K).

Preliminary analysis of **1-THF** via Mössbauer spectroscopy revealed that all the iron atoms are in high spin sate at 77 K. Therefore, the most reasonable explanation for the measured magnetic properties of 1-THF is the presence of a strong antiferromagnetic coupling that persists at room temperature.[38]

The values of $\chi_M T$ for **2-THF** and **2-py** reach values of about 7 emuK/mol (μ = 7.50 μ_B) and about 4.3 emuK/mol (μ about 5.7 μ_B) respectively at room temperature decreasing slightly in the range 300-30 K, while they drop rapidly below 30 K to reach a value of about 3 emu K/mol (μ = 4.90 μ_B) and 2 emu K/mol (μ = 4.0 μ_B) respectively at 5 K probably due to Zeeman effect and zero field splitting (Figure 12).

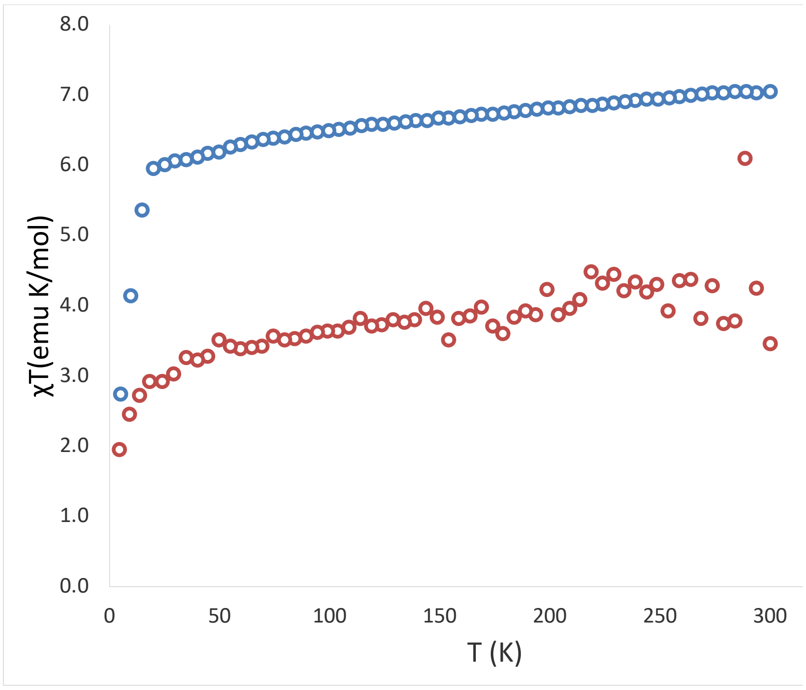

Figure 12. χ_MT vs. T graphic for **2-THF** (blue) and for **2-py** (red) (10^3 Oe, 300-5 K).

For the [Fe(III)Fe(II)(cyclo-salophen)]$^{3-}$ moieties present in both **2-THF** and **2-py** four possible combination of spin state of the iron atoms are possible: HS Fe(III)-HS Fe(II), LS Fe(III)-LS Fe(II), HS Fe(III)-LS Fe(II) and LS Fe(III)-HS Fe(II). For all this conformation is possible to calculate the expected χ_MT and μ values for non-interacting ions by summing the contribution of the single atom. In the case of both HS iron atoms the expected χ_MT is 7.38 emuK/mol (μ = 7.68 μ_B), while in the case of both atoms in LS configuration the expected χ_MT is 0.37 emuK/mol (μ = 1.73 μ_B). Both these values do not match with the experimental data. In the case of HS Fe(III)-LS Fe(II) the expected χ_MT is 4.38 emuK/mol (μ = 5.92 μ_B), and in the case of LS Fe(III)-HS Fe(II) the expected χ_MT is 3.37 emuK/mol (μ = 5.19 μ_B).

From the values reported in Figure 12 is possible to see that in **2-py** are present an HS Fe(III) and a LS Fe(II), while the values for **2-THF** seems to be due to two non-interacting [Fe(III)Fe(II)(cyclo-salophen)]$^{3-}$ dimers.

Regarding **3-THF** and **3-py**, the values of χ_MT remain relatively constant in the temperature range 60-300 K (Figure 12) while they drop rapidly for both complexes below 60 K to reach a value of about 10 emu K/mol at 5 K probably due to Zeeman effect and zero field splitting (Figure 13).

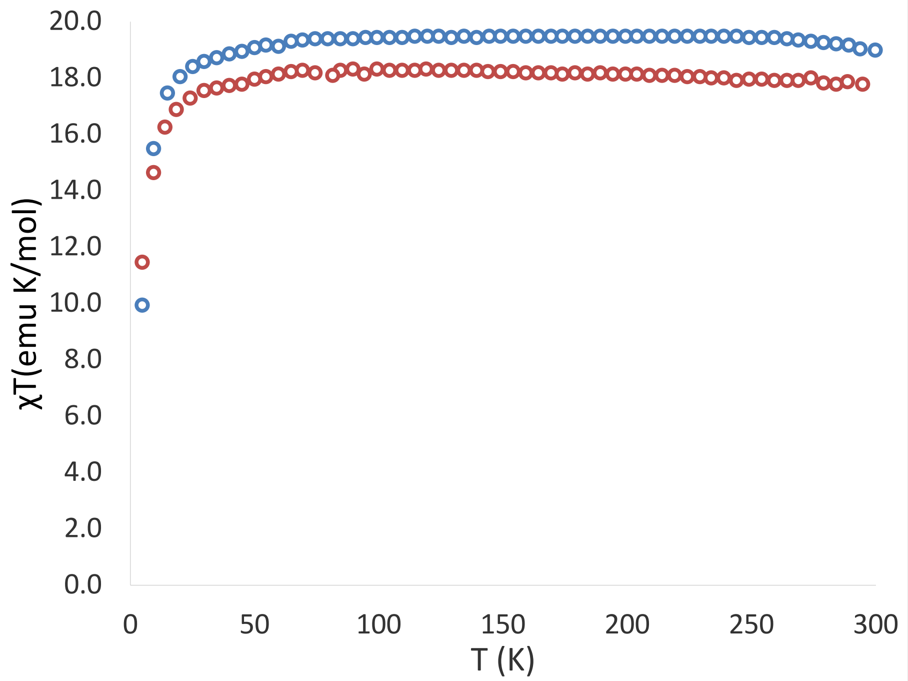

Figure 13. $\chi_M T$ *vs.* T graphic for **3-THF** (blue) and **3-py** (red) (10^3 Oe, 300-5 K).

The values of $\chi_M T$ found for each [Fe$_3$(tris-cyclo-salophen)]$^{6-}$ moiety in **3-THF** (19.4 emuK/mol at 300 K and μ = 12.45 μ_B at 300 K) and **3-py** (17.7 emuK/mol and μ = 11.90 μ_B at 300 K) are much higher than the expected value for three non-interacting Fe(II) (9 emuK/mol) with g = 2. This suggests the presence of a strong ferromagnetic interaction between the Fe centres in the core which is maintained at room temperature. These values are only slightly lower than the 21 emuK/mol expected for a system with S = 6 ground state (g = 2). Only one example of a trinuclear Fe(II) cluster with a stable high spin state (S = 6) at room temperature was previously reported.[27] The previously reported triangular system supported by an hexamido ligand showed Fe(II)-Fe(II) distances comparable to complexes **3-THF** and **3-py** and a similar weak-field environment. A high-spin state was observed in weak-field tri- and hexa-nuclear iron clusters. This was interpreted as weak Fe-Fe interactions that result in three or six atom clusters behaving as a large single spin[27,39,40,41] approximating that of a single metal ion. A similar type of direct magnetic exchange is likely to be at the origin of the high-spin state in **3-THF** and **3-py.**

Electrochemical characterization of the compounds

Since compounds **1-THF** resulted poorly soluble in THF, the electrochemical characterization was performed in pyridine solution. The cyclic voltammogram (CV) of [Fe(salophen)py$_2$] was obtained in pyridine solution in presence of NBu$_4$PF$_6$ 0.1 M as electrolyte at room temperature (Figure 14).

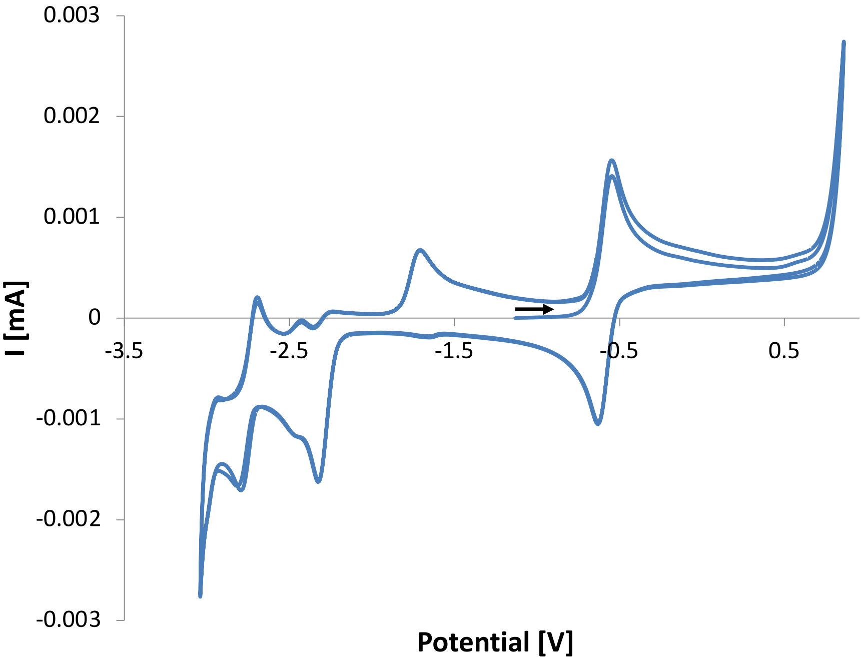

Figure 14. CV of [Fe(salophen)] (4 mM) in py solution in presence of NBu_4PF_6 0.1 M, using a Pt electrode at a scan rate of 100 mV/s (the arrow indicated the starting potential and the direction).

Starting from [Fe(salophen)], a reversible one electron process with E_0 = -0.55 V is observed. This feature is assigned to the oxidation of the metal centre forming the known $[Fe^{III}(salophen)]^+$ cationic specie. Upon the return wave, two irreversible features are observed at -2.31 V and -2.43 V, and one quasi-reversible process at -2.80 V vs $FeCp_2/FeCp_2^+$. The intensity of each waves presents a linear response towards the square root of the scan rate, indicating that all the species act as molecular compounds in the diffusion limit regime. The wave at reduction potential of -2.31 V is attributed to the formation of compound **1-py**, while, the wave at reduction potential of -2.43 V is attributed to the formation of compound **2-py**. The assignment of the redox event is supported by the CV obtained starting from **1-py** and **2-py** (Figure 15, 16).

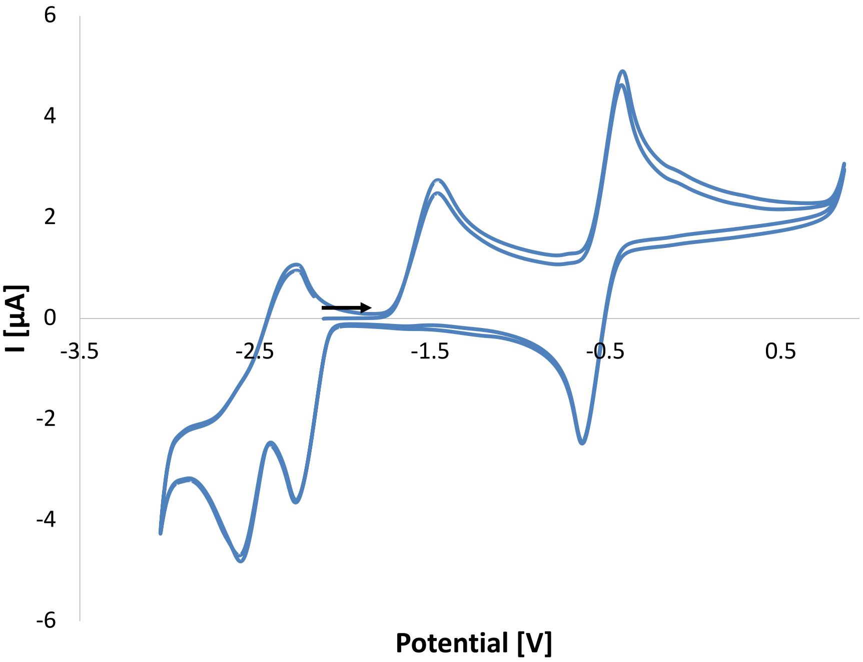

Figure 15. CV of **1-py** (4 mM) in py solution in presence of NBu_4PF_6 0.1 M, using a Pt electrode at a scan rate of 100 mV/s (the arrow indicated the starting potential and the direction).

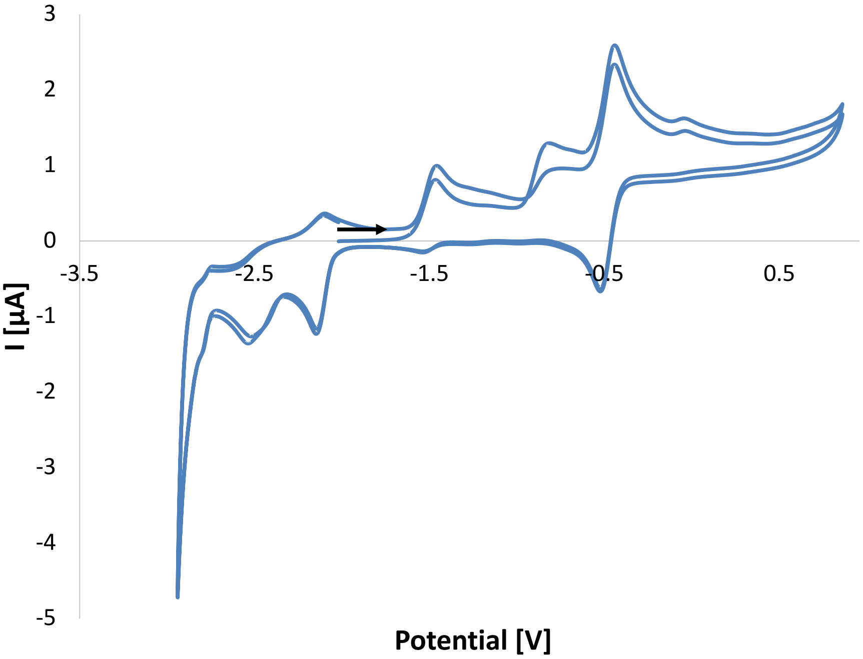

Figure 16. CV of **2-py** (4 mM) in py solution in presence of NBu_4PF_6 0.1 M, using a Pt electrode at a scan rate of 100 mV/s (the arrow indicated the starting potential and the direction).

The CV obtained starting from **2-py** shows an oxidation event at about -0.8 V not visible in the case of [Fe(salophen)] or **1-py**. The hypothesis that this feature is due to the sodium ions present in solution was excluded because it persists even after the addition of 2.2.2-cryptand (Figure S18). The third wave at reduction potential of -2.80 V is instead attributed to the two electron reduction product of

[Fe(salophen)]. Considering the importance of the cation in the determination of the product, compounds like **3-crypt** are most likely to be formed in the experimental conditions due to the presence of non-coordinating cations. However, the formation of cluster such as [Fe$_3$(tris-cyclo-salophen)]$^{6-}$ or other species that than rearrange could not be excluded. Also in this case the CV obtain starting from **3-py** result different from the one obtained from [Fe(salophen)], probably for interaction between **3-py** and the oxidized species formed at the electrode (Figure 17). Again, the hypothesis that the behaviour was due to the presence of coordinating Na$^+$ cation can be excluded because it persists even after the addition of excess 2.2.2 cryptand (Figure S19).

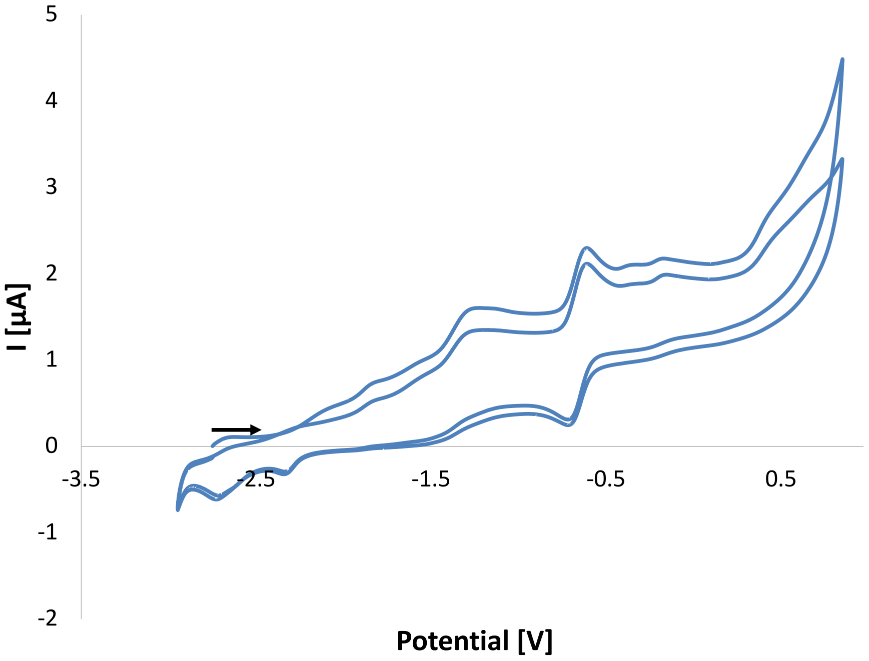

Figure 17. CV of **3-py** (4 mM) in py solution in presence of NBu$_4$PF$_6$ 0.1 M, using a Pt electrode at a scan rate of 100 mV/s (the arrow indicated the starting potential and the direction).

Finally, the signal at -1.72 V is assigned to the oxidation of **1-py** and **2-py** formed electrochemically (Figure S16).

Electrochemical response in presence of CO$_2$. In order to study the ability of the complex to promote the electrocatalytic reduction of carbon dioxide and to better understand the reactivity (*vide infra*), the electrochemical response of [Fe(salophen)py$_2$] in presence of CO$_2$ was tested (Figure 18). Upon the addition of a saturated solution of CO$_2$ in py only two feature irreversible features were visible. The presence of carbon dioxide did not cause any significant change in the potential of the first reduction process, but an increase of the Faradaic current was observed. This suggests that the formation of **1-py** proceed in the same way in presence or in absence of CO$_2$, that does not bind the starting [Fe(salophen)] under the experiment conditions. However, once compound **1-py** is formed, CO$_2$ is capable to react causing the increase of the current. The second feature is observed at -2.68 V and it could represent the reactivity of **2-py** with carbon dioxide. The Faradaic current is about three time bigger than the one observed in absence of carbon dioxide, suggesting that [Fe(salophen)] is capable to act as electrocatalyst. In the return wave, is possible to observe the oxidation process visible also in absence of CO_2. However, the signal is shifter to -1.45 V and a second shoulder is visible at a potential of -1.16 V. This could indicate that the presence of multiple species in solution and suggest that the reduction products (CO_3^{2-} and CO) binds the complexes, causing the shift of the potential. A shift of the potential is also observed for the oxidation (-0.61 V) and two small features at -0.14 V and 0.63 V are visible.

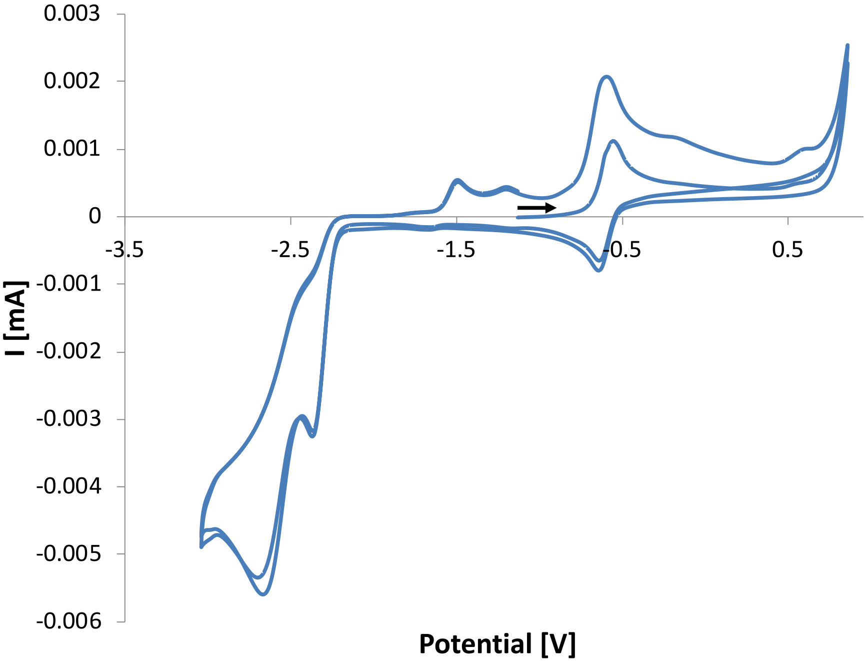

Figure 18. CV of [Fe(salophen)] (4 mM) in presence of CO_2 and in presence of NBu_4PF_6 0.1 M, using a GC electrode at a scan rate of 100 mV/s (the arrow indicated the starting potential and the direction).

Reactivity

One of the most attractive properties of metal complexes supported by non-innocent ligands is their ability to store electrons. Complexes **1-py**, **2-py** and **3-py** are capable of storing two, three and six electrons in C–C bonds, respectively. As has been shown, those electrons may be used for redox reactions, and in some cases are capable of activating small molecules that are normally considered inert. For this reason, we studied the reactivity of the complexes towards carbon dioxide in order to test the availability of the electrons stored in the C–C bonds.

The addition of CO_2 (6 equiv.) to a pyridine solution of **3-py** (Scheme 7) resulted in a colour change of the solution from dark brown to dark green. The ^1H NMR spectrum recorded after one hour of the reaction mixture showed the formation of [Fe(salophen)] as only product visible by ^1H NMR spectroscopy. The residue that was obtained after removal of the solvent was analysed by ^{13}C NMR spectroscopy in basic D_2O (pD = 13.4) and a resonance at 168 ppm was assigned to CO_3^{2-}. The addition of ^{13}AcONa as an internal standard allowed quantitative determination of the carbonate formed during the reaction. that resulted to be 100% (Figure S7). The quantitative formation of carbonate indicates that the complex **3-py** promotes the reductive disproportionation of CO_2 to carbonate and CO. The signal of ^{13}CO could not be detected in the used reaction conditions.

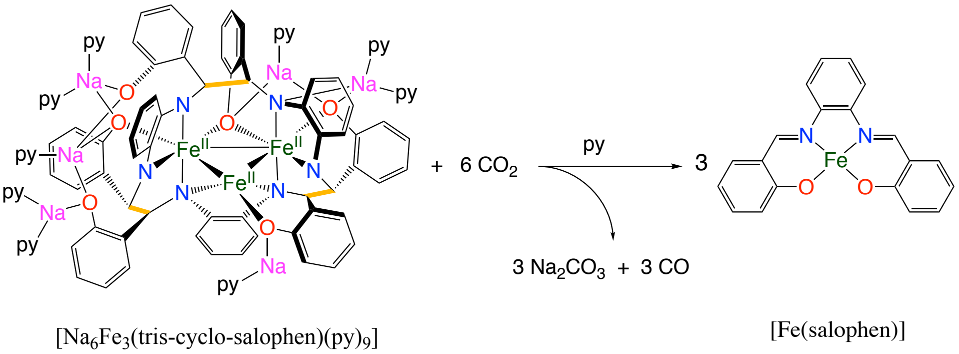

Scheme 7. Reaction of **3-py** with CO_2.

The reaction of **3-py** with CO_2 was also performed with sub-stoichiometric amount of CO_2 (4 equiv. and 2 equiv.) to study the reaction pathway. The reaction proceeds trough the formation of **2-py** and **1-py**, evident from the ^1H NMR spectrum of the crude reaction mixture. Again, after removal of the solvent and dissolution of the residue in basic D_2O (pD = 13.4), only CO_3^{2-} was observed.

Similar reactivity was performed also with **2-py** and **1-py** with stoichiometric and sub-stoichiometric amount of carbon dioxide, resulting in the quantitative reductive disproportionation of CO_2 and formation of the starting [Fe(salophen)] complex (Scheme 8).

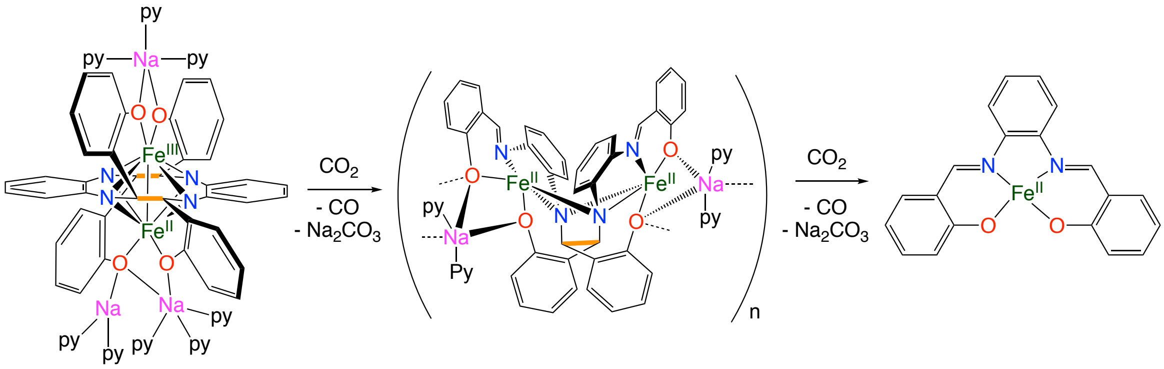

2-py **1-py** Fe(salophen)

Scheme 8. Reaction of **2-py** and **1-py** with CO_2.

The reaction of **3-py**, **2-py** and **1-py** with carbon dioxide proceeds very differently in comparison with the analogous Co complex, which showed only reversible binding of the substrate or attack of the ligand scaffold in the case of more reduced species. [26]

Conclusion

In conclusion, we have found that the one electron reduction of [Fe(salophen)] promoted by Na is ligand centred and affords the complex [Na_2Fe_2(bis-salophen)S_2] (S = THF or py), where the two salophen units are connected through a C-C bond. Further reduction of the complex affords a mixed valence Fe(III)Fe(II) specie with four electrons stored in two C-C bond, where part of the electron needed for the formation of the second bond is given by one of the iron centres. The two electron reduction of [Fe(salophen)] leads to the formation of a macrocyclic dodecadentate ligand perfectly suited for binding three Fe(II) centres at short distances allowing for strong magnetic coupling. Finally, the rearrangement of the electrons in the trinuclear complex is possible by simply cation exchange, affording an Fe(I) specie. It has been proven that the electrons stored in the ligand become available for the reduction of carbon dioxide with selective formation of carbonate. Future works imply the study of those complexes for the electrochemical reduction of carbon dioxide, and the modification of the ligand to study different kind of assembly.

Experimental

General Considerations.

Unless otherwise noted, all manipulations were carried out under an inert argon atmosphere using Schlenk techniques and an MBraun glovebox equipped with a purifier unit. The water and oxygen level were always kept at less than 0.1 ppm. Glassware was dried overnight at 150°C prior to use.

Unless otherwise noted, reagents were acquired from commercial sources and used without further purification. The solvents were purchased from Sigma Aldrich or Cortecnet (deuterated solvents) in their anhydrous form, conditioned under argon and vacuum distilled from K/benzophenone (THF, THF-d8), Na sand/benzophenone (*n*-hexane) or dried with molecular sieves 3 Å (py, py-d5).The synthesis were performed using glass covered stirring bars. Na metal and [$FeCl_2$] were purchase from Sigma Aldrich and used without further purification. Schiff-base ligands were prepared in air by the condensation of 1,2- phenylenediamine with salicylaldehyde (1:2 stoichiometric ratio) in ethanol under reflux in according with published procedures.[22] ^{1}H and ^{13}C NMR experiments were carried out using NMR tubes adapted with J. Young valves. The NMR spectra were recorded on Bruker 400 MHz or 600 MHz. ^{1}H chemical shifts are reported in ppm and were measured relative to residual solvent peaks, which were assigned relative to an external TMS standard set at 0.00 ppm. Elemental analyses were performed under helium by the analytical service at EPFL. The UV-Vis-NIR spectrum was performed with PerkinElmer Lambda 750. The IR spectrum was performed with PerkinElmer Frontier spectrometer. The magnetic measurements were performed using a QuantumDesign MPMS-5T superconducting quantum interference device (SQUID) magnetometer in a temperature range between 5 and 300 K. The microcrystalline samples were enclosed in a quartz tube flame sealed under vacuum. The samples were strained with eicosane to prevent the torqueing during the measurement. The magnetic moment was also measured in THF and pyridine solutions respectively using Evans method. For the reaction of the complexes with $^{13}CO_2$ or CO_2, the compound was dissolved in py-d5 inside the glovebox and transfer in an NMR tube equipped with J. Young valves. The tube was brought outside of the glovebox, attached to a Schlenk line and degassed with three freeze-pump-thaw cycle.

Starting materials.

Na_2salophen. ^{1}H NMR (200 MHz, THF-d_8, 298 K): $\delta = 8.6$ (s, 2H), 7.4 (d, 2H), 6.9-7.3 (m, 8H), 6.5 (t, 2H).

[Fe(salophen)(THF)]. A solution of Na_2salophen (1.87 g, 3.9 mmol, 1 equiv.) in THF (25 mL) was added at room temperature to a suspension of $FeCl_2$ (500 mg, 3.9 mmol, 1eq) in THF (25 mL). The mixture was stirred at room temperature for 7 days affording a dark suspension. The mixture was filtered to remove NaCl and the solvent volume was reduced under vacuum to approximately 10 mL. Storage of the resulting concentrated solution at -40 °C afforded dark green crystals of [Fe(salophen)(THF)] (1.40 g, 80 % yield). The magnetic data measured in solution and in the solid state are comparable to those reported in the literature[28] ($\chi_M T = 3.7$ emu K/mol in solid state and $\chi_M T = 3.5$

emu K/mol in THF solution at 300 K). ^{1}H NMR spectrum of the crystals in py-d5 (400 MHz, py-d5, 298 K): δ = 60.72 (s, 1H), 44.11 (s, 1H), 14.77 (s, 1H), 10.63 (s, 2H), -7.51 (s, 1H), -17.04 (s, 1H). Elemental analysis calc. for [Fe(salophen)(THF)] (444.2 g mol^{-1}): C, 59.86; H, 4.27; N, 6.18. Found: C, 59.66; H, 4.59; N, 5.80.

Syntheses of the complexes.

[Na$_2$Fe$_2$(bis-salophen)(THF)$_4$]$_n$, 1-THF. Na (7.8 mg, 0.339 mmol, 1 equiv.) were added to a solution of [Fe(salophen)(THF)] (150 mg, 0.339 mmol, 1 equiv.) in of THF (6 mL) at -40 °C. The reaction was stirred overnight at -40 °C affording a brown solution. The solvent volume was reduced under vacuum to (1 mL) and the precipitate obtained was recovered by centrifugation. 157 mg of product were recovered (73% yield). Crystals suitable for X-ray diffraction were obtained by slow diffusion of hexane into a THF solution **1-THF**. Recrystallization of **1-THF** in pyridine afforded **1-py**. ^{1}H NMR of **1-py** (400 MHz, py-d5, 298 K): δ = 25.76 (s, 2H), 25.57 (s, 2H), 21.11 (s, 2H), 17.76 (s, 2H), 17.20 (s, 2H), 14.22 (s, 2H), -1.24 (s, 2H), 0.65 (s, 2H), -1.70 (s, 2H), -20.37 (s, 2H). ^{1}H NMR of 1 (400 MHz, py-d5, 233 K): δ = 24.28 (s, 1H), 24.07 (s, 1H), 19.65 (s, 1H), 16.24 (s, 1H), 15.71 (s, 1H), 12.77 (s, 1H), -0.29 (s, 1H), -2.20 (s, 1H), -3.32 (s, 1H), -21.88 (s, 1H). Elemental analysis calc. for [Na$_2$Fe$_2$(bis-salophen)(THF)$_{6.6}$] (1262 g mol^{-1}): C, 62.29; H,5.23 ; N, 5.59. Found: C, 62.05; H, 5.13; N, 5.66.

[Fe$_2$(bis-salophen)][Na(cryptand)]$_2$, 1-crypt. 2.2.2-cryptand (20 mg, 0.053 mmol, 2 equiv.) were added to a brown dispersion of **1-THF** (30 mg, 0.026 mmol, 1 equiv.) in THF (2 mL) at room temperature. The reaction was stirred two hours forming a brown precipitate and a clear supernatant. The precipitate obtained was recovered by centrifugation. 40 mg of product were recovered (96% yield). Crystals suitable for X-ray diffraction were obtained by slow diffusion of a solution of 2.2.2-cryptand into a THF solution **1-THF**. ^{1}H NMR of **1-crypt** (400 MHz, py-d5, 298 K): δ = 51.38 (s, 2H), 41.32 (s, 2H), 32.33 (s, 2H), 31.09 (s, 2H), 24.73 (s, 2H), 19.83 (s, 2H), 2.00 (s, 12H), 1.89 (s, 12H), 1.06 (s, 12H), -4.49 (s, 2H), -5.39 (s, 2H), -12.56 (s, 2H), -15.87 (s, 2H), -35.41 (s, 2H). Elemental analysis calc. for [Fe$_2$(bis-salophen)][Na(cryptand)]$_2$.0.5THF (1575.37 g mol^{-1}): C, 59.47; H,6.65 ; N, 7.11. Found: C, 59.54; H, 6.64; N, 7.17.

[Na$_6$Fe$_4$(cyclo-salophen)(THF)$_{10}$], 2-THF. Na (3.9 mg, 0.169 mmol, 1.5 eq) was added to a solution of [Fe(salophen)(THF)] (50 mg, 0.113 mmol, 1 eq) in THF (4 mL) at -40 °C. The reaction was stirred overnight at -40 °C affording a purple solution. 40 mg of black solid precipitated out from the solution after one night at room at -40 °C (64% yield). Crystals suitable for X-ray diffraction were obtained by slow diffusion of hexane into a THF solution 2-THF. Recrystallization of **2-THF** in pyridine solution afforded **2-py**. ^{1}H NMR of **2-THF** (400 MHz, THF-d8, 298 K): δ = 35.96 (s), 30.51 (s), -13.85 (s), -31.09 (s). ^{1}H NMR of **2-py** (400 MHz, py-d5, 298 K): δ = 36.31 (s), -13.61 (s), -33.57 (s). Elemental analysis calc. for [Na_6Fe_4(cyclo-salophen)$_2$(THF)$_8$] (2194.9 g mol^{-1}): C, 61.27; H, 5.51; N, 5.10. Found: C, 60.93; H, 5.61; N, 5.14.

[Na_6Fe_3(tris-cyclo-salophen)(py)$_9$], 3-py and **[Na_6Fe_3(tris-cyclo-salophen)(THF)$_7$]$_2$, 3-THF**. Sodium metal (20.8 mg, 0.904 mmol, 2 eq) was added to a solution of [Fe(salophen)(THF)] (200 mg, 0.452 mmol, 1 eq) in THF (4 mL) at room temperature. The reaction was stirred overnight at room temperature affording a brown solution and an orange precipitate. The precipitate was separated from the solution by centrifugation and the resultant solid was washed three times with THF (2 mL). Dissolution of the orange precipitate in pyridine afforded a dark brown solution. Diffusion of hexane into the pyridine solution afforded the complex [Na_6Fe_3(tris-cyclo-salophen)(py)$_9$], **3-py** (188 mg, 72 % yield). Crystals suitable for X-ray diffraction were obtained by slow diffusion of *n*-hexane into a pyridine solution of **3-py**.

The ^{1}H NMR spectrum of **3-py** in py-d5 did not show any resonance attributable to the complex when recorded either at -40 °C or at room temperature. A magnetic moment $\mu = 10.8\ \mu_B$ ($\chi_M T = 14.6$ emu K mol^{-1}) was measured for **3-py** in pyridine solution at 298 K using the Evans method. Elemental analysis calcd. for [Na_6Fe_3(tris-cyclo-salophen)(py)$_7$] (1801.5 g mol^{-1}): C, 63.34; H, 4.31; N, 10.11. Found: C, 63.02; H, 4.55; N, 10.23.

SQUID magnetometry was performed in samples containing different amounts of pyridine (7-10) due to different exposure times of the isolated solid to vacuum. No significant differences were observed among the measurements.

The orange precipitate obtained from the reduction of [Fe(salophen)(THF)] in THF could also be solubilized in THF but this required stirring the solid for 4 weeks at room temperature and led to a dark red solution. Slow diffusion of hexane into the resulting solution afforded the complex [Na_6Fe_3(tris-cyclo-salophen) (THF)$_7$]$_2$, **3-THF** as dark brown microcrystalline solid (205 mg, 84% yield). The ^{1}H NMR spectrum of **3-THF** in THF-d8 did not show any resonance attributable to the complex when recorded either at -40 °C or at room temperature.

Crystals suitable for X-ray diffraction were obtained by slow diffusion of *n*-hexane into a THF solution **3-THF**. Elemental analysis calcd. for [$Na_{12}Fe_6$(tris-cyclo-salophen)$_2$(THF)$_{14}$] (3506.4 g mol^{-1}): C, 60.29; H, 5.63; N, 4.79. Found: C, 60.64; H, 5.28; N, 4.86.

A magnetic moment $\mu = 11.2\ \mu_B$ ($\chi_M T = 15.7$ emu K mol^{-1}) was measured for **3-THF** at 298 K in THF solution by Evans method.

The amount of coordinated THF is dependent on the drying time. The amount of THF present in the solid, detected by elemental analysis, does not affect the magnetometry measurements, suggesting that the trinuclear structure is retained independently on the amount of coordinated THF.

[(Fe(salophen))$_2$Na][Na@2.2.2-cryptand]$_3$, 3-crypt. 2.2.2 cryptand (23.6 mg, 0.063 mmol, 9 eq) were added to a solution of **3-THF** (20 mg, 0.007 mmol, 1 eq) in THF (2 mL) at room temperature. Crystals, **3-crypt**, precipitated out from the solution after one night was recovered by centrifugation (38 mg, 88 % yield). ^1H NMR of **3-crypt** (400 MHz, py-d5, 298 K): $\delta = 1.95$ (s), 0.84 (s). Elemental analysis calc. for [Na(Fe(salophen))$_2$][Na(cryptand)]$_3$.THF (2033.9 g mol^{-1}): C, 57.87; H, 7.14; N, 6.89. Found: C, 57.58; H, 7.04; N, 6.56.

Reaction with $^{13}CO_2$. The complex **3-py** (10 mg, 0.0028 mmol, 1 eq) was dissolved in py-d5 (0.4 mL) in an NMR tube equipped with a J Young valve under an argon atmosphere. The solution was degassed by three cycles of freeze-pump-thawing. $^{13}CO_2$ (6 eq) was added to the frozen solution. The reaction mixture rapidly changed colour from dark brown to dark green upon thawing and a dark precipitate formed. The ^1H NMR spectrum was recorded after one night at 298 K, this showed only the resonances assigned to [Fe(salophen)(THF)]. Volatiles were removed under vacuum and basic D_2O (pD = 13.4) was added to the residue. The ^{13}C NMR spectrum in D_2O showed the presence of a signal at 168 ppm assigned to CO_3^{2-}. A reproducible yield in carbonate of 98(5)% (calculated with respect to the reaction of **1-py** with 6 CO_2 molecules) was measured by quantitative $^{13}C\{^1H\}$ NMR spectroscopy using a labelled $CH_3{}^{13}COONa$ solution as an internal standard. No dependence of the yield in carbonate from the concentration of **3-py** was found.

For the reaction of **2-py** and **1-py** the same experimental procedure was followed except for the equivalents of carbon dioxide added to the tube.

Electrochemical characterization. Cyclic voltammetry data were carried out at room temperature in an argon-filled glovebox. All electroanalytic experiments were performed using a Princeton Applied Research Model 273 potentiostat or a Biologic SP-300 potentiostat. Glassy carbon working electrode (1 mm^2) was used. Non aqueous Ag/AgCl pseudo reference was generated by depositing AgCl on a silver wire surface by oxidation with dilute aqua regia and was confined a glass capillary provided of glass wool septum and stored in a solution of the electrolyte prior to use. A Pt wire was used as counter electrode. All the CV experiments were performed in a modified scintillator vial as single channel cell with the cap modified with ports for the electrodes. All data were referenced to an internal standard ($FeCp_2^+/FeCp_2$).

All samples concentration was about 4 mM with 0.1 M [Bu_4N][PF_6] supporting electrolyte in pyridine solution.

References

1 J. S. Anderson, J. Rittle and J. C. Peters, *Nature*, 2013, **501**, 84–87.
2 I. Čorić and P. L. Holland, *J. Am. Chem. Soc.*, 2016, **138**, 7200–7211.
3 Y. Li, Y. Li, B. Wang, Y. Luo, D. Yang, P. Tong, J. Zhao, L. Luo, Y. Zhou, S. Chen, F. Cheng and J. Qu, *Nat. Chem.*, 2013, **5**, 320–326.
4 P. J. Chirik and K. Wieghardt, *Science*, 2010, **327**, 794–795.
5 P. J. Chirik, *Acc. Chem. Res.*, 2015, **48**, 1687–1695.
6 D. L. J. Broere, R. Plessius and J. I. van der Vlugt, *Chem. Soc. Rev.*, 2015, **44**, 6886–6915.
7 G. N. George, C. Costa, J. J. G. Moura and I. Moura, *J. Am. Chem. Soc.*, 1999, **121**, 2625–2626.
8 J. W. Jurss, R. S. Khnayzer, J. A. Panetier, K. A. El Roz, E. M. Nichols, M. Head-Gordon, J. R. Long, F. N. Castellano and C. J. Chang, *Chem. Sci.*, 2015, **6**, 4954–4972.
9 D. Z. Zee, M. Nippe, A. E. King, C. J. Chang and J. R. Long, *Inorg. Chem.*, 2020, **59**, 5206–5217.
10 G. Nocton and L. Ricard, *Chem. Commun.*, 2015, **51**, 3578–3581.
11 E. B. Hulley, P. T. Wolczanski and E. B. Lobkovsky, *J. Am. Chem. Soc.*, 2011, **133**, 18058–18061.
12 G. Nocton, W. W. Lukens, C. H. Booth, S. S. Rozenel, S. A. Medling, L. Maron and R. A. Andersen, *J. Am. Chem. Soc.*, 2014, **136**, 8626–8641.
13 M. J. Monreal and P. L. Diaconescu, *J. Am. Chem. Soc.*, 2010, **132**, 7676–7683.
14 F. Franceschi, E. Solari, C. Floriani, M. Rosi, A. Chiesi-Villa and C. Rizzoli, *Chem. - Eur. J.*, 1999, **5**, 708–721.
15 C. Floriani, E. Solari, F. Franceschi, R. Scopelliti, P. Belanzoni and M. Rosi, *Chem. - Eur. J.*, 2001, **7**, 3052–3061.
16 S. De Angelis, E. Solari, E. Gallo, C. Floriani, A. Chiesi-Villa and C. Rizzoli, *Inorg. Chem.*, 1996, **35**, 5995–6003.
17 S. Gambarotta, F. Urso, C. Floriani, A. Chiesi-Villa and C. Guastini, *Inorg. Chem.*, 1983, **22**, 3966–3972.
18 Sandro Gambarotta,a Mazinella Mazzanti,a Carlo Floriani, and Margareta Zehnder, *Chem. Commun.*, 1984, **730**, 3.
19 E. Solari, C. Maltese, F. Franceschi, C. Floriani, A. Chiesi-Villa and C. Rizzoli, *J. Chem. Soc. Dalton Trans.*, 1997, 2903–2910.
20 E. Gallo, E. Solari, N. Re, C. Floriani, A. Chiesi-Villa and C. Rizzoli, *J. Am. Chem. Soc.*, 1997, **119**, 5144–5154.
21 C. Camp, V. Mougel, P. Horeglad, J. Pécaut and M. Mazzanti, *J. Am. Chem. Soc.*, 2010, **132**, 17374–17377.
22 C. Camp, V. Guidal, B. Biswas, J. Pécaut, L. Dubois and M. Mazzanti, *Chem. Sci.*, 2012, **3**, 2433.
23 C. Camp, J. Andrez, J. Pécaut and M. Mazzanti, *Inorg. Chem.*, 2013, **52**, 7078–7086.
24 C. Camp, D. Toniolo, J. Andrez, J. Pécaut and M. Mazzanti, *Dalton Trans.*, 2017, **46**, 11145–11148.
25 N. Jori, M. Falcone, R. Scopelliti and M. Mazzanti, *Organometallics*, 2020, **39**, 1590–1601.
26 J. Andrez, V. Guidal, R. Scopelliti, J. Pécaut, S. Gambarelli and M. Mazzanti, *J. Am. Chem. Soc.*, 2017, **139**, 8628–8638.
27 E. V. Eames, T. D. Harris and T. A. Betley, *Chem Sci*, 2012, **3**, 407–415.
28 A. Nabei, T. Kuroda-Sowa, T. Shimizu, T. Okubo, M. Maekawa and M. Munakata, *Polyhedron*, 2009, **28**, 1734–1739.
29 C. R. Hess, T. Weyhermüller, E. Bill and K. Wieghardt, *Angew. Chem. Int. Ed.*, 2009, **48**, 3703–3706.

30 A. K. Bartholomew, J. J. Teesdale, R. Hernández Sánchez, B. J. Malbrecht, C. E. Juda, G. Ménard, W. Bu, D. A. Iovan, A. A. Mikhailine, S.-L. Zheng, R. Sarangi, S. G. Wang, Y.-S. Chen and T. A. Betley, *Proc. Natl. Acad. Sci.*, 2019, **116**, 15836–15841.
31 A. S. Yang and B. J. Gaffney, *Biophys. J.*, 1987, **51**, 55–67.
32 M. Adelhardt, M. J. Chalkley, F. W. Heinemann, J. Sutter, A. Scheurer and K. Meyer, *Inorg. Chem.*, 2014, **53**, 2763–2765.
33 P. Power, *J. Am. Chem. Soc.*, 2007, **129**, 8396–8396.
34 C. M. Zall, D. Zherebetskyy, A. L. Dzubak, E. Bill, L. Gagliardi and C. C. Lu, *Inorg. Chem.*, 2012, **51**, 728–736.
35 L. Fohlmeister, S. Liu, C. Schulten, B. Moubaraki, A. Stasch, J. D. Cashion, K. S. Murray, L. Gagliardi and C. Jones, *Angew. Chem. Int. Ed.*, 2012, **51**, 8294–8298.
36 T. M. Powers, A. R. Fout, S.-L. Zheng and T. A. Betley, *J. Am. Chem. Soc.*, 2011, **133**, 3336–3338.
37 J. M. Smith, A. R. Sadique, T. R. Cundari, K. R. Rodgers, G. Lukat-Rodgers, R. J. Lachicotte, C. J. Flaschenriem, J. Vela and P. L. Holland, *J. Am. Chem. Soc.*, 2006, **128**, 756–769.
38 Y. Sanakis, S. J. Yoo, F. Osterloh, R. H. Holm and E. Münck, *Inorg. Chem.*, 2002, **41**, 7081–7085.
39 R. Hernández Sánchez, A. K. Bartholomew, T. M. Powers, G. Ménard and T. A. Betley, *J. Am. Chem. Soc.*, 2016, **138**, 2235–2243.
40 R. Hernández Sánchez and T. A. Betley, *J. Am. Chem. Soc.*, 2015, **137**, 13949–13956.
41 Q. Zhao, T. D. Harris and T. A. Betley, *J. Am. Chem. Soc.*, 2011, **133**, 8293–8306.

Chapter 4 Carbon dioxide reduction by lanthanide(III) complexes supported by redox-active Schiff base ligands.‡

Introduction

The redox-chemistry of lanthanide complexes has attracted increasing attention in recent years because of the unique reactivity of Ln(II) ions in small molecule activation and in particular their ability to reduce N_2, CO_2 or CO.[1,2] However, lanthanides can only undergo one electron transfer processes and therefore reduction of CO_2 or other small molecules (N_2, CO) can only occur by simultaneous electron transfer by several mononuclear complexes[3-8] or by suitably designed polynuclear compounds.[9-11]

An alternative approach for implementing multielectron transfer in lanthanide complexes takes advantage of redox-active ligands for the storage and release of electrons. Redox-active ligands are increasingly used across the periodic table to facilitate metal-based multielectron transfer reactivity and catalytic activity.[12-18] Redox-active ligands can either directly store electrons during reactivity by forming stable radicals or through the formation of new reversible C-C bonds in the ligand backbone.[19,20,21,22,23]

Recently it has been shown that multiple redox state can become accessible to lanthanides when associated to redox active ligand.[21,22,24-29] Those ligand were also found to provide a pathway for magnetic coupling in Ln(III) chemistry leading to molecular magnet behaviour,[30,31] and were also found to enable redox-switchable catalysis in rare-earth promoted polymerization chemistry.[32,33] However only two systems reported in literature show that the electrons stored in the ligand scaffold of lanthanide complexes can be used for the reductive transformation of substrates such as S8, Se or 9,10-phenanthrenequinone.[34,35]

The ability of Schiff bases to act as electrons reservoirs and to enable the multi-electrons reduction of small molecules such as carbon dioxide has been identified in complexes of d block metals[36-43] and more recently in complexes of uranium.[19,44-46]

---

‡ This chapter is part of a paper: Nadir Jori, Davide Toniolo, Bang C. Huynh, Rosario Scopelliti and Marinella Mazzanti, "*Carbon dioxide reduction by lanthanide(III) complexes supported by redox-active Schiff base ligands*", in submission.

Authors contributions: B.C.H. performed the preliminary experiments and obtained the structure of **4-Ln** and **3-Eu**, N.J. obtained the structure of **2-Nd**, optimized its synthesis, D.T. obtained the structure of **2-Sm** and optimized the synthesis of **4-Ln**, **3-Eu** and **2-Sm** and performed the reactivity with carbon dioxide together with N.J.. R.S. performed the X ray analysis and M.M. originated the central idea and coordinated the work. MM and NJ wrote the manuscript.

In contrast, the use of Schiff base ligands in lanthanide chemistry has been essentially limited to Ln(III) complexes that have found application as catalysts[47] and as efficient Near-IR and visible luminescence emitters,[48-50] and have shown attractive physical properties.[51-53] However, the reductive chemistry of lanthanide Schiff base complexes remains so far practically unexplored.[29,34,54] Our group recently demonstrated that the tetradentate salophen Schiff base (salophen: N,N′-disalicylidene-o-phenylenediaminate) acts as redox active ligands also when combined to lanthanide ions.[34] Notably we showed that the reduction of mono-ligand and bis-ligand Ln(III) complexes of salophen leads to results in the reduction of the imino groups of the ligand followed by formation of intermolecular or intramolecular C–C bonds (Scheme 1). The electrons stored in the C-C bonds could be used in the reduction of I_2 or 9,10-phenanthrenequinone but could not affect the reduction of less reactive substrates.

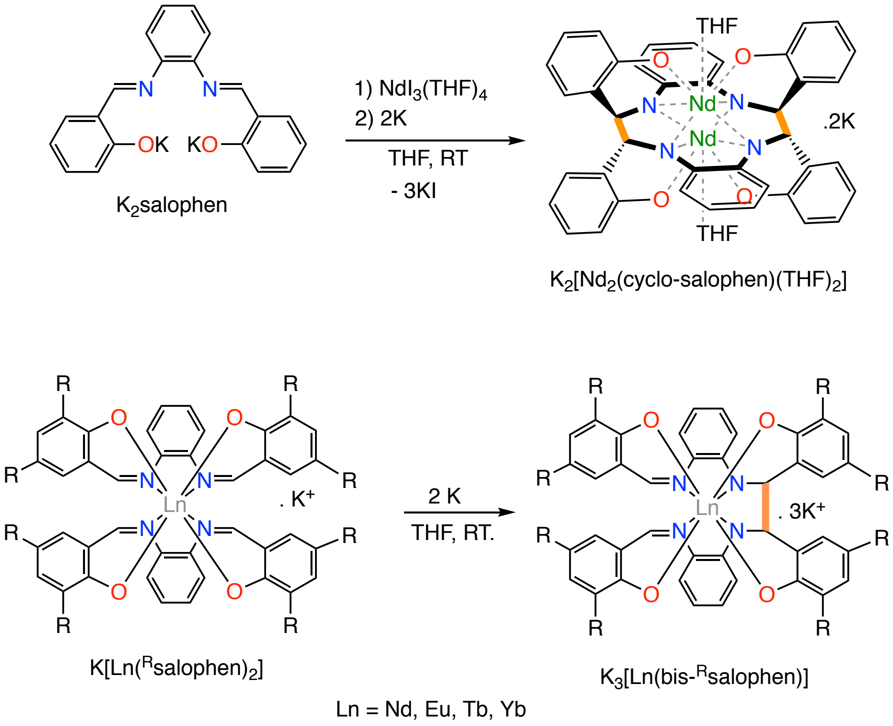

Scheme 1. The two-electron reduction of mono- (top) and bis-(bottom) Schiff base complexes of Nd(III) with alkali metals leads to intermolecular (top) or intramolecular C–C bond formation(bottom). The electrons stored in the C–C bonds can be used to reduce oxidizing substrates

Here we report the reductive chemistry of the Ln(III) complexes of the tripodal trianionic heptadentate Schiff base H_3trensal (2,2’,2”-tris(salicylideneimino)triethylamine), [Ln^{III}(trensal)], **1-Ln** (Ln=Sm, Nd, Eu). [Ln^{III}(trensal)] complexes have been synthesised and crystallographically characterized for a wide range of ions because of the interest for their magnetic properties,[51-53,55] but their reductive chemistry was never explored. Here we show that the reduction of the [Eu^{III}(trensal)] leads to the Eu(II) analogue. In contrast the one and two electron reduction of the [Nd^{II}(trensal)] and [Sm^{III}(trensal)] leads to the intermolecular reductive coupling of the imino groups of the trensal ligand and formation of one and two C-C bonds leaving the metal centre in the +3 oxidation state in a similar way for what it as recently found for U(IV) (Scheme 2).[46] The resulting reduced complexes are able to promote the reductive disproportionation of carbon dioxide by transferring the electrons stored in the C-C bonds to the CO$_2$ to selectively afford carbonate and CO. The selectivity of the reaction differs significantly with the formation of multiple CO$_2$ reduction products previously reported for a U(IV) system.

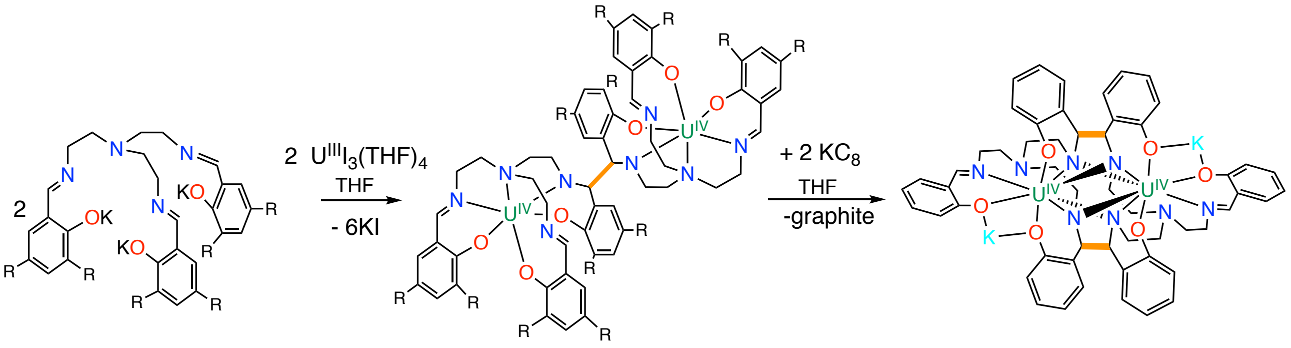

K$_3$trensal [U$_2$(bis-trensal)] [K$_2$U$_2$(cyclo-trensal)]

Scheme 2. Synthesis of [U$_2$(bis-^{R}trensal)] and [K$_2$U$_2$(cyclo-^{R}trensal)].

Results and discussion

Reduction of [Ln(trensal)] complexes.

1-Ln were prepared using a salt metathesis procedure where one equiv. of trensalK$_3$ salt was reacted with the anhydrous [LnX$_3$] (Ln = Sm, Eu, Nd; X = Cl, I) precursors in THF. This procedure, previously used in the synthesis of the [U^{IV}(trensal)I] complex,[56] prevents the use of protic solvents and avoid the presence of water or protic solvents in the isolated complexes.[57] The formation of **1-Ln** via salt metathesis was confirmed by 1H NMR spectroscopy (Figure S1-S3)

The "in situ" addition of one equivalent of KC$_8$ to the reaction mixture obtained from the reaction of K$_3$trensal with [LnX$_3$] in THF afforded the complexes [{K(THF)$_3$}$_2$Ln$_2$(bis-trensal)], **2-Ln** in 70 % (Ln = Sm) and 53% (Ln = Nd) yield (Scheme 3). Alternatively, **2-Sm** can also be synthetized from the reaction of the divalent [SmI$_2$] with one equiv. of the ligand salt.

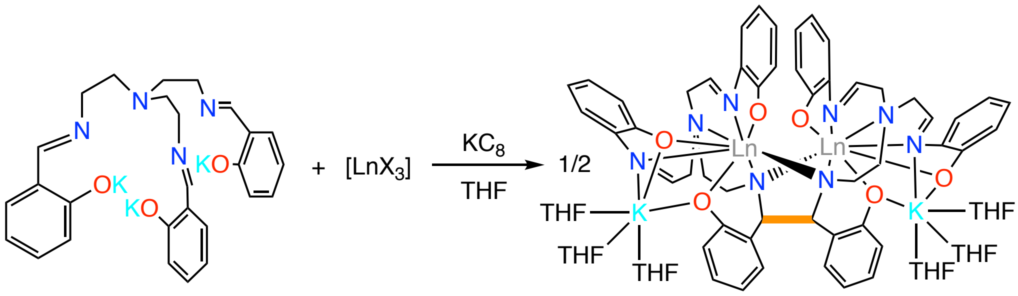

K_3trensal

[{K(THF)$_3$}$_2$Ln$_2$(bis-trensal)], **2-Ln**

Scheme 3. Synthesis of [{K(THF)$_3$}$_2$Ln$_2$(bis-trensal)], **2-Ln**, Ln = Nd, Sm.

The two dimeric **2-Nd** and **2-Sm** complexes crystallize in the C2/c group and are isostructural. Their solid state structure shows the presence of two neodymium(III) (Figure 1) and samarium(III) (Figure S9) cations coordinated by the octa-anionic bis-trensal ligand, formed by C–C coupling of the two imino groups of the original trensal ligands. The formation of the bis-trensal ligand was previously reported by our group from the reduction of the trensal ligand by UI_3 yielding the [U^{IV}_2(bis-trensal)] complex.[46] The resulting dinucleating ligand in **2-Ln** holds the two metal centres in close proximity (Nd–Nd = 3.8922(3)Å and Sm–Sm = 3.8389(4) Å) (Table 1).

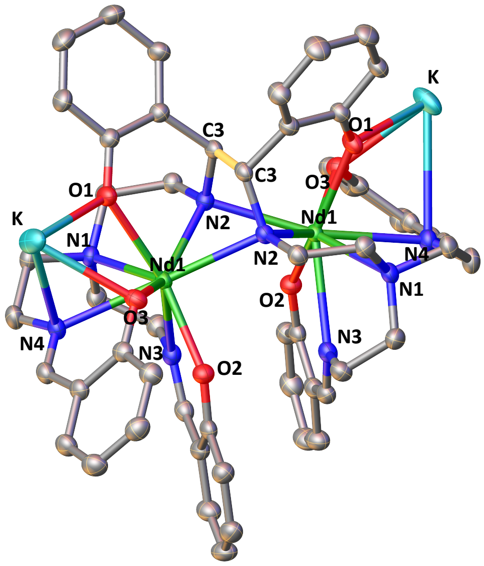

Figure 1. Molecular structure of complex **2-Nd** (C-C bond between imine highlighted in yellow, 50% probability ellipsoids). Hydrogen atoms and coordinated solvent molecules have been omitted for clarity.

The **2-Ln** complexes present two equivalent octacoordinated Ln centres coordinated by two imino nitrogen (avg Ln–N$_{im}$ = 2.67(4) Å for Nd and 2.63(5) Å for Sm), one amino nitrogen (Ln–N$_{am}$= 2.782(2) Å for Nd and 2.745(4)Å for Sm), two bridging amido nitrogen (Ln–N$_{amido}$= 2.478(2) Å for

Nd and 2.50(7) Å for Sm) and three phenoxide oxygen atoms (average Ln–O = 2.38(4) Å for Nd and 2.36(4) Å) of the bis-trensal ligand. Two of the phenoxide oxygen atoms (O1 and O3) coordinate a potassium cation, together with three molecules of THF.

The structural parameters of **2-Ln** (Table 1) clearly show that the reduction has occurred on the imino groups of the ligands rather than on the metal ions. The values of the C–C bond distance (1.573(6) Å for **2-Nd** and 1.586(7) for **2-Sm**) compares well with the intermolecular C–C bonds found in the previously reported [Na_2U(bis-salophen)][19] (1.559(7) Å), K_3[Nd(bis-salophen))][34] (1.56(2) Å) and [U_2(bis-^{tBu}trensal)][46] (1.59(2) Å). The C–N_{amido} bond distances (1.487(4) Å for **2-Nd** and 1.485(5) Å for **2-Sm**) of the ligand backbone are much longer than C–N_{imino} distances (1.287(2) Å for **2-Nd** and 1.288(6) Å for **2-Sm**) in the same complex. The Ln–N_{amido} distances for **2-Nd** (2.48(7) Å) and **2-Sm** (2.50(7) Å) are also shorter than the Ln-N_{imino} distances (2.573 (4) Å and 2.531(4) Å, respectively) for **1-Ln**, supporting the reductive coupling of two imino moieties from different trensal units. These distances compare well with the values reported for [Nd(bis-salophen)]$^{3-}$ (Nd–N_{am} (2.45(2) Å) and Nd–N_{im} (2.64(4) Å).

Table 1. Mean values of selected bond lengths (Å) for the complexes presented in this and previous works.[34]

Complex	C-C	C-N_{imino}	C-N_{amido}	M-N_{imino}	M-N_{amido}	M-M
1-Nd	-	1.280(6)	-	2.573(4)	-	-
1-Sm	-	1.274(8)	-	2.531(4)	-	-
1-Eu	-	1.277(16)	-	2.535(7)	-	-
2-Nd	1.573(6)	1.287(2)	1.487(4)	2.67(4)	2.48(7)	3.8922(3)
[Nd(bis-salophen)]$^{3-}$	1.56(2)	1.29(2)	1.45(1)	2.64(4)	2.45(2)	-
2-Sm	1.586(7)	1.288(6)	1.485(5)	2.63(5)	2.50(7)	3.8389(4)
3-Eu	-	1.272(6)	-	2.63(5)	-	-
4-Nd	1.558(3)	1.273(3)	1.472(4)	2.6895(16)	2.6(1)	3.42619(19)
[Nd_2(cyclo-salophen)]$^{2-}$	1.622(3)	-	1.459(3)	-	2.416(9)	3.54(1)
4-Sm	1.560(6)	1.263(6)	1.470(3)	2.679(9)	2.61(12)	3.4077(4)

The ^{1}H NMR spectrum of **2-Nd** and **2-Sm** in THF-d8 (Figure 2, 3) show 25 and 22 signals respectively in the paramagnetic range, consistent with a fully asymmetric compound in solution.

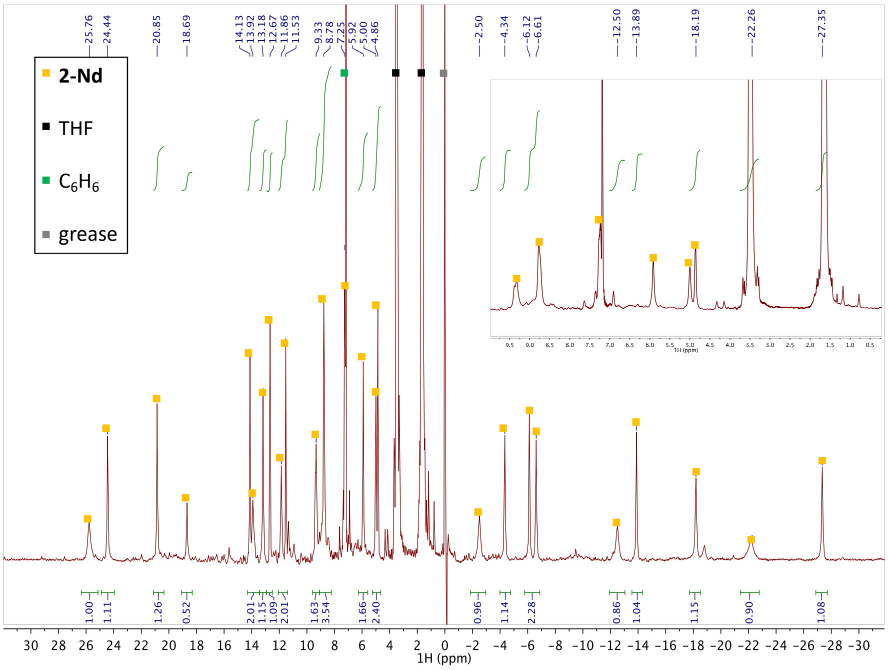

Figure 2. ^{1}H NMR spectrum of **2-Nd** in THF-d8 (THF-d8, 400 MHz, 298 K).

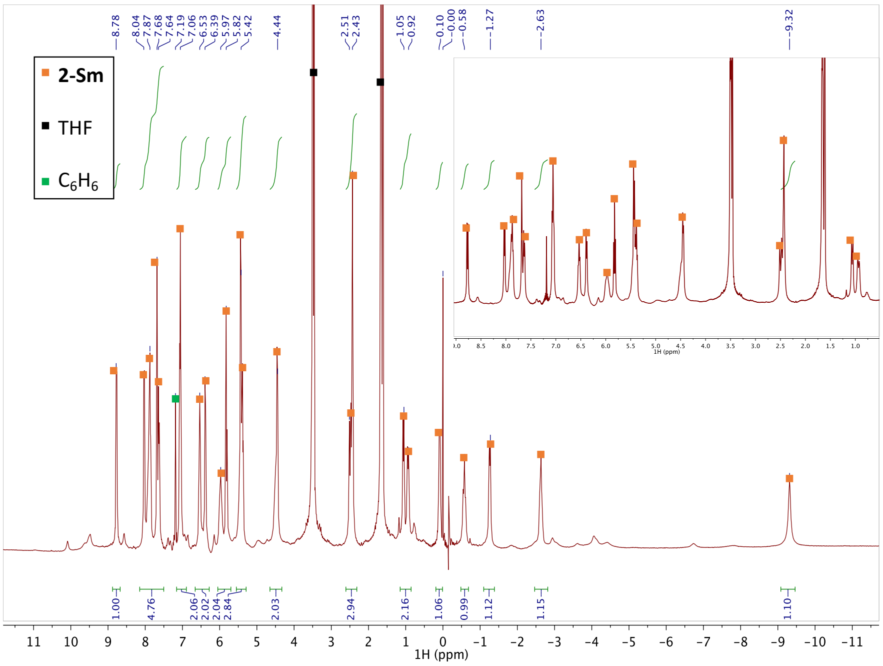

Figure 3. ^{1}H NMR spectrum of **2-Sm** in THF-d8 (THF-d8, 400 MHz, 298 K).

In contrast what observed with Nd and Sm the reduction of **1-Eu** did not afford the Eu(III) bis-trensal complex, but instead an Eu(II) complex of the trensal ligand $[\{K(\mu\text{-THF})(THF)_2\}_2\{Eu^{II}(trensal)\}_2]$, **3-Eu** (Scheme 4).

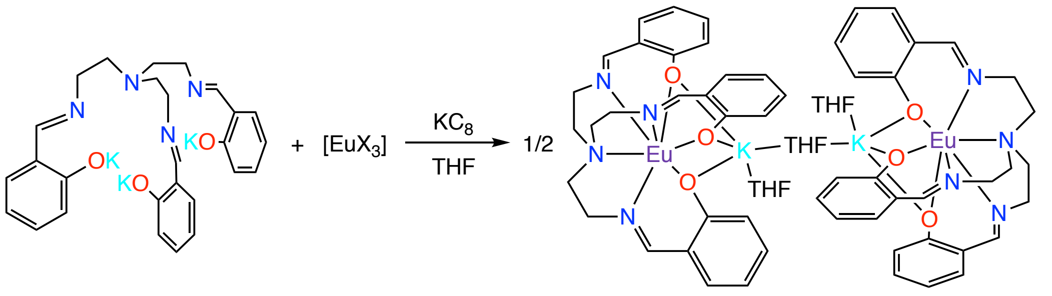

K_3trensal

[{K(μ-THF)(THF)$_2$}$_2${Eu^{II}(trensal)}$_2$], **3-Eu**

Scheme 4. Synthesis of [{K(μ-THF)(THF)$_2$}$_2${Eu^{II}(trensal)}$_2$], **3-Eu** (X = Cl, I, OTf).

No ^{1}H NMR spectrum was observed as expected for the 4f^7 configuration of Eu(II) .

The molecular structure of **3-Eu** (Figure 4) shows two potassium-bound [Eu(II)(trensal)] complexes bridged by a THF molecule. Each [Eu(II)(trensal)] moiety binds a potassium counterion trough three phenoxide oxygen atoms, the latter being also coordinated by one terminal THF molecule and one bridging the two [Eu(trensal)] moieties.

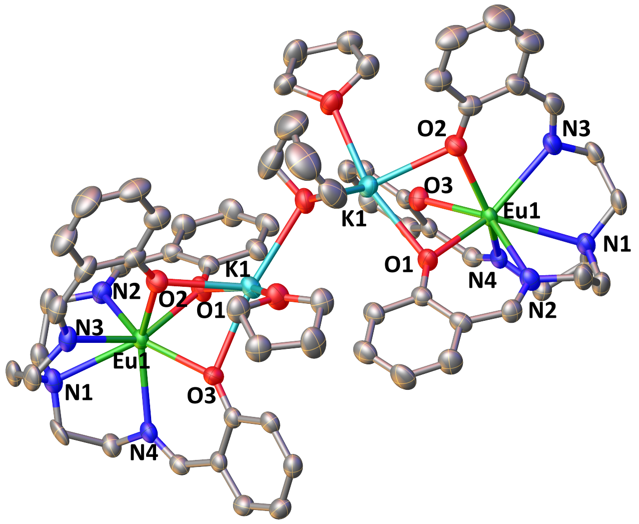

Figure 4. Molecular structure of complex **3-Eu** (50% probability ellipsoids). Hydrogen atoms were omitted for clarity.

The europium centres are heptacoordinated by the amino nitrogen (Eu–N$_{amino}$=2.826(4) Å), the three imino nitrogen (avg Eu–N$_{imino}$= 2.66(4) Å) and the three phenoxide oxygen atoms (avg Eu–O= 2.45(1) Å) from the trensal ligand. The average Eu–N and Eu–O distances are consistent with the formation of a divalent europium complex,[58] and the C–N distances (1.272(6) Å) remain unchanged compared to those found in the crystal structure of the H_3trensal ligand (average 1.266(3) Å).[59] The Eu-N distances are longer compared to those reported for the [Eu^{III}(trensal)] complex (Eu–N$_{amino}$=2.761(9) Å, Eu–N$_{imino}$=2.535(7) Å, Eu–O = 2.233(6) Å),[55] as expected for a metal centre in a lower oxidation state.

These results indicate that while for **1-Nd** and **1-Sm** the reduction of the ligand occurs before the reduction of the metal centre, in the case of **1-Eu** reduction occurs first on the metal centre, probably due to its lower redox potential (Eu^{3+}/Eu^{2+} = -0.35 V, Sm^{3+}/Sm^{2+} = -1.55 V, Nd^{3+}/Nd^{2+} = - 2.6 V). This result differs significantly from what was observed with the Eu(III) complex of the salophen Schiff base K[Eu(salophen)$_2$], where the reduction following the addition of alkali metal occurs on the ligand scaffold.[34] This indicate that the trensal ligand is better suited to stabilize the divalent oxidation state in europium compounds.

Complexes **2-Nd** and **2-Sm** can be further reduced in a controlled fashion by the addition of excess KC_8 (three equiv.) to the in situ synthetized [Ln(trensal)] in THF, affording the complexes [{K(THF)$_3$}$_4$Ln$_2$(cyclo-trensal)], **4-Ln** in 77 % (Ln = Sm) and 78 % (Ln = Nd) yield (Scheme 5). When the reduction was conducted with only 2 equiv. of KC_8 it yielded a mixture of **2-Ln** and **4-Ln**.

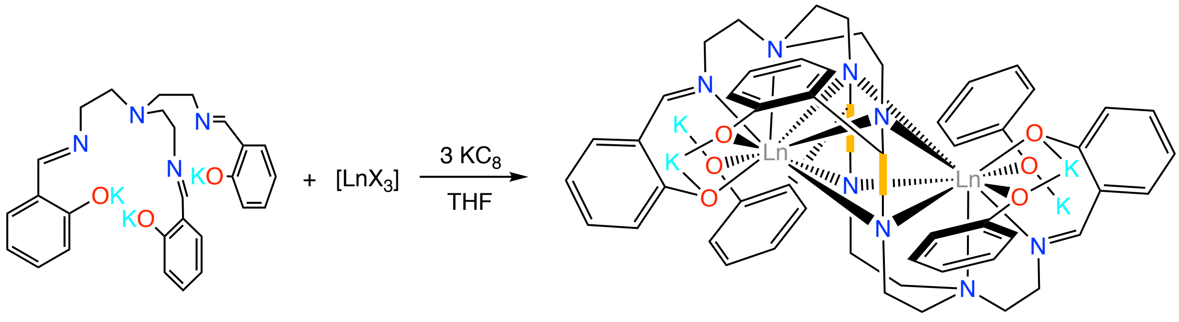

K$_3$trensal

[{K(THF)$_3$}$_4$Ln$^{III}_2$(cyclo-trensal)], **4-Ln**

Scheme 5. Synthesis of [{K(THF)$_3$}$_2${K(THF)}$_2$Ln$_2$(cyclo-trensal)], **4-Ln,** Ln = Nd, Sm (coordinated THF molecules have been omitted for clarity).

The two complexes **4-Nd** and **4-Sm** crystallize in the $P2_1/n$ group and are isostructural. The molecular structure of the **4-Ln** complexes shows the presence of two Nd(III) (Figure 5) or Sm(III) cations (Figure S10) bound by the dodecadentate decaanionic amidophenolate macrocyclic ligand cyclo-trensal produced in the reductive coupling of two imino groups of the trensal ligand. The dinucleating cyclo-trensal ligand in **4-Ln** holds the two Ln centres in close proximity, with a Ln-Ln distances of 3.42619(19) Å for Nd and 3.4077(4) Å for Sm, shorter than those found in **2-Ln** or in the macrocyclic complex [Nd$_2$(cyclo-salophen)]$^{4-}$ (Table 1).[34]

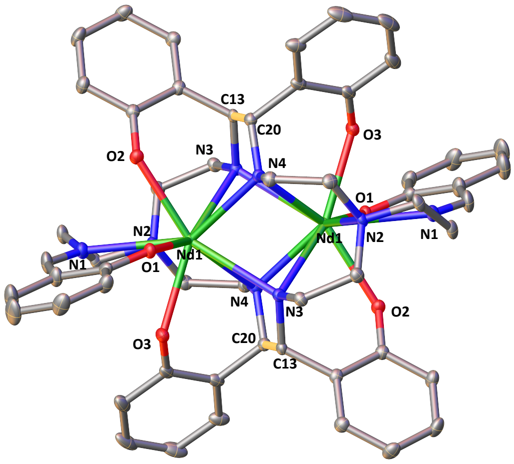

Figure 5. Molecular structure of complex **4-Nd** (C-C bonds between imine highlighted in yellow, 50% probability ellipsoids). Hydrogen atoms, potassium counterions and coordinated solvent molecules have been omitted for clarity.

The **4-Ln** complexes present two equivalent Ln(III) centres in a tricapped trigonal prismatic geometry nonacoordinated by four amido nitrogens (avg Ln–N_{amido}= 2.6 (1) Å for Nd and 2.61(12) Å for Sm), one imino nitrogen (Ln–N_{imino} = 2.6895(16) Å for Nd and 2.679(9) Å for Sm), one amino nitrogen (Ln–N_{amino} = 2.7209(15) Å for Nd and 2.706(3) Å) and three phenoxide oxygen atoms (avg Ln–O = 2.47(1) Å for Nd and 2.45(1) Å for Sm). The six phenoxide oxygen atoms coordinate also four potassium counterions, whose coordination sphere is completed by three THF molecules.

When comparing the selected bond distances shown in Table 1, the C–N_{amido} bond distances (mean C–N_{am} = 1.472(4) Å for Nd and 1.470(3) Å for Sm) of the ligand backbone are much longer than those of the remaining imino group (C–N_{imino} = 1.273(3) Å for Nd and 1.263(6) Å for. Sm) or the values observed for the free ligand (avg. C-N_{im}=1.266(3) Å).[59] These data are in agreement with the presence of four amido groups. The value of the C–C bond distances (1.558(3) Å for Nd and 1.560(3) Å for Sm) fall again in the range of those reported for the intermolecular and intramolecular C–C bonds in [Na_2U(bis-salophen)] (1.559(7) Å),[19] [Nd_2(cyclo-salophen)]$^{2-}$ (1.622(3) Å)[34] and [Nd(bis-salophen))]$^{3-}$ (1.56(2) Å).[34]

The ^{1}H NMR spectra of **4-Nd** and **4-Sm** (Figure 6 and 7 respectively) show only one set of 11 and 14 signals respectively, suggesting the presence of D2h symmetric solution species in agreement with the observed D2h pseudo-symmetry of the solid state structure.

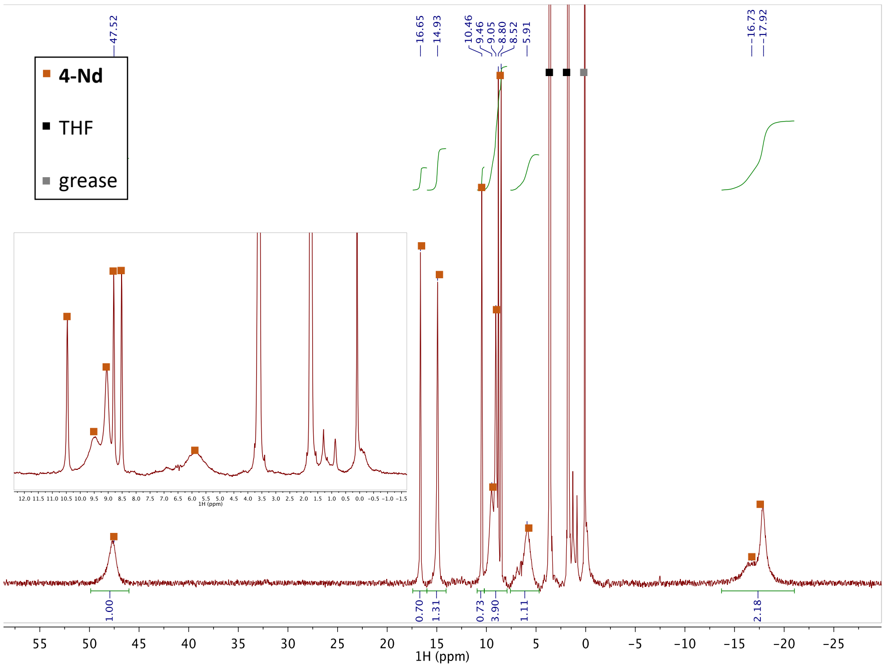

Figure 6. ^{1}H NMR spectrum of **4-Nd** in THF-d8 (THF-d8, 400MHz, 298 K).

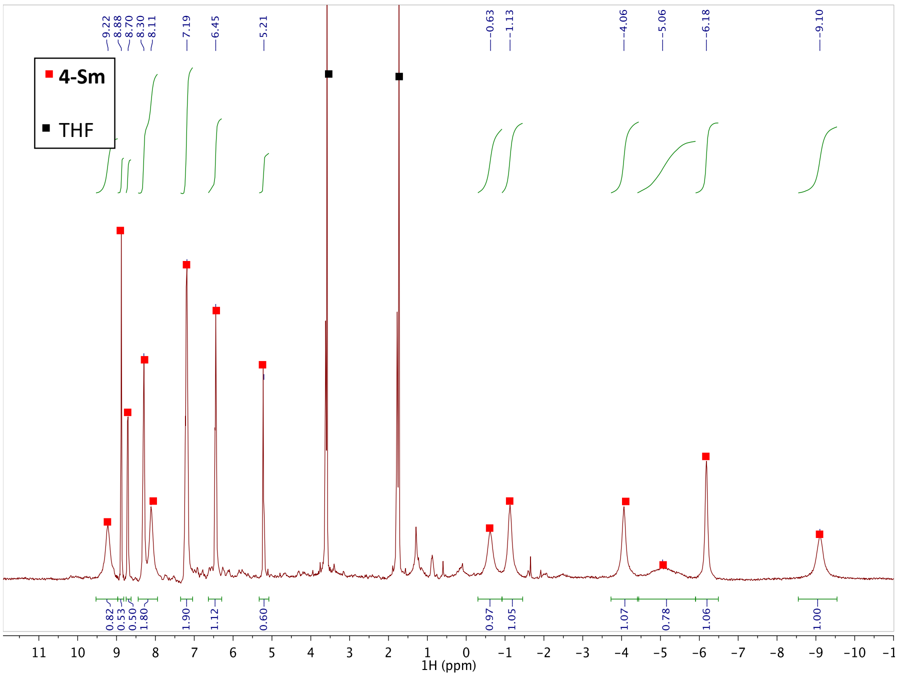

Figure 7. ^{1}H NMR spectrum of **4-Sm** in THF-d8 (THF-d8, 400MHz, 298 K).

CO_2 reduction studies

The **2-Ln** complexes present two electrons stored in the C–C bond of the bis-trensal ligand as found for the previously reported K_3[Ln(bis-^{R}salophen)] complexes.[34] It was shown that the electrons in the K_3[Ln(bis-^{R}salophen)] are available for the reduction of oxidizing substrates such as Ag^+, molecular iodine or 9,10-phenanthrenequinone. However, the K_3[Ln(bis-^{R}salophen)] complexes could not affect the reduction of carbon dioxide.

Differently, **2-Ln** react rapidly and irreversibly with carbon dioxide. The addition of 2 equiv. of CO_2 to a THF solution **2-Ln** resulted in a colour change of the solution from yellow/orange to pale yellow, with the concomitant formation of an insoluble product. The ^1H NMR spectra recorded after the formation of the solid products showed the disappearance of the signals assigned to **2-Ln**. The low solubility of the precipitate formed in the reaction mixture preclude a quantitative analysis od the product via NMR spectroscopy. However, in the case of **2-Nd**, the ^1H NMR spectrum of the precipitate in py-d5 after the separation from the supernatant showed a set of seven signal that resemble the one found for **1-Nd**. Quantitative $^{13}C\{^1H\}$ NMR spectra recorded in basic D_2O (pD = 13.4) in presence of $^{13}AcO^-$ as internal standard showed the formation of $^{13}CO_3^{2-}$ in about 100 % conversion for both **2-Ln** complexes (Figure S5, S7). (Scheme 6 top).

The presence of carbonate indicated that the electrons stored in C–C bond in complexes **2-Ln** can affect the reductive disproportionation of CO_2, showing a significant increase in reactivity towards CO_2 compared to the one of K_3[Nd(bis-^{R}salophen)]. The reactivity of **2-Ln** differs also from that of the recently reported U(IV) analogue, [U_2(bis-trensal)], that only undergoes insertion of the CO_2 into the U-N bond.

The difference in reactivity between the **2-Ln** complexes and the [U_2(bis-trensal)] maybe explain considering the different bridging mode adopted by the amido nitrogen in **2-Ln,** that may results in a less basic character compared to the non-bridging amido nitrogen in [U_2(bis-trensal)] preventing the insertion of CO_2 into the Ln-N_{amido} bond. Moreover, the close proximity of the Ln centres in the **2-Ln** centres should promote CO_2 activation via cooperative binding to the two metal centres.

In contract to **2-Ln**, complex **3-Eu** did not show any reactivity with CO_2.

In a similar way, the reactivity of **4-Ln** with carbon dioxide was tested and compared with the previously reported K_2[Nd_2(cyclo-salophen)] and [$\{K(THF)_3\}_2U_2$(cyclo-trensal)]. Like in the previous case, the K_2[Nd_2(cyclo-salophen)] complexes were found able to transfer the four electrons stored in the two C-C bonds but it was not able to reduce CO_2 or CS_2. In contrast we found that **4-Ln** display a significant increased reactivity towards CO_2. The addition of 4 equiv. of CO_2 to a solution of **4-Ln** in THF leads to an immediate colour change of the solution from red/orange to pale yellow with concomitant formation of a precipitate. The ^1H NMR spectra recorded after formation of the solid products showed the disappearance of the signals assigned to **4-Ln**. The ^{13}C NMR spectra recorded after one day showed the formation of ^{13}CO (181 ppm) as only visible product in THF solution (Figure S3).

The quantitative $^{13}C\{^1H\}$ NMR spectra recorded in presence of $^{13}AcO^-$ as internal standard (Figure S6, S8) showed the formation of $^{13}CO_3^{2-}$ in 97 % (Ln = Sm) and 100 % conversion (Ln = Nd) (Scheme 6 bottom).

These results show that the four electrons stored in the two C-C bonds of the cyclo-trensal ligands are quantitatively used for the reductive disproportionation of CO_2. The clean quantitative reductive disproportionation effected by the **4-Ln** complexes contrasts remarkably with the multiple reaction pathways previously reported for the reaction of the analogue U(IV) complex $[\{K(THF)_3\}_2U_2$(cyclo-trensal)] with CO_2. Such pathways included reductive disproportionation of CO_2, insertion of CO_2 in the U–N_{amido} bonds, CO_2 cleavage and further addition of the formed CO to the U–N_{amido} bonds.

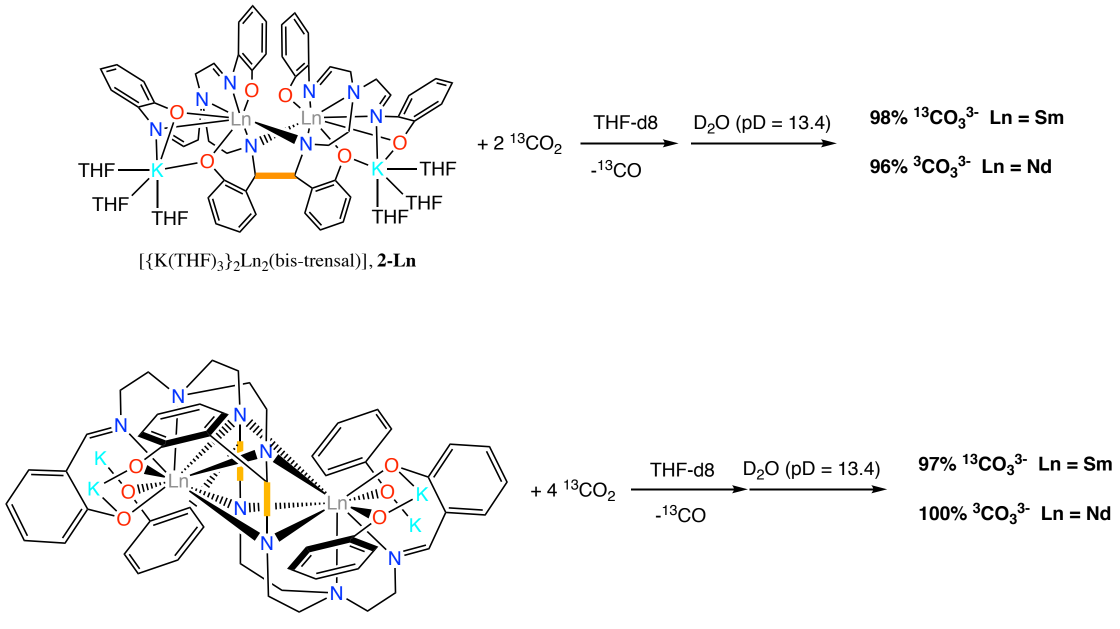
+ 2 $^{13}CO_2$
THF-d8
-^{13}CO
D_2O (pD = 13.4)
98% $^{13}CO_3^{3-}$ Ln = Sm
96% $^{3}CO_3^{3-}$ Ln = Nd
+ 4 $^{13}CO_2$
THF-d8
-^{13}CO
D_2O (pD = 13.4)
97% $^{13}CO_3^{3-}$ Ln = Sm
100% $^{3}CO_3^{3-}$ Ln = Nd

$[\{K(THF)_3\}_2Ln_2$(bis-trensal)], **2-Ln**

$[\{K(THF)_3\}_4Ln^{III}_2$(cyclo-trensal)], **4-Ln**

Scheme 6. Reactivity of **2-Ln** (top) and **4-Ln** (bottom) with 2 and 4 equiv. of $^{13}CO_2$, respectively.

Conclusion

In this work we studied the reductive chemistry of Ln complexes supported by trensal ligand. Like it was found for other kind of Schiff base, the trensal ligand is capable of acting as redox active ligand, storing electrons in one or two C-C bonds and maintaining the oxidation state of the metal centres unchanged. We have demonstrated that the reduced compounds are able to release the electrons to relatively inert substrates like CO_2, forming selectively carbonate and carbon monoxide. This characteristic makes the compounds presented here unique, being the first example of lanthanides supported by Schiff base capable of reducing carbon dioxide. Another difference from the [Ln(^{R}salophen)] derivatives equivalents is that the redox processes are sensitive to the nature of the Ln ion, reducing the ligand in the cases of Nd and Sm, and the metal in the case of Eu. Since the electronic properties of Schiff base are easily tuneable by adding substituent on the phenyl rings, a variety of ligands can be synthesized to afford lanthanide complexes with optimized redox properties. Future studies will be directed to investigate the influence of the ligand substituents on the redox properties with the final objective of perform electrocatalytic reduction of carbon dioxide.

Experimental

Materials and methods

General Considerations Unless otherwise noted, all manipulations were carried out at ambient temperature under an inert argon atmosphere using Schlenk techniques and an MBraun glovebox equipped with a purifier unit. The water and oxygen levels were always kept at less than 1 ppm. Glassware was dried overnight at 150°C before use.

NMR experiments were carried out using NMR tubes adapted with J. Young valves. ^{1}H and ^{13}C NMR spectra were recorded on a Bruker 400 MHz spectrometer. NMR chemical shifts are reported in ppm with solvent residual signal as internal reference.

Elemental analyses were performed using a Thermo Scientific Flash 2000 Organic Elemental Analyzer at the Institute of Chemistry and Chemical Engineering at EPFL.

Starting materials Unless otherwise noted, reagents were purchased from commercial suppliers and used without further purification. The solvents were purchased from Aldrich or Cortecnet (deuterated solvents) in their anhydrous form, conditioned under argon and vacuum distilled from K/benzophenone (toluene, hexane, pyridine and THF). Depleted uranium was purchased from Ibilabs, Florida, USA. The ligand K_3trensal ligand salt were prepared according to the published procedures.[56] $^{13}CO_2$ (93.13% ^{13}C) was purchased from Cortecnet and transferred prior to use in a flask in equipped with a Young valve and containing activated 3 Å molecular sieves.[LnX_3] (Ln = Eu, Sm, Nd; X = Cl, I, OTf) were purchased from Sigma Aldrich and used without purification. [SmI_2] was purchased from Sigma Aldrich.

Synthetic procedures

[Ln(trensal)] were prepared by reacting 1 equiv. of K_3trensal salt with the anhydrous [LnX_3] (Ln =Sm, Eu, Nd; X = Cl, I, OTf) precursors in THF. Because of the low solubility of the **1-Ln** complexes in THF we did not attempt to separate of the potassium salts, and resulting crude mixture was used as such for further reduction. The **1-Ln** complexes were characterized by ^{1}H NMR spectroscopy.

[Nd(trensal)], **1-Nd**. ^{1}H NMR (py-d5, 400 MHz, 298 K) δ =27.20 (s, 3H), 11.28 (s, 3 H), 9,29 (s, 3H), 8.14 (s, 3H), 7.28 (s, 3H), 4.15 (s, 6H) and -5.28 (s, 6H).

[Sm(trensal)], **1-Sm**. ^{1}H NMR (py-d5, 400 MHz, 298 K) δ =8.11 (d, 3H), 7.68 (s, 3H), 7,13 (t, 3H), 6.83 (t, 3H), 6.79 (d, 3H), 3.02 (s, 6H) and -0.42 (s, 6H).

[Eu(trensal)], **1-Eu**. ^{1}H NMR (py-d5, 400 MHz, 298 K) δ =9.12 (s, 6H), 7.18 (s, 3 H), 5.68 (s, 3H), 3.84 (s, 3H), 3.09 (s, 3H), 1.36 (s, 6H) and -23.78 (s, 3H).

Synthesis [{K(THF)$_3$}$_2$Nd$_2$(bis-trensal)], 2-Nd. An off-white suspension of trensalK$_3$ (86.0 mg, 0.150 mmol, 1 equiv.) in THF (2.0 mL) was added to the light green solid [NdI$_3$(THF)$_4$] (78.9 mg, 0.150 mmol, 1 equiv.) and the resulting suspension was stirred for 4 h at room temperature affording an off-white suspension. A bronze suspension of KC$_8$ (20.2 mg, 0.150 mmol, 1 equiv.) in THF. (1.0 mL) was added and the reaction mixture was stirred at room temperature for 4 h. The resulting dark suspension was filtered at room temperature to remove the graphite and the KI formed during the reaction, yielding a yellow-orange solution. The solution was concentrated until approx. 1.5 mL. Slow diffusion of hexane into the solution resulted in the formation after 3 days of yellow coloured X-ray quality crystals in 53 % yield (49.5 mg). ^{1}H NMR (THF-d8, 400 MHz, 298 K) δ = 25.76 (s, 2H), 24.44 (s, 2H), 20.85(s, 2H), 18.69(s, 2H), 14.13 (s, 2H), 13.92 (s, 2H), 13.18 (s, 2H), 12.67 (s, 2H), 11.89 (s, 2H), 11.83 (s, 2H), 9.33 (s, 2H), 8.78 (s, 4H), 7.25 (s, 4H), 5.92 (s, 2H), 5.00 (s, 2H), 4.86 (s, 2H), -2.50 (s, 2H), -4.34 (s, 2H), -6.12 (s, 2H), -6.61 (s, 2H), -12.50 (s, 2H), -13.89 (s, 2H), -18.19 (s, 2H), -22.26 (s, 2H), -27.35 (s, 2H). Elem. anal. calc. (%) for [K$_2$Nd$_2$(bis-trensal)]: C, 50.76%; H, 4.26%; N, 8.77%. Found: C, 50.38%; H, 4.26%; N, 8.36%.

Synthesis [{K(THF)$_3$}$_2$Sm$_2$(bis-trensal)], 2-Sm. An off-white suspension of trensalK$_3$ (43.4 mg, 0.0753 mmol, 1 equiv.) in THF (2.5 mL) was added to a suspension of [SmI$_3$] (40 mg, 0.0753 mmol, 1 equiv.) in THF (2.5 mL). The resulting off-white suspension was stirred at room temperature for 4 h affording a pale yellow suspension. Then a bronze suspension of KC$_8$ (10.1 mg, 0.0753 mmol, 1 equiv.) in THF (1.0 mL) was added and the reaction mixture was stirred at room temperature for 4 h. The resulting dark grey suspension was filtered to remove the graphite and the KI formed during the reaction, yielding a pale orange solution. Slow diffusion of hexane into the solution afforded 38 mg of compound (70 % yield). ^{1}H NMR (THF-d8, 400 MHz, 298 K) δ = 8.78 (s, 2H), 8.04 (s, 2H), 7.87 (s, 2H), 7.68 (s, 2H), 7.64 (s, 2H), 7.19 (s, 2H), 7.06 (s, 4H), 6.53 (s, 2H), 6.39 (s, 2H), 5.97 (s, 2H), 5.82 (s, 2H), 5.42 (s, 6H), 4.44 (s, 4H), 2.51 (s, 2H), 2.43 (s, 4H), 1.05 (s, 2H), 0.92 (s, 2H), 0.10 (s, 2H) -0.58 (s, 2H), -1.27 (s, 2H), -2.63 (s, 2H), -9.32 (s, 2H). Elem. anal. calc. (%) for [K$_2$Sm$_2$(bis-trensal)(THF)$_{2.5}$]: C, 52.28%; H, 5.07%; N, 7.62%. Found: C, 52.18%; H, 4.73%; N, 7.24%. Crystals of **2-Sm** suitable for X-ray diffraction were obtained by storing a concentrated solution of the compound in THF at -40 °C.

Synthesis [{K(μ-THF)(THF)$_2$}$_2${Eu^{II}(trensal)}$_2$], 3-Eu. An off-white suspension of trensalK$_3$ (50.1 mg, 0.0843 mmol, 1 equiv.) in THF (2.5 mL) was added to a suspension of [EuCl$_3$(THF)$_3$] (40 mg, 0.0843 mmol, 1 equiv.) in THF (2.5 mL). The resulting off-white suspension was stirred at room temperature for 4 h affording an off-white suspension. Afterwards a bronze suspension of KC$_8$ (11.4 mg, 0.0843 mmol, 1 equiv.) in THF (1 mL) was added and the reaction mixture was stirred at room temperature for 4 h. The resulting deep purple suspension was filtered to remove the graphite and the KI formed during the reaction, affording a deep purple solution. Slow diffusion of hexane into a THF solution of the complex afforded 44.3 mg of compound (75 % yield). Elem. anal. calc. (%) for [KEu(trensal)(THF)$_{0.75}$]: C, 51.43%; H, 4.75%; N, 8.00%. Found: C, 51.16%; H, 4.83%; N, 7.71%. Crystals suitable for X-ray diffraction were obtained by slow diffusion of hexane into a THF solution of **3-Eu**.

Synthesis [{K(THF)$_3$}$_2${K(THF)}$_2$Sm$_2$(cyclo-trensal)], 4-Sm. A suspension of trensalK$_3$ (43.4 mg, 0.0753 mmol 1 equiv.) in THF (2.5 mL) was added to a suspension of [SmI$_3$] (40 mg, 0.0753 mmol 1 equiv.) in THF (2.5 mL) and left to react at room temperature for 4 h. A bronze suspension of KC$_8$ (30.5 mg, 0.226 mmol, 3 equiv.) was added and the mixture was stirred at room temperature for 4 h affording a pale yellow suspension. The mixture was filtered at room temperature to remove the graphite and the KI formed during the reaction, affording a red solution. Slow diffusion of hexane into the THF solution afforded after one night 45 mg of compound (77 % yield). ^{1}H NMR (THF-d8, 400 MHz, 298 K) δ = 9.23 (s, 4H), 8.88 (s, 2H), 8.70 (d, 2H), 8.30 (s, 4H), 8.11 (s, 2H), 7.19 (d, 8H), 6.45 (m, 4H), 5.22 (s, 4H), -0.63 (s, 2H), -1.13 (s, 4H), -4.06 (br, 4H), -5.05. (br, 2H), -6.19 (br, 4H), -9.12 (br, 4H). Elem. anal. calc. (%) for [K$_4$Sm$_2$(cyclo-trensal)(THF)$_{2.5}$]: C, 49.64%; H, 4.82%; N, 7.24%. Found: C, 49.81%; H, 4.55%; N, 7.11%. Crystals suitable for X-ray diffraction were obtained by slow diffusion of hexane into a THF solution of **4-Sm**.

Synthesis [{K(THF)$_3$}$_2${K(THF)}$_2$Nd$_2$(cyclo-trensal)], 4-Nd. An off-white suspension of trensalK$_3$ (141.1 mg, 0.0246 mmol, 1 equiv.) in THF (1.5 mL) was added to a light blue suspension of [NdI$_3$(THF)$_4$] (129.2 mg, 0.447 mmol 1 equiv.) in THF (2.5 mL) and left to react at room temperature overnight. A bronze suspension of KC$_8$ (181.2 mg, 1.340 mmol, 3 equiv.) in THF (2.0 mL) was added and the mixture was stirred at room temperature for 5 h affording a dark orange suspension. The mixture was filtered at room temperature to remove the graphite and the KI formed during the reaction, affording a dark orange solution. Slow diffusion of n-hexane into the THF solution afforded after one night 141.4 mg of compound (78 % yield). ^{1}H

NMR (THF-d8, 400 MHz, 298 K) δ = 47.52 (s, 4H), 16.65 (s, 2H), 14.93 (s, 4H), 10.46 (s, 2H), 9.46 (s, 2H), 9.05 (s, 2H), 8.80 (s, 2H), 8.52 (s, 2H), 5.91 (s, 4H), -16.73 (s, 4H), -17.92 (s, 4H).
Elem. anal. calc. (%) for [K_4Nd_2(cyclo-trensal)$(THF)_{1.5}$]: C, 49.22%; H, 4.54%; N, 7.65%. Found: C, 48.82%; H, 5.04%; N, 7.65%. Crystals suitable for X-ray diffraction were obtained by slow diffusion of hexane into a THF solution of **4-Nd**.

Reactivity with CO_2.

Reaction of 2-Ln with 2 equiv. of $^{13}CO_2$. Complexes **2-Ln** were prepared in situ from the reaction between [$NdI_3(THF)_4$] (12.8 mg, 0.0157 mmol, 1 equiv.) or [SmI_3] (10.0 mg, 0.0188 mmol, 1 eq), K_3trensal with a suspension of KC_8 (1 equiv.) as described before. After removal of KI and graphite, the resulting yellow solution of **2-Ln** was degassed by and 2 equiv. of $^{13}CO_2$ were added. Upon addition of CO_2 the solution turned from yellow to colourless with the concomitant formation of a precipitate.
Upon removal of the solvent under vacuum and after dissolution in basic D_2O (pD = 13.4), quantitative $^{13}C\{^1H\}$ NMR experiments were performed (^{13}C-labelled sodium acetate as reference). The yields in carbonate correspond to 96% and 98% for Nd and Sm, respectively.

Reaction of 4-Ln with 4 equiv. of $^{13}CO_2$ Complexes **4-Ln** were prepared in situ from the reaction between [$NdI_3(THF)_4$] (9.3 mg, 0.0114 mmol, 1 equiv.) or [SmI_3] (10.0 mg, 0.0188 mmol, 1 equiv.), K_3trensal with a suspension of KC_8 (3 equiv.) as described before. After removal of KI and graphite, the resulting dark orange solution of **4-Ln** was degassed and 4 equiv. of $^{13}CO_2$ were added. Upon addition of CO_2 the solution turned from yellow to colourless and a pale yellow precipitate formed.
Upon removal of the solvent in vacuo and after dissolution in basic D_2O (pD = 13.4), quantitative $^{13}C\{^1H\}$ NMR experiments were performed (^{13}C-labelled sodium acetate as reference).
The yields in carbonate correspond to 100% and 97% for Nd and Sm, respectively.

References

1 K. A. Grice, *Coord. Chem. Rev.*, 2017, **336**, 78–95.

2 P. Yang, E. Zhou, B. Fang, G. Hou, G. Zi and M. D. Walter, *Organometallics*, 2016, **35**, 2129–2139.

3 J. Andrez, J. Pécaut, P.-A. Bayle and M. Mazzanti, *Angew. Chem. Int. Ed.*, 2014, **53**, 10448–10452.

4 D. Heitmann, C. Jones, D. P. Mills and A. Stasch, *Dalton Trans.*, 2010, **39**, 1877.

5 W. J. Evans, C. A. Seibel and J. W. Ziller, *Inorg. Chem.*, 1998, **37**, 770–776.

6 W. J. Evans, S. A. Kozimor and J. W. Ziller, *J. Am. Chem. Soc.*, 2003, **125**, 14264–14265.

7 W. J. Evans, D. S. Lee and J. W. Ziller, *J. Am. Chem. Soc.*, 2004, **126**, 454–455.

8 M. Xémard, V. Goudy, A. Braun, M. Tricoire, M. Cordier, L. Ricard, L. Castro, E. Louyriac, C. E. Kefalidis, C. Clavaguéra, L. Maron and G. Nocton, *Organometallics*, 2017, **36**, 4660–4668.

9 A. R. Willauer, D. Toniolo, F. Fadaei-Tirani, Y. Yang, M. Laurent and M. Mazzanti, *Dalton Trans.*, 2019, **48**, 6100–6110.

10 D. Toniolo, A. R. Willauer, J. Andrez, Y. Yang, R. Scopelliti, L. Maron and M. Mazzanti, *Chem. – Eur. J.*, 2019, **25**, 7831–7834.

11 D. Cui, O. Tardif and Z. Hou, *J. Am. Chem. Soc.*, 2004, **126**, 1312–1313.

12 C. Camp, D. Toniolo, J. Andrez, J. Pécaut and M. Mazzanti, *Dalton Trans.*, 2017, **46**, 11145–11148.

13 P. J. Chirik, *Acc. Chem. Res.*, 2015, **48**, 1687–1695.

14 P. J. Chirik and K. Wieghardt, *Science*, 2010, **327**, 794–795.

15 D. L. J. Broere, R. Plessius and J. I. van der Vlugt, *Chem. Soc. Rev.*, 2015, **44**, 6886–6915.

16 O. R. Luca and R. H. Crabtree, *Chem Soc Rev*, 2013, **42**, 1440–1459.

17 S. V. Klementyeva, N. P. Gritsan, M. M. Khusniyarov, A. Witt, A. A. Dmitriev, E. A. Suturina, N. D. D. Hill, T. L. Roemmele, M. T. Gamer, R. T. Boeré, P. W. Roesky, A. V. Zibarev and S. N. Konchenko, *Chem. - Eur. J.*, 2017, **23**, 1278–1290.

18 S. V. Klementyeva, A. N. Lukoyanov, M. Yu. Afonin, M. Mörtel, A. I. Smolentsev, P. A. Abramov, A. A. Starikova, M. M. Khusniyarov and S. N. Konchenko, *Dalton Trans.*, 2019, **48**, 3338–3348.

19 C. Camp, V. Mougel, P. Horeglad, J. Pécaut and M. Mazzanti, *J. Am. Chem. Soc.*, 2010, **132**, 17374–17377.

20 M. J. Monreal and P. L. Diaconescu, *J. Am. Chem. Soc.*, 2010, **132**, 7676–7683.

21 G. Nocton, W. W. Lukens, C. H. Booth, S. S. Rozenel, S. A. Medling, L. Maron and R. A. Andersen, *J. Am. Chem. Soc.*, 2014, **136**, 8626–8641.

22 G. Nocton and L. Ricard, *Chem. Commun.*, 2015, **51**, 3578–3581.

23 C. C. Hojilla Atienza, C. Milsmann, S. P. Semproni, Z. R. Turner and P. J. Chirik, *Inorg. Chem.*, 2013, **52**, 5403–5417.

24 K. Vasudevan and A. H. Cowley, *Chem. Commun.*, 2007, 3464.

25 I. L. Fedushkin, A. N. Lukoyanov and E. V. Baranov, *Inorg. Chem.*, 2018, **57**, 4301–4309.

26 I. L. Fedushkin, D. S. Yambulatov, A. A. Skatova, E. V. Baranov, S. Demeshko, A. S. Bogomyakov, V. I. Ovcharenko and E. M. Zueva, *Inorg. Chem.*, 2017, **56**, 9825–9833.

27 S. S. Galley, S. A. Pattenaude, R. F. Higgins, C. J. Tatebe, D. A. Stanley, P. E. Fanwick, M. Zeller, E. J. Schelter and S. C. Bart, *Dalton Trans.*, 2019, **48**, 8021–8025.

28 H. Sugiyama, I. Korobkov, S. Gambarotta, A. Möller and P. H. M. Budzelaar, *Inorg. Chem.*, 2004, **43**, 5771–5779.

29 C. D. Bérubé, S. Gambarotta, G. P. A. Yap and P. G. Cozzi, *Organometallics*, 2003, **22**, 434–439.

30 C. A. Gould, L. E. Darago, M. I. Gonzalez, S. Demir and J. R. Long, *Angew. Chem.*, 2017, **129**, 10237–10241.

31 S. Demir, M. Nippe, M. I. Gonzalez and J. R. Long, *Chem Sci*, 2014, **5**, 4701–4711.

32 Y.-L. Duan, J.-X. He, W. Wang, J.-J. Zhou, Y. Huang and Y. Yang, *Dalton Trans.*, 2016, **45**, 10807–10820.

33 Y. Pan, W. Li, N.-N. Wei, Y.-M. So, Y. Li, K. Jiang and G. He, *Dalton Trans.*, 2019, **48**, 3583–3592.

34 C. Camp, V. Guidal, B. Biswas, J. Pécaut, L. Dubois and M. Mazzanti, *Chem. Sci.*, 2012, **3**, 2433.

35 E. J. Coughlin, M. Zeller and S. C. Bart, *Angew. Chem.*, 2017, **129**, 12310–12313.

36 S. De Angelis, E. Solari, E. Gallo, C. Floriani, A. Chiesi-Villa and C. Rizzoli, *Inorg. Chem.*, 1996, **35**, 5995–6003.

37 F. Franceschi, E. Solari, C. Floriani, M. Rosi, A. Chiesi-Villa and C. Rizzoli, *Chem. - Eur. J.*, 1999, **5**, 708–721.

38 C. Floriani, E. Solari, F. Franceschi, R. Scopelliti, P. Belanzoni and M. Rosi, *Chem. - Eur. J.*, 2001, **7**, 3052–3061.

39 E. Solari, C. Maltese, F. Franceschi, C. Floriani, A. Chiesi-Villa and C. Rizzoli, *J. Chem. Soc. Dalton Trans.*, 1997, 2903–2910.

40 S. Gambarotta, F. Urso, C. Floriani, A. Chiesi-Villa and C. Guastini, *Inorg. Chem.*, 1983, **22**, 3966–3972.

41 J. Andrez, V. Guidal, R. Scopelliti, J. Pécaut, S. Gambarelli and M. Mazzanti, *J. Am. Chem. Soc.*, 2017, **139**, 8628–8638.

42 A. W. Nichols, S. Chatterjee, M. Sabat and C. W. Machan, *Inorg. Chem.*, 2018, **57**, 2111–2121.

43 D. Toniolo, R. Scopelliti, I. Zivkovic and M. Mazzanti, *J. Am. Chem. Soc.*, 2020, **142**, 7301–7305.

44 C. Camp, J. Andrez, J. Pécaut and M. Mazzanti, *Inorg. Chem.*, 2013, **52**, 7078–7086.

45 C. Camp, L. Chatelain, V. Mougel, J. Pécaut and M. Mazzanti, *Inorg. Chem.*, 2015, **54**, 5774–5783.

46 N. Jori, M. Falcone, R. Scopelliti and M. Mazzanti, *Organometallics*, 2020, **39**, 1590–1601.

47 S. Matsunaga and M. Shibasaki, *Chem Commun*, 2014, **50**, 1044–1057.

48 H. Uh, P. Badger, S. Geib and S. Petoud, *Helv. Chim. Acta*, 2009, **92**, 2313–2329.

49 R. D. Archer, H. Chen and L. C. Thompson, *Inorg. Chem.*, 1998, **37**, 2089–2095.

50 X. Yang, R. A. Jones and S. Huang, *Coord. Chem. Rev.*, 2014, **273–274**, 63–75.

51 M. J. Giansiracusa, E. Moreno-Pineda, R. Hussain, R. Marx, M. Martínez Prada, P. Neugebauer, S. Al-Badran, D. Collison, F. Tuna, J. van Slageren, S. Carretta, T. Guidi, E. J. L. McInnes, R. E. P. Winpenny and N. F. Chilton, *J. Am. Chem. Soc.*, 2018, **140**, 2504–2513.

52 M. Perfetti, E. Lucaccini, L. Sorace, J. P. Costes and R. Sessoli, *Inorg. Chem.*, 2015, **54**, 3090–3092.

53 E. Lucaccini, L. Sorace, M. Perfetti, J.-P. Costes and R. Sessoli, *Chem Commun*, 2014, **50**, 1648–1651.

54 T. Dubé, S. Gambarotta and G. Yap, *Organometallics*, 1998, **17**, 3967–3973.

55 P. V. Bernhardt, B. M. Flanagan and M. J. Riley, *Aust. J. Chem.*, 2000, **53**, 229–231.

56 R. Faizova, S. White, R. Scopelliti and M. Mazzanti, *Chem. Sci.*, 2018, **9**, 7520–7527.

57 P. V. Bernhardt, B. M. Flanagan and M. J. Riley, *Aust. J. Chem.*, 2001, **54**, 229.

58 J. Andrez, G. Bozoklu, G. Nocton, J. Pécaut, R. Scopelliti, L. Dubois and M. Mazzanti, *Chem. – Eur. J.*, 2015, **21**, 15188–15200.

59 N. Gunduz, T. Gunduz and M. B. Hursthouse, *J. Chem. Soc. Perkin Trans.*, 1985, **4**, 899–902.

Chapter 5. A Tetranuclear Samarium(II) Inverse Sandwich from Direct Reduction of Toluene by a Samarium(II) Siloxide§

Introduction

Multi-decker sandwich complexes of the f-elements are of high interest because of their anticipated unique electrical and magnetic properties. Bridging organic spacers may facilitate intermetallic electronic communication, leading to potential application in molecular electronics and molecular magnetism.[1-4] However, the development of this area is hampered by the limited number of multi-metallic sandwich complexes reported in the literature.[4,5] Multi-decker complexes based on bridging COT ligands (COT = η^8-cyclooctatetraenyl) are the most developed family of multi-decker f-element sandwich complexes.[1,4,6-9] Arenes are attractive alternative ligands for the synthesis of multi-decker complexes with potentially interesting magnetic and electronic properties[2,10], but arene-bridged polynuclear complexes of lanthanides are rare.[4,5] Only very recently, we reported a unique example of an arene-bridged Ce^{II} tetradecker complex supported by siloxide ligands.[11] The pentanuclear $[K(2.2.2\text{-crypt})]_2[\{(KL_3Ce)(\mu\text{-}\eta^6{:}\eta^6\text{-}C_7H_8)\}_2Ce]$ complex was obtained by reduction of the Ce^{III} complex, $[KCeL_4]$ (L = $OSi(O^tBu)_3$), with 10 equiv. of K in toluene, affording the first example of a multi-decker complex obtained from the reduction of a trivalent lanthanide complex in a carbocyclic solvent. Reports of the formation of dinuclear arene-bridged $Ln^{II/III}$ complexes from the reduction of trivalent lanthanides complexes are more numerous.[5,12-17] Although Ln^{II} intermediates are likely to be involved in these reactions, the reduction of toluene or benzene by authenticated Ln^{II} complexes has not been confirmed. Here, we report a unique example of an arene-bridged triple-decker Sm^{II} complex that formed upon dissolution of the dinuclear Sm^{II} siloxide complex, $[Sm_2L_4(DME)]$ (L = $OSi(OtBu)_3$), in toluene. In contrast, the reduction of the Sm^{III} siloxide complex, $[SmL_3]_2$,[18] with KC_8 afforded the unusual arene-bridged Sm^{II} dimer, $[\{KSmL_3\}_2(\mu\text{-}\eta^6{:}\eta^6\text{-}C_7H_8)]$, among other products.

---

§ Part of this chapter has been published: R. P. Kelly, D. Toniolo, F. F. Tirani, L. Maron, M. Mazzanti, *Chem. Commun.* 2018, 54, 10268– 10271.
Authors contributions: R.P.K. and D.T. performed the synthesis and the characterizations of the complexes. In particular D.T. optimized the synthesis and obtained the crystal structure of **2** and **3**. F.F.T. performed the X ray analysis and M.M. coordinated the work. R.P.K. and M.M wrote the manuscript.

Results and Discussion

The reduction of the previously reported [SmL$_3$]$_2$[18] complex with 1 equiv. of KC$_8$ per Sm atom in toluene at −40 °C afforded a mixture of several compounds that crystallized rapidly during reduction. Single crystals of the Sm^{II} complex, [KSm$_2$L$_5$], **1** (see appendix), and of the arene-bridged complex, [{KSmL$_3$}$_2$(μ-η^6:η^6-C$_7$H$_8$)], **2**, were isolated from the reaction mixture (Scheme 1). The ^{1}H NMR spectrum of the crude reaction mixture after removal of graphite (and crystallized reduction products) shows the presence of a major set of signals assigned to the previously reported Sm^{III} complex, [SmL$_4$K],[19] and minor signals assigned to complex **2**. Quantitative integration of the signals assigned to [SmL$_4$K] indicates a 30 % conversion of the starting material into [SmL$_4$K].

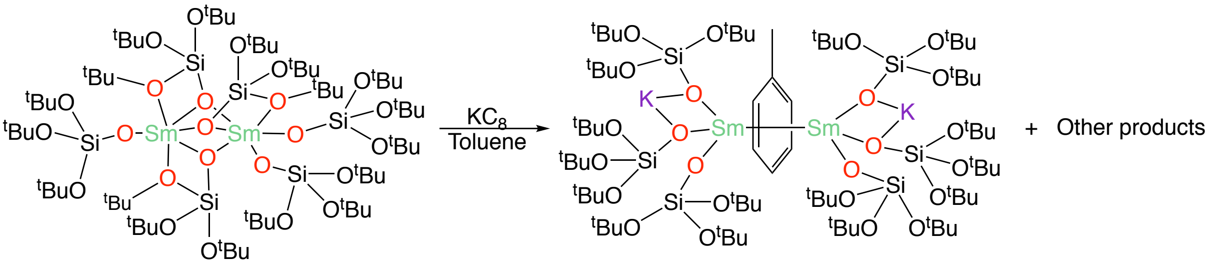

[Sm$_2$L$_6$]

[Sm$_2$L$_6$K$_2$(tol)], **2**

Scheme 1. Synthesis of **3** followed by its reaction with toluene to make **4**

^{1}H NMR studies showed that, once isolated, complex **2** decomposes quickly in toluene solution at room temperature and (more slowly) at −40 °C, yielding [SmL$_4$K] and unidentified products. The presence of multiple reduction products, the low stability of **1** and **2**, and their low solubility, prevented their isolation in reasonable amounts. Performing the reaction in the presence of cryptand also led to a mixture of compounds, with [K(2.2.2-cryptand)][SmL$_4$] being the major species. These results differ significantly from what is observed in the reduction of [Ln(Cp^R)$_3$] complexes (Cp^R = Cp’ = C$_5$H$_4$(SiMe$_3$); or Cp” = C$_5$H$_3$(SiMe$_3$)$_2$-1,3; or Cp^{tt} = C$_5$H$_3$-(^{t}Bu)$_2$-1,3;; and Ln = Ce or La) with 3–4 equivalents of K/KC$_8$, which is usually accompanied by loss of an anionic ligand (Cp’ = C$_5$H$_4$(SiMe$_3$) and formation of stable arene-bridged Ln^{II} complexes of the general formula [{Ln(Cp^R)$_2$}$_2$(μ-η^6:η^6-arene)] (arene = C$_6$H$_6$ or C$_7$H$_8$)$^{1-/2-}$).[12,13,20]

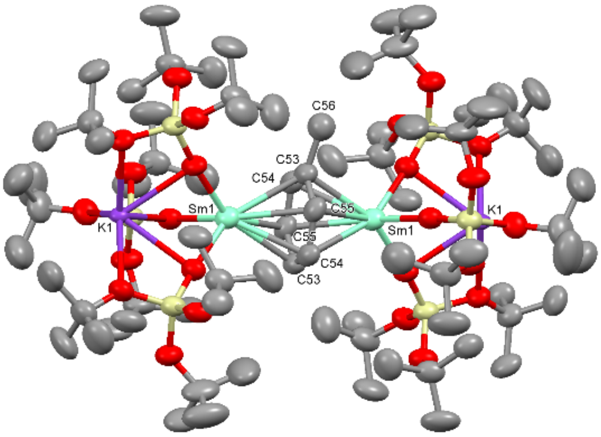

Figure 1. Molecular structure of complex **2** shown with 50 % probability thermal ellipsoids. Hydrogen atoms have been omitted for clarity. Selected bond lengths (Å): Sm–O = 2.219(5)−2.241(5), Sm–C = 2.686(9)–2.752(8), mean $C_{aromatic}$–$C_{aromatic}$ = 1.416(8).

The solid-state structure of **2** (figure 1) shows a central toluene bridging two identical {$KSmL_3$} units. The two potassium ions are both six-coordinate, while the two samarium ions are also both six-coordinate and feature a three-legged piano stool coordination geometry. The Sm–O bond lengths range from 2.219(5)−2.241(5) Å, and they are shorter the Sm–$O_{terminal}$ bond length in the Sm^{II} complex, [SmL_4K_2] (2.381(2) Å).[15] The average toluene C–C bond length of 1.416(8) Å is not significantly different from that of free toluene, and so its charge could not be assigned from these distances alone. The Sm–C bond lengths (2.686(9)–2.752(8) Å) are much longer than those found in **4** (*vide infra*). The latter values are consistent with the presence of a Sm^{II}-toluene^{0}-Sm-^{II} species. Several examples of Ln^{II}-neutral arene complexes have been reported where the arene is unsupported,[21, 22] or more often, it is a substituent in N- or S-donor ligands.[23-29] Lanthanide complexes of neutral arene ligands[5] have also been reported that contain Ln^{III} [30] and Ln^{0} [31-33] ions.

In view of these results, we decided to investigate the direct reaction of isolated Ln^{II} complexes with toluene.

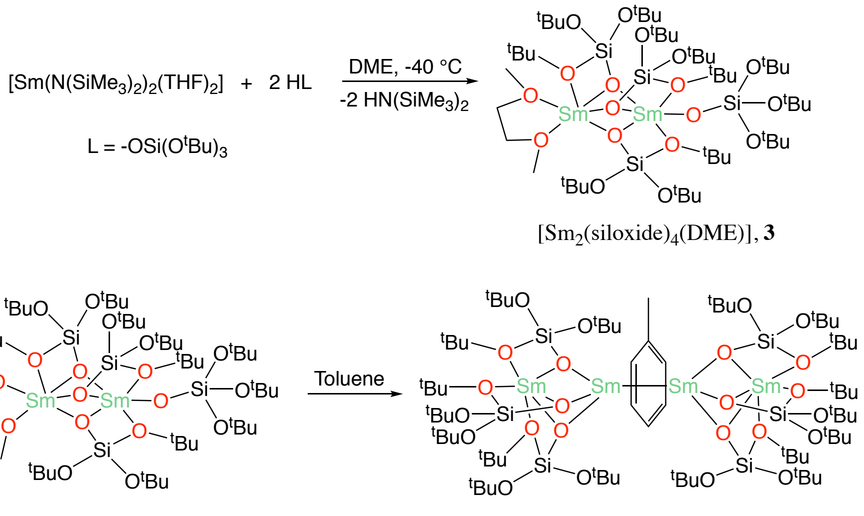

$[Sm_2(siloxide)_4(DME)]$, **3**

$[Sm_2L_4(DME)]$, **3**

$[Sm_4L_6(tol)]$, **4**

Scheme 2. Synthesis of **3** followed by its reaction with toluene to make **4**.

The dissolution of the previously reported Sm^{II} complex, $[SmL_4K_2]$, in toluene at room temperature or at −40 °C led to the decomposition of the Sm^{II} species, affording $[SmL_4K]$ in quantitative yield. While reduced toluene species are probably formed in this reaction, no arene-bridged intermediate was isolated from this reaction. In order to identify an alternative route to more stable arene bridged complexes, we explored the possibility of preparing an alkali-metal-free, low-coordinate Sm^{II} complex. The dinuclear Sm^{II} siloxide complex, $[Sm_2L_4(DME)]$ (**3**, L = $OSi(O^tBu)_3$), was prepared in 77 % yield by treating $[Sm\{N(SiMe_3)_2\}_2(THF)_2]$ with two equivalents of $HOSi(O^tBu)_3$ in DME at −40 °C (Scheme 2). Complex **3** represents a rare Ln^{II} siloxide complex, with only a handful of others known. [11, 18, 19, 34] Storage of a concentrated solution of **3** in DME at −40 °C afforded dark brown single crystals of **3** that were suitable for X-ray diffraction studies. The molecular structure of **3** features two six-coordinate Sm ions unsymmetrically coordinated by four siloxide ligands and one DME molecule (Figure 2). Sm1 is coordinated by one terminal κ^1-siloxide ligand, two bridging κ^2-siloxide ligands and one bridging κ^1-siloxide ligand. On the other hand, Sm2 is coordinated by two bridging κ^1-siloxide ligands, one bridging κ^2-siloxide ligand and one terminal κ^2-dme molecule. The $Sm–O_{siloxide}$ bond lengths range from 2.383(12)–2.692(13) Å, similar to the range observed in the Sm^{II} siloxide complex, $[K_2SmL_4]$ (2.381(2)–2.6659(18) Å). [15]

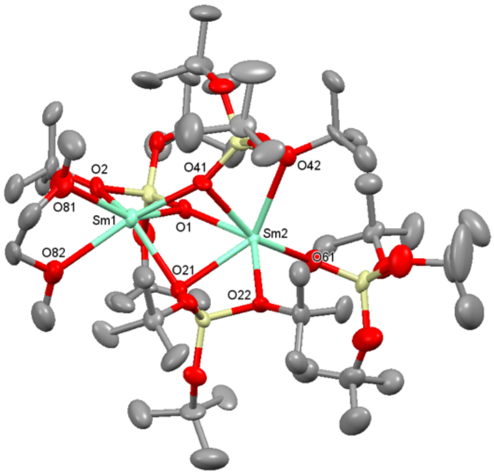

Figure 2. Molecular structure of complex **3** shown with 50 % probability thermal ellipsoids. Solvent of crystallization and hydrogen atoms have been omitted for clarity. Selected bond lengths (Å): Sm–$O_{siloxide}$ = 2.383(12)–2.692(13); Sm–O_{dme} = 2.681(15)–2.710(14).

Complex **3** is highly soluble in non-polar and polar solvents, and it shows moderate stability in THF at room temperature, with only some decomposition evident after 36 h at room temperature. The decomposition reaction proceeds with the formation of Sm^{III}, as evidenced by the detection of $[SmL_3(THF)_2]$ by ^1H NMR spectroscopy. This highlights the marked reactivity of complex **3**, although it is much more stable in THF than the previously reported Sm^{II} complex, $[SmL_4K_2]$[19]. Complex **3** is also stable for up to a week in toluene at −40 °C but reacts slowly with toluene at room temperature. Storage of a concentrated toluene solution (~70 mM) of **3** for three days at room temperature and one night at −40 °C afforded dark brown crystals of the tetranuclear Sm inverse sandwich complex, $[\{Sm_2L_3\}_2(\mu\text{-}\eta^6\text{:}\eta^6\text{-}C_7H_8)]$, **4**, in 44 % yield (Scheme 1). ^1H NMR studies showed that the amount of complex **4** continued to increase after dissolution of **3** in toluene until saturation of the solution occurs after three days. The stoichiometry of the reaction leading to **4** requires the formation of a second species, and the ^1H NMR spectrum of the evaporated reaction mixture in THF-d8 indicated it to be the Sm^{III} complex, $[SmL_3(THF)_2]$,[18] also obtained in 44 % yield (as confirmed by quantitative ^1H NMR spectroscopy). Complex **4** is poorly soluble in toluene and only moderately soluble in THF, where its decomposition begins rapidly. The molecular structure of **4** (Fgure 3) features four Sm ions, six siloxide ligands and one central bridging toluene ligand. The two terminal six-coordinate Sm1 ions have the same coordination environment and they are each bound by three bridging κ^2-siloxide ligands. The two Sm(II) ions are bound by three bridging κ^1-siloxide ligands and they both sandwich a bridging $\eta^6\text{:}\eta^6\text{-}C_7H_8$ molecule (Sm(II)–centroid–Sm(II) = 180°). The Sm–O bond lengths range from 2.395(4)–2.620(4) Å, similarly to those found in **1** and $[SmL_4K_2]$, thus supporting the presence of Sm ions in the +2 oxidation state. The Sm2–C bond lengths range from 2.523(5)–2.607(5) Å, and the average $C_{aromatic}$–$C_{aromatic}$ bond length (1.462(7) Å) is indicative of a reduced toluene molecule.[12-14 35-39] .

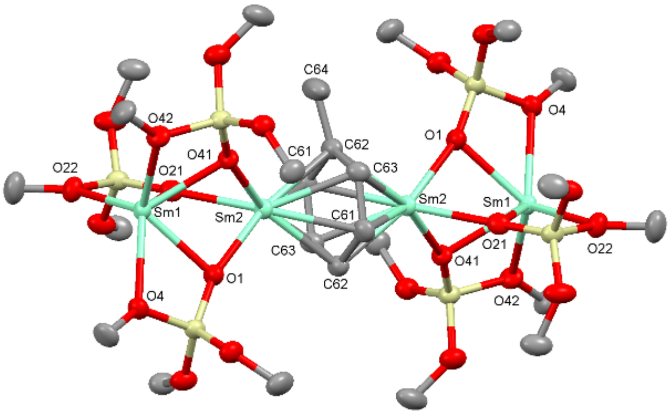

Figure 3. Molecular structure of complex **4** shown with 50 % probability thermal ellipsoids. Disordered components, the methyl groups of the tBu groups and hydrogen atoms have been omitted for clarity. Selected bond lengths (Å): Sm–O = 2.395(4)–2.620(4), Sm2–$C_{aromatic}$ = 2.523(5)–2.607(5), mean $C_{aromatic}$–$C_{aromatic}$ = 1.462(7) Å)

The UV-Vis-NIR spectra of **2** and **4** in in toluene show broad, intense bands in the visible region, consistent with f-d and/or charge-transfer transitions typical of samarium(II).[40]

Unrestricted DFT calculations were carried out on the whole molecules of **2** and **4** to further investigate their electronic structure. Geometry optimization was carried out at the DFT level (B3PW91) with explicit f electrons, as already done for similar complexes.[11,41] Using the f-in-core method, it was possible to confirm the oxidation state of all four samarium centres as +2 in complex **4**. The obtained geometry is in excellent agreement with the one obtained with explicit f electrons, confirming the +2 oxidation state of the four samarium centres. The optimized structure obtained with explicit f electrons and a spin state of 25 is in good agreement with the experimental one (Sm–O between 2.50 and 2.60 Å; and Sm2–C around 2.60 Å). The average $C_{aromatic}$–$C_{aromatic}$ bond length is 1.42 Å, in line with a reduced toluene species. This is further highlighted by the nature of the highest doubly occupied molecular orbital of the system (as there are also 24 singly occupied MOs), which is a δ-bond (figure 4) involving the toluene π* orbital, and this is consistent with a toluene^{2-}. This work provides a proof that the first La^{II} complex reported by Lappert and coworkers[14,41] was indeed a genuine La^{II} arene anion complex. For the sake of comparison, calculations were also carried out with explicit f electrons on complex **2**. In this complex, the two samarium ions are also in the +2 oxidation state, and the toluene is not reduced; the δ-bond is the LUMO (see appendix). A weak bonding interaction between the toluene π orbital and the 5d Sm^{II} orbitals was also found in both complexes.

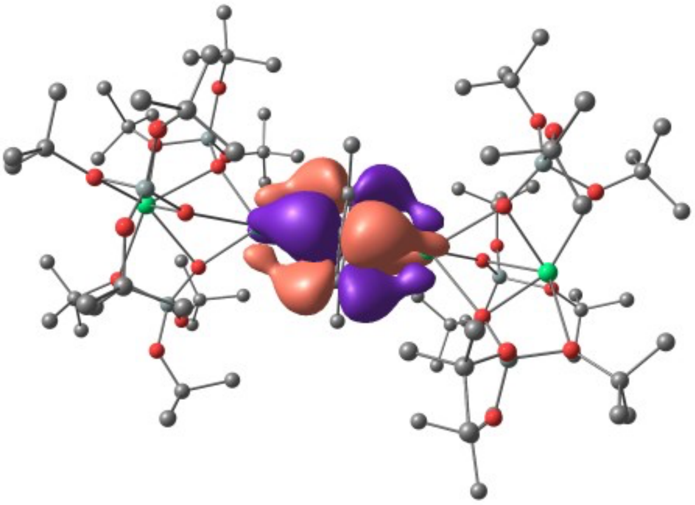

Figure 4. Highest doubly occupied MO of complex **4**.

Thus, computational studies support the formulation of [{$KSmL_3$}$_2$(μ-η^6:η^6-C_7H_8)] as a Sm^{II}-toluene^0-Sm^{II} complex, and the formulation of [{Sm_2L_3}$_2$(μ-η^6:η^6-C_7H_8)] as a (Sm^{II})$_2$-toluene^{2-}-(Sm^{II})$_2$. [{Sm_2L_3}$_2$(μ-η^6:η^6-C_7H_8)] is the second example of an arene-bridged Ln^{II} multidecker complex. However, it differs from the recently reported Ce^{II} tetra-decker, [{($KCeL_3$)(μ-η^6:η^6-C_7H_8)}$_2$Ce], in that it formed without the presence of an alkali metal reductant in the reaction mixture. The reactivity of the dimeric [Sm_2L_4(DME)] complex is remarkable, as it is the first case of a clear-cut toluene reduction by a Sm^{II} complex, demonstrating its unusual reducing power. These results provide a simple and attractive route to arene-bridged multidecker Ln complexes and future studies will be directed to investigating the possibility of obtaining similar systems with later lanthanide ions.

Experimental

General methods.

Unless otherwise noted, all reactions were performed using either standard Schlenk line techniques or in an inert atmosphere glovebox under an atmosphere of purified argon (<1 ppm O_2/H_2O). Glassware was dried overnight at 150 °C prior to use. Unless otherwise noted, reagents were acquired from commercial sources and used without further purification. The solvents were purchased from Aldrich or Eurisotop (deuterated solvents) in their anhydrous form, conditioned under argon and vacuum distilled from K/benzophenone or Na dispersion/benzophenone (hexane, toluene, and THF) and degassed prior to use. Syntheses were performed using glass covered stirring bars [$Sm(HMDS)_2(THF)_2$][42], [SmL_3]$_2$[18] and [SmL_4K_2][19] (L = $OSi(O^tBu)^3$) were prepared using literature procedures. NMR experiments were carried out using NMR tubes adapted with J. Young valves. NMR spectra were recorded on a Bruker 400 MHz NMR spectrometer. ^{1}H chemical shifts are reported in ppm and are referenced to residual protio solvent peaks. Elemental analyses were performed under helium by the analytical service at the EPFL. The UV-Vis-NIR spectra were performed with a PerkinElmer Lambda 750. Experimental details concerning X-ray structural determinations are reported below.

Reduction of SmL_3 in toluene, isolation of [Sm_2L_5K], 1, and [$\{K_2Sm_2L_6\}(\mu\text{-}\eta^6\text{:}\eta^6\text{-}C_7H_8)$] , 2.

KC_8 (2.9 mg, 0.0213 mmol, 1 eq) was added to a solution of [SmL_3] (L = $OSi(O^tBu)_3$) (20 mg, 0.0213 mmol, 1 eq) in toluene (5 mL) at -40 °C. The reaction was stirred at -40 °C for two days. The reaction was followed by ^{1}H NMR spectroscopy and only after two days all the starting material was consumed. The graphite was removed from the solution together with part of crystalline products formed during the reaction (due to the low solubility of complex 2 it was impossible to recover it from the reaction mixture). The ^{1}H NMR spectrum of the resulting red-pink solution (Tol-d8, 400 MHz, 298 K) shows a peak at $\delta = 1.27$ ppm assigned to [SmL_4K] as well as other peaks assigned to 2 (ratio of 2 : [SmL_4K] ≅ of 2 : 44) and to unidentified species (see appendix, figure S1). The quantitative integration of the signal (with respect to DME as internal standard) showed a 35% conversion of the starting [SmL_3] into [SmL_4K]. The solution was concentrated (0.5 mL) and left stand one night at -40 °C affording crystals of 1 and 2. A few crystals of compound 2 could be isolated by letting the solution warm up at room temperature and washing with cold toluene to remove 1. ^{1}H NMR of 2 (tol-d8, 400 MHz, 298 K): δ 1.62 (54 H, $OSi(O^tBu)_3$), δ 1.37 (108 H, $OSi(O^tBu)_3$). Complex 2 resulted to be stable in the reaction mother liquor at -40 °C for several days but decomposes in two days at room temperature affording [SmL_4K] and other minor species (see appendix, figures S2 and S3). The presence of multiple products in the reaction and the low thermal stability of complexes 1 and 2 prevented the isolation of the compounds 1 and 2 analytically pure in reasonable amounts to perform elemental analysis.

Similar mixture of products was obtained when the reduction of [SmL_3] with KC_8 is performed in the presence of 2.2.2-cryptand at -40 °C.

Reaction of [SmL_4K_2] with toluene.

[SmL_4K_2] (30 mg) was dissolved in tol-d8 (0.5 mL) at -40°C affording a red-pink solution. The ^{1}H NMR spectra of the resulting solution (tol-d8, 400 MHz, 233 K) showed the presence of a peak at $\delta = 1.31$ ppm corresponding to [SmL_4K] together with a peak at $\delta = 2.32$ ppm of an unknown compound in ratio 10:1 (see appendix, figure S4). Quantitative integration of the signal assigned to [SmL_4K] (with respect to naphtalene as internal standard) indicate a 98% conversion of [SmL_4K_2] into [SmL_4K] (Figure S5).

Synthesis of [Sm_2L_4(DME)], 3.

A cold (-40 °C) solution of HL (403 mg, 1.52 mmol) in DME (2.5 mL) was added to a stirring solution of [$Sm(HMDS)_2(THF)_2$] (469 mg, 0.762 mmol) in DME (2.5 mL). The resulting dark brown solution was stirred overnight at −40 °C and then the solvent volume was reduced to 2.5 mL. Storage of the concentrated solution at −40 °C yielded large dark crystals of [Sm_2L_4(DME)], 3 (183 mg). Further concentration of the supernatant and storage at −40 °C yielded an overall 426 mg of 2 as dark crystalline product (77% yield). Elemental analysis calcd. for $C_{52}H_{118}O_{18}Si_4Sm_2$ (1444.56 g mol^{-1}): C, 43.24; H, 8.23. Found: C, 43.37; H, 8.01. ^{1}H NMR (THF-d8, 400 MHz, 298 K): δ = 3.49 (s, 4H, $CH_3O(\mathit{CH_2})_2OCH_3$), 3.32 (s, 6H, $\mathit{CH_3}O(CH_2)_2O\mathit{CH_3}$), 2.07 (s, 108H, $OSi(O^t\mathit{Bu})_3$) (Figure S7). ^{1}H NMR (tol-d8, 400 MHz, 298 K): δ = 2.46 (s, 106H), 3.93 ppm (s, 12H).

NMR studies of the reaction between [Sm_2L_4(DME)] and toluene.

The evolution of solutions of 3 (20 mg, 0.014 mmol) in tol-d8 (0.5 mL) at both -40 °C (see appendix, figures S8) and room temperature (see appendix, figures S9-S14) was followed by ^{1}H NMR spectroscopy along the time.

At this concentration no evolution was observed at -40 °C for a week (see appendix, figure S8).

The ^{1}H NMR spectra measured at room temperature show the continuous evolution of compound 3 in tol-d8 after the dissolution. The peaks assigned to complex 3 decrease in intensity during the time and the peak assigned to complex 4 appears after one day and increases with time (see appendix, figures S9-S11). After 6 days crystals of 4 begun to form in the NMR tube resulting in a decrease of the signal assigned to complex 4 (see appendix, figure S12). After 12 days new peaks appeared in the spectrum (see appendix, figure S13).

The [SmL_3] formed during the reaction is not visible in the NMR spectra of the crude mixture in tol-d8 probably due to interaction with unreacted 3. When a small amount of [SmL_3] was added to the reaction mixture in toluene no new peaks were observed confirming that the two species are exchanging in toluene solution. [SmL_3] and unreacted 3 were both detected after taking to dryness the reaction mixture and dissolving the residue in THF-d8.

Reaction of 3 with toluene, synthesis of [{Sm_4L_6}(μ-η^6:η^6-C_7H_8)], 4.

Complex 3 (100 mg, 0.069 mmol) was dissolved in toluene (1 mL). Storage of this solution at room temperature for three days and then at -40 °C for 4 hours deposited dark brown crystals of complex 4 (23 mg, 44% yield). The evolution of the solution with time was followed by ^{1}H NMR spectroscopy (see appendix, figure S16-S18). After removal of crystals of 4 the resulting solution was taken to dryness and the residual was dissolved in THF-d8. Quantitative integration of the solution with naphthalene showed 43% yield for [SmL$_3$] with 50% of unreacted 3 still present in THF solution remaining (see appendix, figure S19). Elemental analysis calcd. for $C_{79}H_{170}O_{24}Si_6Sm_4$ (2274.16 g mol^{-1}): C, 41.72; H, 7.53. Found: C, 41.36; H, 8.07. ^{1}H NMR (THF-d8, 400 MHz, 298 K): δ 0.92 (162H, OSi(*OtBu*)$_3$) (Figure S20).

References

1 O. T. Summerscales, S. C. Jones, F. G. N. Cloke and P. B. Hitchcock, *Organometallics*, 2009, **28**, 5896-5908.

2 W. L. Huang, J. J. Le Roy, S. I. Khan, L. Ungur, M. Murugesu and P. L. Diaconescu, *Inorg. Chem.*, 2015, **54**, 2374-2382.

3 J. J. Le Roy, M. Jeletic, S. I. Gorelsky, I. Korobkov, L. Ungur, L. F. Chibotaru and M. Murugesu, *J. Am. Chem. Soc.*, 2013, **135**, 3502-3510.

4 F. T. Edelmann, *New J. Chem.*, 2011, **35**, 517-528.

5 M. N. Bochkarev, *Chem. Rev.*, 2002, **102**, 2089-2117.

6 W. J. Evans, M. A. Johnston, M. A. Greci and J. W. Ziller, *Organometallics*, 1999, **18**, 1460-1464.

7 W. J. Evans, R. D. Clark, M. A. Ansari and J. W. Ziller, *J. Am. Chem. Soc.*, 1998, **120**, 9555-9563.

8 T. Li, J. Wiecko, N. A. Pushkarevsky, M. T. Gamer, R. Koppe, S. N. Konchenko, M. Scheer and P. W. Roesky, *Angew. Chem. Int. Ed. Engl.*, 2011, **50**, 9491-9495.

9 A. Edelmann, S. Blaurock, V. Lorenz, L. Hilfert and F. T. Edelmann, *Angew. Chem. Int. Ed. Engl.*, 2007, **46**, 6732-6734.

10 S. S. Liu, J. W. Ziller, Y. Q. Zhang, B. W. Wang, W. J. Evans and S. Gao, *Chem. Commun.*, 2014, **50**, 11418-11420.

11 R. P. Kelly, L. Maron, R. Scopelliti and M. Mazzanti, *Angew. Chem. Int. Ed. Engl.*, 2017, **56**, 15663-15666.

12 C. M. Kotyk, M. E. Fieser, C. T. Palumbo, J. W. Ziller, L. E. Darago, J. R. Long, F. Furche and W. J. Evans, *Chem. Sci.*, 2015, **6**, 7267-7273.

13 Y. K. Gun'ko, P. B. Hitchcock and M. F. Lappert, *Organometallics*, 2000, **19**, 2832-2834.

14 M. C. Cassani, D. J. Duncalf and M. F. Lappert, *J. Am. Chem. Soc.*, 1998, **120**, 12958-12959.

15 M. D. Fryzuk, L. Jafarpour, F. M. Kerton, J. B. Love, B. O. Patrick and S. J. Rettig, *Organometallics*, 2001, **20**, 1387-1396.

16 M. D. Fryzuk, L. Jafarpour, F. M. Kerton, J. B. Love and S. J. Rettig, *Angew. Chem. Int. Ed. Engl.*, 2000, **39**, 767-768.

17 M. C. Cassani, Y. K. Gun'ko, P. B. Hitchcock, M. F. Lappert and F. Laschi, *Organometallics*, 1999, **18**, 5539-5547.

18 M. Nishiura, Z. M. Hou and Y. Wakatsuki, *Organometallics*, 2004, **23**, 1359-1368.

19 J. Andrez, J. Pecaut, P.-A. Bayle and M. Mazzanti, *Angew. Chem. Int. Ed. Engl.*, 2014, **53**, 10448-10452.

20 M. C. Cassani, Y. K. Gunko, P. B. Hitchcock and M. F. Lappert, *Chem. Commun.* , 1987-1988.

21 S. I. Troyanov, Russ. J. Coord. Chem., 1998, **24**, 591-597.

22 A. A. Fagin, M. N. Bochkarev, S. A. Kozimor, J. W. Ziller and W. J. Evans, *Z. Anorg. Allg. Chem.*, 2005, **631**, 2848-2853.

23 I. V. Basalov, O. S. Yurova, A. V. Cherkasov, G. K. Fukin and A. A. Trifonov, *Inorg. Chem.*, 2016, **55**, 1236-1244.

24 D. Heitmann, C. Jones, D. P. Mills and A. Stasch, *J. Chem. Soc.-Dalton Trans.*, 2010, **39**, 1877-1882.

25 M. G. Gardiner, A. N. James, C. Jones and C. Schulten, *J. Chem. Soc.-Dalton Trans.*, 2010, **39**, 6864-6870.

26 D. Heitmann, C. Jones, P. C. Junk, K. A. Lippert and A. Stasch, *J. Chem. Soc.-Dalton Trans*, 187-189.

27 A. Cofone and M. Niemeyer, *Z. Anorg. Allg. Chem.*, 2006, **632**, 1930-1932.

28 M. E. Fieser, C. T. Palumbo, H. S. La Pierre, D. P. Halter, V. K. Voora, J. W. Ziller, F. Furche, K. Meyer and W. J. Evans, *Che . Sci.*, 2017, **8**, 7424-7433.

29 D. P. Halter, C. T. Palumbo, J. W. Ziller, M. Gembicky, A. L. Rheingold, W. J. Evans and K. Meyer, *J. Am. Chem. Soc.*, 201, **140**, 2587-2594.

30 F. A. Cotton and W. Schwotzer, *J. Am. Chem. Soc.*, 1986, **108**, 4657-4658.

31 P. L. Arnold, M. A. Petrukhina, V. E. Bochenkov, T. I. Shabatina, V. V. Zagorskii, G. B. Sergeev and F. G. N. Cloke, *J. Organomet. Chem.*, 2003, **688**, 49-55.

32 F. G. N. Cloke, *Chem. Soc. Rev.*, 1993, **22**, 17-24.

33 D. M. Anderson, F. G. N. Cloke, P. A. Cox, N. Edelstein, J. C. Green, T. Pang, A. A. Sameh and G. Shalimoff, *J. Chem. Soc. Chem. Commun.*, 1989.

34 D. J. Duncalf, P. B. Hitchcock and G. A. Lawless, *J. Organomet. Chem.*, 1996, **506**, 347-349.

35 P. L. Diaconescu, P. L. Arnold, T. A. Baker, D. J. Mindiola and C. C. Cummins, *J. Am. Chem. Soc.*, 2000, **122**, 6108-6109.

36 W. L. Huang, F. Dulong, T. P. Wu, S. I. Khan, J. T. Miller, T. Cantat and P. L. Diaconescu, *Nat. Commun.*, 2013, **4**.

37 B. Vlaisayljevich, P. L. Diaconescu, W. L. Lukens, Jr., L. Gagliardi and C. C. Cummins, *Organometallics*, 2013, **32**, 1341-1352.

38 C. Camp, V. Mougel, J. Pecaut, L. Maron and M. Mazzanti, *Chem. Eur. J.*, 2013, **19**, 17528-17540.

39 D. P. Mills, F. Moro, J. McMaster, J. van Slageren, W. Lewis, A. J. Blake and S. T. Liddle, *Nat. Chem.*, 2011, **3**, 454-460.

40 M. R. MacDonald, J. E. Bates, J. W. Ziller, F. Furche and W. J. Evans, *J. Am. Chem. Soc.*, 2013, **135**, 9857-9868.

41 P. B. Hitchcock, M. F. Lappert, L. Maron and A. V. Protchenko, *Angew. Chem. Int. Ed. Engl.*, 2008, **47**, 1488-1491.

42 W. J. Evans, D. K. Drummond, H. Zhang and J. L. Atwood, *Inorg. Chem.*, **1988**, *27*, 575–579

Chapter 6. CS_2 Reductive Coupling to Acetylenedithiolate by a Dinuclear Ytterbium(II) Complex**

Introduction

The activation of CS_2 by transition metals is of interest for the development of catalysts that can convert the CS_2 pollutant, largely used as feedstock in viscose industrial production, into less toxic or useful products.[1] Numerous studies have also been driven by its similarity to CO_2, a potential abundant and renewable source of carbon and the possibility of creating new C-C bonds.[2] Metal complexes of the d[2b,2c,3] and 5f block[2d,4,5], were shown to promote a wide range of reactions such as CS_2 reduction to CS_2^{2-}, disproportionation to CS_3^{2-} and CS, head-to-head reductive C-C coupling to afford tetrathioxalate, head-to-tail reductive C-S coupling, or cleavage of one C-S bond leading to CS and sulphide complexes. Complete disassembly of the CS_2 molecule has also been reported in three cases.[1b,6]

Divalent lanthanide ions display a broad range of reactivity with small unreactive molecules,[7] but only few examples of CS_2 activation have been reported. CS_2 activation by lanthanide ions so far resulted in CS_2 disproportionation or reductive C-S or C-C coupling to afford thiocarbonate, thiooxalate and thioformyl carbonotrithioate ($(SCSCS_2)^{2-}$) respectively.[8] Very recently the first example of a rare CS_2^{2-} dianion trapped between two Yb(III) ions was also reported.[9]

CO reductive coupling by samarium(II) and uranium(III) complexes was reported to afford ketene carboxylate and ynediolate $O\text{-}C{=}C\text{-}O^{2-}$ (that act as a linear κ^2-O,O' bridging ligand) respectively.[10] In contrast the formation of the acetylenedithiolate dianion analogue $(S\text{-}C{\equiv}C\text{-}S)^{2-}$ from CS_2 or CS reduction was never reported. Acetylenedithiolate is of interest as bridging ligand because of its potential to support electronic communication between metal centres, but, due to its low stability, only a few acetylenedithiolate complexes were so far reported.[11]

All the reported examples of CS_2 reduction by lanthanides involve two one-electron transfers by two metal complexes compounds, but experimental and computational studies suggest that cooperative

---

** Part of this chapter was published: D. Toniolo, A. R. Willauer, J. Andrez, Y. Yang, R. Scopelliti, L. Maron, M. Mazzanti, *Chem. Eur. J.*, 2019, **25**, 7831– 7834
Authors contributions: D.T. and A.R.W. optimized the synthesis and the characterization of the compounds. J.A. started the project and obtained the first crystal structure of **2** and **3**, Y.Y. and L.M. performed the DFT calculations, R.S. performed the X-ray single crystal analysis and M.M. coordinated the work.

binding of the substrate by bimetallic intermediate is crucial in the outcome of the reduction.[8c, 12] As such, the reaction of polynuclear lanthanide complexes with CS_2 is of interest because it may allow to trap reactive intermediates or stabilize unusual reaction products.

Here we report the reduction of CS_2 by the dinuclear Yb(II) complex $[Yb_2L_4]$, **1**, (L = $(O^tBu)_3SiO^-$) complex which allowed to trap for the first time a product of CS coupling from CS_2 reduction in the complex $[Yb_2L_4(C_2S_2)]$, **2** together with the CS_2^{2-} bridged key intermediate $[Yb_2L_4(CS_2)]$, **3**.

Results and Discussion

Crystal of the homoleptic complex **1**, were obtained by recrystallization from hexane at -40 °C of the $[Yb_2L_4(DME)]$ complex prepared as previously described for $[Sm_2L_4(DME)]$.[13] The solid state structure of **1** is presented in Figure 1 and shows the presence of a dimer where two Yb(II) ions are bridged by three oxygen atoms from three different siloxide ligands in a non-symmetric fashion. The Yb-$O_{siloxide}$ bond lengths in **1** range from 2.265(2) – 2.570(3) Å, and are consistent with the values previously reported for the divalent ytterbium complex $[YbL_4K_2]$ (2.251(6) – 2.571(6) Å).[1b]

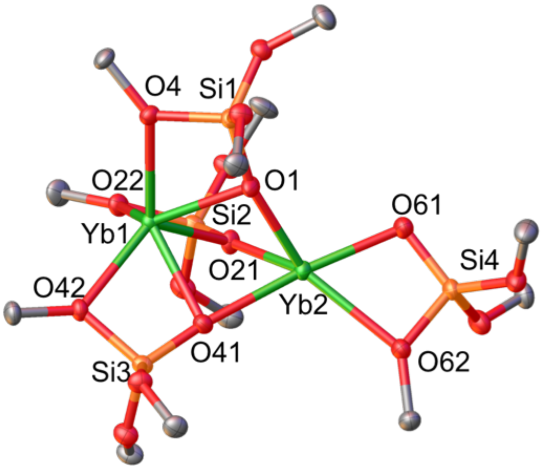

Figure 1. Solid-state molecular structures of **1** (50% probability ellipsoids). Hydrogen atoms, methyl groups and solvent molecule are omitted for clarity.

The addition of 1 - 2 equivalents of $^{13}CS_2$ to a C_6D_{12} solution of **1** at room temperature, resulted reproducibly in the immediate complete conversion of **1**, and the formation of the new species, **2** and **3**, as indicated in Scheme 1. The ^1H NMR spectrum of the reaction mixture shows the presence of the same species in the same ratios independently of the conditions used (see appendix, Figures S3-S6).

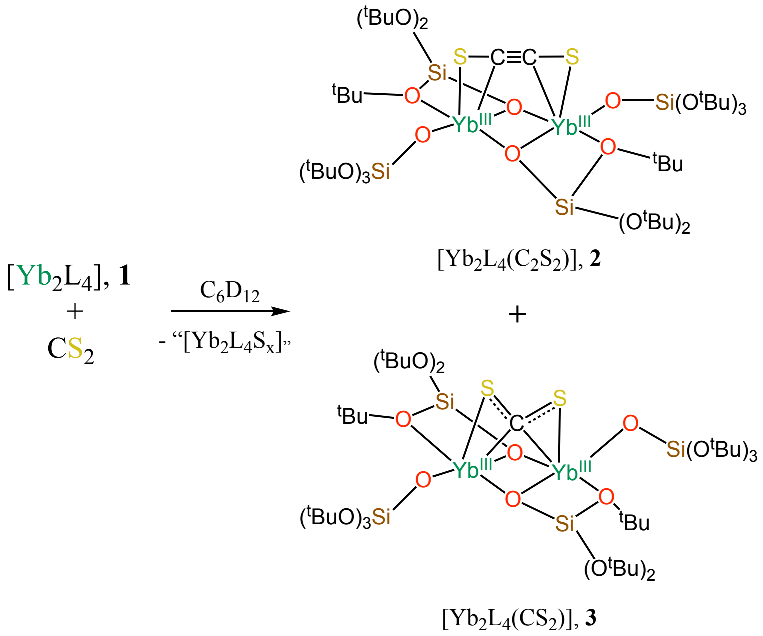
[Yb₂L₄], 1
+
CS₂
C₆D₁₂
- "[Yb₂L₄Sₓ]"
[Yb₂L₄(C₂S₂)], 2
+
[Yb₂L₄(CS₂)], 3
(ᵗBuO)₂
ᵗBu
(ᵗBuO)₃Si
Si(OᵗBu)₃
(OᵗBu)₂
Si
S
C
O
Ybᴵᴵᴵ

Scheme 1. Reaction of **1** with carbon disulphide in cyclohexane.

Storage of a concentrate solution of the reaction mixtures at room temperature resulted in the isolation of the complex [$Yb_2L_4(C_3S_5)$], **4** as a minor product (5 % yield). Storage of a concentrated hexane solution of the reaction mixture at -40 °C, after removal of [$Yb_2L_4(C_3S_5)$]**,** allowed the isolation of pale orange crystals of the co-crystallized species [$Yb_2L_4(\mu\text{-}C_2S_2)$], **2** and [$Yb_2L_4(\mu\text{-}CS_2)$], **3**, with **2**/**3** ratios of 0.24/0.76, 0.18/0.82 or 0.10/0.90 obtained from X-ray diffraction measurements on different crystals.

In one occasion, crystals containing only complex **3** were also isolated.

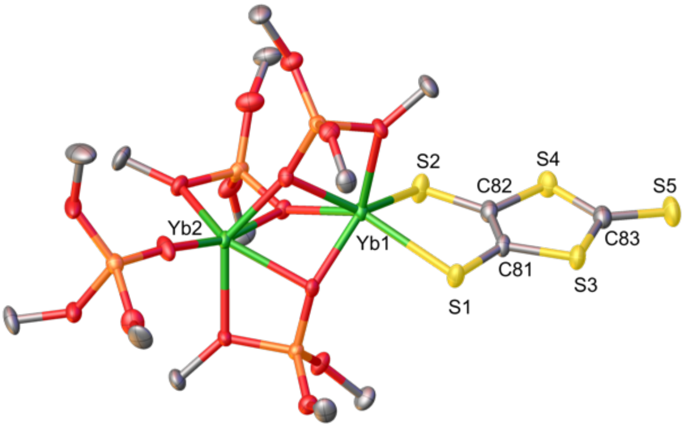
S2
S4
S5
C82
Yb2
Yb1
C83
C81
S1
S3

Figure 2. Solid-state molecular structure of **4** (50% probability ellipsoids). Hydrogen atoms and methyl groups were omitted for clarity.

Complex **4** (Figure 2) shows the presence of the product of CS_2 reductive coupling, $C_3S_5^{2-}$ (dmit^{2-} = 1,3-dithiole-2-thione-4,5-dithiolate) that binds in a bidentate fashion one of the Yb(III) cations formed after the oxidation. To our knowledge metal complexes of the dmit of lanthanides were not so far structurally characterized.

More interestingly, the structure of **2** (Figure 3) shows the presence of a dimer where the $C_2S_2^{2-}$ ligand bridges the two Yb(III) ions in an unprecedented linear μ-η^2-C,S:-η^2-C',S' fashion. The observed binding mode is consistent with the formulation of the ligand acetylenediolate and differs significantly from the side-on bridging mode (μ-η^2-C,C') found in homo and heterobimetallic complexes of d-block metals.[11a-f]

The Yb-Yb distance in **2** (3.2460(2) Å) is slightly longer than in **1** (3.2303(3) Å). The Yb–$O_{siloxide}$ distances (2.068(2) – 2.337(2) Å) are consistent with those found in the homoleptic trivalent complex [YbL_3] (2.029 (3) – 2.339 (2) Å).[14] The value of the C–C bond distance in the $C_2S_2^{2-}$ moiety (1.16(2) Å) is characteristic of a triple bond (1.2 Å in acetylene) and is slightly shorter than what found in other Ln(III)-bound acetylides (1.202(4) Å).[15] The two C–S bonds (1.71(2) and 1.72(2) Å) are longer than the CS double bond in CS_2 (1.55 Å) and in the range of values previously reported for the C-S bond in ethylenedithionate complexes.[11a,16] The mean value of the Yb(III)-C bond distance at 2.62(2) Å is shorter than the value found in the Yb(II) η^2-acetylene complex [$(Me_5C_5)_2Yb(\eta^2\text{-}MeC\equiv CMe)$ (2.850(1) Å)[17] but consistent with the difference in ionic radii (0.16 Å).The $C_2S_2^{2-}$ moiety is nearly linear with C2B–C1B–S1B and C1B–C2B–S2B angles of 176(2)° and 177(2)°.

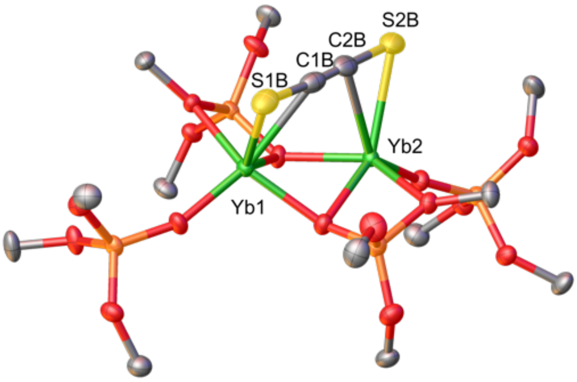

Figure 3. Solid-state molecular structure of **2** (50% probability ellipsoids). Hydrogen atoms, methyl groups and co-crystallized **3** were omitted for clarity. Selected bond lengths (Å): C1B–C2B = 1.16(4); C1B–S1B = 1.71(2); C2B–S2B = 1.72(2); Yb1-S1B = 2.566(6); Yb2-S2B = 2.664(6).

The complex **3** crystallizes in the monoclinic space group $P2_1/c$ as a dimer with six-coordinated metal centre. The structure presented in Figure 4 shows that the reduced CS_2^{2-} moiety bridges the two trivalent ytterbium ions in a symmetric μ-η^2(CS):η^2(CS') fashion. The two C–S bond distances have similar values (1.673(18) and 1.68(2) Å) and are longer than free CS_2 (1.55 Å), consistent with the two-electron reduction of carbon disulphide. The symmetrical binding mode adopted by the CS_2^{2-} in complex **3** differs significantly from those found in the only other reported lanthanide complex of CS_2^{2-} $[Yb_2(DippForm)_4(CS_2)]$[9] (μ-η³(S,C,S′):η²(S,C)) or in the U(IV) complexes, $[U\{(OSi(O^tBu)_3)_3\}_2(\mu\text{-}CS_2)]$,[4b] (μ-η²(S,C):η²(S,S')) and $[(CH_3C_5H_4)_3U]_2(\mu\text{-}CS_2)]$,[4a] ((μ-η²(S,C):η¹(S')) isolated from the reduction of CS_2 by two mononuclear Yb(II) and U(III) complexes respectively.

Only two examples of dinuclear complexes presenting a similar symmetrical coordination mode with two side-on bound C-S fragments were reported so far for d-block metals.[2c, 3c]

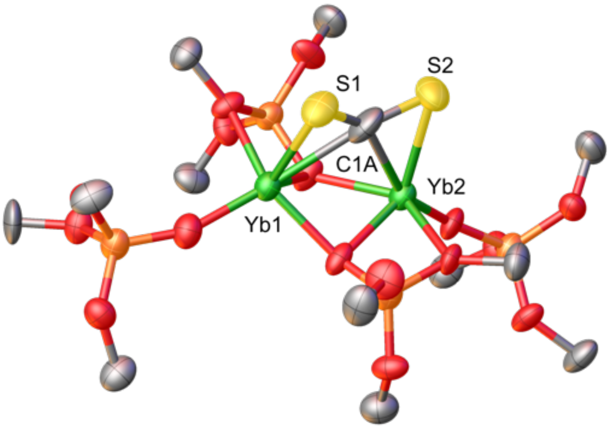

Figure 4. Solid-state molecular structure of **3** (50% probability ellipsoids). Hydrogen atoms and methyl groups were omitted for clarity. Selected bond lengths (Å): C1A–S1 = 1.673(18); C1A–S2 = 1.68(2), Yb1–S1 = 2.656(4); Yb2–S2 = 2.645(5); Yb1–C1A = 2.52(2); Yb2–C1A = 2.531(17).

The complexes **2** and **3** co-crystallize and could not be isolated separately for analytical purposes, but they can be isolated together in good yield from the other reaction products by crystallization. The ¹H NMR spectrum of the isolated mixtures of **2** and **3** shows only the presence of three NMR signals for the siloxide ligands of the two complexes.

The ¹³C NMR signals of the bound $C_2S_2^{2-}$ and CS_2^{2-} dianions could not be observed in the isolated mixtures of **2** and **3** probably due to the paramagnetism of the Yb(III) cation. However, after addition of two equivalents of pyHCl, the quantitative ¹³C NMR in DMSO-d6 shows the presence of two signals at δ = 257.2 ppm and 246.3 ppm assigned to the products obtained after protonation of the $C_2S_2^{2-}$ and CS_2^{2-} dianions in **2** and **3** respectively (see appendix, Figure S12-14).

The reactivity of **1** with CS_2 differs significantly from that reported for the mononuclear ytterbium complex $[YbL_4K_2]$, that resulted in the formation of multiple product such as $C_2S_4^{2-}$, $C_3S_5^{2-}$, CS_3^{2}.[8a] Due to the sterically encumbered environment of the Yb(II) centre in $[YbL_4K_2]$, the CS_2 reduction products were quickly released and metal bound intermediates could not be isolated. In spite of the lower number of siloxide supporting ligands and anticipated lower reducing power, the dinuclear complex [Yb_2L_4] promotes the reduction of CS_2 and allowed to trap the reduction products. The high stability of the CS_2^{2-} intermediate **3** and the formation of the acetylenediolate reduction product may be ascribed to the unusual binding mode imposed in the CS_2^{2-} intermediate by the dinuclear nature of the [Yb_2L_4] complex and the cooperative reduction by the two metal centres. The formation of $C_2S_2^{2-}$ must be accompanied by the formation of a sulphide or polysulphide complex that could be identified by ^{1}H NMR studies by performing the reaction of **1** with elemental sulphur, but that could not be isolated. Previous studies showed that the reaction of Ln(II) with sulphur can yield dinuclear sulphide, disulphide, trisulphide and polysulphide complexes or fascinating sulphide bridged cluster compounds.[9,18]

The reduction of CS_2 to acetylenediolate is unprecedented both in f- and d-block metal chemistry. Therefore, DFT calculations (B3PW91) were carried out in order to get some insights on this peculiar reactivity (Figure 5).

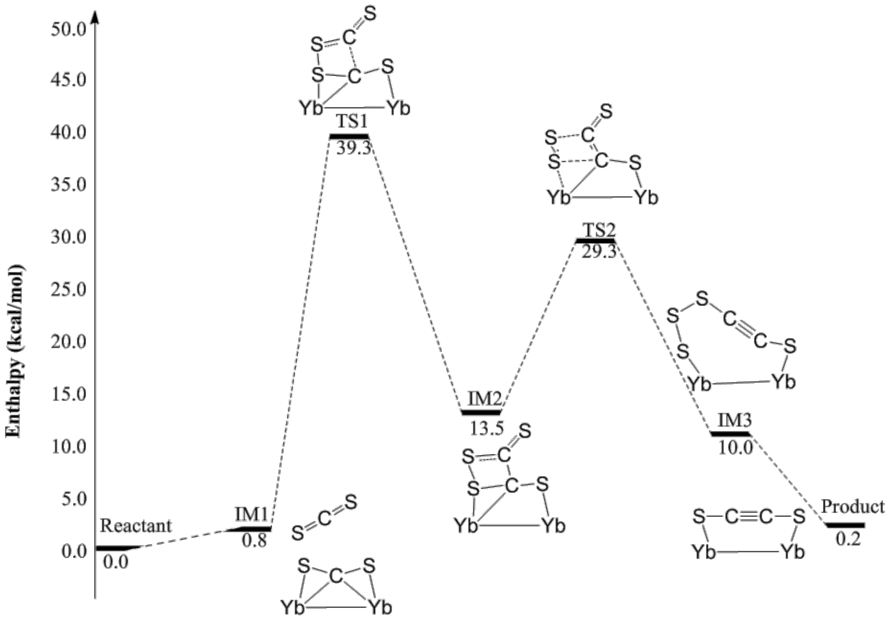

Figure 5. Computed enthalpy profile for the reaction of **1** with CS_2 at room temperature.

The reaction begins with the double reduction of CS_2 by complex **1**, yielding the dinuclear “key intermediate” (complex **3**). This step is found to be exothermic by 22.4 kcal/mol as found in other reactions. From complex **3**, the direct CS bond breaking to yield thiocarbonate is computed to be kinetically difficult (barrier of 46.6 kcal/mol, see appendix, Figure S15). Complex **3** can then further react with another CS_2 molecule but in a very different way from what found for mononuclear

U(III),[4c] or Sm(II)[8c] complexes. Indeed, rather than a nucleophilic addition, the system is undergoing a [2+2] cycloaddition. This peculiar reactivity is associated with the CS_2 binding mode in complex **3**. Indeed, unlike previously reported $(CS_2)^{2-}$ complexes, the HOMO indicates a bonding interaction between the carbon of CS_2 and the two Yb centres (Figure 4), reversing the bond polarity in the CS_2 molecule by relocalizing negative charge on the sulphur atoms (-0.13). Therefore, the best overlap of the incoming CS_2 molecule and complex **3** involves sulphur-sulphur and carbon-carbon interactions, as found in TS1 (cycloaddition TS). The cycloaddition product formation (IM2) appears to be endothermic by 13.7 kcal/mol so that the system evolves through the easy release of S_2 (TS2), yielding the final product whose formation is athermic from complex 3. Then, S2 is either trapped directly by a Yb(II) dimer or by other S2 molecules to form S8, that reacts further with unreacted complex 1.

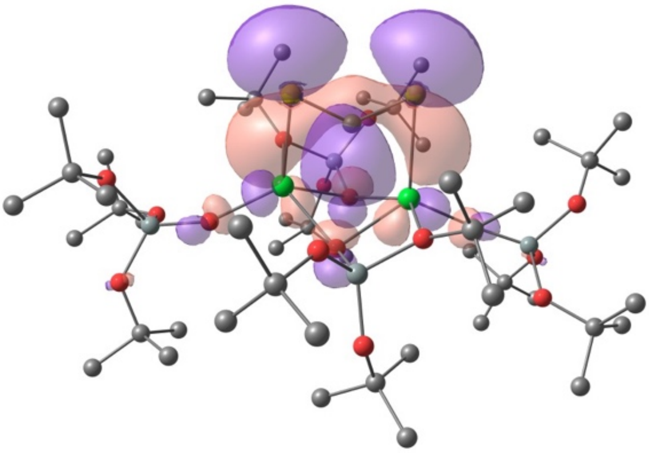

Figure 6. 3D representation of the HOMO of complex **3**

In conclusion, CS_2 reduction by a dinuclear Yb(II) complex supported by siloxide ligands, proceeds very differently from what previously found for other mononuclear Ln(II) or U(III) complexes highlighting the important effect of multimetallic cooperativity in the outcome of CS_2 activation. Notably, we isolated the first example of acetylenedithiolate complex formed from the metal reduction of CS_2. DFT studies suggest that this unusual reactivity arises from the rare symmetric double side-on binding mode found in the stable dinuclear Yb(III)-CS_2^{2-} intermediate.

Experimental

General consideration. Unless otherwise noted, all reactions were performed either using standard Schlenk line techniques or in an inert atmosphere MBraun glovebox under an atmosphere of purified argon (<1 ppm O2/H2O). Glassware was dried overnight at 150 °C prior to use. Syntheses were performed using glass covered stirring bars. Unless otherwise noted reagents were acquired from commercial suppliers and used without further purification. HOSi(OtBu)3 and pyHCl were purchased from Aldrich and purified by sublimation prior to use. The complex [U2(OSi(O^{t}Bu)$_3$)$_6$(CS$_2$)] was prepared according to the published procedure.[19] The ^{13}C NMR of [U2(OSi(O^{t}Bu)$_3$)$_6$(CS$_2$)], containing the CS$_2$$^{2-}$ fragment was measured in the same conditions (upon addition of pyHCl to release CS$_2$$^{2-}$) as used for the mixture of the complexes [Yb$_2$L$_4$(C$_2$S$_2$)] and [Yb$_2$L$_4$(CS$_2$)], to identify the signal corresponding to the CS$_2$$^{2-}$ fragment from complex [Yb$_2$L$_4$(CS$_2$)]. The solvents were purchased from Aldrich, Eurisotop or Cortecnet (deuterated solvents) in their anhydrous form, conditioned under argon and vacuum distilled from K/benzophenone or Nadispersion/benzophenone and degassed prior to use. DMSO-d6 was freeze-degassed and stored over activated 3 Å molecular sieves. NMR experiments were carried out using NMR tubes adapted with J. Young valves. NMR spectra were recorded on Bruker 400 or 600 MHZ spectrometers. ^{1}H and ^{13}C chemical shifts are reported in ppm and were measured relative to residual solvent peaks. Quantitative ^{13}C NMR was measured using an adapted sequence (zgig) and by measuring the relaxation delays for the signals of interest. CHN elemental microanalysis were obtained using a Thermo Scientific Flash 2000 Organic Elemental Analyzer and performed under helium by the analytical service at EPFL. GC- MS analysis were performed under Argon by the analytical service at EPFL, using an Agilent 7890B GC equipped with an HP-5MS UI column (60 m × 0.25 mm × 0.25 μm) coupled to an MS detector.

Synthesis of [Yb$_2$L$_4$], 1.[20]

The complex [Yb$_2$L$_4$(DME)] (L = (O^{t}Bu)$_3$SiO$^-$) was first prepared as previously described for the analogous [Sm$_2$L$_4$(DME)].[13] A cold (-40°C) solution of HL (82.9 mg, 0.31 mmol, 2 eq.) in DME (2 mL) was added to a stirring solution of [Yb(HMDS)2(THF)2] (100 mg, 0.16 mmol, 1 eq.) in DME (1 mL) at -40 °C. The resulting orange solution was stirred overnight at -40°C. Concentration of the solution to about 1 mL and storage at -40 °C yielded dark orange crystals of [Yb2L4(DME)] in 78 % yield (93 mg, 0.063 mmol). Anal. Calc. for [Yb2(OSi(OtBu)3)4(DME)] (1489.92 g mol-1): C52H118O18Si4Yb2: C, 41.92; H, 7.98. Found: C, 41.81; H, 7.86. 1H NMR (Tol-d8, 400 MHz, 298 K): δ = 3.22 ppm (s, 10 H, DME), 1.51 ppm (s, 108 H, tBu). 1H NMR (THF-d8, 400 MHz, 298 K): δ = 3.43 ppm (s, 4H, DME), 3.28 ppm (s, 6H, DME), 1.37 ppm (s, 108 H, ^{t}Bu). Successive recrystallizations of [Yb2L4(DME)] at -40 °C in n-hexane allowed the isolation of green crystals in 70% yield. 1H NMR studies showed the complete removal of the DME. 1H NMR (Tol-d8, 400 MHz, 298 K): δ = 1.52 ppm (s, 108 H, tBu). 1H NMR (THF-d8, 400 MHz, 298 K): δ = 1.37 ppm (s, 108 H, ^{t}Bu). Dark brown crystals suitable for X-ray diffraction analysis of [Yb$_2$L$_4$], 1, were obtained from a saturated n-hexane solution at -40 °C.

Reactivity of [Yb_2L_4], 1, with 1 equivalent $^{13}CS_2$ at room temperature.

a) 2.2 µL $^{13}CS_2$ (0.036 mmol, 1 eq.) were added to a solution of **1** (50 mg, 0.036 mmol) in n-hexane (1 mL) at room temperature. The colour of the solution changed from dark brown to light brown. The solution was stirred overnight at room temperature leading to a yellow precipitate in a light brown supernatant. Filtration of the suspension yielded [$Yb_2L_4(C_3S_5)$], **4**, as a yellow solid in 5 % yield (3 mg, 0.0019 mmol) (yield calculated as a percentage of the total Yb content in **1**). The ^{13}C NMR of the yellow solid (DMSO-d_6, 400 MHz, 298 K) shows the signals at $\delta = 202.8$ ppm and 146.2 ppm corresponding to $C_3S_5^{2}$. Storage of the light brown filtrate at -40 °C overnight yielded 22.4 mg of orange crystals of the co-crystallized complexes [$Yb_2L_4(C_2S_2)$], 2 / [$Yb_2L_4(CS_2)$], 3. The ^1H NMR spectrum of the isolated mixture of 2 / 3 complexes (C_6D_{12}, 400 MHz, 298 K) shows signals at 31.97 ppm, 1.48 ppm and -18.79 ppm assigned to the protons of the co-crystallized products.

b) 6.6 µL $^{13}CS_2$ of a 1.66 M solution in C_6D_{12} (0.011 mmol, 1 eq.) were added to a solution of **1** (15 mg, 0.011 mmol) in C_6D_{12} (0.3 mL) at room temperature. The colour of the solution changed from dark brown to light brown and the solution was kept at room temperature overnight. The ^1H NMR spectrum of the reaction mixture (C_6D_{12}, 400 MHz, 298 K) shows signals at 31.98 ppm, 6.13 ppm, 1.48 ppm 0.14 ppm, -0.24 ppm and -18.79 ppm. ^{13}C NMR (C_6D_{12}, 400 MHz, 298 K): $\delta = 193.0$ ppm (free CS_2). No changes in the ^1H and ^{13}C NMR spectra could be observed over time. The reaction mixture was filtered. Positive ESI-MS (m/z): 1497.47 ([$Yb_2L_4(S_3) + H]^+$), 1491.59 ([$Yb_2L_4(^{13}C_2S_2) + H]^+$), 1478.53 ([$Yb_2L_4(^{13}CS_2) + H]^+$), 1465.49 ([$Yb_2L_4(S_2) + H]^+$), 1433.53 ([$Yb_2L_4(S) + H]^+$). Pale orange crystals of the co-crystallized complexes [$Yb_2L_4(C_2S_2)$], 2 / [$Yb_2L_4(CS_2)$], 3 suitable for X-ray diffraction were obtained overnight from a concentrated n-hexane solution at -40 °C. Two crystals showing different co-crystallization ratio (ratio: 0.24/0.76, 0.18/0.82) were measured by X-ray diffraction analysis. Pale orange crystals of the co-crystallized [$Yb_2L_4(C_2S_2)$], 2 / [$Yb_2L_4(CS_2)$], 3 suitable for X-ray diffraction were also obtained when the reaction was performed in n-hexane at -40 °C (ratio: 0.22/0.78) and when a lower amount of $^{13}CS_2$ (0.66 eq.) was used (ratio: 0.14/0.86).

c) 6.6 µL $^{13}CS_2$ of a 1.66 M solution in C_6D_{12} (0.011 mmol, 1 eq.) were added to a solution of **1** (15 mg, 0.011 mmol) in C_6D_{12} (0.3 mL) at room temperature and the solution was kept at room temperature overnight. The solvent and excess $^{13}CS_2$ were removed under vacuum. ^{13}C NMR (DMSO-d_6, 400 MHz, 298 K): $\delta = 202.9$ ppm and 145.9 ppm ($C_3S_5^{2-}$).

d) 6.6 µL $^{13}CS_2$ of a 1.66 M solution in C_6D_{12} (0.011 mmol, 1 eq.) were added to a solution of **1** (15 mg, 0.011 mmol) in C_6D_{12} (0.3 mL) at room temperature and then the solution was kept at room temperature overnight. The solvent and excess $^{13}CS_2$ were removed under vacuum. The residue was dissolved in n-hexane (0.4 mL) and two equivalents of pyHCl (2.5 mg, 0.022 mmol) were added, in order to release the bound reduced CS_2 species. Stirring the solution for three days at room temperature resulted in a blurry green suspension that was taken to dryness and dissolved in DMSO-d_6 (0.3 mL). The quantitative ^{13}C NMR spectrum (DMSO-d_6, 600 MHz, 298 K) shows the presence of two signals. The first signal at $\delta = 246.3$ ppm is assigned to the decomposition product of $[Yb_2L_4(CS_2)]$, 3 and the second one at $\delta = 257.2$ ppm is assigned to the decomposition product of $[Yb_2L_4(C_2S_2)]$, 2. The was assignment performed on the base of the results obtained by applying the same procedure to the complex $[U_2L_6(CS_2)]$[19], where the quantitative ^{13}C NMR spectrum (DMSO-d_6, 600 MHz, 298 K) only displayed one signal at $\delta = 245.7$ ppm.

Reactivity of $[Yb_2L_4]$, 1, with 2 equivalents $^{13}CS_2$ at room temperature.

a) 13.2 µL $^{13}CS_2$ of a 1.66 M solution in C_6D_{12} (0.022 mmol, 2 eq.) were added to a solution of **1** (15 mg, 0.011 mmol) in C_6D_{12} (0.3 mL) at room temperature. The colour of the solution changed from dark brown to light brown and the solution was kept at room temperature overnight. The ^1H NMR spectrum of the reaction mixture (C_6D_{12}, 400 MHz, 298 K) shows signals at 31.99 ppm 6.07 ppm, 1.48 ppm, 0.14 ppm, -0.23 ppm and -18.80 ppm. ^{13}C NMR (C_6D_{12}, 400 MHz, 298 K): $\delta = 193.0$ ppm (free CS_2). No changes in the ^1H and ^{13}C NMR spectra could be perceived over time. Letting stand the solution at room temperature for 3 days allowed the isolation of X-ray diffraction suitable crystals of $[Yb_2L_4(C_3S_5)]$, **4**. The solution was filtered. Positive ESI-MS (m/z): 1497.57 ($[Yb_2L_4(S_3) + H]^+$), 1491.60 ($[Yb_2L_4(^{13}C_2S_2) + H]^+$), 1478.46 ($[Yb_2L_4(^{13}CS_2) + H]^+$), 1465.50 ($[Yb_2L_4(S_2) + H]^+$), 1433.54 ($[Yb_2L_4(S) + H]^+$). Pale orange crystals of the co-crystallized 2 / 3 species suitable for X-ray diffraction were obtained overnight from a concentrated n-hexane solution of the filtrate at -40 °C (Ratio: 0.10/0.90). Furthermore, pale orange crystals suitable for X-ray diffraction of $[Yb_2L_4(CS_2)]$, 3 were also obtained overnight from a concentrated n-hexane solution at -40 °C.

b) 4.4 µL $^{13}CS_2$ (0.072 mmol, 2 eq.) were added to a solution of **1** (50 mg, 0.036 mmol) in n-hexane (1 mL) at room temperature. The colour of the solution changed from dark brown to light brown. The solution was stirred overnight at room temperature overnight leading to a yellow precipitate in a light brown supernatant. Filtration of the suspension yielded the yellow solid corresponding to **4** in 9 % yield (5.4 mg, 0.0034 mmol), respectively to the total Yb content from **1.** Anal. Calc. for $[Yb_2(OSi(O^tBu)_3)_4(C_3S_5)]$, 4 (1596 g mol^{-1}): $C_{51}H_{108}O_{16}Si_4S_5Yb_2$: C, 38.38; H, 6.82. Found: C, 38.16; H, 6.87. Storage of the light brown filtrate at -40 °C overnight yielded 18.5 mg of orange crystals of the co-crystallized complexes 2 / 3. Anal. Calc. for $[Yb_2L_4(CS_2)].C_6H_{14}$ (1562 g mol^{-1}): $C_{55}H_{122}O_{16}Si_4S_2Yb_2$: C, 42.29; H, 7.87. Anal. Calc. for $[Yb_2L_4(C_2S_2)].C_6H_{14}$ (1574 g mol^{-1}): $C_{56}H_{122}O_{16}Si_4S_2Yb_2$: C, 42.73; H, 7.81. Found: C, 42.61; H, 7.54. Elemental analysis does not allow to determine a reliable ratio between 2 and 3. The ^{1}H NMR spectrum of the isolated 2 / 3 complexes (C_6D_{12}, 400 MHz, 298 K) shows signals at 31.98 ppm, 1.48 ppm and -18.80 ppm assigned to the protons of the co-crystallized products.

c) 13.2 µL **$^{13}CS_2$** of a 1.66 M solution in C_6D_{12} (0.022 mmol, 2 eq.) were added to a solution of **1** (15 mg, 0.011 mmol) in C_6D_{12} (0.3 mL) at room temperature and the solution was kept at room temperature overnight. The solvent and excess **$^{13}CS_2$** were removed under vacuum. ^{13}C NMR (DMSO-d_6, 400 MHz, 298 K): $\delta = 203.0$ ppm and 145.9 ppm ($C_3S_5^{2-}$).

d) 13.2 µL **$^{13}CS_2$** of a 1.66 M solution in C_6D_{12} (0.022 mmol, 2 eq.) were added to a solution of **1** (15 mg, 0.011 mmol) in C_6D_{12} (0.3 mL) at room temperature and the solution was kept at room temperature overnight. The solvent and excess $^{13}CS_2$ were removed under vacuum. The residue was dissolved in n-hexane (0.4 mL) and two equivalents of pyHCl (2.5 mg, 0.022 mmol) were added, in order to release the bound reduced CS_2 species. Stirring the solution for three days at room temperature resulted in a blurry green suspension that was taken to dryness and dissolved in DMSO-d_6 (0.3 mL). The quantitative ^{13}C NMR spectrum (DMSO-d_6, 600 MHz, 298 K) shows the presence of two signals. The first signal at $\delta = 246.2$ ppm is assigned to the decomposition product of $[Yb_2L_4(CS_2)]$, 3 and the second one at $\delta = 256.7$ ppm is assigned to the decomposition product of $[Yb_2L_4(C_2S_2)]$, 2. The assignment was performed by applying the same procedure to the complex $[U_2L_6(CS_2)]$[19], where the quantitative ^{13}C NMR spectrum (DMSO-d_6, 600 MHz, 298 K) only displayed one signal at $\delta = 245.7$ ppm.

Reactivity of $[Yb_2L_4]$ with 1/8 equivalent S_8 at room temperature.

In order to verify the possible presence of sulphide products arising from the reaction with CS_2 we reacted complex 1 with elemental sulphur. 34 µL of a 0.013 M concentrated S_8 solution in C_6D_{12} (0.45 µmol, 0.125 eq.) were added to a solution of **1** (5 mg, 3.6 µmol) in C_6D_{12} (0.4 mL) at room temperature. The colour of the solution changed from dark brown to pale yellow during addition. The ^{1}H NMR spectrum of the reaction mixture (C_6D_{12}, 400 MHz, 298 K) shows signals at 38.45 ppm, 16.81 ppm, 9.66 ppm, 7.14 ppm, 5.97 ppm, 2.38 ppm, 1.47 ppm, 0.15 ppm and -0.20 ppm. The signals at $\delta = 5.97$ ppm, 1.47 ppm, 0.15 ppm and -0.22 ppm correspond to unidentified Yb(III) sulfide species, “Yb-S”, that were also identified in the reaction mixture after the addition of 1 eq. or 2 eq. $^{13}CS_2$ in a C_6D_{12} solution of 1.

References

1 (a) L. D. Wang, W. He, Z. K. Yu, *Chem. Soc. Rev.*, 2013, **42**, 599-621; (b) X. F. Jiang, H. Huang, Y. F. Chai, T. L. Lohr, S. Y. Yu, W. Z. Lai, Y. J. Pan, M. Delferro, T. J. Marks, *Nat. Chem.*, 2017, **9**, 188-193.

2 (a) I. S. Butler, A. E. Fenster, *J. Organomet. Chem.*, 1974, **66**, 161-194; (b) K. K. Pandey, *Coord. Chem. Rev.*, 1995, **140**, 37-114; (c) A. F. R. Kilpatrick, J. C. Green, F. G. N. Cloke, *Organometallics*, 2015, **34**, 4816-4829; (d) O. P. Lam, F. W. Heinemann, K. Meyer, *Angew. Chem. Int. Ed. Engl.*, 2011, **50**, 5965-5968.

3 (a) A. R. Johnson, W. M. Davis, C. C. Cummins, S. Serron, S. P. Nolan, D. G. Musaev, K. Morokuma, *J. Am. Chem. Soc.* **1998**, *120*, 2071-2085; (b) W. S. Ren, H. B. Song, G. F. Zi, M. D. Walter, *J. Chem. Soc.-Dalton Trans.* **2012**, *41*, 5965-5973; (c) P. Haack, C. Limberg, T. Tietz, R. Metzinger, *Chem. Commun.,* 2011, **47**, 6374-6376.

4 (a) J. G. Brennan, R. A. Andersen, A. Zalkin, *Inorg. Chem.*, 1986, **25**, 1756-1760; (b) V. Mougel, C. Camp, J. Pecaut, C. Coperet, L. Maron, C. E. Kefalidis, M. Mazzanti, *Angew. Chem. Int. Ed. Engl.*, 2012, **51**, 12280-12284; (c) O. P. Lam, L. Castro, B. Kosog, F. W. Heinemann, L. Maron, K. Meyer, *Inorg. Chem.*, 2012, **51**, 781-783; (d) E. M. Matson, W. P. Forrest, P. E. Fanwick, S. C. Bart, *J. Am. Chem. Soc.*, 2011, 133, 4948-4954.

5 (a) P. L. Arnold, C. J. Stevens, N. L. Bell, R. M. Lord, J. M. Goldberg, G. S. Nichol, J. B. Love, *Chem. Sci.*, 2017, **8**, 3609-3617; (b) C. Camp, O. Cooper, J. Andrez, J. Pecaut, M. Mazzanti, *J. Chem. Soc.-Dalton Trans.*, 2015, **44**, 2650-2656.

6 (a) J. Ballmann, A. Yeo, B. A. MacKay, S. van Rijt, B. O. Patrick, M. D. Fryzuk, *Chem. Commun.*, 2010, **46**, 8794-8796; (b) S. I. Kallane, T. Braun, M. Teltewskoi, B. Braun, R. Herrmann, R. Laubenstein, *Chem. Commun.*, 2015, **51**, 14613-14616.

7 (a) M. G. Gardiner, D. N. Stringer, *Materials*, 2010, **3**, 841-862; (b) W. J. Evans, *J. Alloys Compd.*, 2009, **488**, 493-510; (c) M. Xemard, V. Goudy, A. Braun, M. Tricoire, M. Cordier, L. Ricard, L. Castro, E. Louyriac, C. E. Kefalidis, C. Clavaguera, L. Maron, G. Nocton, *Organometallics*, 2017, **36**, 4660-4668; (d) F. T. Edelmann, *Angew. Chem. Int. Ed.*, 1995, **34**, 2466-2488.

8 (a) J. Andrez, J. Pecaut, P.-A. Bayle, M. Mazzanti, *Angew. Chem. Int. Ed. Engl.*, 2014, **53**, 10448-10452; (b) J. Andrez, G. Bozoklu, G. Nocton, J. Pecaut, R. Scopelliti, L. Dubois, M. Mazzanti, *Chem. Eur. J.*, 2015, **21**, 15188-15200; (c) L. Castro, D. P. Mills, C. Jones, L. Maron, *Eur. J. Inorg. Chem.*, 2016, 792-796; (d) G. B. Deacon, P. C. Junk, J. Wang, D. Werner, *Inorg. Chem.*, 2014, **53**, 12553-12563; (e) D. Heitmann, C. Jones, D. P. Mills, A. Stasch, *Dalton Trans.*, 2010, **39**, 1877-1882; (f) L. Castro, S. Labouille, D. R. Kindra, J. W. Ziller, F. Nief, W. J. Evans, L. Maron, *Chem. Eur. J.*, 2012, **18**, 7886-7895.

9 D. Werner, G. B. Deacon, P. C. Junk, *Inorg. Chem.*, 2019, **58**, 1912-1918.

10 (a) W. J. Evans, D. S. Lee, J. W. Ziller, N. Kaltsoyannis, *J. Am. Chem. Soc.*, 2006, **128**, 14176-14184; (b) A. S. Frey, F. G. N. Cloke, P. B. Hitchcock, I. J. Day, J. C. Green, G. Aitken, *J. Am. Chem. Soc.*, 2008, **130**, 13816-13817; (c) P. L. Arnold, Z. R. Turner, R. M. Bellabarba, R. P. Tooze, *Chem. Sci.*, 2011, **2**, 77-79; (d) B. M. Gardner, J. C. Stewart, A. L. Davis, J. McMaster, W. Lewis, A. J. Blake, S. T. Liddle, *Proc Natl Acad Sci USA,* 2012, **109**, 9265-9270; (e) S. M. Mansell, N. Kaltsoyannis, P. L. Arnold, *J. Am. Chem. Soc.*, 2011, **133**, 9036-9051.

11 (a) W. W. Seidel, M. J. Meel, F. Hupka, J. J. Weigand, *Dalton Trans.*, 2010, **39**, 624-631; (b) W. W. Seidel, M. J. Meel, U. Radius, M. Schaffrath, T. Pape, *Inorg. Chem.*, 2007, **46**, 9616-9629; (c) W. W. Seidel, M. J. Meel, M. Schaffrath, T. Pape, *Eur. J. Org. Chem.*, 2007, 3526-3532; (d) W. W. Seidel, M. Schaffrath, T. Pape, *Angew. Chem. Int. Ed.*, 2005, **44**, 7798-7800; (e) W. W. Seidel, M. Schaffrath, T. Pape, *Chem. Commun.*, 2006, 3999-4000; (f) W. W. Seidel, W. Dachtler, J. Semmler, M. Tanzler, M. Folk, A. Villinger, *Chem. Eur. J.*, 2013, **19**, 14702-14711; (g) Y. Sunada,

Y. Hayashi, H. Kawaguchi, K. Tatsumi, *Inorg. Chem.*, 2001, **40**, 7072-7078; (h) H. Sugiyama, Y. Hayashi, H. Kawaguchi, K. Tatsumi, *Inorg. Chem.*, 1998, **37**, 6773-6779.

12 L. Castro, L. Maron, *Chem. Eur. J.*, 2012, **18**, 6610-6615.

13 R. P. Kelly, D. Toniolo, F. F. Tirani, L. Maron, M. Mazzanti, *Chem. Commun.*, 2018, **54**, 10268-10271.

14 G. Lapadula, M. P. Conley, C. Coperet, R. A. Andersen, *Organometallics*, *2015*, **34**, 2271-2277.

15 V. Goudy, M. Xemard, S. Karleskind, M. Cordier, C. A. Lamsfus, L. Maron, G. Nocton, *Inorganics,* 2018, **6**.

16 W. W. Seidel, M. D. I. Arias, M. Schaffrath, M. C. Jahnke, A. Hepp, T. Pape, *Inorg. Chem.*, 2006, **45**, 4791-4800.

17 C. J. Burns, R. A. Andersen, *J. Am. Chem. Soc.*, 1987, **109**, 941-942.

18 (a) M. Kuhling, R. McDonald, P. Liebing, L. Hilfert, M. J. Ferguson, J. Takats, F. T. Edelmann, *J. Chem. Soc.-Dalton Trans.*, 2016, **45**, 10118-10121; (b) J. F. Corbey, M. Fang, J. W. Ziller, W. J. Evans, *Inorg. Chem.*, 2015, **54**, 801-807; (c) Y. Z. Ma, S. Bestgen, M. T. Gamer, S. N. Konchenko, P. W. Roesky, *Angew. Chem. Int. Ed.*, 2017, **56**, 13249-13252; (d) A. Kornienko, T. J. Emge, G. A. Kumar, R. E. Riman, J. G. Brennan, *J. Am. Chem. Soc.*, 2005, **127**, 3501-3505; (e) J. H. Melman, M. Fitzgerald, D. Freedman, T. J. Emge, J. G. Brennan, *J. Am. Chem. Soc.*, 1999, **121**, 10247-10248.

19 V. Mougel, C. Camp, J. Pécaut, C. Copéret, L. Maron, C. E. Kefalidis, M. Mazzanti, *Angew. Chem.* **2012**, *124*, 12446–12450.

20 A. Willauer, D. Toniolo, F. Fadaei-Tirani, Y. Yang, L. Maron, M. Mazzanti, *Dalton Trans.,* 2019, **48**, 6100– 6110.

Chapter 7. Carbon Dioxide Reduction by Dinuclear Yb(II) and Sm(II) Complexes Supported by Siloxide Ligands††

Introduction

The potential application of CO_2 as a low-cost, widely available, abundant C1 feedstock for the synthesis of value-added organic compounds and fuels[1] has generated increasing interest towards the reduction of heteroallenes and other C1 substrates (such as CO) by f-element complexes.[2,3a,3c,3d,3j,4,5] The first example of CO_2 reduction by a lanthanide ion was reported by Evans more than twenty years ago. A Sm(II) bis-cyclopentadienyl complex ($[Cp^*_2Sm(THF)_2]$) was shown to promote the reductive coupling of CO_2 to afford selectively oxalate.[4j,6] Examples of reduction of CO_2 to oxalate remain rare both in d-[7] and f-block[3a,3n,4h,4j,6,8] metal chemistry. Moreover, oxalate formation is usually not selective and accompanied by formation of other reduction or insertion products. Solvent effects were shown to play a key role in the outcome of the CO_2 reduction by d-block metal complexes.[7c] The importance of steric effects in determining the formation of oxalate versus carbonate formation in the reduction of CO_2 by mixed sandwich uranium(III) complexes incorporating a cyclo-pentadienyl ligand and a dianionic aromatic cyclooctatetraene was recently demonstrated in an elegant study by Cloke and coworkers.[8b] Cloke and coworkers also demonstrated, using a "harder" bis-aryloxide supporting ligand, the importance of temperature and CO_2 pressure in determining the oxalate/carbonate ratio in CO_2 reduction by U(III) complexes.[4h]

In a related study on CO_2 reduction by mononuclear sandwich complexes of Sm(II) Nocton and coworkers showed the selective formation of carbonate and CO, when bulky cyclopentadienyls ligands are used as supporting ligands rather than Cp*, as a result of both steric and electronic effects.[9] A similar selectivity towards carbonate formation had been reported for macrocyclic organosamarium(II) complex[3d] In contrast we showed previously that both oxalate and carbonate products were formed from the CO_2 reduction by a electron-rich mononuclear complex of Yb(II) supported by a polydentate tris(*tert*-butoxy) siloxide ligand.[8c]

[††] Part of this chapter has been published: A. Willauer, D. Toniolo, F. Fadaei-Tirani, Y. Yang, L. Maron, M. Mazzanti, *Dalton Trans.* 2019, **48**, 6100– 6110.
Authors contributions: A.W. and D.T. performed the synthesis and the characterizations of the compounds, F.F.T. performed the X ray analysis, Y.Y. and L.M. performed the DFT calculations and M.M. coordinated the work.

These studies underline the important role that the nature of the metal and of the supporting ligand play in the CO_2 reduction.

It has also become increasingly evident that another key parameter in the reduction of heteroallenes is the nuclearity of the metal complex. Notably, cooperative binding of heteroallenes by bimetallic complexes provides an attractive route for promoting their activation and reduction.[10,5g,11]

In most cases, the reduction of heteroallenes and other small molecules such as N_2, O_2, NO, or CO by f-elements involves two one-electron transfers by two metal complexes and results in dinuclear compounds where two metals are bridged by the reduction product.[2b,3a,3c,3d,3m,4a,4g,4j,5c,6,8b,12,13]

Computational studies corroborated the importance of bimetallic cooperativity in the reduction of heteroallenes by uranium and lanthanides complexes.[3h-3j,3l,3n,5g,8d,14]

However, the use of polymetallic complexes of f-elements in the activation of small molecules is extremely rare[5f, 8a, 15] and only one example of dinuclear complex able to reduce CO_2 has been reported for lanthanide ions. Notably, the dinitrogen complex $[\{(C_5Me_4H)_2Lu(THF)\}_2(N_2)]$ reacts with CO_2 affording selectively the oxalate bridged complex $[\{(C_5Me_4H)_2Lu\}_2(C_2O_4)]$.[8a, 16]

Here we report two dinuclear complexes of lanthanides(II) supported by the polydentate tris(*tert*-butoxy) siloxide ligand ($[Yb_2L_4]$, **1-Yb** and $[Sm_2L_4]$, **1-Sm**, ($L = (O^tBu)_3SiO^-$). We show that these complexes are able to reduce CO_2 in spite of the presence of only two electron-rich siloxide ligands and that the nature of the lanthanide ion, the solvent and the number of siloxide ligands play an important role on the ratio of oxalate versus carbonate formed in the reduction. Unprecedented tetranuclear $Yb_2(II)Yb_2(III)$-μ-C_2O_4 oxalate-bridged and $Yb_4(III)(\mu_3\text{-}CO_3\text{-}\kappa^4\text{-}O,O',O'')_2$ carbonate bridged complexes were isolated and crystallographically characterized.

It is remarkable that in the presence of dinuclear low coordinated metal complexes the CO_2 reduction involves more than two metal centres. Experimental and computational studies show that both intermolecular and intramolecular activation of carbon dioxide may occur in these dinuclear complexes.

Results and Discussion

Syntheses of divalent lanthanide complexes

The divalent lanthanide complexes $[Yb_2L_4]$, **1-Yb** and $[Sm_2L_4]$, **1-Sm**, ($L = (O^tBu)_3SiO^-$) were obtained in 81% and 74% yield respectively, by treating $[Yb\{N(SiMe_3)_2\}_2(THF)_2]$ or $[Sm\{N(SiMe_3)_2\}_2(THF)_2]$ with two equivalents of $HOSi(O^tBu)_3$ in DME at -40 °C. Coordinated DME was removed completely by multiple recrystallizations of the reaction mixture residues from hexane (Scheme 1). Elemental analysis and ^1H NMR in Tol-d8 and C_6D_{12} of the resulting solids confirmed complete removal of DME. Crystals of **1-Ln** suitable for X-ray diffraction were obtained by storage of a concentrated hexane solution of the complexes at -40 °C.

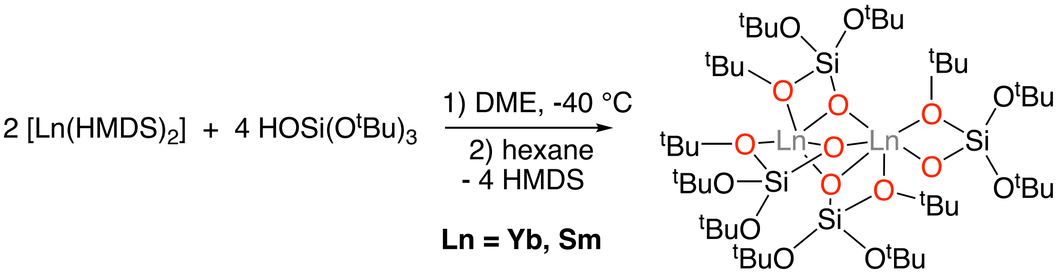

[Ln$_2$L$_4$]

Scheme 1. Synthesis of complexes **1-Yb** and **1-Sm**.

The complexes **1-Yb** and **1-Sm** crystallize in the triclinic space group $P\bar{1}$ and are isostructural. The structure of **1-Sm** is presented in Figure 1 and shows the presence of a dimer where two lanthanide ions are bridged by three oxygen atoms from three different siloxide ligands. One lanthanide ion in the structure of **1-Sm** is five-coordinated by a terminal siloxide ligand in a bidentate fashion and by three bridging siloxides while the second metal ion is six-coordinated by three bridging siloxide ligands in a bidentate fashion. The crystal structure of the solvate complex [Sm$_2$L$_4$(DME)],[17] was reported previously. The removal of the bound DME solvent from [Sm$_2$L$_4$(DME)], does not results in a decreased stability of the resulting Sm(II) complex **1-Sm** because of the multiple coordination modes of the siloxide ligand. Notably, in both complexes the two Sm(II) ions show the same coordination number and in **1-Sm** the two DME oxygen donors are replaced by siloxide ones.

On the other hand , the Sm-O$_{\text{siloxide}}$ bond lengths in **1-Sm** fall in a slightly larger range (2.387(5) – 2.735(5) Å) compared to the mononuclear [SmL$_4$K$_2$] complex (2.381(2) – 2.6659(18) Å)[8c] and the dimeric [Sm$_2$L$_4$(DME)] complex (2.383(12) – 2.692(13) Å).[17]

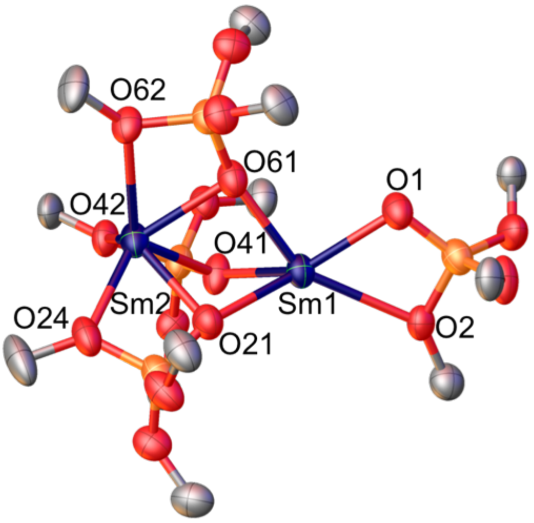

Figure 1. Solid-state molecular structure of **1-Sm** (50% probability ellipsoids). Hydrogen atoms and methyl groups are omitted for clarity. Selected Sm–$O_{siloxide}$ bond lengths (Å): 2.387(5) – 2.735(5)

The complexes **1-Yb** and **1-Sm** are highly soluble in both polar and non-polar solvents. The ^1H NMR spectrum of **1-Yb** in Tol-d8 and C_6D_{12} shows a single narrow signal corresponding to the 108 protons of the siloxide ligands in agreement with the presence of fluxional species in solution. The ^1H NMR spectrum of **1-Sm** shows one broad signal in Tol-d8 and two signals in C_6D_{12} corresponding to the 108 protons of the siloxide ligands suggesting a reduced fluxionality of the samarium species in solution. The ^1H NMR spectra of both complexes **1-Yb** and **1-Sm** in THF-d8 shows a single signal for all siloxide ligands in agreement with the presence of fluxional species and solvent binding.

Although **1-Yb** and **1-Sm** are stable in solid state and in solution at -40 °C, ^1H NMR studies indicated a lower stability in solution at room temperature showing evidence of decomposition in THF and in toluene after 36h. Notably, a decrease of ^1H NMR signal assigned to the siloxide ligands is observed over time for both **1-Yb** and **1-Sm.**

The complex [Sm_2L_4(DME)] was previously shown to slowly react at room temperature with toluene affording, after few days, the tetranuclear divalent samarium sandwich complex [$\{Sm_2L_3\}_2(\mu\text{-}\eta^6{:}\eta^6\text{-}C_7H_8)$].[17] Spectroscopic ^1H NMR study of **1-Sm** in Tol-d8 at room temperature shows that the removal of the DME molecule from the coordination environment of the samarium metal centre does not impact the formation of this multiple decker complex. The complex **1-Yb** also decomposes in toluene but we were not able to isolate the reaction products.

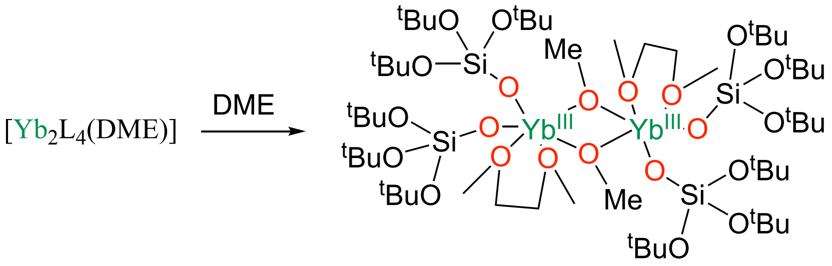

$[Yb_2L_4(OMe)_2(DME)_2]$

Scheme 2. Decomposition of **1-Yb** in DME at room temperature.

The complex **1-Yb** also reacts with DME over time at room temperature. After 3 weeks at room temperature, highly insoluble colourless crystal of $[Yb_2L_4(\mu\text{-}OMe)_2(DME)_2]$, **2**, were isolated in low yield (Scheme 2). The complex **2** crystallizes in the triclinic space group $P\bar{1}$ and is presented in Figure 2. The centrosymmetric structure features a trivalent binuclear ytterbium complex with six-coordinated metal ions. Each ytterbium ion is coordinated by two siloxide ligands in a k^1 fashion, a k^2-DME molecule and two μ_2-κ^1-methoxy groups. The Yb–$O_{siloxide}$ distances are consistent with values reported for Yb^{III} tris(tert-butoxy)siloxide ligands.[8c,18]

The cleavage of the C–O bond in DME by divalent ytterbium complexes has been observed previously in the literature.[19] The Yb–O3A distances (2.205(4) and 2.272(4) Å) in **2** are similar to the Yb-OMe distances in the analogous complexes $[Yb_2I_4(\mu\text{-}OMe)_2(DME)_2]$ (2.152(4) and 2.210(6) Å),[19a] $[Yb_2\{N(SiMe_3)C_6H_4\text{-}2\text{-}OMe\}_4(\mu\text{-}OMe)_2]$ (2.217(2) and 2.221(2) Å),[19c] and $[Yb_2(OAr)_4(\mu\text{-}OMe)_2(DME)_2]$ (2.191(2) and 2.258(2) Å).[19b]

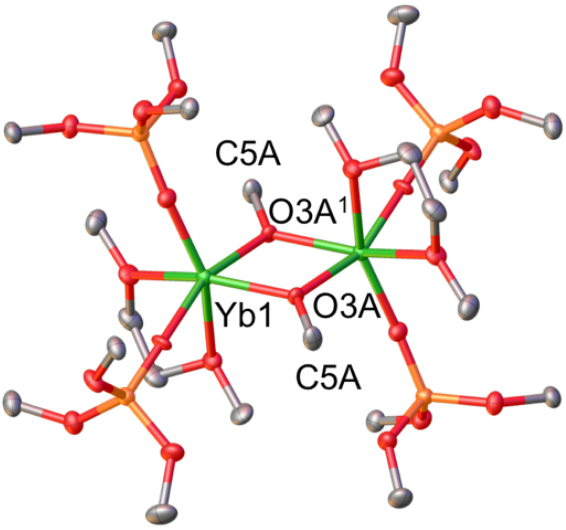

Figure 2. Solid-state molecular structure of **2** (50% probability ellipsoids). Hydrogen atoms and methyl groups from ^{t}Bu are omitted for clarity. Selected bond lengths (Å): Yb–$O_{siloxide}$ = 2.101(4) – 2.125(4); Yb1–O3A = 2.205(4); Yb1–O3A^1 = 2.272(4); O3A–C5A = 1.430(7). Symmetry transformation used to generate equivalent atoms: ^{1}1-x, 1-y, 1-z.

Reactivity with carbon dioxide

In previous studies we reported the synthesis and structure of the mononuclear homoleptic complexes [$Ln^{II}(OSi(OtBu)_3)_4K_2$] for Sm, Eu and Yb. The presence of four electron-rich tris(tert-butoxy)siloxide ligands imparts stability and unusual reactivity to the metal centre leading to the first example of CS_2 and CO_2 activation by a Yb(II) complex. Notably, [YbL_4K_2], reacts with CO_2 affording quantitatively oxalate and carbonate in ratio 1:2.2 and CO. However, the bulky siloxide ligands enforce the labile binding of the reduction products preventing the isolation of reaction intermediates where the substrate or reduction products are metal-bound.

In the dinuclear complexes **1-Yb** and **1-Sm** the presence of only two tris(tert-butoxy)siloxide ligands per metal centre should allow the isolation of reaction intermediates. However, the lower number of ligands will also result in an overall lower reducing power of the complexes compared to the ate analogues [YbL_4K_2] and [SmL_4K_2] that could prevent CO_2 reduction. Indeed, the reactivity of Ln(II) complexes is ligand dependent[20] and it was recently shown, that the dinuclear, neutral, low coordinated [$Sm^{II}(OTf)_2(DME)_2]_2$ complex[15d] does not reduces carbon dioxide in contrast with reports describing CO_2 reduction by neutral Sm(II) complexes supported by Cp,[4j, 9] or porphyrinogen ligands.[3d]

In order to understand how the number of siloxide ligands and the complex nuclearity affect the reduction of CO_2 by divalent lanthanides we investigated the reactivity of **1-Yb** and **1-Sm** with CO_2. **1-Yb** and **1-Sm** react immediately with CO_2 at room temperature affording CO and carbonate or oxalate. However, the ratio between carbonate and oxalate is different for **1-Yb** and **1-Sm** compared to $[YbL_4K_2]$ and $[SmL_4K_2]$ in the same solvent. Moreover, the carbonate : oxalate ratio was found to vary depending on the solvent and the lanthanide ions (Table 1).

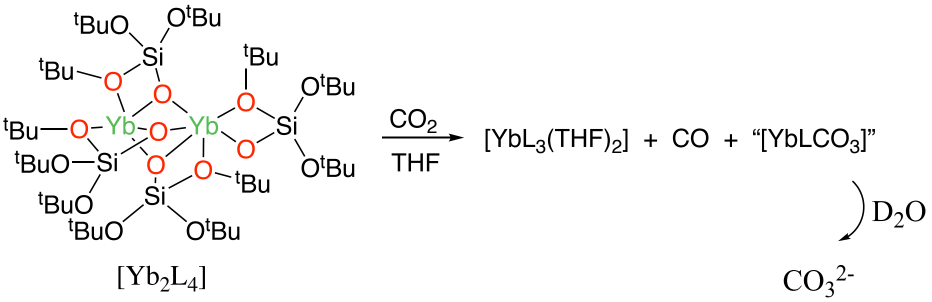

Scheme 3. Reaction of **1-Yb** with carbon dioxide in THF-d8.

When $^{13}CO_2$ (~5 equivalents) was added to a THF-d8 solution of **1-Yb**, an immediate colour change was observed from orange to yellow (Scheme 3). The ^1H NMR spectrum of the reaction mixture in THF-d8, recorded immediately after addition, shows the complete disappearance of the signal assigned to **1-Yb** and the apparition of new signals. A signal assigned to the trivalent species $[YbL_3(THF)_2]$ (δ = -16.93 ppm) increases over time reaching approximately 50% yield after 10 days. These data suggest that mononuclear Yb(III) complexes containing bound reduction products are also present in solution.

The ^{13}C NMR spectrum of the reaction mixture in THF-d8 shows the presence of free ^{13}CO and $^{13}CO_2$ as well as a signal at δ = 169.95 ppm that was assigned to the bound carbonate product. No change in the ^{13}C NMR spectrum could be detected over time. The quantitative ^{13}C NMR spectrum of the residue (after removal of the solvent) in basic (pD = 13) deuterated water confirmed the presence of carbonate (δ = 168.26 ppm) as the single product of carbon dioxide reduction with 90% conversion.

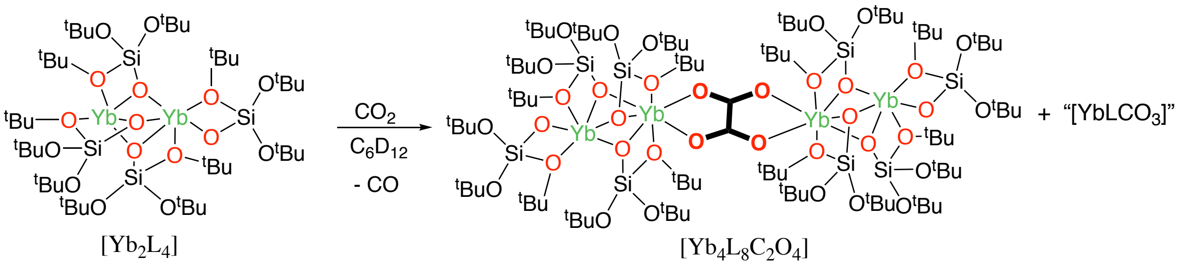

Scheme 4. Reaction of $[Yb_2L_4]$, **1-Yb**, with carbon dioxide in cyclohexane (oxalate highlight in bold).

When excess $^{13}CO_2$ (~5 equivalents) was added to a C_6D_{12} solution of **1-Yb** an immediate colour change was observed from brown to yellow (Scheme 4). The ^1H NMR spectrum in C_6D_{12} of the reaction mixture, immediately after addition of $^{13}CO_2$ showed the apparition of three new signals and unreacted **1-Yb**. After three days, the ^1H NMR spectrum showed the complete disappearance of **1-Yb**.

The ^{13}C NMR spectrum after two weeks shows only excess CO_2. The solvent and the excess $^{13}CO_2$ were removed and the residue was dissolved in deuterated water at pD = 13 in order to release the products of carbon dioxide reduction from the ytterbium metal centres. A very basic pH is required to release completely the bound oxalate and carbonate. The quantitative ^{13}C NMR spectrum showed the presence of carbonate (δ = 167.62 ppm) and oxalate (δ = 179.72 ppm) in a ratio of 50: 1 with 94 % total conversion (carbonate + oxalate).

These results show that in THF the reduction of CO_2 by **1-Yb** only leads to the formation of carbonate, but oxalate is also formed when a non-polar solvent is used. Compared to the tetra-siloxide $[YbL_4K_2]$ complex (ratio oxalate : carbonate 1 : 2.2),[8c] the bis-siloxide, **1-Yb**, leads to a higher selectivity for carbonate formation probably as a result of lower steric hindrance at the metal centre. In the reaction of [YbL4K2] with CO2 the reduction products are rapidly released and it was impossible to isolate intermediates.[8c] Attempts to isolate the Yb-bound carbonate species from THF or hexane solutions were also unsuccessful probably due to the presence of multiple products (only single crystals of $[YbL_3(THF)_2]$ could be isolated).

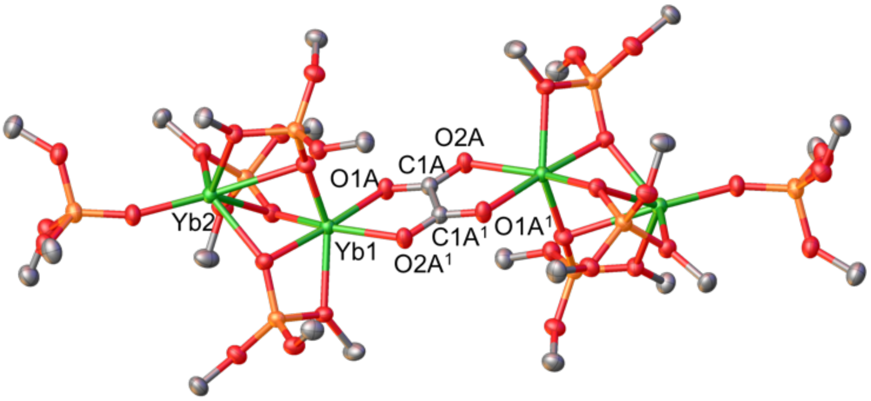

Figure 3. Solid-state molecular structure of **3** (50% probability ellipsoids). Hydrogen atoms and methyl groups were omitted for clarity. Selected bond lengths (Å): Yb1–$O_{siloxide}$ = 2.0945(12) – 2.3649(12); Yb2–$O_{siloxide}$ = 2.2143(12) – 2.7426(14); Yb1– O1A = 2.2993(13); Yb1–O2A^1 = 2.3025(13); O1A–C1A = 1.256(2); O2A–C1A = 1.251(2); C1A–C1A^1 = 1.554(3). Symmetry transformation used to generate equivalent atoms: ^{1}1-x, 1-y, 1-z.

However, storage at -40 °C of a concentrated hexane solution overnight of the reaction mixture obtained after reaction of **1-Yb** with ~5 equivalents CO_2 at room temperature performed in C_6D_{12} allowed the isolation of crystals suitable for X-ray diffraction of the tetranuclear mixed-valence complex $[Yb_4L_8(C_2O_4)]$, **3** (Figure 3). The complex **3** crystallizes in the triclinic space group $P\bar{1}$ as a tetramer. The solid-state structure shows the presence of a $C_2O_4^{2-}$ ligand bridging two $[Yb^{II}L_2Yb^{III}L_2]$ dinuclear moieties. The two moieties are composed of two six-coordinated ytterbium. The first ytterbium is coordinated to one terminal k^1-siloxide ligands, two bridging k^2-siloxide ligands and one bridging k^1-siloxide ligand. The second ytterbium metal centre is coordinated to one bridging k^2-siloxide ligand, two bridging k^1-siloxide ligands and one k^2-C_2O_4 ligand. The Yb1–O$_{siloxide}$ (2.0945(12) – 2.3649(12) Å) distances and the Yb2–O$_{siloxide}$ (2.2143(12) – 2.7426(14) Å) distances fall in the range of Yb^{III}–O$_{siloxide}$ (2.029(3) – 2.339(2) Å)[18] and Yb^{II}–O$_{siloxide}$ distances (2.251(6) – 2.571(6) Å),[8c] respectively, in agreement with the presence of mixed-valence $[Yb^{II}L_2Yb^{III}L_2]$ dimeric moieties. The C1A–C1A^1 bond lengths is 1.554(3) Å which is consistent with the formation of a single C–C bond (1.54 Å in ethane). The isolation of complex **3** suggests that two complexes **1-Yb** interact with two CO_2 molecules in their dinuclear form when the reaction is carried out in a non-coordinating solvent. However, only one of the Yb(III) centres in **1-Yb** transfers one electron to the CO_2 molecule while the second Yb centre remains in the oxidation state +II probably due its lowered redox potential in the presence of the Yb(III) ion. Thus, two Yb(II) centres from two dinuclear complexes transfer one electron to two CO_2 molecules resulting in their reductive coupling to oxalate.

The high yield in oxalate + carbonate (94%) indicates that complex **3** is a moderately stable intermediate that must react further with CO_2 to afford additional reduction products. Indeed, once the reaction is finished all Yb(II) complexes have reacted to afford oxalate or carbonate reduction products.

In order to assess the influence of the nature of the lanthanide ion on the reactivity we also investigated the reactivity of **1-Sm**.

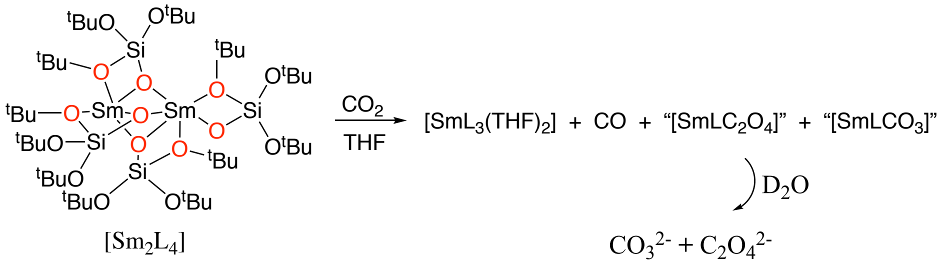

[Sm$_2$L$_4$]
CO$_2$
THF
[SmL$_3$(THF)$_2$] + CO + "[SmLC$_2$O$_4$]" + "[SmLCO$_3$]"
D$_2$O
CO$_3^{2-}$ + C$_2$O$_4^{2-}$

Scheme 5. Reaction of $[Sm_2L_4]$, **1-Sm**, with carbon dioxide in THF-d8.

The reaction of **1-Sm** with $^{13}CO_2$ (~5 equivalents) in THF-d8 afforded a colour change from dark brown to colourless over few minutes (Scheme 5). The ^1H NMR spectrum of the reaction mixture in

THF-d8, immediately after addition, shows the complete disappearance of the signal assigned to **1-Sm** and the apparition of signals assigned to [$SmL_3(THF)_2$]. The signals continuously increased over two days, reaching approximately 50 % conversion of **1-Sm** into [$SmL_3(THF)_2$]. The ^{13}C NMR spectrum in THF-d8 shows the presence of free ^{13}CO and $^{13}CO_2$ as well as new signals at $\delta = 174.61$ ppm and 174.38 ppm that shift over time.

The solvent and the excess $^{13}CO_2$ were removed after two days and the residue was dissolved in basic (pD = 13) deuterated water. The quantitative ^{13}C NMR spectrum in D_2O showed the presence of carbonate and oxalate in a 104 : 1 ratio and in 90 % total yield (carbonate + oxalate).

These results indicate that while in THF the reduction of CO_2 by **1-Yb** only leads to the formation of carbonate, the reduction of CO_2 by **1-Sm** also leads to the formation of a low amount of oxalate. No intermediate Sm(II) complexes containing bound carbonate or carboxylate could be isolated from THF.

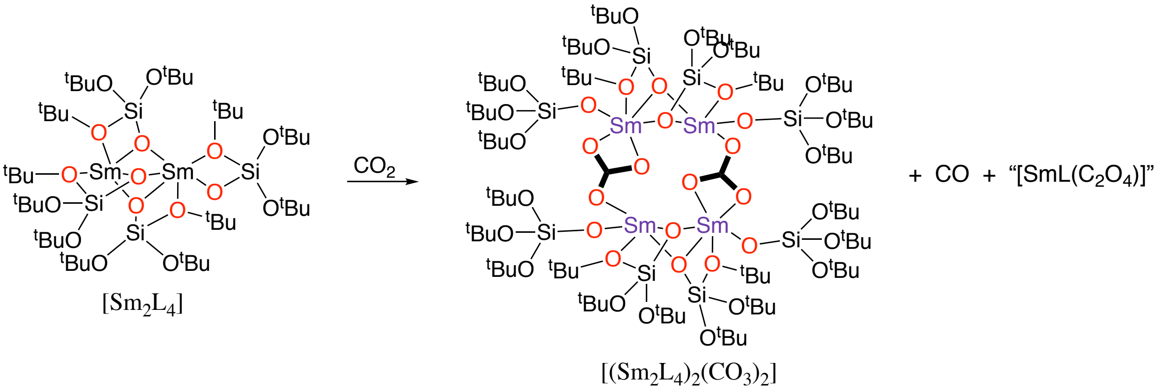

Scheme 6. Reaction of [Sm_2L_4], **1-Sm**, with carbon dioxide in cyclohexane (carbonate highlight in bold)

The reaction of [Sm_2L_4], **1-Sm** with $^{13}CO_2$ (~5 equivalents) in C_6D_{12} afforded a less radical colour change, compared to THF-d8, from dark brown to light brown (Scheme 6). The ^{1}H NMR spectrum of the reaction mixture in C_6D_{12} shows the immediate disappearance of **1-Sm** and the appearance of new signals. The ^{13}C NMR spectrum in C_6D_{12} shows the presence of $^{13}CO_2$ in excess and free ^{13}CO as well as the presence of additional signals assigned to Sm-bound CO_2 reduction products. After four days at room temperature the solution turned colourless. The broad ^{1}H NMR spectrum did not show any detectable change over time, but important changes were observed in the number and chemical shift of the ^{13}C NMR signals over time (see appendix, figure S16, 18). These changes may be due to changes occurring over time in the binding mode of the CO_2 reduction products to the Sm complex. The quantitative ^{13}C NMR spectrum of the reaction mixture in basic (pD = 13) D_2O after 10 days showed the presence of oxalate and carbonate in a 1 : 17 ratio and in 98 % total yield.

These results indicate that the reduction of CO_2 by **1-Sm** in C_6D_{12} leads to higher amounts of oxalate compared to the reduction in THF-d8 or to the reduction of CO_2 by **1-Yb** in THF or C_6D_{12} but no intermediate containing bound oxalate could be isolated.

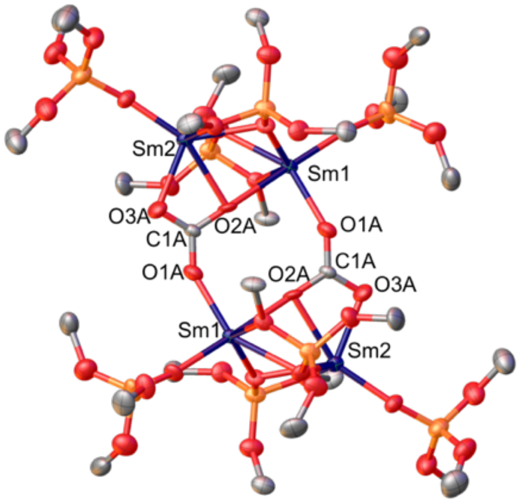

Figure 4**.** Solid-state molecular structure of **4** (50% probability ellipsoids). Hydrogen atoms and methyl groups were omitted for clarity. Selected bond lengths (Å): Sm–$O_{siloxide}$ = 2.150(6) – 2. 479(6); Sm1–O1A = 2.258(7); Sm1–O2A^1 = 2.420(7); Sm2–O2A = 2.485(6); Sm2–03A = 2.295(7); C1A–O = 1.274(10) – 1.287(11). Symmetry transformation used to generate equivalent atoms: ^{1}3/2-x, 1/2-y, 1-z.

In contrast, storage for 2 days at -40 °C of a concentrated hexane solution of **1-Sm** after reaction with $^{13}CO_2$ (~5 equivalents) in C_6D_{12} at room temperature allowed the isolation of X-ray diffraction suitable crystals of $[Sm_4L_8(\mu_3\text{-}CO_3\text{-}\kappa^4\text{-}O,O',O'')_2]$, **4.** The molecular structure of **4** (Figure 4) shows the presence of a Sm(III) tetrameric complex where each metal centre is six-coordinated. The dimer is built from two identical $[Sm_2L_2(\mu\text{-}L)_2]$ moieties each composed of two samarium(III) ions coordinated to one terminal siloxide ligand in a k^1 fashion, one bridging k^1-siloxide ligand and one bridging k^2-siloxide ligand. The two $[Sm_2L_2(\mu\text{-}L)_2]$ moieties are bridged by two carbonate groups in a $\mu_3\text{-}\kappa^4$-O,O',O'' fashion. The Sm–$O_{siloxide}$ distances (2.150(6) – 2. 479(6) Å) are similar to those found in the previously reported Sm(III) complexes.[22] A similar tetranuclear carbonate Sm(III) complex was reported very recently using triflate as supporting ligand ($[Sm_4(CO_3)_2(OTf)_8(THF)_{10}]$).[15d] However, the Sm(II) precursor $[Sm(OTf)_2(DME)_2]$ did not react directly with CO_2 but only via formation of a oxo complex of Sm(III) after reaction with a O-transfer agent. The carbonate C–O distances (1.274(10) – 1.287(11) Å) and the O–C–O angles (117.3(8) – 122.2(8)°) in **4** are similar to those found in the samarium triflate complex (1.263(2) –1.315(2) Å and 115.8(2) – 125.1(2)°).

Furthermore, the Sm–O$_{carbonate}$ bond lengths are in the range of previously reported trivalent samarium carbonate complexes.[9,15d]

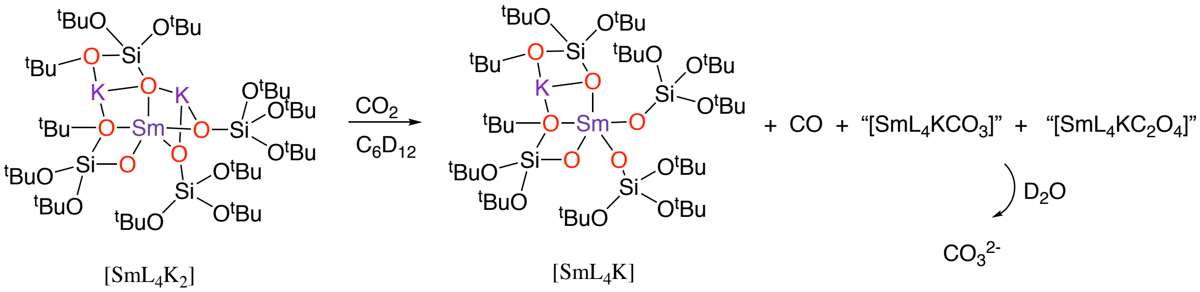

[SmL_4K_2] [SmL_4K]

Scheme 7. Reaction of [SmL_4K_2], with carbon dioxide in cyclohexane

In order to compare the reactivity with carbon dioxide between the bis-siloxide complex **1-Sm** and the previously reported tetra-siloxide [SmL_4K_2] complex, the reaction of [SmL_4K_2] with $^{13}CO_2$ (~5 equivalents) in C_6D_{12} was performed (Scheme 7). This afforded a colour change of the solution from red to colourless. ^1H NMR spectroscopy studies showed the complete disappearance of the signal assigned to [SmL_4K_2] and the appearance of a single signal at δ = 0.55 ppm corresponding to the trivalent species [SmL_4K] in approximately 50% yield, determined by NMR using naphthalene as internal standard. The ^{13}C NMR spectrum in C_6D_{12} shows the formation of new signals assigned to Sm-bound reduced CO_2 species. No evolution in the ^1H NMR or ^{13}C NMR spectra could be observed suggesting a faster reaction compared to **1-Sm**.

The quantitative ^{13}C NMR spectrum in basic D_2O (pD = 12) showed the presence of oxalate (δ = 173.36 ppm) and carbonate (δ = 168.22 ppm) in a ratio of 1:0.8 and in 92 % total yield (carbonate and oxalate). The same ratio was observed when the reaction was performed in Tol-d8.

These results indicate that the use of the bulkier tetra-siloxide [SmL_4K_2] complex leads to the formation of oxalate in higher yield compared to **1-Sm**, becoming the major product of CO_2 reduction.

Table 1. Oxalate : Carbonate molar ratios from the reaction of [Ln_2L_4] (Ln = Yb, Sm, 25 mM) and [LnL_4K_2] (Ln = Yb, Sm, 25 mM) with CO_2 after release of the CO_2 reduction products in basic D_2O (pD = 12-13).

Reagents	Solvent	$C_2O_4^{2-}$: CO_3^{2-}
[Yb_2L_4]	THF-d8	0 : 1
[YbL_4K_2]	THF-d8	1 : 3
[Yb_2L_4]	C_6D_{12}	1 : 50
[YbL_4K_2]	Tol-d8	1 : 1.5
[Sm_2L_4]	THF-d8	1 : 104
[Sm_2L_4]	C_6D_{12}	1 : 17
[SmL_4K_2]	C_6D_{12}	1 : 0.8
[SmL_4K_2]	Tol-d8	1 : 0.8

Computational studies

DFT calculations were carried out in order to determine possible reaction pathways and to explain the observed trend of product formation. Previous studies on Sm(II) catalysed CO_2 reduction[3d,9] have demonstrated that carbonates are formed, that are kinetic products, while others[3h,3n,4j] reported the formation of oxalate, that is the thermodynamic product. The preferential carbonate formation was easily explained by the fact that the "key intermediate", a Sm(III)-$(CO_2)^{2-}$-Sm(III) complex, is η2(C-O) bonded to the Sm centre(s) and therefore favouring O-C rather than C-C bond formation with an incoming CO_2. Recent reports on Ti(III)[23] and Th(III)[3a] chemistry have shown that the donation ability of the ligand can allow the formation of a transient dioxocarbene species that favours the C-C bond formation over the O-C one. In a same way, a seminal work by Tsoureas et al. on uranium(III) complexes[4] demonstrated that the carbonate : oxalate ratio can also be tuned by changing the sterics around the metal centres. In all the above studies only mononuclear complexes were involved in the reaction with CO_2. Experimentally, during the reaction of the dimeric **1-Sm** and **1-Yb** with CO_2, the formation of tetrametallic complexes was observed, which are difficult to handle computationally. A calculation was undertaken on the tetrametallic "key intermediate" [$L_4Sm_2(CO_2)L_4Sm_2$]. The geometry of this complex indicates a dioxocarbene structure that would favour oxalate formation. Moreover, the stabilization of this tetrametallic "key intermediate" with respect to the separated reactants (2 dimers and CO_2) is similar as the one found for the bimetallic intermediate [$L_2Sm(CO_2)L_2Sm$] formed from the reaction of one dimer and a CO_2.

The carbonate and oxalate formation pathways with **1-Sm** were therefore computed on dimers and are reported in Figure 5. It should however be kept in mind that the formation of the “key intermediate” from two dimers, although favourable energetically would be disfavoured entropically as it goes from three particles to one with respect to the ”key intermediate” formed from one dimer.

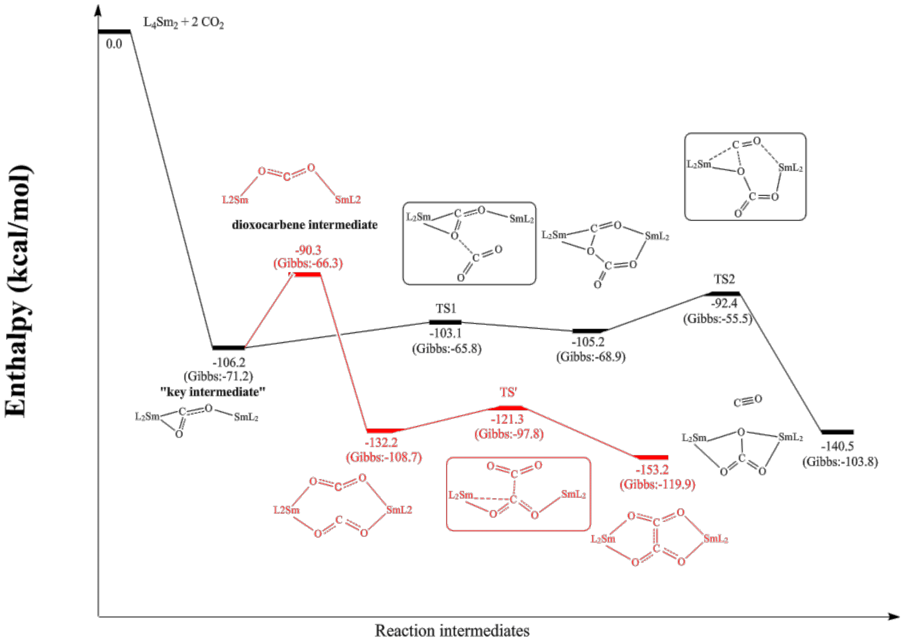

Figure 5. Computed enthalpy profile (room temperature) for the CO_2 reaction with **1-Sm**. The black profile is the carbonate formation whereas the red one is the oxalate formation pathway

The reaction mechanism for the carbonate formation from the reaction of **1-Sm** with CO_2, is classical and similar to previous reports for mononuclear complexes. [3d, 9] The formation of the key intermediate is exoergic by 106.2 kcal/mol and in this compound the CO_2^{2-} moiety is (μ:μ:η(C-O)) bonded to the two samarium centres. No oxo formation is observed in line with the bulkiness of the ligand but a concerted reaction mechanism where the incoming CO_2 forms a C-O bond with the CO_2^{2-} and then releases CO, is found. The highest barrier is 12.8 kcal/mol for the latter and is associated to the need to have the two Sm fragments relatively close increasing the steric repulsion. On the other hand, the formation of the oxalate implies the formation a dioxocarbene intermediate as found with the tetramer. The dioxocarbene intermediate (Figure 5) is 15.9 kcal/mol less stable that the “key intermediate” making this pathway less favourable than the carbonate formation even though the subsequent formation of the CO_2 adduct to the dioxocarbene is highly favourable (-41.9 kcal/mol). The oxalate formation is then achieved with an equivalent barrier (10.9 kcal/mol) as the carbonate. This is associated with the formation of a transient dioxocarbene that decreases the steric congestion at the transition state but this intermediate is less stable than the “key intermediate” involved in the carbonate formation. Thus, the formation of the oxalate from the dimer and CO_2 is favoured thermodynamically but kinetics and the formation of tetrametallic intermediate still allow carbonate formation.

Conclusion

In summary we have shown that dinuclear complexes containing low-coordinate lanthanide(II) ions can be stabilized by the polydentate tris(tertbutoxy) siloxide ligand. In spite of the presence of only two siloxide ligands bound to the metal centre the complexes $[Yb_2L_4]$, 1-Yb and $[Sm_2L_4]$, 1-Sm, (L = $(O^tBu)_3SiO^-$) are highly reactive as indicated by the observed cleavage of the DME C-O bond over time at room temperature to afford crystals of $[Yb_2L_4(\mu\text{-}OMe)_2(DME)_2]$, 2. More importantly the 1-Yb and 1-Sm complexes effect the reduction of CO_2 in ambient conditions leading to both carbonate and oxalate formation. The selectivity of the reduction towards oxalate or carbonate changes depending on the solvent polarity and on the nature of the ion. For both lanthanides carbonate formation is favoured but oxalate formation increases in non-polar solvents. These results suggest that dimeric species favours oxalate formation. Notably, in non-polar solvents the 1-Yb and 1-Sm complexes are present in solution as dimers, while the formation of monomeric species is anticipated in polar solvents. Computational studies confirmed that the formation of oxalate is favoured with respect to carbonate formation in the reaction of the dimeric lanthanide complexes with CO_2. However, the formation of tetrametallic intermediates likely to result in the concomitant formation of carbonate. Crystals of the tetranuclear mixed-valence oxalate intermediate $[Yb_4L_8(C_2O_4)]$, 3 were isolated from hexane and shows the presence of a $C_2O_4^{2-}$ ligand bridging two $[Yb^{II}L_2Yb^{III}L_2]$ dinuclear moieties. Crystals of the tetranuclear di-carbonate product $[Sm_4L_8(\mu_3\text{-}CO_3\text{-}\kappa^4\text{-}O,O',O'')_2]$, 4 were isolated from hexane. The structures of 3 and 4 suggest that the CO_2 activation in non-polar solvents involves the interaction of two dimers with CO_2 molecules at least to some extent. Such cooperative interaction results both in oxalate and carbonate formation.

Experimental

General considerations

Unless otherwise noted, all reactions were performed either using standard Schlenk line techniques or in an inert atmosphere glovebox under an atmosphere of purified argon (<1 ppm O_2/H_2O). Glassware was dried overnight at 150 °C prior to use. Unless otherwise noted reagents were acquired from commercial suppliers and used without further purification. The solvents were purchased from Aldrich or Eurisotop (deuterated solvents) in their anhydrous form, conditioned under argon and vacuum distilled from K/benzophenone or Nadispersion/benzophenone (n-hexane, Toluene, DME, cyclohexane and THF) and degassed prior to use or dried over molecular sieves for one week (DMSO). Syntheses were performed using glass covered stirring bars. HOSi(OtBu)3, azobenzene and naphthalene were purchased from Aldrich and purified by sublimation prior to use. [Yb(HMDS)$_2$(THF)$_2$], [Sm(HMDS)$_2$(THF)$_2$][25], and [SmL$_4$K$_2$][8c] (L = OSi(OtBu)$_3$) were prepared using literature procedures. The amount of THF was determined by 1H NMR using naphthalene as internal reference. NMR experiments were carried out using NMR tubes adapted with J. Young valves. NMR spectra were recorded on Bruker 400 and 600 MHZ spectrometers. 1H and 13C chemical shifts are reported in ppm and were measured relative to residual solvent peaks. Elemental analyses were performed under helium by the analytical service at EPFL.

Syntheses

Synthesis of [Sm$_2$L$_4$], 1-Sm. A cold (-40 °C) solution of HL (84.6 mg, 0.32 mmol, 2 eq.) in DME (2.5 mL) was added to a stirring solution of [Yb(HMDS)$_2$(THF)$_2$] (100 mg, 0.16 mmol, 1 eq.) in DME (1.5 mL). The resulting dark brown solution was stirred overnight at -40 °C. The solvent was removed under vacuum affording a dark brown powder. The solid was dissolved in cold n-hexane (3 mL), stirred at -40 °C for 15 min and then taken to dryness. This operation was repeated three times affording a dark brown solution to completely remove coordinated DME. Removal of DME by heating under vacuum was avoided because it leads to decomposition. The solution was filtered and concentrated. Storage of the solution at -40 °C yielded dark brown crystals of [Sm$_2$L$_4$], 1-Sm in 74 % yield (89 mg, 0.068 mmol). Anal. Calc. for [Sm$_2$(OSi(OtBu)$_3$)$_4$] (1354.4 g mol^{-1}): $C_{48}H_{108}O_{16}Si_4Sm_2$: C, 42.57; H, 8.04. Found: C, 42.45; H, 8.03. ^{1}H NMR (Tol-d8, 400 MHz, 298 K): δ = 2.80 ppm (s, 108 H). ^{1}H NMR (THF-d8, 400 MHz, 298 K): δ = 2.07 ppm (s, 108 H). ^{1}H NMR (C_6D_{12}, 400 MHz, 298 K): δ = 2.39 ppm (s), 1.65 ppm (s). Dark brown crystals suitable for X-ray diffraction analysis were obtained from a saturated solution of **1-Sm** in hexane at -40 °C.

Synthesis of [Yb$_2$L$_4$] (1-Yb). A cold (-40 °C) solution of HL (294.9 mg, 1.11 mmol, 2 eq.) in DME (4 mL) was added to a stirring solution of [Yb(HMDS)$_2$(THF)$_2$] (355.8 mg, 0.56 mmol, 1 eq.) in DME (2 mL). The resulting orange solution was stirred overnight at -40 °C. The solvent was removed under vacuum affording an orange powder. The solid was dissolved in cold n-hexane (3 mL), stirred at -40 °C for 15 min and then taken to dryness. This operation was repeated three times affording a dark brown solution to completely remove coordinated DME. Removal of DME by heating under vacuum was avoided because it leads to decomposition. The solution was filtered and concentrated. Storage of the solution at -40 °C yielded green crystals of [Yb$_2$L$_4$], 1-Yb in 81 % yield (315 mg, 0.23 mmol). Anal. Calc. for [Yb$_2$(OSi(O^{t}Bu)$_3$)$_4$] (1399.7 g mol^{-1}): $C_{48}H_{108}O_{16}Si_4Yb_2$: C, 41.19; H, 7.78.

Found: C, 41.25; H, 7.75. ^{1}H NMR (Tol-d8, 400 MHz, 298 K): δ = 1.52 ppm (s, 108 H). ^{1}H NMR (THF-d8, 400 MHz, 298 K): δ = 1.37 ppm (s, 108 H). ^{1}H NMR (C_6D_{12}, 400 MHz, 298 K): δ = 2.69 ppm (s, 108 H).

Stability studies of complexes 1-Yb and 1-Sm

Stability of 1-Yb. The evolution of solutions of **1-Yb** (15 mg, 0.01 mmol) in Tol-d8 (0.3 mL), THF-d8 (0.3 mL), C_6D_{12} (0.3 mL) at room temperature was followed by ^{1}H NMR spectroscopy over time (400 MHz, 298 K). 1-Yb only shows evidence of decomposition after 36 hours at room temperature in Tol-d8 and THF-d8. After 5 days at room temperature, the ^{1}H NMR spectra show a decrease of 15% of the signals of 1-Yb in Tol-d8 and THF-d8. No appearance of new signals was observed over time that could be assigned to the decomposition products. Furthermore, the orange solution of **1-Yb** (30 mg, 0.021 mmol) in DME (0.3 mL) slowly fades over time at room temperature. After 15 days colourless single crystals suitable for X-ray diffraction of [Yb_2L_4(μ-$OMe)_2(DME)_2$] (2) could be isolated in a low yield. ^{1}H NMR spectroscopy of 1-Yb in C_6D_{12} showed that the complex is stable for weeks at room temperature in a C_6D_{12} solution.

Stability of 1-Sm. The evolution of solutions of **3-Sm** (15 mg, 0.01 mmol) in Tol-d8 (0.3 mL), THF-d8 (0.3 mL), C_6D_{12} (0.3 mL) at room temperature was followed by ^{1}H NMR spectroscopy over time. 1-Sm only shows evidence of decomposition after 36 hours at room temperature in THF-d8. After 5 days at room temperature, the ^{1}H NMR spectra show a decrease of 20% of the signals of 1-Sm in THF-d8. No significant new signals were observed over time that could be assigned to the decomposition products. ^{1}H NMR spectroscopy of 1-Sm in C_6D_{12} showed that the complex is stable for weeks at room temperature in in a C_6D_{12} solution. ^{1}H NMR study of 1-Sm in Tol-d8 at room temperature showed a decrease of the intensity of the signals assigned to 1-Sm, reaching 20 % of decomposition in Tol-d8 after 5 days, and the apparition of a signal at δ = 1.08 ppm corresponding to the reduced toluene adduct [$\{Sm_2L_3\}_2(\mu\text{-}\eta^6\text{:}\eta^6\text{-}C_7H_8)$].[17]

Reactivity

Reactivity of 1-Yb with CO_2 in THF-d8. $^{13}CO_2$ (~5 equivalents) was added to a liquid nitrogen frozen solution of 1-Yb (10 mg, 0.007 mmol, 1 eq.) in THF-d8 (0.3 mL). The solution was allowed to warm up at room temperature resulting in a colour change of the solution from orange to yellow. The ^{1}H NMR spectrum of the resulting solution (THF-d8, 400 MHz, 298 K) shows complete disappearance of the signals of 1-Yb, the appearance of a signal assigned to the [$YbL_3(THF)_2$] complex at δ = -16.93 ppm and of a new set of signals at δ = 1.23 ppm, 0.82 ppm and -0.01 ppm. The formation of [$YbL_3(THF)_2$] increased over 10 days reaching a conversion of approximately 50 %, determined by ^1H NMR using naphthalene as internal standard. ^{13}C NMR (THF-d8, 400 MHz, 298 K): δ = 185.02 ppm (free CO), 169.95 ppm (bound CO_3^2), 125.84 ppm (free CO_2), 99.97 ppm (siloxide), 37.67 ppm (siloxide), 31.65 ppm (siloxide) and 10.47 ppm (siloxide). No change in the ^{13}C NMR spectrum is perceived over time. The quantitative ^{13}C NMR of the evaporated reaction mixture after removing the excess of $^{13}CO_2$ in D_2O (D_2O, 600 MHz, 298 K, pD-13) shows a single signal at δ =168.26 ppm assigned to CO_3^{2-} in 90% yield using ^{13}C-labelled sodium acetate as internal standard.

Reactivity of 1-Yb with CO_2 in C_6D_{12}. $^{13}CO_2$ (~5 equivalents) was added to a liquid nitrogen frozen solution of 1-Yb (10 mg, 0.007 mmol, 1 eq.) in C_6D_{12} (0.3 mL). The solution was allowed to warm up at room temperature resulting in a colour change of the solution from dark brown to yellow. The ^1H NMR spectrum of the resulting solution (C_6D_{12}, 400 MHz, 298 K) shows signals at δ = 7.31 ppm, 1.54 ppm, 1.47 ppm (1-Yb) and 1.41 ppm. After 3 days at room temperature the signals at 1.54 ppm, 1.47 ppm (1-Yb) and 1.41 ppm disappeared and two new signals at δ = 1.51 ppm and 1.44 ppm can be identified. The ^{13}C NMR (C_6D_{12}, 400 MHz, 298 K) spectrum of the reaction mixture immediately after addition of $^{13}CO_2$: δ = 159.2 ppm, 125.82 ppm (free CO_2), 31.77 ppm (siloxide). ^{13}C NMR spectroscopy studies over time (C_6D_{12}, 400 MHz, 298 K) show the continuous decrease of the signal at δ = 159.20 ppm and the complete disappearance of it after 2 weeks at room temperature. The quantitative ^{13}C NMR spectrum of the evaporated reaction mixture after removing the excess of $^{13}CO_2$ in D_2O (D_2O, 600 MHz, 298 K, pD-13) shows two signals at δ = 167.62 ppm assigned to CO_3^{2-} and 179.72 ppm assigned to $C_2O_4^{2-}$ in 94 % total yield (oxalate and carbonate, using ^{13}C-labelled sodium acetate as internal standard) with a ratio of 1 : 50 (oxalate : carbonate). Here, the chemical shift of the signal assigned to oxalate is shifted from about 6 ppm compared to free oxalate suggesting that oxalate binding to Yb(III) may still occur at pH = 13. Pale yellow crystals of [$Yb_4L_8(C_2O_4)$] (**3**) suitable for X-ray diffraction were obtained overnight from a concentrated hexane solution of 1-Yb at -40 °C after addition of ~5 equivalents of CO_2 at room temperature.

Reactivity of 1-Sm with CO_2 in THF-d8. $^{13}CO_2$ (~5 equivalents) was added to a liquid nitrogen frozen solution of 1-Sm (10 mg, 0.007 mmol) in THF-d8 (0.3 mL). The solution was allowed to warm up at room temperature resulting in a colour fading of the solution from dark brown to colourless in few minutes. The ^1H NMR spectrum of the resulting solution (THF-d8, 400 MHz, 298 K) shows the complete disappearance of the signal assigned to 1-Sm and the formation of signals at δ = 1.51 ppm ([$SmL_3(THF)_2$]) and 1.31 ppm, growing over two days. The quantitative ^1H NMR spectrum shows, after two days, a yield of approximately 50%, determined by NMR using naphthalene as internal standard, for [$SmL_3(THF)_2$]. ^{13}C NMR (THF-d8, 400 MHz, 298 K); immediately after addition: δ =

185.20 ppm (free CO), 175.86 ppm, 174.43 ppm, 174.21 ppm, 125.94 ppm (free CO_2), 72.37 ppm (siloxide) and 32.97 ppm (siloxide). The quantitative ^{13}C NMR after 10 days of the evaporated reaction mixture after removing the excess of $^{13}CO_2$ in D_2O (D_2O, 600 MHz, 298 K, pD-13) shows two signals at δ = 168.32 ppm assigned to CO_3^{2-} and 173.36 ppm assigned to $C_2O_4^{2-}$ in 90 % total yield (oxalate and carbonate, using ^{13}C-labelled sodium acetate as internal standard) with a ratio of 1 : 104 (oxalate : carbonate).

Reactivity of 1-Sm with CO_2 in C_6D_{12}. $^{13}CO_2$ (~5 equivalents) was added to a liquid nitrogen frozen solution of 1-Sm (10 mg, 0.007 mmol) in C_6D_{12} (0.3 mL). The solution was allowed to warm up at room temperature resulting in a colour change of the solution from dark brown to light brown. The ^1H NMR spectrum of the resulting solution (C_6D_{12}, 400 MHz, 298 K) shows the formation of three sets of peaks at δ = -4.17 ppm, -4.45 ppm and -5.75 ppm. ^{13}C NMR (C_6D_{12}, 400 MHz, 298 K); immediately after addition: δ = 192.43 ppm (bound $C_2O_4^{2-}$/CO_3^{2-}), 191.72 ppm (bound $C_2O_4^{2-}$/CO_3^{2-}), 185.02 ppm (free CO), 128.70 ppm, 125.80 (free CO_2) and 32.14 ppm (siloxide). After 4 days, the colour of the solution turned colourless. No change in the ^1H NMR spectrum. ^{13}C NMR (C_6D_{12}, 400 MHz, 298 K); after four days at room temperature: δ = 185.02 ppm (free CO), 166.52 ppm, 164.99 ppm, 164.24 ppm, 128.70 ppm, 125.80 (free CO_2) and 32.14 ppm (siloxide). The quantitative ^{13}C NMR of the evaporated reaction mixture after removing the excess of $^{13}CO_2$ in D_2O (D_2O, 600 MHz, 298 K, pD-13) shows signals at 173.25 ppm ($C_2O_4^{2-}$) and 168.31 ppm (CO_3^{2-}) in a 1 : 17 ratio with a total yield of 98% (oxalate and carbonate, using ^{13}C-labelled sodium acetate as internal standard). Colourless crystals of $[Sm_4L_8(CO_3)_2]$ **(4)** suitable for X-ray diffraction were obtained from a concentrated hexane solution of 1-Sm left at -40 °C for 2 days after addition of ~5 equivalents of CO_2 at room temperature.

Reactivity of $[SmL_4K_2]$ with CO_2 in C_6D_{12}. $^{13}CO_2$ (~5 equivalents) was added to a liquid nitrogen frozen solution of $[SmL_4K_2]$ (10 mg, 0.008 mmol) in C_6D_{12} (0.3 mL). The solution was allowed to warm up at room temperature resulting in a colour change of the solution from red to colourless. The quantitative ^1H NMR in C_6D_{12} shows the complete disappearance of the signal assigned to $[SmL_4K_2]$ (δ = 2.41 ppm) and the formation of $[SmL_4K]$ (δ = 0.55 ppm) in approximately 50% yield, determined by NMR using naphthalene as internal standard. ^{13}C NMR (C_6D_{12}, 400 MHz, 298 K): δ = 202.05 ppm, 198.84 ppm, 168.43 ppm, 157.97 ppm, 156.52 ppm, 156.02 ppm, 125.80 (free CO_2), 72.29 ppm (siloxide), 32.37 ppm (siloxide). ^1H NMR and ^{13}C NMR spectroscopy studies did not show any changes in the spectra. The quantitative ^{13}C NMR of the evaporated reaction mixture after removing the excess of $^{13}CO_2$ in D_2O (D_2O, 600 MHz, 298 K, pD-13) shows two signals at δ = 173.36 ppm assigned to $C_2O_4^{2-}$ and δ = 168.22 ppm assigned to CO_3^{2-} in 92 % total yield (oxalate and carbonate, using ^{13}C-labelled sodium acetate as internal standard) with a ratio of 1 : 0.8 (oxalate : carbonate).

References

1 (a)W. B. Tolman, *Activation of Small Molecules: Organometallic and Bioinorganic Perspectives*, Wiley-VCH, Verlag, 2006; (b)C. Finn, S. Schnittger, L. J. Yellowlees and J. B. Love, *Chem. Commun.*, 2012, **48**, 1392-1399; (c)E. E. Benson, C. P. Kubiak, A. J. Sathrum and J. M. Smieja, *Chem. Soc. Rev.*, 2009, **38**, 89-99; (d)K. Huang, C. L. Sun and Z. J. Shi, *Chem. Soc. Rev.*, 2011, **40**, 2435-2452; (e)M. Aresta and A. Dibenedetto, *J. Chem. Soc.-Dalton Trans.*, 2007, 2975-2992; (f)M. Aresta, *Carbon Dioxide as a Chemical Feedstock*, Wiley VCH, 2010.

2 (a)K. A. Grice, *Coord. Chem. Rev.*, 2017, **336**, 78-95; (b)P. L. Arnold and Z. R. Turner, *Nat. Rev. Chem.*, 2017, **1**.

3 (a)A. Formanuik, F. Ortu, C. J. Inman, A. Kerridge, L. Castro, L. Maron and D. P. Mills, *Chem. Eur. J.*, 2016, **22**, 17976-17979; (b)O. P. Lam and K. Meyer, *Polyhedron*, 2012, **32**, 1-9; (c)I. Castro-Rodriguez and K. Meyer, *Chem. Commun.*, 2006, 1353-1368; (d)N. W. Davies, A. S. P. Frey, M. G. Gardiner and J. Wang, *Chem. Commun.*, 2006, 4853-4855; (e)G. B. Deacon, P. C. Junk, J. Wang and D. Werner, *Inorg. Chem.*, 2014, **53**, 12553-12563; (f)D. Heitmann, C. Jones, D. P. Mills and A. Stasch, *J. Chem. Soc.-Dalton Trans.*, 2010, **39**, 1877-1882; (g)I. Castro-Rodriguez, H. Nakai, L. N. Zakharov, A. L. Rheingold and K. Meyer, *Science*, 2004, **305**, 1757-1759; (h)L. Castro, S. Labouille, D. R. Kindra, J. W. Ziller, F. Nief, W. J. Evans and L. Maron, *Chem. Eur. J.*, 2012, **18**, 7886-7895; (i)L. Castro and L. Maron, *Chem. Eur. J.*, 2012, **18**, 6610-6615; (j)O. P. Lam, L. Castro, B. Kosog, F. W. Heinemann, L. Maron and K. Meyer, *Inorg. Chem.*, 2012, **51**, 781-783; (k)J. G. Brennan, R. A. Andersen and A. Zalkin, *Inorg. Chem.*, 1986, **25**, 1756-1760; (l)L. Castro, O. P. Lam, S. C. Bart, K. Meyer and L. Maron, *Organometallics*, 2010, **29**, 5504-5510; (m)I. Castro-Rodriguez and K. Meyer, *J. Am. Chem. Soc.*, 2005, **127**, 11242-11243; (n)L. Castro, D. P. Mills, C. Jones and L. Maron, *Eur. J. Inorg. Chem.*, 2016, 792-796.

4 (a)A. C. Schmidt, A. V. Nizovtsev, A. Scheurer, F. W. Heinemann and K. Meyer, *Chem. Commun.*, 2012, **48**, 8634-8636; (b)I. Korobkov and S. Gambarotta, in *Progress in Inorganic Chemistry, Vol 54*, ed. K. D. Karlin, 2005, vol. 54, pp. 321-348; (c)B. M. Gardner and S. T. Liddle, *Eur. J. Inorg. Chem.*, 2013, **2013**, 3753-3770; (d)O. T. Summerscales and F. G. N. Cloke, *Organometallic and Coordination Chemistry of the Actinides*, 2008, **127**, 87-117; (e)H. S. La Pierre and K. Meyer, in *Prog. Inorg. Chem.*, ed. K. D. Karlin, 2014, vol. 58, pp. 303-415; (f)S. T. Liddle, *Angew. Chem. Int. Ed. Engl.*, 2015, **54**, 8604-8641; (g)R. J. Kahan, F. G. N. Cloke, S. M. Roe and F. Nief, *New J. Chem.*, 2015, **39**, 7602-7607; (h)C. J. Inman, A. S. P. Frey, A. F. R. Kilpatrick, F. G. N. Cloke and S. M. Roe, *Organometallics*, 2017, **36**, 4539-4545; (i)C. L. Webster, J. W. Ziller and W. J. Evans, *Organometallics*, 2013, **32**, 4820-4827; (j)W. J. Evans, C. A. Seibel and J. W. Ziller, *Inorg. Chem.*, 1998, **37**, 770-776.

5 (a)A. S. P. Frey, F. G. N. Cloke, M. P. Coles, L. Maron and T. Davin, *Angew. Chem. Int. Ed. Engl.*, 2011, **50**, 6881-6883; (b)O. T. Summerscales, F. G. N. Cloke, P. B. Hitchcock, J. C. Green and N. Hazari, *J. Am. Chem. Soc.*, 2006, **128**, 9602-9603; (c)O. T. Summerscales, F. G. N. Cloke, P. B. Hitchcock, J. C. Green and N. Hazari, *Science*, 2006, **311**, 829-831; (d)M. B. Gardiner, J. C. Stewart, A. L. Davis, J. McMaster, W. Lewis, A. J. Blake and S. T. Liddle, *Proc Natl Acad Sci USA*, 2012, **109**, 9265-9270; (e)P. L. Arnold, Z. R. Turner, R. M. Bellabarba and R. P. Tooze, *Chem. Sci.*, 2011, **2**, 77-79; (f)V. Mougel, C. Camp, J. Pecaut, C. Coperet, L. Maron, C. E. Kefalidis and M. Mazzanti, *Angew. Chem. Int. Ed. Engl.*, 2012, **51**, 12280-12284; (g)O. Cooper, C. Camp, J. Pécaut, C. E. Kefalidis, L. Maron, S. Gambarelli and M. Mazzanti, *J. Am. Chem. Soc.*, 2014, **136**, 6716-6723; (h)C. Camp, O. Cooper, J. Andrez, J. Pecaut and M. Mazzanti, *J. Chem. Soc.-Dalton Trans.*, 2015, **44**, 2650-2656.

6 W. J. Evans, J. M. Perotti, J. C. Brady and J. W. Ziller, *J. Am. Chem. Soc.*, 2003, **125**, 5204-5212.

7 (a)U. R. Pokharel, F. R. Fronczek and A. W. Maverick, *Nat. Commun.*, 2014, **5**; (b)R. Angamuthu, P. Byers, M. Lutz, A. L. Spek and E. Bouwman, *Science*, 2010, **327**, 313-315; (c)C. T. Saouma,

C. C. Lu, M. W. Day and J. C. Peters, *Chem. Sci.*, 2013, **4**, 4042-4051; (d)L. J. Farrugia, S. Lopinski, P. A. Lovatt and R. D. Peacock, *Inorg. Chem.*, 2001, **40**, 558-559; (e)C. C. Lu, C. T. Saouma, M. W. Day and J. C. Peters, *J. Am. Chem. Soc.*, 2007, **129**, 4-5.

8 (a)W. J. Evans, S. E. Lorenz and J. W. Ziller, *Inorg. Chem.*, 2009, **48**, 2001-2009; (b)N. Tsoureas, A. F. R. Kilpatrick, C. J. Inman and F. G. N. Cloke, *Chem. Sci.*, 2016, **7**, 4624-4632; (c)J. Andrez, J. Pecaut, P.-A. Bayle and M. Mazzanti, *Angew. Chem. Int. Ed. Engl.*, 2014, **53**, 10448-10452; (d)A.-C. Schmidt, F. W. Heinemann, C. E. Kefalidis, L. Maron, P. W. Roesky and K. Meyer, *Chem. Eur. J.*, 2014, **20**, 13501-13506.

9 M. Xemard, V. Goudy, A. Braun, M. Tricoire, M. Cordier, L. Ricard, L. Castro, E. Louyriac, C. E. Kefalidis, C. Clavaguera, L. Maron and G. Nocton, *Organometallics*, 2017, **36**, 4660-4668.

10 (a)G. Fachinetti, C. Floriani and P. F. Zanazzi, *J. Am. Chem. Soc.*, 1978, **100**, 7405-7407; (b)S. Gambarotta, F. Arena, C. Floriani and P. F. Zanazzi, *J. Am. Chem. Soc.*, 1982, **104**, 5082-5092.

11 (a)J. P. Krogman, B. M. Foxman and C. M. Thomas, *J. Am. Chem. Soc.*, 2011, **133**, 14582-14585; (b)J. H. Jeoung and H. Dobbek, *Science*, 2007, **318**, 1461-1464.

12 (a)W. J. Evans, N. T. Allen and J. W. Ziller, *J. Am. Chem. Soc.*, 2001, **123**, 7927-7928; (b)W. J. Evans, G. Zucchi and J. W. Ziller, *J. Am. Chem. Soc.*, 2003, **125**, 10-11; (c)W. J. Evans, K. A. Miller and J. W. Ziller, *Angew. Chem. Int. Ed. Engl.*, 2008, **47**, 589-592; (d)O. P. Lam, S. C. Bart, H. Kameo, F. W. Heinemann and K. Meyer, *Chem. Commun.*, 2010, **46**, 3137-3139; (e)W. J. Evans, *J. Alloys Compd.*, 2009, **488**, 493-510.

13 (a)A. S. P. Frey, F. G. N. Cloke, M. P. Coles and P. B. Hitchcock, *Chem. Eur. J.*, 2010, **16**, 9446-9448; (b)O. T. Summerscales, A. S. P. Frey, F. Geoffrey, N. Cloke and P. B. Hitchcock, *Chem. Commun.*, 2009, 198-200; (c)S. M. Mansell, N. Kaltsoyannis and P. L. Arnold, *J. Am. Chem. Soc.*, 2011, **133**, 9036-9051; (d)W. J. Evans, J. W. Grate, I. Bloom, W. E. Hunter and J. L. Atwood, *J. Am. Chem. Soc.*, 1985, **107**, 405-409.

14 E. Louyriac, P. W. Roesky and L. Maron, *J. Chem. Soc.-Dalton Trans.*, 2017, **46**, 7660-7663.

15 (a)M. Falcone, L. Barluzzi, J. Andrez, F. F. Tirani, I. Zivkovic, A. Fabrizio, C. Corminboeuf, K. Severin and M. Mazzanti, *Nat. Chem.*, 2019, **11**, 154–160; (b)M. Falcone, L. Chatelain, R. Scopelliti, I. Zivkovic and M. Mazzanti, *Nature*, 2017, **547**, 332-335; (c)P. L. Arnold, C. J. Stevens, N. L. Bell, R. M. Lord, J. M. Goldberg, G. S. Nichol and J. B. Love, *Chem. Sci.*, 2017, **8**, 3609-3617; (d)M. Xemard, M. Cordier, E. Louyriac, L. Maron, C. Clavaguera and G. Nocton, *J. Chem. Soc.-Dalton Trans.*, 2018, **47**, 9226-9230.

16 W. J. Evans, D. S. Lee, D. B. Rego, J. M. Perotti, S. A. Kozimor, E. K. Moore and J. W. Ziller, *J. Am. Chem. Soc.*, 2004, **126**, 14574-14582.

17 R. P. Kelly, D. Toniolo, F. F. Tirani, L. Maron and M. Mazzanti, Chem. Commun., 2018, 54, 10268–10271.

18 G. Lapadula, M. P. Conley, C. Coperet and R. A. Andersen, Organometallics, 2015, 34, 2271–2277.

19 (a) D. J. Duncalf, P. B. Hitchcock and G. A. Lawless, Chem. Commun., 1996, 269–271; (b) G. B. Deacon, P. C. Junk and G. J. Moxey, Z. Anorg. Allg. Chem., 2008, 634, 2789–2792; (c) G. B. Deacon, C. M. Forsyth and N. M. Scott, Eur. J. Inorg. Chem., 2000, 2501–2506.

20 E. Prasad, B. W. Knettle and R. A. Flowers, *J. Am. Chem. Soc.*, 2002, **124**, 14663-14667.

21 C. Camp, J. Pecaut and M. Mazzanti, *J. Am. Chem. Soc.*, 2013, **135**, 12101-12111.

22 M. Nishiura, Z. M. Hou and Y. Wakatsuki, *Organometallics*, 2004, **23**, 1359–1368.

23 A. Paparo, J. S. Silvia, C. E. Kefalidis, T. P. Spaniol, L. Maron, J. Okuda and C. C. Cummins, *Angew. Chem. Int. Ed. Engl.*, 2015, **54**, 9115-9119.

24 N. Tsoureas, L. Castro, A. F. R. Kilpatrick, F. G. N. Cloke and L. Maron, *Chem. Sci.*, 2014, **5**, 3777-3788.

25 W. J. Evans, D. K. Drummond, H. M. Zhang and J. L. Atwood, *Inorg. Chem.*, 1988, **27**, 575–579.

Chapter 8. Anhydrous conditions enable the catalyst-free carboxylation of aromatic alkynes with CO2 under mild conditions.[7]

Introduction

The utilization of CO_2 as a C1 source is attractive due to its low toxicity, low price and abundance.[1,2] CO_2 is the main cause of global warming and hence its emission in the atmosphere must be limited.[3] The development of synthetic methods employing CO_2 as the reactive synthon allows for the replacement of harmful, petrochemical-based chemicals that are routinely used. Recent years have seen the emergence of many reactions building complexity with CO_2.[4] Examples include the synthesis of cyclic carbonates[5,6], methylated amines[7], formylated amines,[8] proprioylic carboxylic acids[9–11] and esters and numerous heterocycles[12]. It is accepted that CO_2 is a thermodynamically stable and kinetically inert molecule that requires robust catalytic tools to be efficiently transformed. Nevertheless, a plethora of reports demonstrate that CO_2 transformation can often be base-catalysed. In this respect, the utilization of Cs_2CO_3 and DMSO appears to be a privileged system for CO_2-related applications.[13]

Of the reactions mentioned above, the carboxylation of alkynes is interesting due to the importance of propyolic acid derivatives in medicinal chemistry.[14] To date, many studies have been carried out to optimize the conditions for the carboxylation of terminal alkynes. Most of previous studies rely on either homogeneous or heterogeneous catalysts mostly based on copper, silver or lanthanide to achieve high conversions under mild conditions (Figure 1).[14,15] However, other metals such as Pd, Mo and rare earth metals have shown catalytic activity.[16,17,18] Typically, the catalyst is believed to facilitate the deprotonation of the alkyne, which leads to a facilitated CO_2 insertion and hence better yields. Many times, a second esterification step is needed to stabilize the product and avoid the decomposition once the carbon dioxide is removed or under the analytical conditions. In Scheme 1 are summarized some of the catalysts and reaction conditions that have been studied.

---

[7] Part of this chapter have been published: D. Toniolo, F. D. Bobbink, P. J. Dyson, M. Mazzanti, *Helvetica Chimica Acta*, 2020, **103**.
Authors contributions: D.T. performed the synthesis and the catalytic experiments. F.D.B. performed the GC analysis, P.J.D. and M.M. coordinated the work.

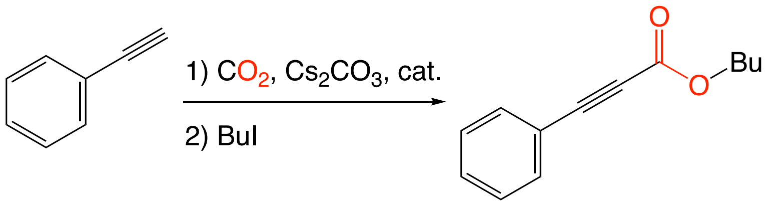

Previous work:

AgI (1 % mol) DMF, 50 °C, 2 bar, 44-96 % yield	$AgBF_4$ (0.05-0.25 % mol) DMSO, 50 °C, 1 bar, 21-99 % yield	NHC-Ag (1 % mol) DMF, RT, 1 bar, 0-85 % yield

Scheme 1. Carboxylation of phenylacetylene using Cs_2CO_3 as the base and CO_2 as the carboxylation reagent.

DFT calculations were performed for both Cu and Ag catalysts, and revealed the active specie to be a $[CuL]^+$ or $[Ag(CO_3)L]^-$ (L = ligand or solvent) complexes capable to coordinate and deprotonate the alkyne in presence of a base, and subsequently insert CO_2 into the M-C bond (Scheme 2).[19,20,21] At the same time, it has been reported that the catalyst-free reaction in DMF or DMSO does not proceed, or only results in poor yields.[22,23] However, good and excellent yields were achieved by Yugen and coworkers when the reaction was carried out in DMF at high temperature (120-160 °C) and pressure (2.5-7 bar), even in absence of catalytic species.[24] Moreover, only recently Huang and coworker report a non-negligible yield (37 %) if the reaction is carried out in DMSO at 60 °C for 6 hours in presence of 1.5 equiv. of Cs_2CO_3 in absence of catalyst, but the result could have been rationalized considering the possibility to have metallic impurities in the reaction mixture.[25]

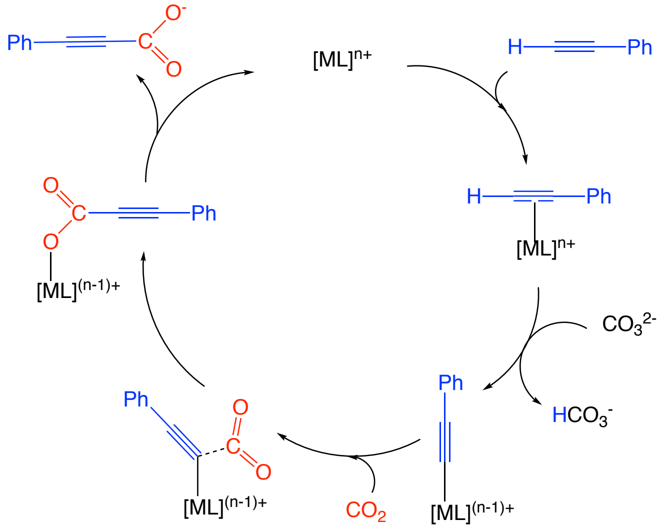

Scheme 2. Proposed mechanism for the carboxylation of terminal alkynes.

Shen and coworkers have demonstrated that trivalent ytterbium acetylide complexes containing bisphenolate ligands undergoes CO_2 insertion into the metal-carbon bond and hence these complexes has the potential to be used as catalysts.[26] Based on the mechanism proposed in previous reports and our own expertise in f-element chemistry, we set-out to develop an Ytterbium complex that would allow to reveal the mechanistic details of the transformation and delineate its accompanying challenges.

Results and Discussion

Following the example of Shen, we tested the catalytic activity of ytterbium bisphenolate complexes. [Yb(MPA)CCPh(THF)], **1,** was prepared by treating the divalent [Yb(HMDS)$_2$] with one equivalent of MPAH$_2$ in hexane, followed by reaction with one equivalent of phenylacetylene in THF. Complex **1** is presumably the first intermediate of the catalytic carboxylation reaction. The crystal structure of **1** (Figure 1) shows and Yb(III) centre hexa-coordinated in a distort tetragonal bi-pyramid geometry with a terminal phenyl acetylene moiety. The coordination sphere is completed with a THF molecule.

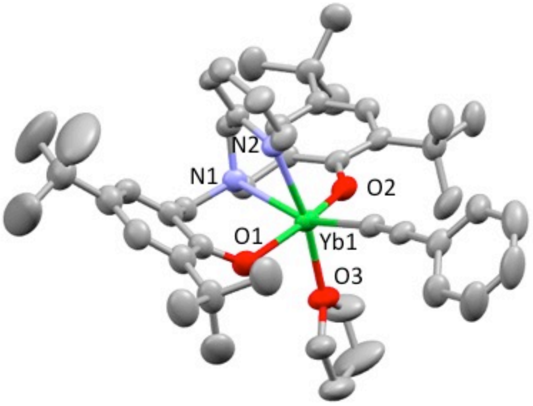

Figure 1. XRD structure of **1** (ellipsoid 50%, hydrogen atoms have been omitted for clarity)

Upon exposure to carbon dioxide, a CO_2 molecule inserts into the M-C bond, affording [Yb(MPA)O$_2$CCCPh]$_2$, **2**. The solid state structure of **2** (Figure2) shows two identical [Yb(III)(MPA)] moieties connected by two bridging propiolate anions. The metal centres are epta-coordinated and are situated in the cavity of the MPA^{2-} ligand.

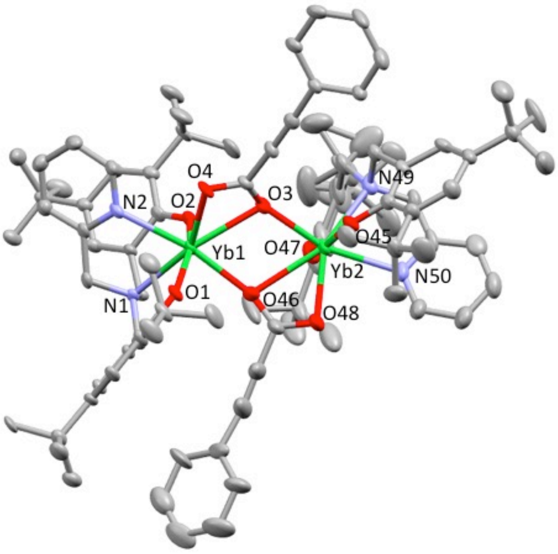

Figure 2. XRD structure of **2** (ellipsoid 50%, hydrogen atoms have been omitted for clarity)

Complexes **1** and **2** represent the two hypothesized intermediates in the catalytic cycle proposed by DFT. In case the two complexes show a catalytic activity and the response is the same, it would be the experimental prove of the proposed mechanism and it would confirm the calculations.

After the successful synthesis of the hypothesized intermediate we moved to the utilization of complexes as catalysts for the carboxylation. Like in most of the previous reported examples we relied on a second esterification step to convert the product into the corresponding more stable ester. We started our investigation at a working temperature of 40 °C but this resulted in poor yields. Differently, when the temperature was increased to 80 °C, the reaction proceeded smoothly and resulted in excellent yields. With a load of 2 mol% catalysis, 99 % conversion was obtained after a 4 hours reaction. Also starting from complex **2**, the same results were obtained, increasing the reliability in the reaction mechanism proposed by DFT.

However, to confirm that complexes **1** and **2** were actually acting as catalyst in the reaction, and to prove that the ligand scaffold plays a role in the catalyst activity, a test was conducted using commercially available ytterbium salts. Interestingly, the use of [$YbCl_3$] also resulted in a quantitative yield in the same reaction conditions. This result was initially rationalized as an indication that the different electronic properties due to the ligands scaffold are not crucial for catalysis, but they are important in order to isolate key reaction intermediates.

After this result a catalytic test was conducted in absence of catalyst. To our surprise, the control experiment resulted as well in excellent conversions. This test in absence of catalyst was repeated several times to confirm the result, because the catalyst free reaction was reported to not proceed, or only result in poor yields. This surprizing discovery suggested that a catalyst specie is not required for the reaction to proceed, and motivated us to further study the reaction to understand the parameters that were influencing the outcome of the reaction.

Phenylacetylene was taken a model substrate. Initially, the reaction was conducted in DMSO at 40 °C for 24 h under 1 atm. CO_2 in presence of two equivalents of Cs_2CO_3. A non-negligible yield of 33% was obtained (Table 1, entry 1) in line with previous results showing that the reaction proceeds to some extent under very mild conditions even in the absence of a catalyst.[25] We found that, on increasing the temperature to 60 °C and then to 80 °C the yields increases up to 99 % in 4 hours (Table 1, entries 2, 3). The increase in yield with temperature is attributed to the increased solubility of the base in DMSO with temperature, and to faster deprotonation kinetics.[27] To demonstrate the ability of the base to deprotonate (at least partially) the acidic C-H bond, the reaction between phenylacetylene and Cs_2CO_3 was monitored by ^1H NMR spectroscopy (see appendix, figure S4). The signal assigned to the aliphatic proton disappeared after 1 h at 80 °C, confirming deprotonation of the alkyne. This result suggest that the rate determining step of the C-H carboxylation reaction is the deprotonation of the alkyne because the subsequent reaction with $^{13}CO_2$ resulted in the fast formation of the 3-phenylpropiolate salt, detected by ^{13}C NMR spectroscopy (appearance of a signal at 155.8 ppm assigned to the carboxylic group, see appendix Figures S6, S7).

The reaction does not proceed when it is conducted in DMF or THF (Table 1 entries 4 and 5), where Cs_2CO_3 is markedly less soluble, indicating that the solubility of Cs_2CO_3 is important for good activity, presumably due to the deprotonation rate that is accelerated when the base is soluble.[18,28] Low yields are also obtained with sub-stoichiometric amounts of anhydrous Cs_2CO_3 (Table 1, entry 6).

Remarkably, at 80 °C the time required for a near-quantitative conversion of the substrate is much shorter compared to those previously reported in literature (14-24 h), even if catalysts are used and/or harsher conditions are applied.[16,18,24,28] Notably, high yields are only reached after 12 h when the $AgPF_6$ catalyst was used in DMF with stoichiometric amounts of Cs_2CO_3 and 2 atm. CO_2.[29] The time-dependent yields measured at 80 °C show that the reaction is essentially first order with respect to the substrate with an estimated kinetic constant of 2 h^{-1}, and reaches the maximum yield after approximately 3 h (Figure 2, Table 1, entries 7-9). To ensure that the carboxylic group is derived from CO_2 and not Cs_2CO_3, an experiment was conducted in absence of CO_2 and no reaction was observed (Table 1, entry 10).

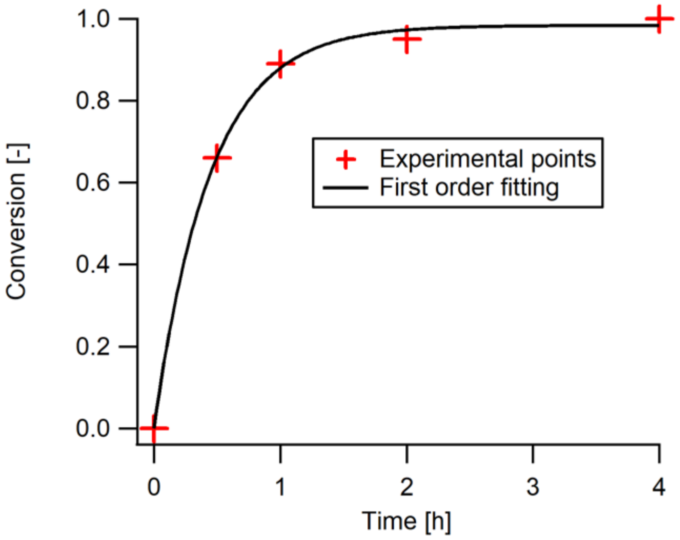

Figure 2. Time-dependent yields for the catalyst-free carboxylation of phenylacetylene. Reaction condition: PhCCH (28 mg, 0.28 mmol), Cs_2CO_3 (183 mg, 0.56 mmol, 2 eq.), CO_2 (1 atm.), DMSO (1 mL), 80 °C.

Table 1. Optimization of reaction conditions. Reaction conditions: phenylacetylene (0.28 mmol), CO_2 (1 atm), Cs_2CO_3 (183 mg, 0.56 mmol, 2 eq.), DMSO (1 mL). Product trapped with butyl iodide (1.1 eq.). [a] Yields determined by GC using n-decane as internal standard. [b] Isolated product. [c] 0.2 eq. of Cs_2CO_3. [d] Without CO_2.

Entry	Solvent	T [°C]	Time [h]	Yield [%][a]
1	DMSO	40	24	33
2	DMSO	60	4	30
3	DMSO	80	4	> 99, 91[b]
4	DMF	80	4	4
5	THF	80	4	< 1
6[c]	DMSO	80	4	6
7	DMSO	80	2	95
8	DMSO	80	1	83
9	DMSO	80	0.5	66
10[d]	DMSO	40	24	< 1

[a]Yields determined by GC using n-decane as internal standard.

[b]Isolated product. [c]0.2 eq. of Cs_2CO_3. [d]Without CO_2.

Our results show that the low to modest yields reported for the catalyst-free reaction in DMSO can be easily optimized by increasing the temperature to 80°C to afford the product in near-quantitative yield. Since the reproducibility of carboxylation reaction promoted by weak bases as Cs_2CO_3 is likely to be affected by the presence of water, even under forcing conditions (high temperature, overpressure),[30] we investigated the effect of stoichiometric amounts of water in the used mild conditions. Addition of carefully controlled amounts of water (0.1, 0.2 and 1 eq. with respect to Cs_2CO_3) to the system leads to a significant reduction in yield (Table 2, entries 1-3, 80, 43 and <1 %, respectively). Hence, to ensure reproducible high yields under catalyst-free conditions, water must be excluded from the reaction mixture and anhydrous solvents and reagents must be used. The detrimental effect of water is not unique to metal free carboxylation reactions. To emphasize the general detrimental effect of water we performed the metal catalysed reaction using the performant $AgPF_6$ under the reported conditions,[29] but in the presence of H_2O (1 eq.). The experiment resulted in negligible yield (Table 2, entry 4). These results indicate that rigorously anhydrous conditions (thoroughly dried solvents, anhydrous Cs_2CO_3 and reagents, rigorous Schlenk techniques) should be used even in presence of a catalytic specie.

Table 2. Effect of water on the catalysed and catalyst-free reaction. Reaction conditions: phenylacetylene (0.28 mmol), CO_2 (1 atm), DMSO (1 mL). Product trapped with butyl iodide (1.1 eq.). Yields determined by GC using n-decane as internal standard.

Entry	**Notes**	**T [°C]**	**Time [h]**	**Yield [%]**
1	0.1 eq H_2O	80	4	80
2	0.2 eq H_2O	80	4	43
3	1 eq H_2O	80	4	< 1
4	$AgPF_6$ (4 %), 1 eq H_2O	80	4	< 1

Knowing the detrimental effect of water in the reaction mixture, to ensure the reproducibility of the experiments is necessary to establish a protocol and an analytic method to measure or estimate the moisture in the solvent and the reagents.

The water content in DMSO and phenylacetylene can be evaluated by ^1H NMR spectroscopy and revealed that the reagents employed in this study do not contain water in sufficient amount to influence the kinetics (see appendix). Probing the water content in Cs_2CO_3 by ^1H NMR spectroscopy in DMSO-d6 revealed that the water signal only becomes apparent when the amount exceeds 1 equiv. of water per equiv. of carbonate (see appendix, figure S5). This suggests that ^1H NMR spectroscopy is unsuited to quantify very low water content in Cs_2CO_3. Nevertheless, the water content in Cs_2CO_3 can conveniently be estimated by elemental analysis, provided the analysis is conducted under inert, dry atmosphere (Table S1). Established water removal methods such as drying over molecular sieves (DMSO and PhCCH) or by drying under high vacuum for several days (Cs_2CO_3) can be employed and dramatically increases the reaction yield.

The catalytic activity of transition metal ions based on copper or silver in DMF (where Cs_2CO_3 is not able to deprotonate terminal alkynes) reported by other authors can be rationalized by the ability of those metals to coordinate the substrate, weakening the C-H bond, and accelerating the deprotonation of the alkyne, as proposed in computational studies.[19,20] However, our results strongly suggest that the carboxylation of aromatic terminal alkynes in DMSO essentially proceeds via an uncatalyzed acid-base reaction and the addition of catalyst is not crucial.

The catalyst-free carboxylation was explored for various phenyl acetylene derivatives under the reaction conditions optimized for phenyl acetylene. Quantitative yields were obtained in four hours for aromatic alkynes with electron withdrawing groups in the aromatic ring and for both p-methyl phenyl acetylene and m-methoxy phenyl acetylene. (Table 3, Entry 1-7), while good yields were instead achieved for less acid alkynes (Table 3, Entry 7-10).

Table 3. Carboxylation of phenyl acetylene derivatives. Reaction conditions: alkyne (0.28 mmol), CO_2 (1 atm), DMSO (1 mL). Product trapped with butyl iodide (1.1 eq.). Yields determined by GC using n-decane as internal standard. [a]Isolated yield.

Entry	*Alkyne*	*Time [h]*	Yield [%]
1	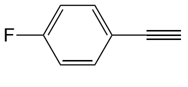	4	> 99, 92[a]
2	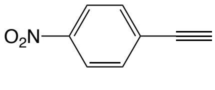	4	> 99
3	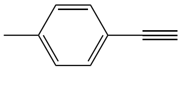	4	> 99
4	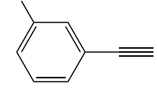	4	> 99, 95[a]

5	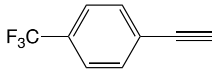	4	> 99
6	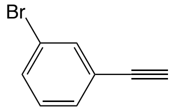	4	> 99
7	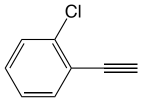	4	> 99
8	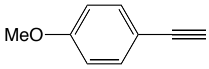	4	88
9	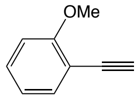	4	75
10	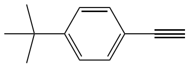	4	60

The mechanism of the base-promoted transformation is therefore postulated to require the following steps: deprotonation of the alkyne by the carbonate base, insertion of CO_2, nucleophilic attack of the carboxylate anion onto the alkyl halide in the final step. Scheme 3 summarizes the key mechanistic steps and postulates the main deactivation pathway due to water, i.e. acidification of the reaction mixture inhibiting the deprotonation of the alkyne.

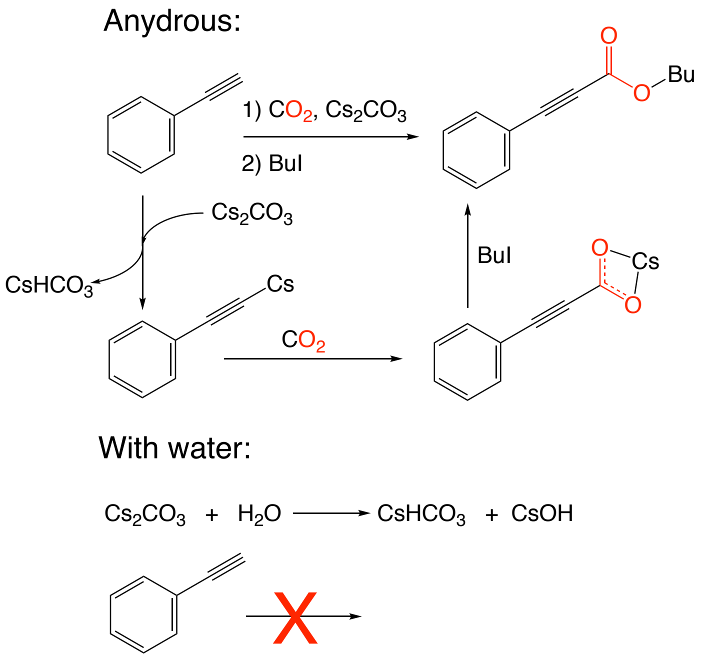
Anydrous:
1) CO2, Cs2CO3
2) BuI
O
O
Bu
Cs2CO3
CsHCO3
Cs
CO2
BuI
O
Cs
O
With water:
Cs2CO3 + H2O → CsHCO3 + CsOH

Scheme 3. Proposed steps for the uncatalysed carboxylation of PhCCH using CO_2 as in the absence (top) and presence (bottom) of water.

Conclusion

In conclusion, we demonstrated that carboxylation of phenylacetylene can be promoted in quantitative yield under anhydrous conditions using Cs_2CO_3 as the base in DMSO under mild conditions and in short reaction times (80 °C, 1 atm. CO_2, 4 h). When moisture is present in the reaction mixture, even reported catalysts such as $AgPF_6$ are unable to catalyse the reaction. Hence, the C-H carboxylation of alkynes proceeds mainly *via* an acid-base mechanism. We believe that these results can be generalized to many base-promoted CO_2 reactions.

Experimental

General methods.

Loading of reagents for carboxylation was carried out under an inert argon atmosphere using an MBraun glovebox equipped with a purifier unit or using standard Schlenk-type techniques. Glassware was dried overnight at 150 °C prior to use. Unless otherwise noted, reagents were acquired from commercial sources and used without further purification. The solvents and the reagents were purchased from Sigma Aldrich or Eurisotop (deuterated solvents) in their anhydrous form, conditioned under argon and dried with molecular sieves (4 Å) for two weeks. Water content in DMSO was tested using quantitative ^1H NMR spectroscopy (see supporting information). Cs_2CO_3 was purchased from Sigma Aldrich and dried under vacuum (10^{-3} bar) for 5 days at 60 °C prior to use. Shorter drying times result in the deleterious presence of water and reduced catalytic performance (see supporting information). ^1H and ^{13}C NMR experiments were carried out using NMR tubes adapted with J. Young valves. The NMR spectra were recorded on Bruker 400 or 800 MHz. ^1H chemical shifts are reported in ppm and were measured relative to residual solvent peaks, which were assigned relative to an external TMS standard set at 0.00 ppm. Gas chromatography-mass spectrometry (GC-MS) of liquid samples was performed on an Agilent 7890B Gas Chromatograph together with Agilent 7000C MS triple quad detector using He as the carrier gas. The yields were determined by the internal standard method using n-decane as the internal standard.

Synthesis of [Yb(MPA)CCPh(THF)].

A dispersion of $MPA(OH)_2$ (250 mg, 0.46 mmol, 1eq) in 6 ml of hexane was slowly added dropwise to a stirring solution of $[Yb(HMDS)_2(THF)_3]$ (325 mg, 0.46 mmol, 1eq) in 6 mL of hexane. After 4 hours of stirring at room temperature the mixture turned brown with formation of a green precipitate.

The suspension was taken to dryness and the solid obtained was dissolved in 5 ml of THF affording a brown solution. ^{1}H NMR (400 MHz, THF-d8, 298 K) of the intermediate: δ = 8.01, 7.39, 6.88, 6.79, 6.75, 6.61, 4.29, 3.53, 3.05, 1.34, 1.22. PhCCH (100 µL 0.92 mmol, 2 eq) was added. The solution was stirred at room temperature for 24 hours. The reaction mixture was taken to dryness and the solid obtained was washed 3 times with 4 ml of hexane. The [Yb(MPA)(CCPh)(THF)] (889.10 g/mol) in form of a pale yellow solid insoluble in hexane was recovered (220 mg, 55% yield). Re-crystallization of this complex by slow diffusion of hexane into a THF solution of the complex afforded yellow crystals suitable for X-ray diffraction. ^{1}H NMR (400 MHz, THF-d_8, 298 K): δ = 65.38, 57.79, 50.40, 44.83, 0.68, 0.52, 0,32, -1.08, -6.33, -14.69, -16.03, -18.89, -55.70, -86.50. Elemental analysis calc. for [Yb(MPA)(CCPh)(THF)]: C, 64.85; H, 7.14; N, 3.15. Found: C, 64.83; H, 7.22; N, 3.04.

Synthesis of [Yb(MPA)(COOCCPh)]$_2$.

70 mg of isolated **1** were dissolved in 3 ml of THF. After removal of the argon headspace, an excess of CO_2 was added and the solution was stirred at room temperature for 3 hours. The solution was taken to dryness affording and 65 mg of [Yb(MPA)(COOCCPh)]$_2$ (1722.7 g/mol) were recovered (88 % yield). ^{1}H NMR (400 MHz, THF-d8, 298 K): δ = 51.05, 38.84, 35.01, 32.00, 21.10, 6.68, -2.60, -5,74, -19.92, -54.03 Elemental analysis calcd. for [Yb(MPA)(O_2CCCPh)]$_2$: C, 62.78 ; H, 6.44 ; N, 3.25. Found: C, 62.57; H, 6.08; N, 2.88.

Typical procedure for the base-promoted carboxylation reaction.

To ensure reproducibility with respect to temperature and time, four reactions were conducted simultaneously.[31] Four 25 mL round bottom flasks were each charged with 183 mg (0.56 mmol, 2 equiv.) of anhydrous Cs_2CO_3, 30 µL of phenyl acetylene (0.28 mmol, 1 equiv.), and 1 mL of DMSO. The individual reaction mixtures were stirred to afford pale yellow suspensions. The mixtures were frozen and then 1 atm CO_2 was introduced to each flask after removing the argon atmosphere under mild vacuum. Subsequently, the mixtures were quickly warmed to 80 °C in a pre-heated oil bath under continuous stirring at 400 rpm for 4 hours. Then each mixture was cooled to 40 °C and 35 µL of 1-iodobutane (0.3 mmol, 1.1 equiv.) were added under air. After 1 h, 53 µL of n-decane (0.28 mmol, 1 eq) were added as internal standard together with 4 ml of AcOEt. The suspension was filtered to remove the cesium carbonate and hydrogen carbonate formed during the reaction and the filtrate was analysed by GC-MS/FID.

For the reaction conduced with other substrates the same procedure described above was used, except that an equimolar amount of other acetylene derivatives was employed.

For the reactions conduced with different solvents, temperature, amount of base or time, the same procedure described above was used, except for that other solvents, other temperature, other amount of base or other times were employed.

For the reaction conduced in presence of $AgPF_6$ the same procedure described above was used, except that $AgPF_6$ was added to the reaction flask under argon atmosphere before the addition of CO_2.

For the reaction conducted without CO_2 the same procedure described above was used, except that CO_2 was not added to the flasks.

For the reactions conduced in presence of water the same procedure described above was used, except that H_2O was added to the flasks trough a septum outside of the glovebox.

Synthesis of the phenylpropiolic esters by direct carboxylation.

A 25 mL round bottom flask was charged with 549 mg (1.68 mmol, 2 eq) of anhydrous Cs_2CO_3, 90 µL of phenyl acetylene (0.84 mmol, 1 eq), and 3 mL of DMSO. The mixture was frozen and then 1 atm CO_2 was introduced in the flask after removing the argon atmosphere under mild vacuum. Subsequently, the mixture was quickly warmed to 80 °C in a pre-heated oil bath and maintained at to 80 °C under continuous stirring at 400 rpm for 4 hours. The mixture was then cooled to 40 °C and 105 µL of 1-iodobutane (0.9 mmol, 1.1 eq) were added under air. After 1 h, water (5 mL) was added to the system and the mixture was extracted three times with Et_2O (4 mL each). The combination of the organic phases was dried under vacuum affording the butyl 3-phenylpropiolate as viscous oil (152 mg, 91% yield).

^1H NMR spectrum of butyl 3-phenylpropiolate (THF-d8, 400 MHz, 298 K): δ = 7.58-7.60 (d, 2H, J = 8 Hz), 7.38-7.48 (m, 2 H), 7.30-7.31 (d, 1H, J = 4 Hz), 4.17-4.20 (t 2H), 1.62-1.69 (m, 2H), 1.37-1.47 (m, 2H), 0.93-0.97 (t, 3H) (see appendix, figure S3). HRMS (APPI/LTQ-Orbitrap) m/z calc. for $C_{13}H_{15}O_2^+$ $[M + H]^+$: 203.1067; Found 203.1064.

The synthesis of 3-p-fluorophenylpropiolate and 3-m-methoxyphenylpropiolate was performed using the same conditions except for the final extraction of the ester from water which was performed using CH_2Cl_2 instead of ether (three times with 4 mL).

^1H NMR spectrum of butyl 3-p-fluorophenylpropiolate (CD_3CN, 400 MHz, 298 K): δ = 7.64-7.68 (m, 2H), 7.17-7.22 (m, 2H), 4.20-4.23 (t, 2H), 1.63-1.70 (m, 2H), 1.36-1.45 (m, 2H), 0.93-0.96 (m, 3H). HRMS (ESI/QTOF) m/z calc. for $C_{13}H_{14}FO_2^+$ $[M + H]^+$: 221.0978; Found 221.0977

^1H NMR spectrum of butyl 3-m-methoxyphenylpropiolate (CD_3CN, 400 MHz, 298 K): δ = 7.33-7.37 (t, 1H), 7.18-7.20 (d, 1H, J = 8 Hz), 7.15 (s, 1H), 7.08-7.10 (m, 1H), 4.20-4.23 (t, 2H), 3.80 (s, 3H)

1.63-1.70 (m, 2H), 1.36-1.46 (m, 2H), 0.93-0.97 (t, 3H). HRMS (ESI/QTOF) m/z calc. for $C_{14}H_{16}O_3Ag^+$ $[M + Ag]^+$: 339.0150; Found 339.0163.

References

1 D. M. D'Alessandro, B. Smit and J. R. Long, *Angew. Chem. Int. Ed.*, 2010, **49**, 6058–6082.

2 B. Smit, A.-H. A. Park and G. Gadikota, Frontiers in Energy Research, 2014, **2**, 2013–2015.

3 R. Monastersky, Nature, 2013, 497, 13–14.

4 Q. Liu, L. Wu, R. Jackstell and M. Beller, *Nat. Commun.*, 2015, **6**, 1–15.

5 F. D. Bobbink, D. Vasilyev, M. Hulla, S. Chamam, F. Menoud, G. Laurenczy, S. Katsyuba and P. J. Dyson, *ACS Catalysis*, 2018, **8**, 2589–2594.

6 F. D. Bobbink and P. J. Dyson, *J. Catal.*, 2016, **343**, 52–61.

7 S. Das, F. D. Bobbink, G. Laurenczy and P. J. Dyson, *Angew. Chem. Int. Ed.*, 2014, **53**, 12876–12879.

8 M. Hulla, F. D. Bobbink, S. Das and P. J. Dyson, *ChemCatChem*, 2016, **8**, 3338–3342.

9 Y. Yuan, C. Chen, C. Zeng, B. Mousavi, S. Chaemchuen and F. Verpoort, *ChemCatChem*, 2017, **9**, 882–887.

10 D. Yu, F. Zhou, D. S. W. Lim, H. Su and Y. Zhang, ChemSusChem, 2017, **10**, 836–841.

11 M. Trivedi, J. R. Smreker, G. Singh, A. Kumar and N. P. Rath, *New J. Chem.*, 2017, **41**, 14145–14151.

12 M. Hulla, S. M. A. Chamam, G. Laurenczy, S. Das and P. J. Dyson, *Angew. Chem. Int. Ed.*, 2017, **56**, 10559–10563.

13 F. D. Bobbink, W. Gruszka, M. Hulla, S. Das and P. J. Dyson, *Chem. Commun.*, 2016, **52**, 10787–10790.

14 F. Manjolinho, M. Arndt, K. Gooßen and L. J. Gooßen, *ACS Catal*., 2012, **2**, 2014–2021.

15 J. Hong, M. Li, J. Zhang, B. Sun and F. Mo, *ChemSusChem*, 2019, **12**, 6–39.

16 M. Trivedi, G. Singh, A. Kumar and N. P. Rath, *Dalton Trans.*, 2015, **44**, 20874–20882.

17 J.-H. Chen, C.-H. Deng, S. Fang, J.-G. Ma and P. Cheng, *Green Chem*., 2018, **20**, 989–996.

18 H. Cheng, B. Zhao, Y. Yao and C. Lu, *Green Chem.*, 2015, **17**, 1675–1682.

19 J. Jover and F. Maseras, J. Org. Chem., 2014, **79**, 11981–11987.

20 C. Liu, Y. Luo, W. Zhang, J. Qu and X. Lu, *Organometallics*, 2014, **33**, 2984–2989.

21 R. Yuan and Z. Lin, ACS Catal., 2014, **4**, 4466–4473.

22 M. Arndt, E. Risto, T. Krause and L. J. Gooßen, *ChemCatChem*, 2012, **4**, 484–487.

23 B. Yu, J.-N. Xie, C.-L. Zhong, W. Li and L.-N. He, *ACS Catal.*, 2015, **5**, 3940–3944.

24 Y. Dingyi and Z. Yugen, Green Chem., 2011, **13**, 1275–1279.

25 Z. Wu, L. Sun, Q. Liu, X. Yang, X. Ye, Y. Hu and Y. Huang, *Green Chem.*, 2017, **19**, 2080–2085.

26 H. Zhou, H. Guo, Y. Yao, L. Zhou, H. Sun, H. Sheng, Y. Zhang and Q. Shen, *Inor. Chem.*, 2007, **46**, 958–964.

27 J. W. Bunting and D. Stefanidis, *Can. J. Chem.*, 1989, **67**, 428–432.

28 S. Li, J. Sun, Z. Zhang, R. Xie, X. Fang and M. Zhou, *Dalton Trans.*, 2016, **45**, 10577–10584.

29 X. Zhang, W.-Z. Zhang, X. Ren, L.-L. Zhang and X.-B. Lu, *Org. Lett.*, 2011, **13**, 2402–2405.

30 O. Vechorkin, N. Hirt and X. Hu, *Org. Lett.*, 2010, **12**, 3567–3569.

31 F. D. Bobbink, S. Das and P. J. Dyson, *Nat. Protoc.*, 2017, **12**, 417.

Conclusions and Perspectives

In this work we explored different ways to build multimetallic systems capable to undergo multielectron transfer for the activation of small molecules.

First, the synthesis of complexes bearing more than one metal atom has been achieved via reduction of redox active ligands supporting the metal centre through the formation of C-C bonds. The in situ formed new ligands resulted capable of force multiple metal centres in close proximity and store electrons. We have shown that the combination of the redox active salophen ligand together with uranium and transition metals provide a versatile route for the synthesis of heterometallic U-M (M = Ni, Co, Fe) compounds, that showed an enhancement of the reactivity compare to the uranium homobimetallic analogue.

In parallel, and inspired by recent work on cobalt, we have also investigated the possibility of building polymetallic complexes of iron by using the salophen ligands. The reduction of the iron complex supported by the salophen ligand undergoes either ligand centred or metal centred reduction depending on the conditions, and the metal ion active participate to transferring electron to the ligand scaffold. An unprecedent self-assembly of a trinuclear divalent iron complex was discovered with an enhancement of the magnetic properties compared to the monometallic system. It has been also confirmed that the electron stored in the C-C bond are available for the reduction of carbon dioxide with selective formation of CO and carbonate.

The redox active trensal ligand has been used to support Eu, Sm and Nd complexes. The reduction of these complexes resulted in the formation of a bimetallic compounds for the Sm and the Nd with two or four electrons stored in C-C bonds. Differently, the reduction of the Eu analogue resulted to be metal centred. The bimetallic Sm and Nd compounds resulted to be more reactive that the previously reported salophen analogues, resulting able to react with carbon dioxide forming selectively CO and carbonate.

It has been showed that dinuclear complexes containing low-coordinate Yb(II) and Sm(II) can be stabilized by the polydentate tris(*tert*-butoxy)siloxide ligand. Both complexes exhibit reaction with carbon dioxide in ambient conditions leading to a mixture of carbonate and oxalate. The selectivity of the reduction depends on the solvent polarity and on the nature of the ion. The ytterbium complexes resulted active towards carbon disulphide, promoting the formation of the rare $C_2S_2^{2-}$ moiety. Also, dissolution of the divalent samarium complex in toluene resulted in the formation of multideker complex providing the first example of toluene reduction from a Sm(II), demostrating the unusual reducing power.

Finally, the mechanism of the carboxylation of terminal alkynes in DMSO solution has been elucidated. It has been proven that the reaction proceeds spontaneously in presence of anhydrous Cs_2CO_3 that act as base for the deprotonation of the alkyne and the addition of “catalytic” species is not needed.

Concerning the study on the complexes supported by Schiff bases, the natural development of the project is the study of the electrocatalytic activity of the complexes presented in this thesis. In particular the iron compounds may have the potential to be used as electrocatalyst for the reduction of CO_2 since the reaction affords the starting compound with the release of the products. Moreover, the addition of organic substituents in the salophen scaffold can change the redox behaviour and potentially the reactivity with small molecules. Other kind of Schiff bases may confer different properties and different ability to coordinate multiple metal centres. Also, the formation of the trimetallic systems is very dependent on the ligand and on the metal and future studies will be focused on the rationalization of the multimetallic assembly.

Regarding the use of tris(*tert*-butoxy)siloxide as redox inactive ligand, the chemistry of the formation of multideker complexes could be extended to metals possessing more unpaired electrons to study the magnetic properties and maybe to increase the understanding of single molecule magnets.
Finally, the use of other kind of siloxide ligand together with divalent lanthanides should be explored because of the unique reactivity promoted by those systems.

In conclusion, in this thesis has been developed two strategies to build homo- and hetero-multimetallic complex that can be further extended to different metals. These methods can be used for the preparation of a large variety of complexes and permit a fine tuning of the sterics and electronic properties. The study of different multimetallic systems will increase our understanding of the metal-metal interaction and will allow to further explore the reactivity with small molecule.

Appendix chapter 2

NMR Spectroscopic Data

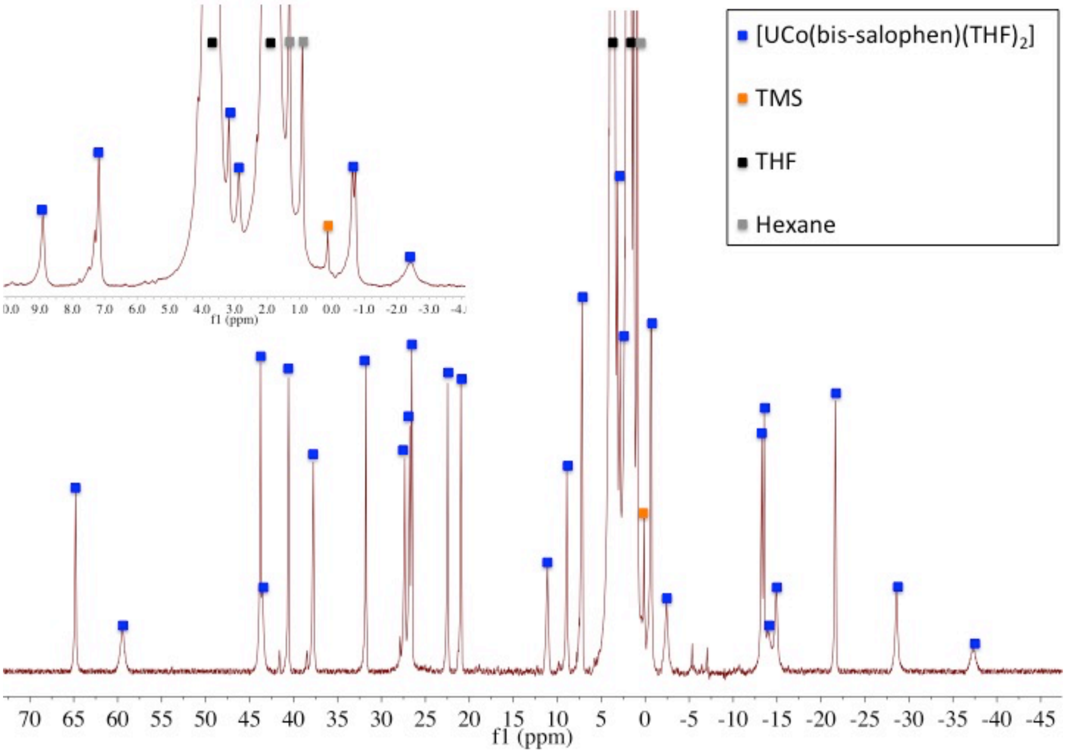

Figure S1. ^{1}H NMR spectrum of **4-2THF** (THF-d8, 298K, 400MHz).

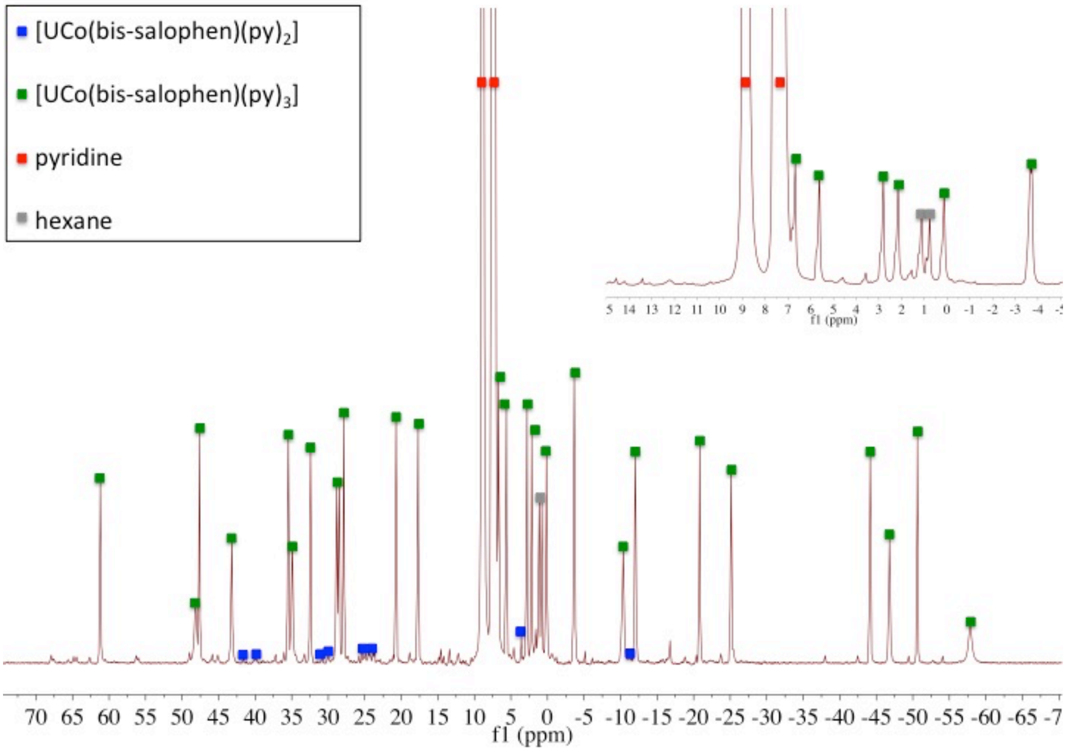

Figure S2. ^{1}H NMR spectrum of **4-3py** immediately after dissolution (py-d5, 298K, 400 MHz).

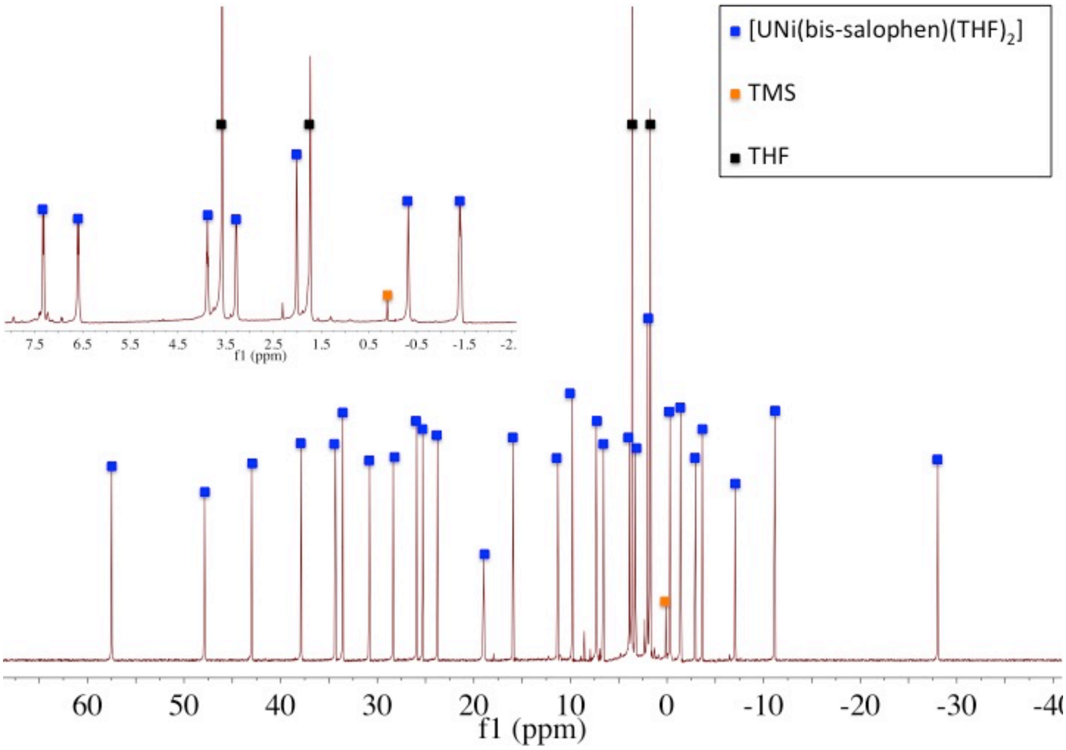

Figure S3. ^{1}H NMR spectrum of **5-THF** (py-d5, 298K, 400 MHz).

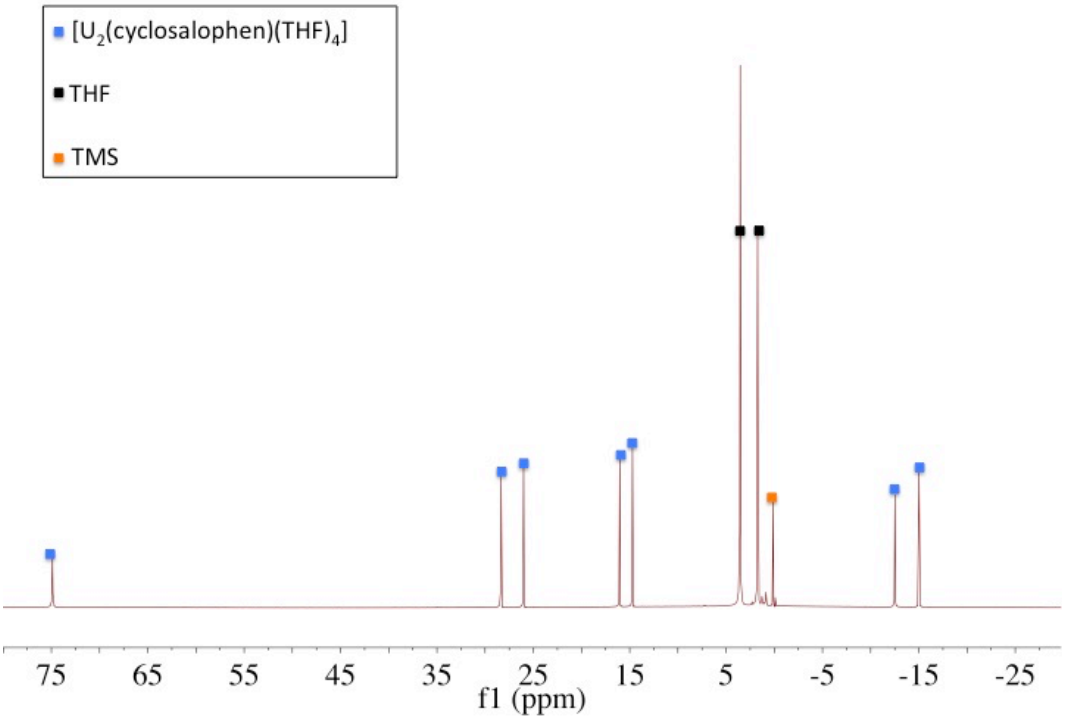

Figure S4. ^{1}H NMR spectrum after reaction of **3** with KC_8 showing only the peaks assigned to [U_2(cyclo-salophen)$(THF)_4$] (THF-d8, 298K, 400 MHz).

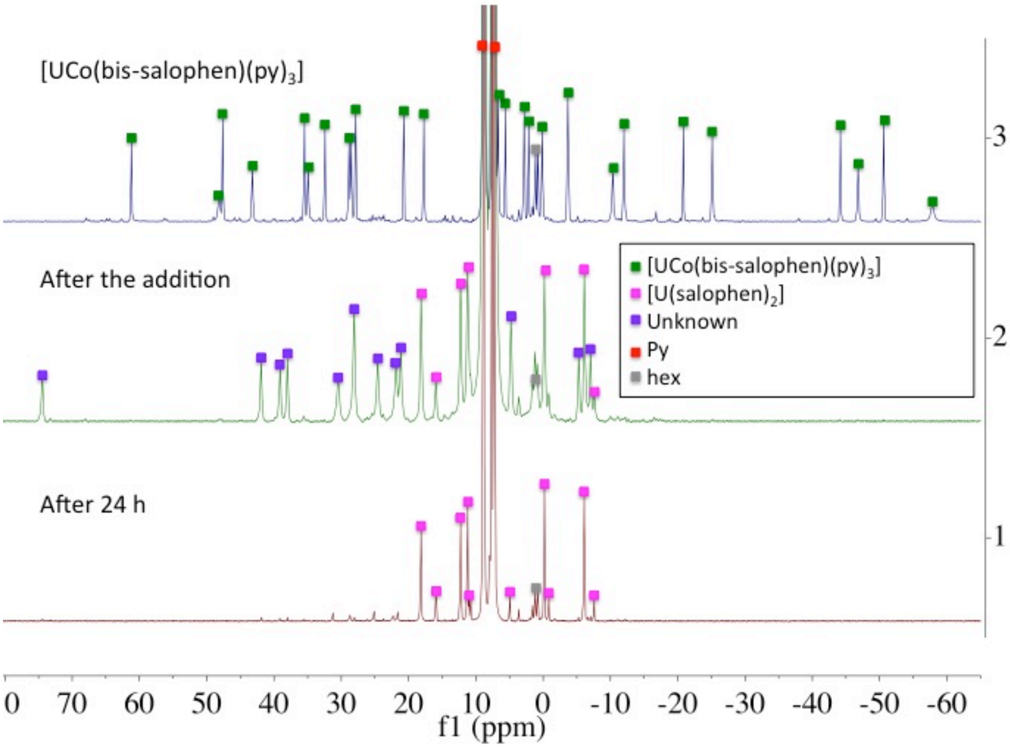

Figure S5. ^{1}H NMR spectrum before (top), immediately after (middle) and 24 hours after the reaction between **4-3py** and 2 equiv. of $^{13}CS_2$ (py-d5, 298K, 400 MHz).

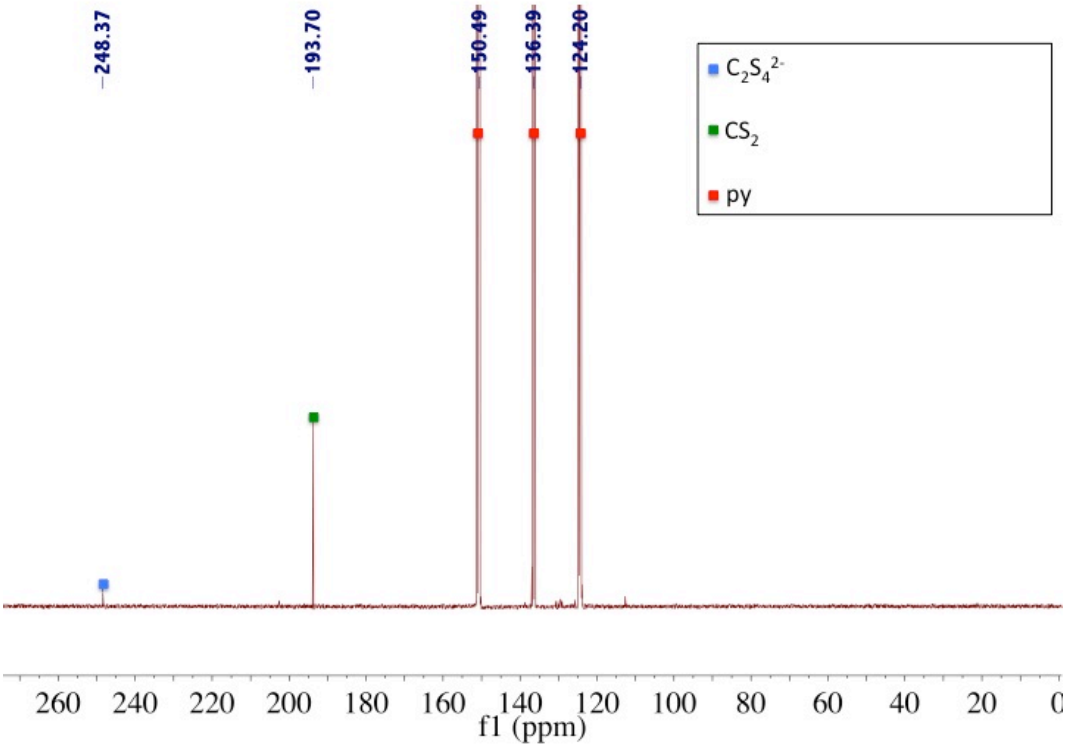

Figure S6. ^{13}C NMR spectrum of the solid obtained from the reaction of **4-3py** with $^{13}CS_2$ (py-d5, 298K, 100.6MHz).

ESI-MS spectrometry data

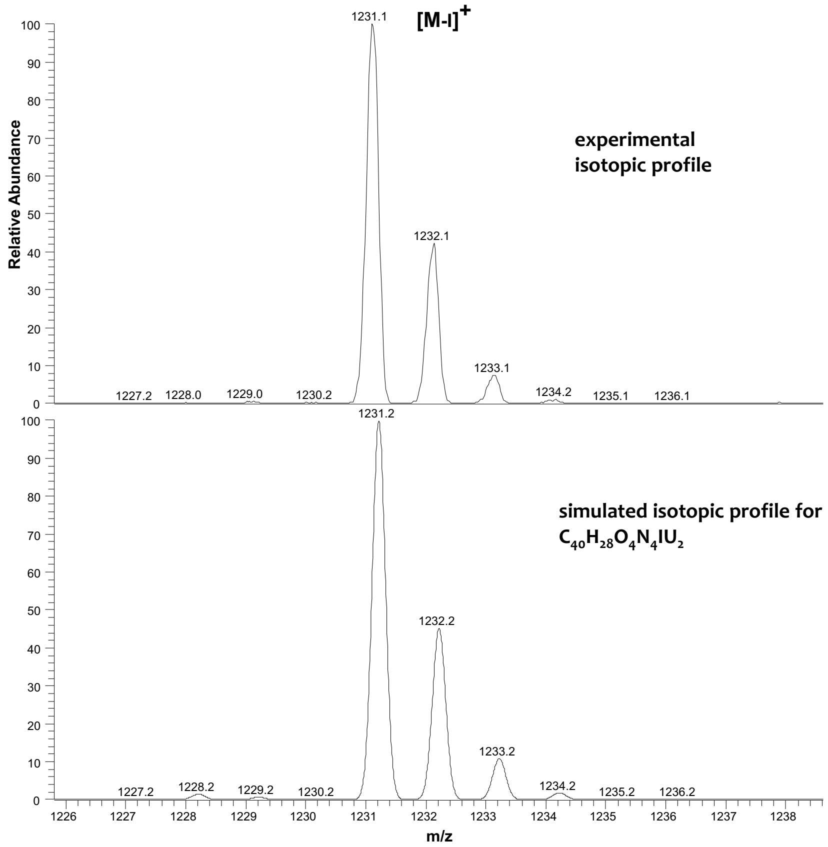

Figure S7. Experimental and simulated ESI-MS spectrum of $[U_2\text{(bis-salophen)}I]^+$ (m/z Calcd for $C_{40}H_{28}N_4O_4IU_2$, 1231.2 $gmol^{-1}$).

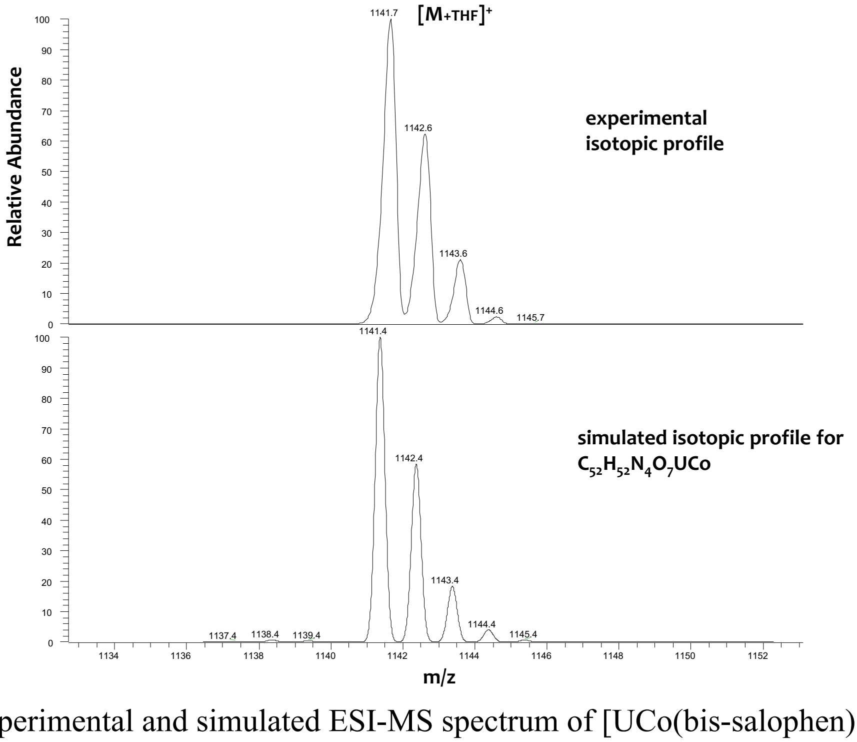

Figure S8. Experimental and simulated ESI-MS spectrum of $[UCo\text{(bis-salophen)}(THF)_3]^+$ (m/z Calcd for $C_{52}H_{52}N_4O_7UCo$: 1141.4 $gmol^{-1}$).

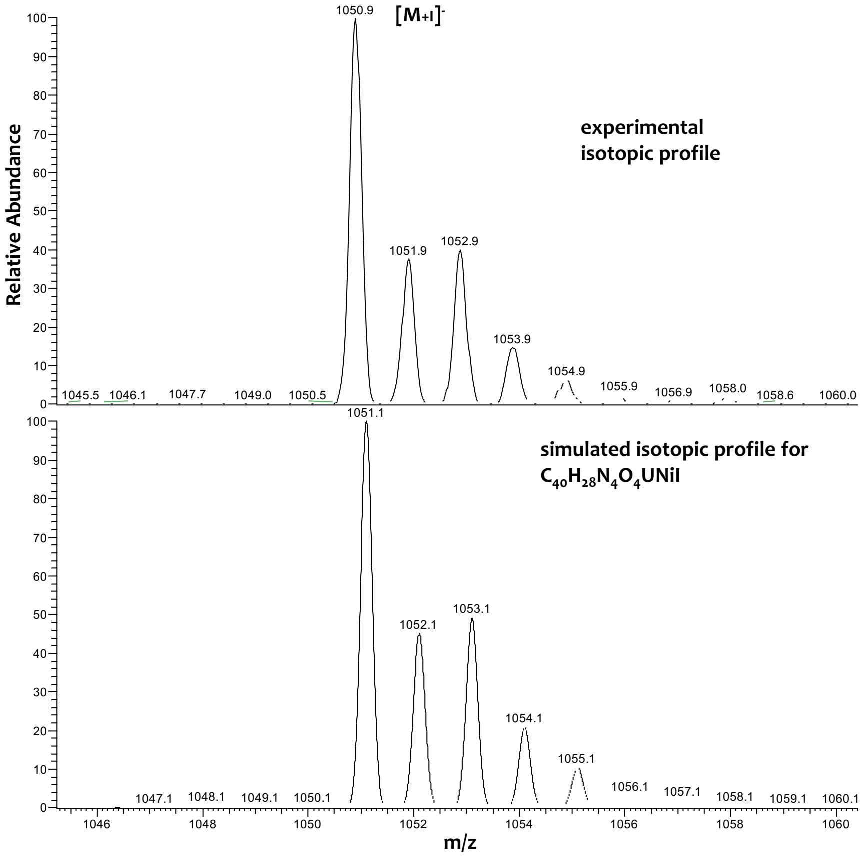

Figure S9. Experimental and simulated ESI-MS spectrum of [UNi(bis-salophen) + I]$^-$ (m/z Calcd for $C_{40}H_{28}N_4O_4UNiI$: 1051.1 gmol^{-1}).

X-ray crystallography data

Experimental details for X-ray data collections of all complexes are given in table S1. X-ray data can be obtained free of charge from the Crystallopgraphic Data Centre via www.ccdc.cam.ac.uk/data_request/cif. CCDC numbers xxx. Figure Graphics are generated using MERCURY 2.4 Supplied with Cambridge Structural Database; CCDC: Cambridge, U.K., 2004-2009. Diffraction data for **2-py**, **4-2py**, **4-THF** and **5-THF** were taken using an Oxford-Diffraction XCalibur S or a Bruker APEX II CCD kappa geometry diffractometers (Mo-Kα radiation, graphite monochromator, λ = 0.71073 Å). The Bragg-intensities of **3** and **4-3py** were measured using Cu *K*α radiation on a Rigaku SuperNova dual system equipped with an Atlas CCD detector. To prevent evaporation of co-crystallised solvent molecules the crystals were coated with light hydrocarbon oil and the data were collected at 150 K or 100 K. The dataset were reduced and corrected for absorption with CrysAlisPro.[1] and then corrected for absorption.

The solution and refinement were performed by SHELXT.[2] The crystal structures were refined using full-matrix least-squares based on F^2 with all non-hydrogen atoms anisotropically defined. Hydrogen atoms were found by Fourier transform and refined isotropically for **4-2py**, placed in calculated positions by means of the "riding" model for **2-py**, **3**, **4-THF**, **4-3py** and **5-THF**.

The crystal structure of **3** included, within the asymmetric unit, three THF solvent molecules. Two of them were correctly modelled, whereas the third one turned out to be highly disordered and, because of this, it was treated by the SQUEEZE algorithm of PLATON.[3] The crystal structure of **4-3py** displayed in the final model two pyridine molecules (as solvent). One of them was very disordered and it was treated by the split model in combination with some geometrical constraints (AFIX card) and rigid bond restraints (SIMU card), during the last stages of refinement.

Table S1. Crystallographic parameters for complexes **2-6**.

Compound	**[U_2(bis-salo-phen)$(py)_6$][I]$_2$.3py, 2-py.3py**	**[UCo(bis-salo-phen)$(py)_2$] 4-2py**	**[UCo(bis-salo-phen)$(THF)_2$].1.5 THF 4-THF.1.5THF**	**[UNi(bis-salo-phen)$(THF)_2$]. 5-THF. 1.5 THF**
Formula	$C_{85}H_{73}N_{13}O_4I_2U_2$	$C_{50}H_{38}N_6O_4CoU$	$C_{56}H_{56}N_4O_{7.5}CoU$	$C_{54}H_{56}N_4O_{7.5}NiU$
Crystal size [mm]	0.43 x 0.34 x 0.06	0.38 x 0.22 x 0.09	0.42 x 0.37 x 0.27	0.17 x 0.10 x 0.08
Crystal system	Monoclinic	Monoclinic	Monoclinic	Monoclinic
Space group	P 2_1/c	C 2/c	C 2/c	C 2/c
Volume [Å^3]	7864.2(8)	8466.5(3)	9138(5)	9151.8(4)
a [Å]	13.3578(11)	26.5567(6)	26.2903(17)	26.2314(8)
b [Å]	15.3976(7)	11.9483(2)	12.927(7)	12.9229(3)
c [Å]	38.2404(17)	26.6871(5)	27.0396(12)	27.1920(7)
α [°]	90	90	90	90
β [°]	90.910(5)	91.1024(16)	96.065(6)	96.858(3)
γ [°]	90	90	90	90
Z	4	8	8	8
Absorption coefficient [mm^{-1}]	4.958	4.267	3.965	4.008
F (000)	3984	4248	4696	4704
T [K]	150.0(1)	150(2)	150(2)	150(2)
Total no. reflexions	31445	25630	26327	28607
Unique reflexions [R(int)]	16050 [R(int) = 0.0671]	12885 [R(int) = 0.0341]	13941 [R(int) = 0.0474]	13862 [R(int) = 0.0485]
Final R indices [I>2σ(I)]	R1 = 0.0801, wR2 = 0.1345	R1 = 0.0369, wR2 = 0.0631	R1 = 0.0581 wR2 = 0.1055	R1 = 0.0467, wR2 = 0.0741
Largest diff. peak and hole [eA^{-3}]	2.35 and -2.29	1.163 and -0.827	2.382 and -1,368	1.114 and -1.166
GOF	1.108	1.022	1.058	1.027

Compound	**[U_2(bis-salo-phen)$Cl_2(THF)_2$].THF, 3-THF**	**[UCo(bis-salo-phen)$(py)_3$].2py 4-3py.2py**	**[UFe(bis-salo-phen)$(py)_3$].py 6.py**
Formula	$C_{52}H_{52}N_4O_7U_2Cl_2$	$C_{65}H_{53}N_9O_4CoU$	$C_{60}H_{48}FeN_8O_4U$
Crystal size [mm]	0.145 x 0.109 x 0.079	0.138 x 0.109 x 0.098	0.21×0.21×0.11
Crystal system	Triclinic	Monoclinic	Monoclinic
Space group	P 1	P 2_1/n	P2_1/n

Volume [Å^3]	5046(3)	5376.44(18)	5009.1(13)
a [Å]	11.7350(5)	11.6829(2)	11.1713(14)
b [Å]	19.9970(7)	23.5857(4)	21.171(4)
c [Å]	22.9587(9)	20.1120(4)	21.180(2)
α [°]	76.376(4)	90	90
β [°]	77.185(3)	104.034(2)	90.466(9)
γ [°]	78.707(3)	90	90
Z	4	4	4
Absorption coefficient [mm^{-1}]	19.340	3.377	3.577
F (000)	2664.0	2628	-
T [K]	100.01(10)	100.01(10)	120.15
Total no. reflexions	38801	70018	43095
Unique reflexions [R(int)]	20295 [R(int) = 0,0464]	13687 [$R_{(int)}$ = 0.0344]	11037 [$R_{(int)}$ = 0.1032]
Final R indices [I>2σ(I)]	R1 = 0.0449 wR2 = 0.0931	R_1 = 0.0277, wR_2 = 0.0543	R_1 = 0.0940, wR_2 = 0.2018
Largest diff. peak and hole [eA^{-3}]	1.543 and -2.638	0.729 and -0.682	0.1032
GOF	0.994	1.050	1.209

Table S2. Selected average bond lengths (Å) and angles (°) for compounds **1-3.**

Compound	U-N$_{imino}$	U-N$_{amido}$	U-O$_{phenolate}$	C-C$_{link}$	C-N$_{amido}$	C-N$_{imino}$
[U(salophen)$_2$][3]	2.61(3)	/	2.22(1)	/	/	1.283(8)
Na$_2$[U(bis-salophen)][3] **1**	2.624(7)	2.387(8)	2.31(1)	1.559(7)	1.46(1)	1.298(3)
[U$_2$(bis-salophen)(py)$_6$]I$_2$.(py)$_3$ **2-py**	2.55(1)	2.44(2) and 2.662(3)	2.15(1)	1.599(15)	1.49(1)	1.303(3)
[U$_2$(bis-salophen)(THF)$_2$Cl$_2$] **3**	2.559(5) and 2.484(5)	2.448(5) and 2.453(5)	2.156(4), 2.170(4), 2.135(5) and 2.154(4)	1.588(8)	1.467(7) and 1.482(8)	1.293(8) and 1.302(9)

EPR spectrum

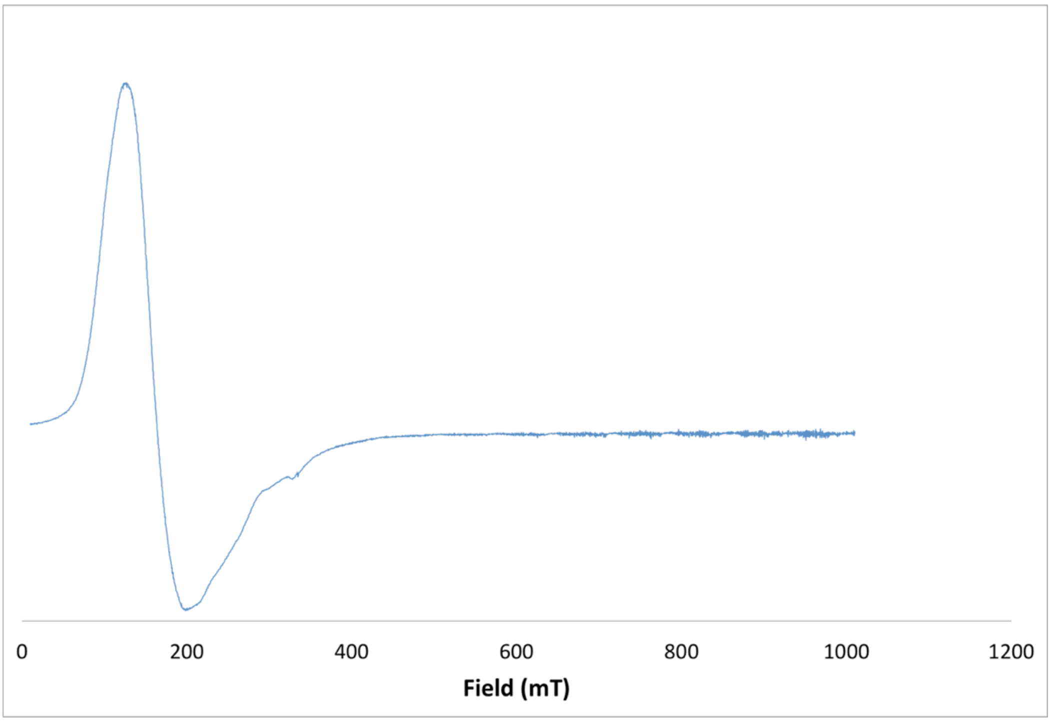

Figure S10. X Band (9.40 GHz) EPR spectrum of the solid obtained from the reaction of 4-3py with $^{13}CS_2$ in a toluene/hexane glass at 5 K (g = 4.04).

References

1 CrysAlisPRO, Rigaku Oxford Diffraction, 2015.
2 G. M. Sheldrick, *Acta Crystallogr., Sect. A*, 2015, 71, 3-8.
3 PLATON and A. L. Spek, *Acta Crystallogr., Sect. C*, 2015, 71, 9-18.

Appendix chapter 3

NMR spectroscopic data

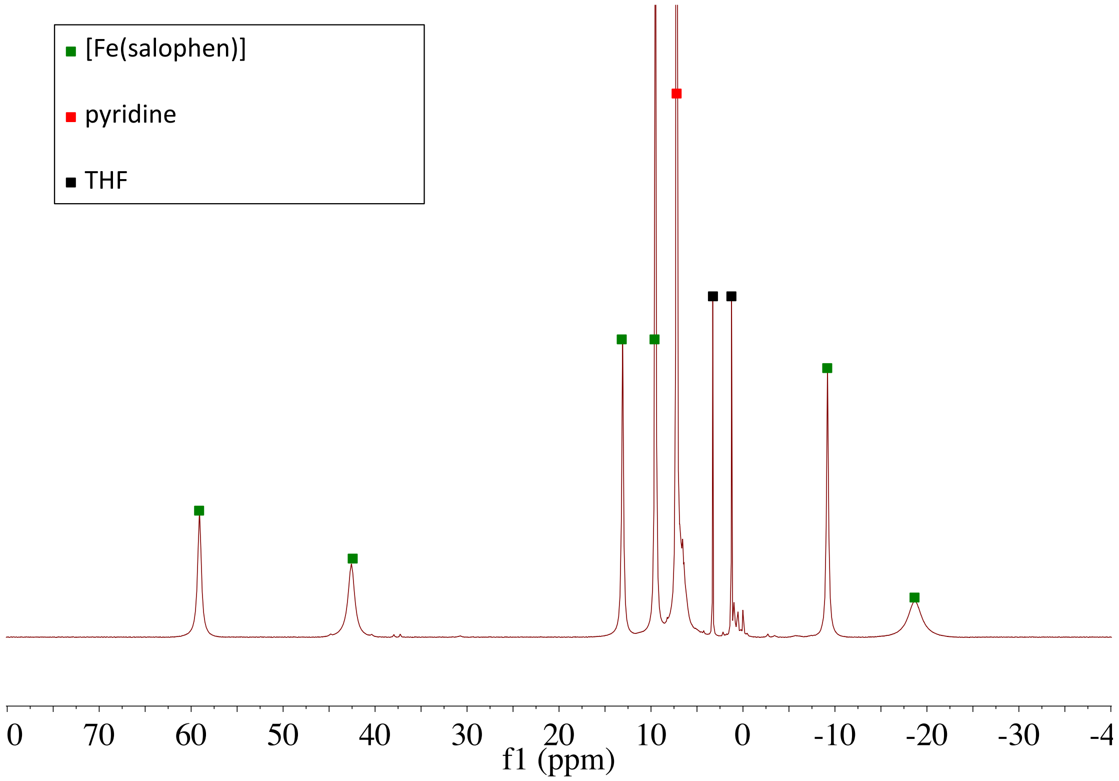

Figure S1. ^{1}H NMR spectrum of [Fe(salophen)] (py-d5, 400 MHz, 298 K).

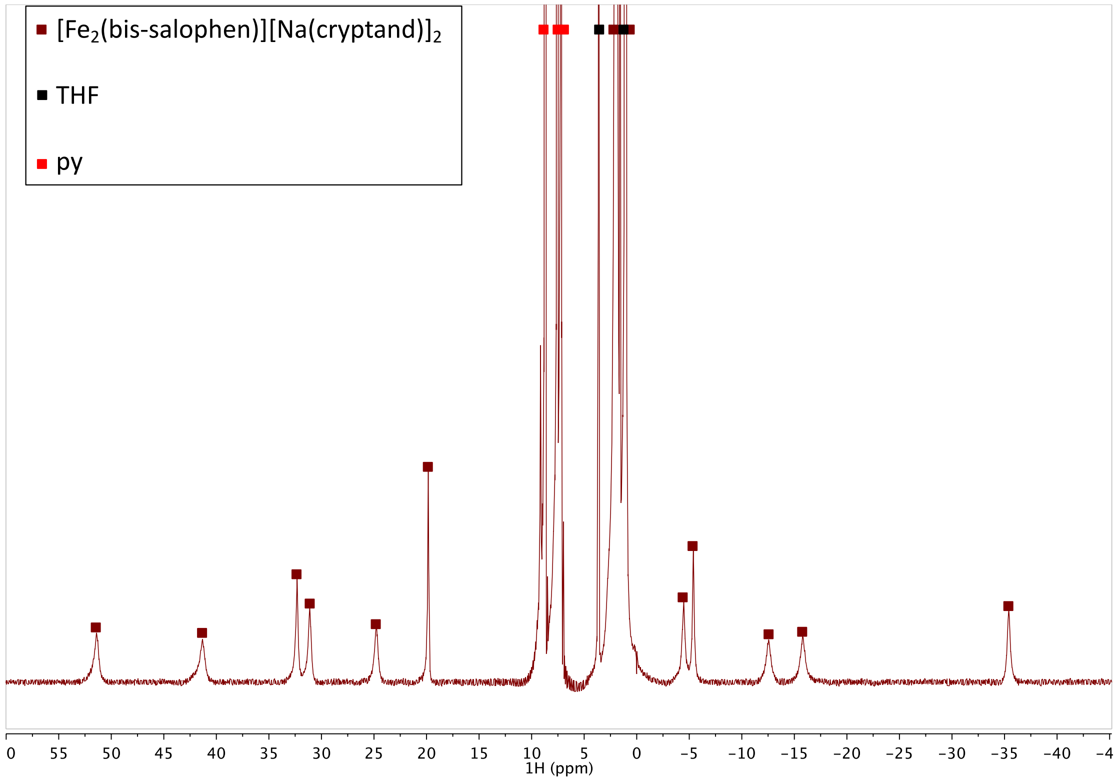

Figure S2. ^{1}H NMR spectrum of [Fe$_2$(bis-salophen)][Na(cryptand)]$_2$, **1-crypt** (py-d5, 400 MHz, 298 K).

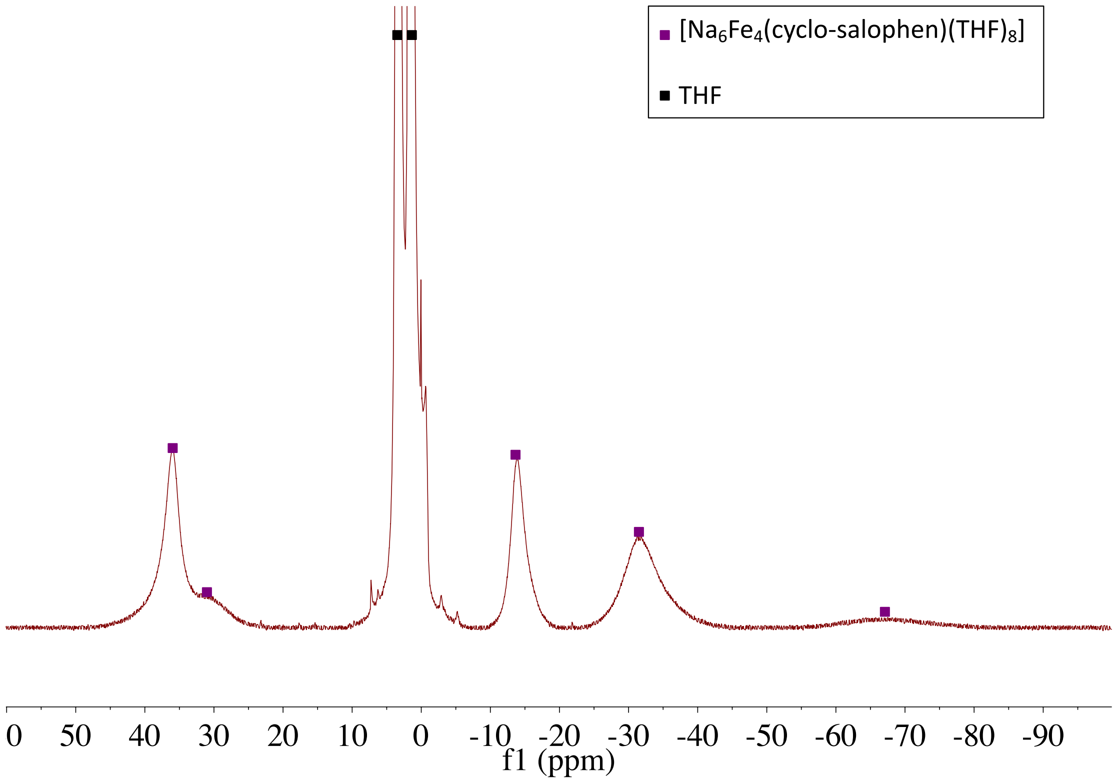

Figure S3.^{1}H NMR spectrum of [Na$_6$Fe$_4$(cyclo-salophen)$_2$(THF)$_{10}$], **2-THF** (THF-d8, 400 MHz, 298 K).

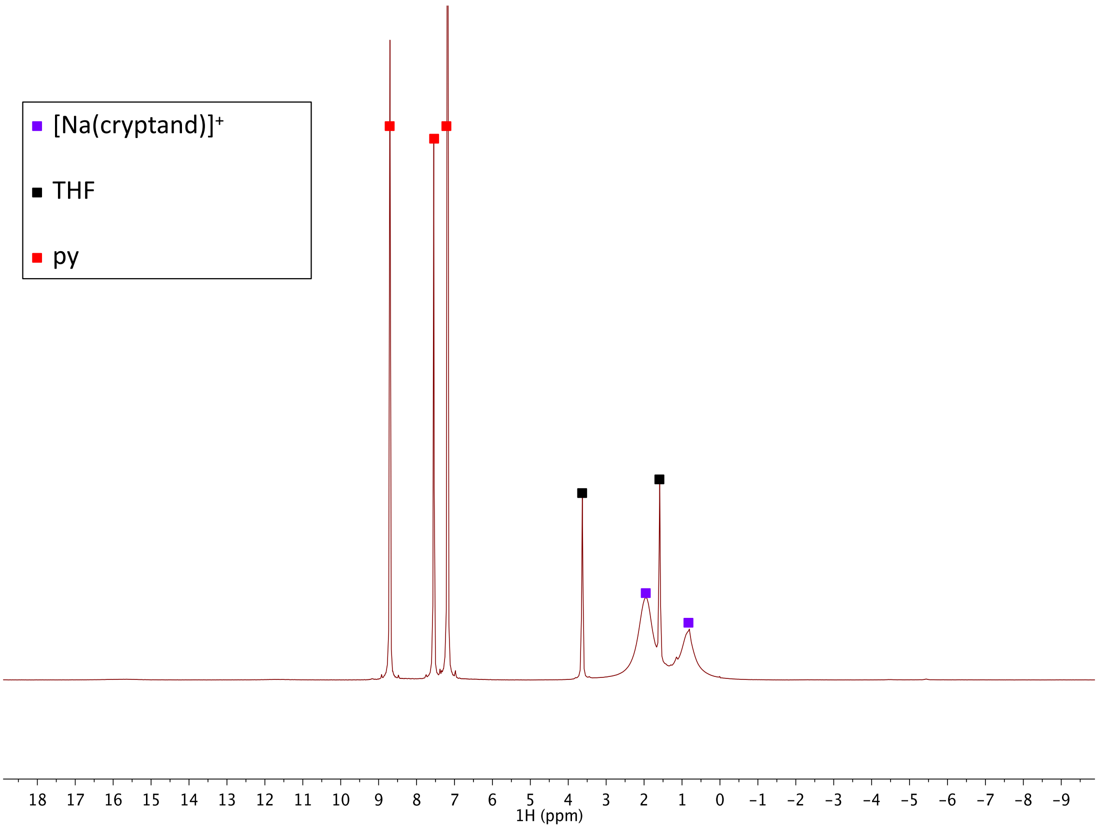

Figure S4. ^{1}H NMR spectrum of $[Na(Fe(salophen))_2][Na(cryptand)]_3$, **3-crypt** (py-d5, 400 MHz, 298 K).

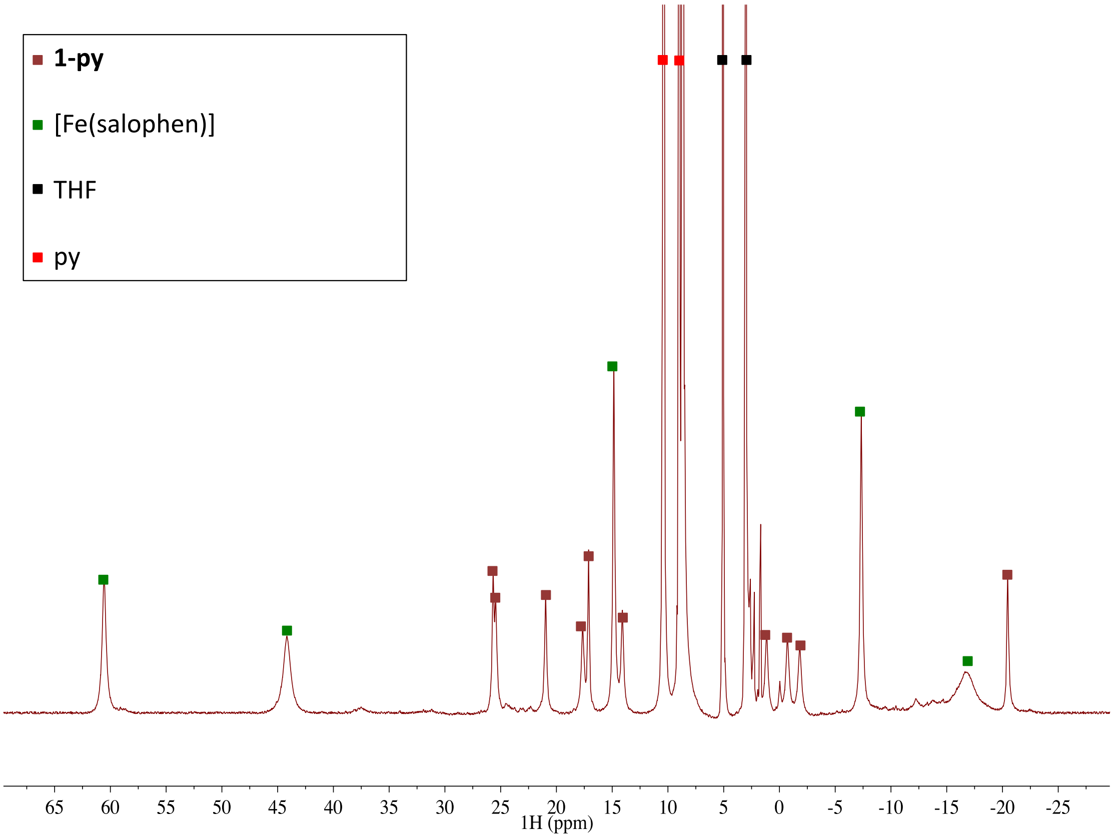

Figure S5. ^{1}H NMR spectrum of the reaction mixture of **2-py** and 2 equiv. of $^{13}CO_2$ (py-d5, 400 MHz, 298 K).

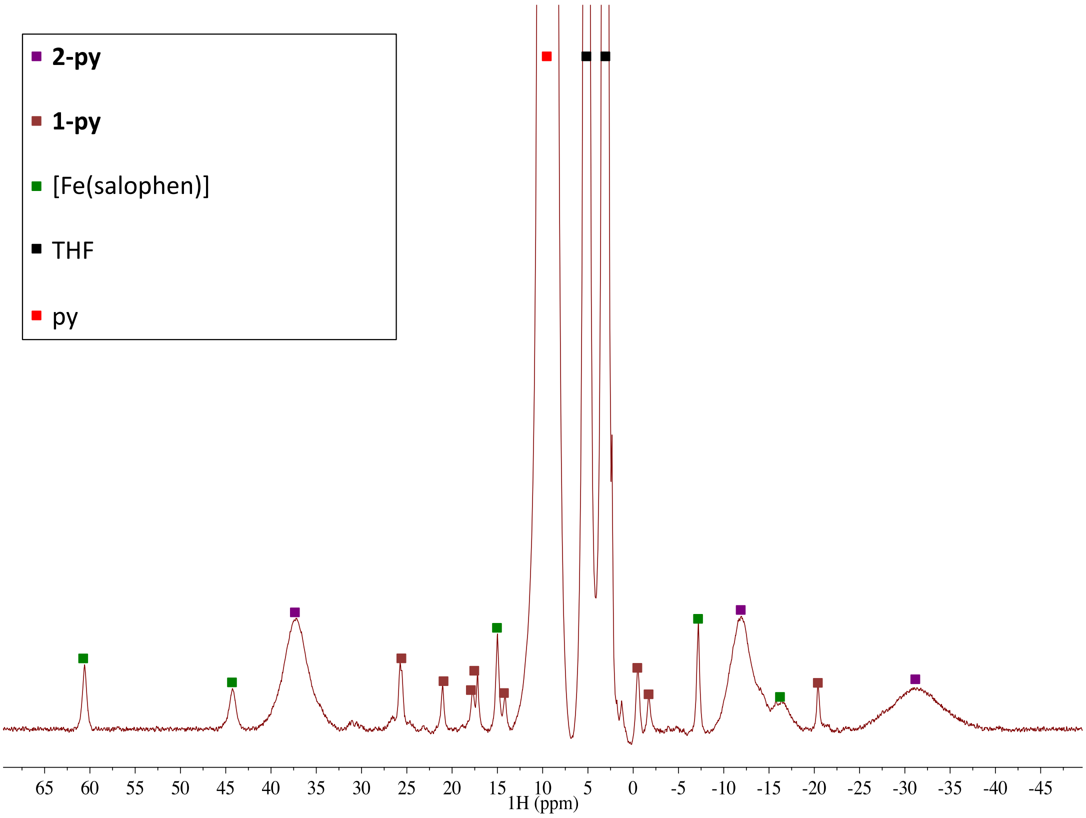

Figure S6. ^{1}H NMR spectrum of the reaction mixture of **3-py** and 2 equiv. of $^{13}CO_2$ (py-d5, 400 MHz, 298 K).

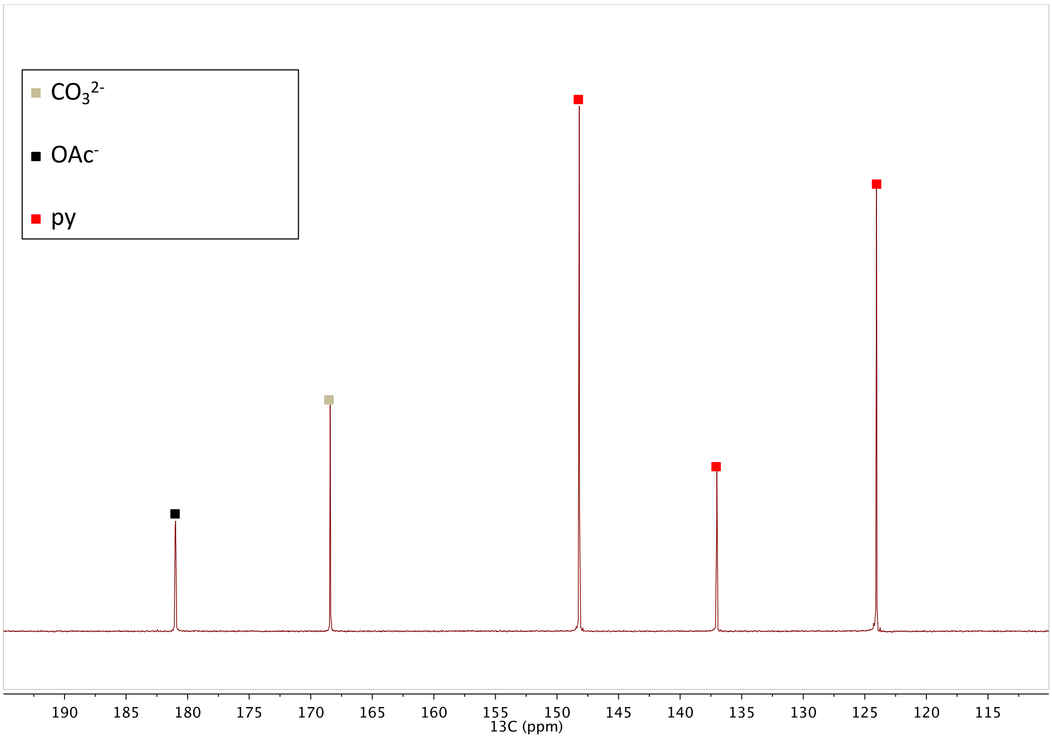

Figure S7. $^{13}C\{^1H\}$ NMR spectrum of the reaction mixture of **3-py** and $^{13}CO_2$ (D_2O, 400 MHz, 298 K).

UV-Vis-NIR and IR spectra

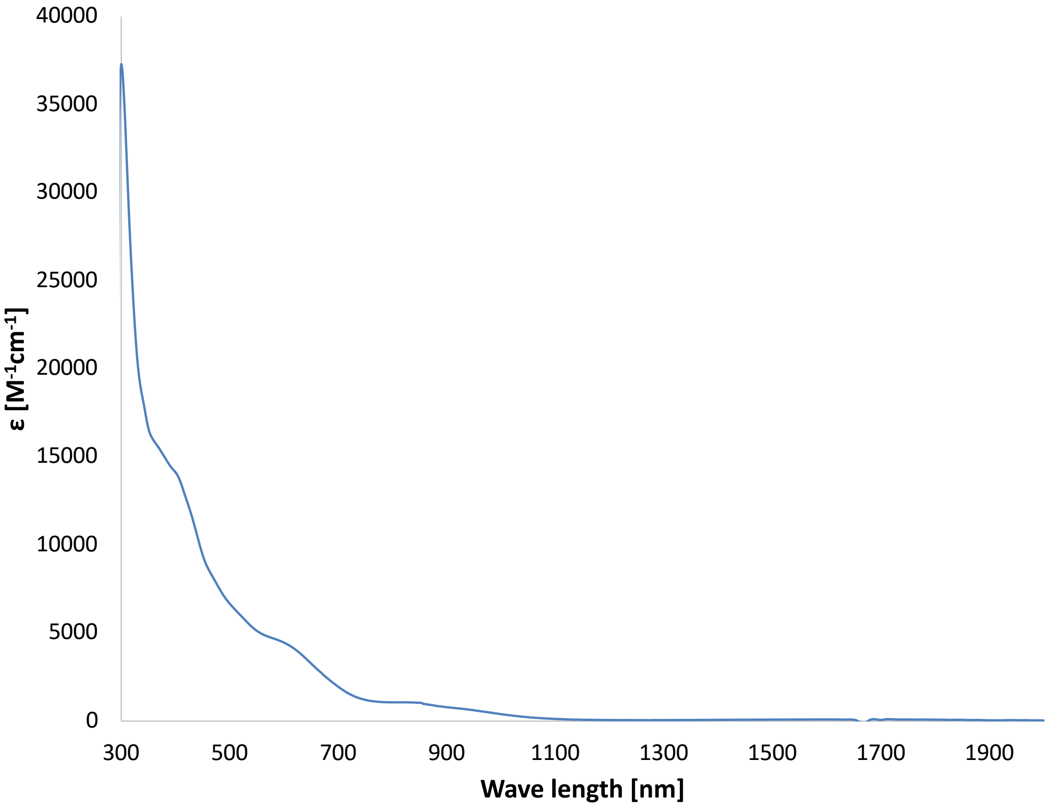

Figure S8. UV-Vis-NIR spectrum of a 0.14 mM solution of **1-THF** in THF.

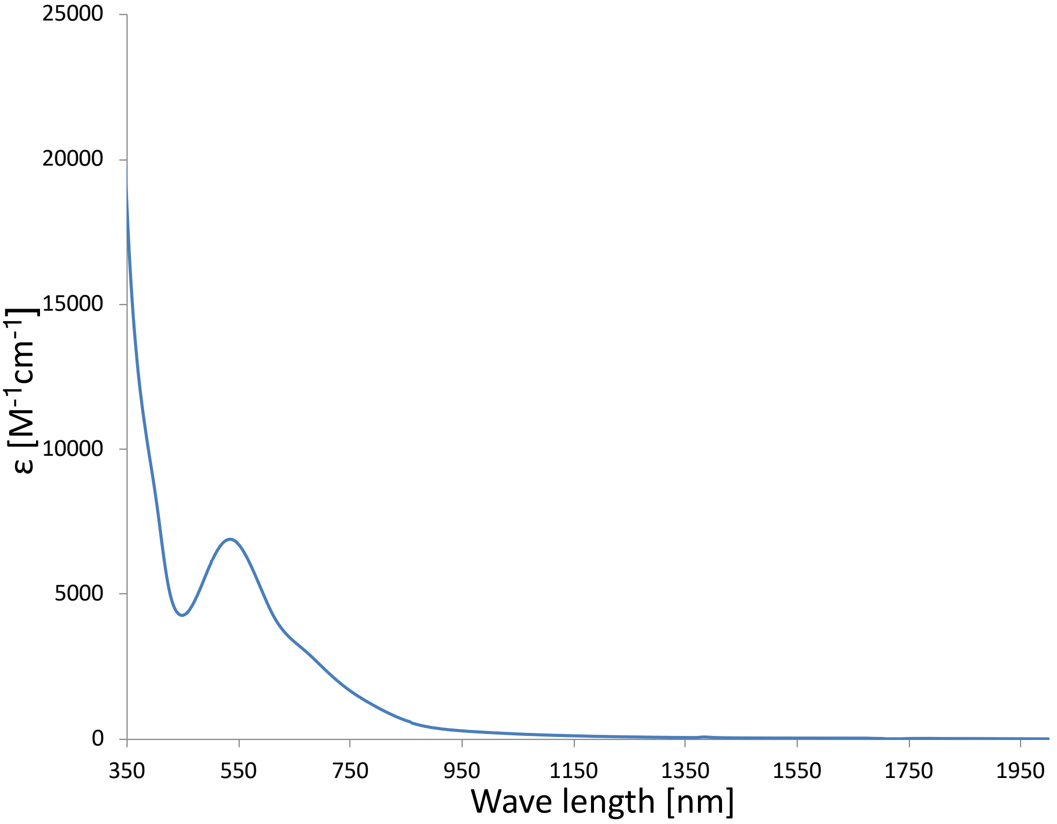

Figure S9. UV-Vis-NIR spectrum of a 0.14 mM solution of **2-THF** in THF.

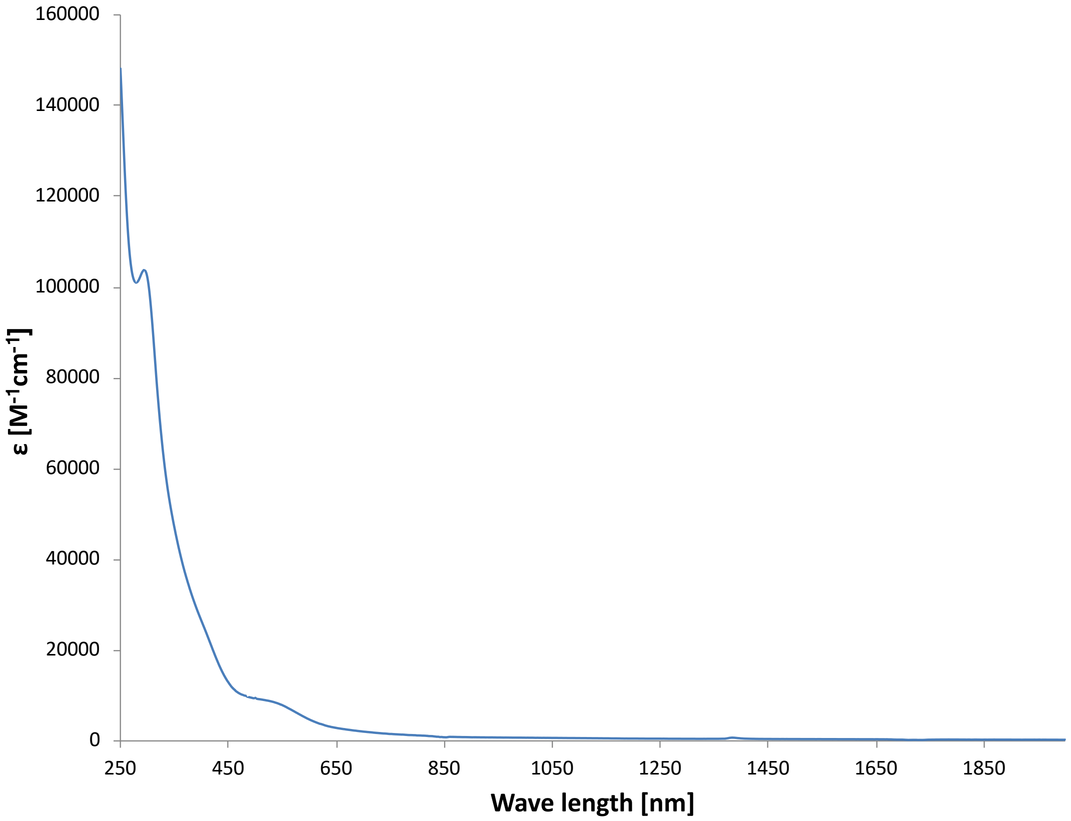

Figure S10. UV-Vis-NIR spectrum of a 0.14 mM solution of **3-THF** in THF.

X-ray crystallography structure determination details

Table S3. Crystallographic parameters.

Compound	**1-THF**	**1-py**	**1-crypt**
Formula	$C_{108}H_{112}Fe_4N_8Na_4O_{15}$	$C_{60}H_{48}Fe_2N_8Na_2O_4$	$C_{76}H_{100}Fe_2N_8Na_2O_{16}$
Crystal size [mm]	0.157 x 0.041 x 0.022	0.184 x 0.054 x 0.049	0.12×0.08×0.03
Crystal system	Monoclinic	Triclinic	monoclinic
Volume [Å^3]	4766.0(4)	2937.5(10)	7347.36(12)
a [Å]	15.6421(9)	14.445(2)	19.41572(20)
b [Å]	18.6208(8)	14.971(3)	13.79102(12)
c [Å]	17.6271(8)	15.609(3	27.8823(3)
α [°]	90	111.015(18)	90
β [°]	111.832(6)	101.878(14)	100.2207(9)
γ [°]	90	101.770(16)	90
Z	2	2	4
Absorption coefficient [mm^{-1}]	0.687	4.514	3.889
F (000)	2168	1140	3256
T [K]	140.00(10)	140.01(10)	139.99(10)
Reflections collected	41826	20765	25650
Independent reflections [R(int)]	11732 [R_{int} = 0.0836]	10386 [R_{int} = 0.1681]	7217 [R_{int} = 0.0199]
Final R indices [I>2σ(I)]	R_1 = 0.0668, wR_2 = 0.1143	R_1 = 0.0868, wR_2 = 0.1926	R_1 = 0.0253, wR_2 = 0.0645
Largest diff. peak and hole [eA^{-3}]	0.513 and -0.517	0.756 and -0.694	0.315 and -0.385
GOF	1.020	0.928	1.033

Compound	**2-THF**	**2-py**	**3-crypt**
Formula	$C_{120}H_{136}Fe_4N_8Na_6O_{18}$	$C_{80}H_{68}Fe_2N_{12}Na_3O_4$	$C_{94}H_{136}N_{10}O_{22}Na_4Fe_2$
Crystal size [mm]	0.391 x 0.188 x 0.093	0.491 x 0.372 x 0.132	0.34×0.10×0.09
Crystal system	Monoclinic	Monoclinic	monoclinic
Volume [Å^3]	6562.3(6)	31496.3(12)	11657.3(9)
a [Å]	18.9709(10)	48.8964(13)	12.5532(5)
b [Å]	17.2638(6)	13.4823(2)	24.3711(12)
c [Å]	21.3084(11	47.8421(9)	38.3971(18)
α [°]	90	90	90
β [°]	109.893(6)	92.991(2)	97.088(4)
γ [°]	90	90	90
Z	2	16	4
Absorption coefficient [mm^{-1}]	4.162	3.553	-
F (000)	2452	11984	-
T [K]	199.99(10)	140.1(3)	140.00(10)
Reflections collected	28186	104981	47531

Independent reflections [R(int)]	7075 [R_{int} = 0.0876]	27799 [R_{int} = 0.0651]	22505 [R_{int} = 0.0727]
Final R indices [I>2σ(I)]	R_1 = 0.0675, wR_2 = 0.1696	R_1 = 0.1265, wR_2 = 0.3606	R_1 = 0.1136, wR_2 = 0.3742
Largest diff. peak and hole [eA^{-3}]	0.401 and -0.557	2.136 and -0.844	0.594 and -0.454
GOF	1.030	1.426	0.962

Compound	[$Na_{12}Fe_6$(tris-cyclo-salo-phen)$_2$(THF)$_{14}$], **3-THF**	[Na_6Fe_3(tris-cyclo-salo-phen)(py)$_9$].2py, **3-py.2py**
Formula	$C_{176}H_{196}Fe_6N_{12}Na_{12}O_{26}$	$C_{115}H_{97}Fe_3N_{17}Na_6O_6$
Crystal size [mm]	0.572 x 0.217 x 0.164	0.339 x 0.269 x 0.089
Wavelength [Å]	1.54184	0.71073
Formula weight	3506.44	2118.58
Space group	$P2_1/c$	$P1$
Crystal system	Monoclinic	Triclinic
Volume [Å^3]	9865.5(5)	2536.26(12)
a [Å]	13.4845(3)	13.3029(3)
b [Å]	33.0195(12)	14.1443(3)
c [Å]	22.9829(7)	15.9246(4)
α [°]	90	112.076(2)
β [°]	105.404(3)	111.146(2)
γ [°]	90	92.244(2)
Z	2	1
Absorption coefficient [mm^{-1}]	4.209	0.516
F (000)	3664	1098
T [K]	140.00(10)	140.00(10)
Reflections collected	69497	55517
Independent reflections [R(int)]	20221 [R_{int} = 0.0584]	33321 [R_{int} = 0.0360]
Final R indices [I>2σ(I)]	R_1 = 0.0958, wR_2 = 0.2570	R_1 = 0.0589, wR_2 = 0.1098
Largest diff. peak and hole [eA^{-3}]	2.379 and -0.752	1.138 and -1.065
GOF	1.073	1.027

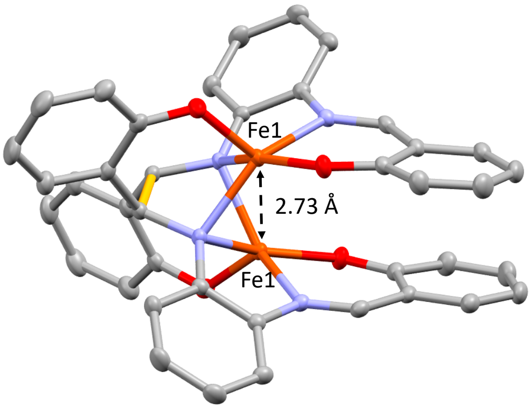
Fe1
2.73 Å
Fe1

Figure S11. XRD structure of **1-crypt** (50% probability ellipsoids). The C-C bond formed by reduction is highlight in yellow. Hydrogen atoms and counterions have been omitted for clarity.

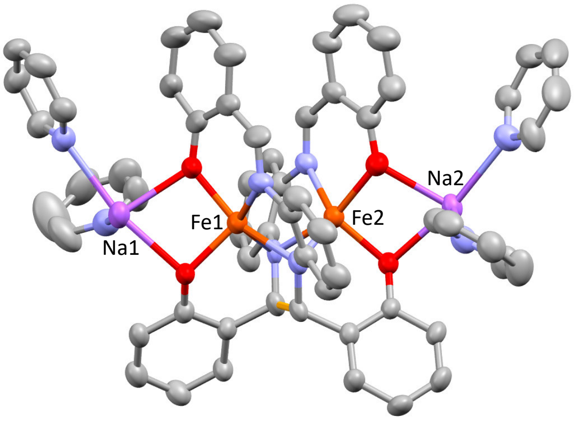
Na2
Fe1
Fe2
Na1

Figure S12. Solid-state structure of the asymmetric unit of **1-py** (50 % probability ellipsoids). The C-C bond formed by reduction is highlight in yellow. Hydrogen atoms have been omitted for clarity.

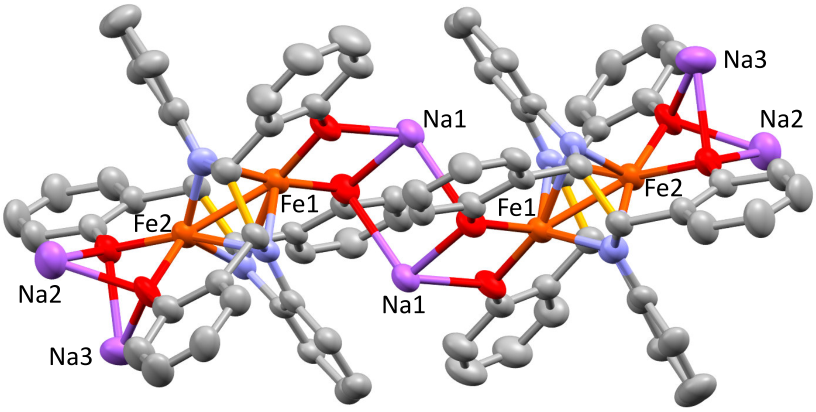
Na3
Na1
Na2
Fe1
Fe2
Fe1
Fe2
Na2
Na1
Na3

Figure S13. Solid-state structure of **2-THF** (50 % probability ellipsoids). The C-C bonds formed by reduction are highlight in yellow. Hydrogen atoms have been omitted for clarity.

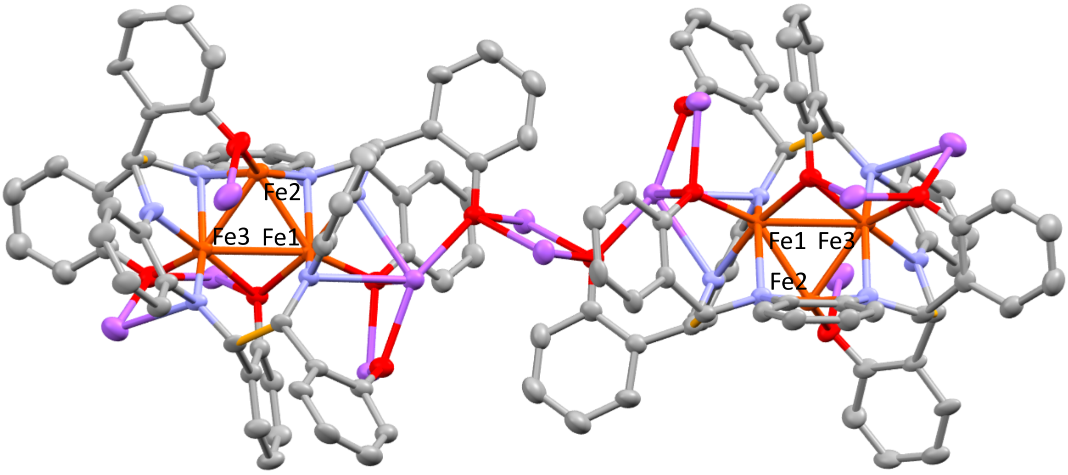

Figure S14. Mercury diagram of the molecular structure of **3-THF** (50% probability ellipsoids). The three C-C bonds formed by reduction of salophen^{2-} are shown in yellow. Hydrogen atoms and the Na-bound THF molecules have been omitted for clarity.

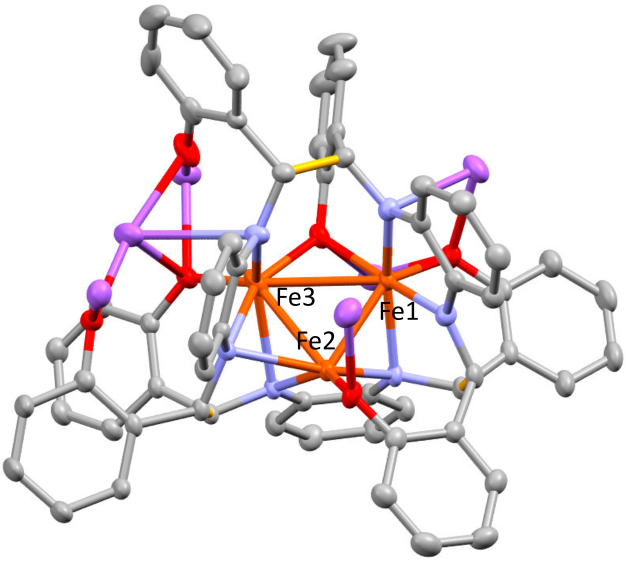

Figure S15. Mercury diagram of the molecular structure of **3-py** (50% probability ellipsoids). The three C-C bonds formed by reduction of salophen^{2-} are shown in yellow. Hydrogen atoms, lattice pyridine molecules and the sodium-bound pyridine molecules have been omitted for clarity.

Electrochemistry data

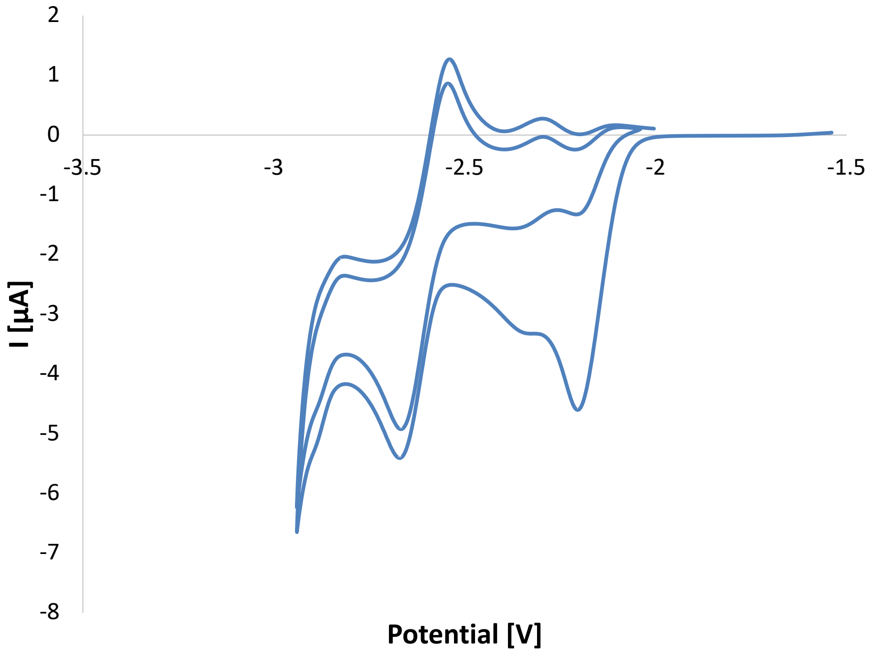

Figure S16. CV of [Fe(salophen)] (4 mM) in py solution in presence of NBu_4PF_6 0.1 M, using a Pt electrode at a scan rate of 100 mV/s (reduced window).

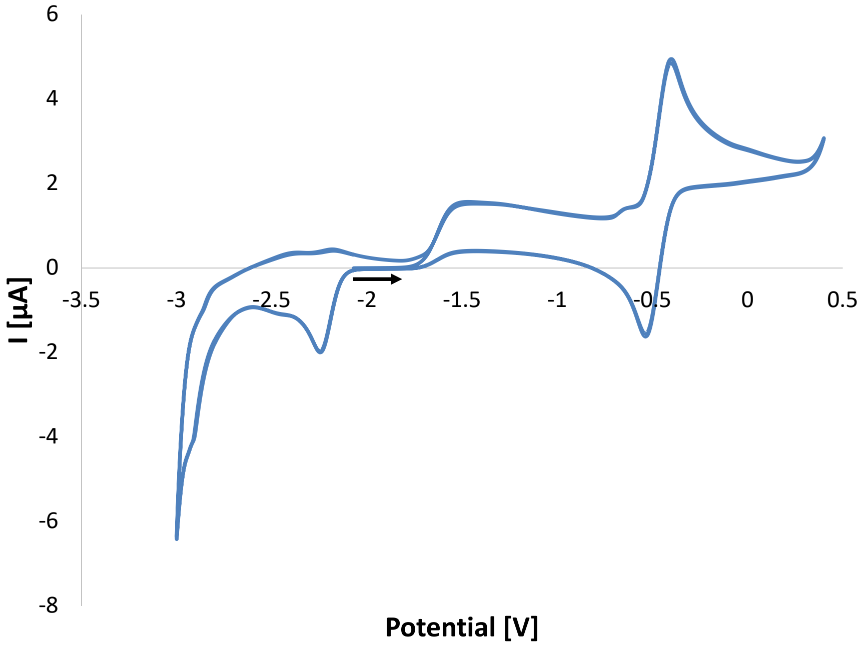

Figure S17. CV of **1-py** (4 mM) in py solution in presence of NBu_4PF_6 0.1 M and excess 2.2.2-cryptand, using a Pt electrode at a scan rate of 100 mV/s (the arrow indicated the starting potential and the direction).

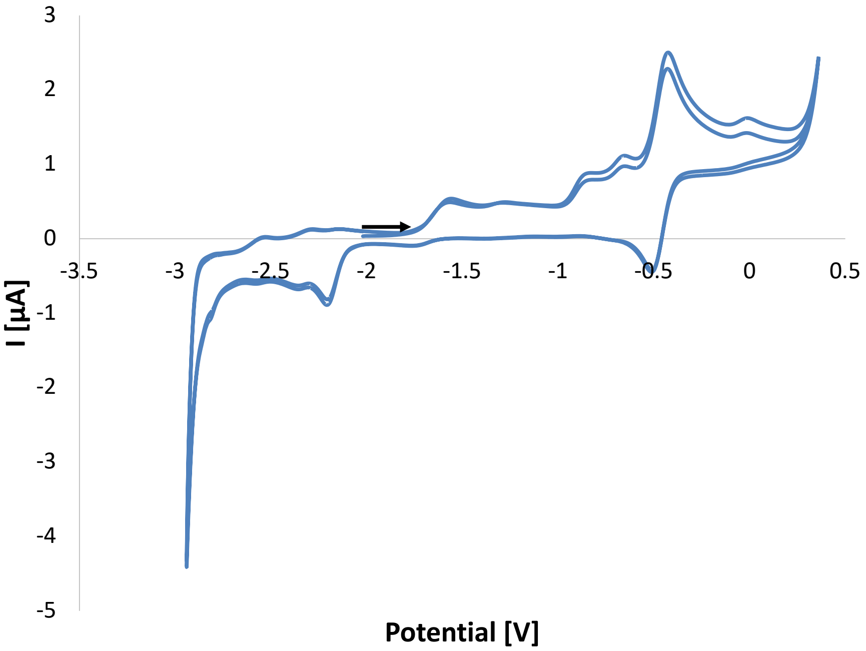

Figure S18. CV of **2-py** (4 mM) in py solution in presence of NBu_4PF_6 0.1 M and excess 2.2.2-cryptand, using a Pt electrode at a scan rate of 100 mV/s (the arrow indicated the starting potential and the direction).

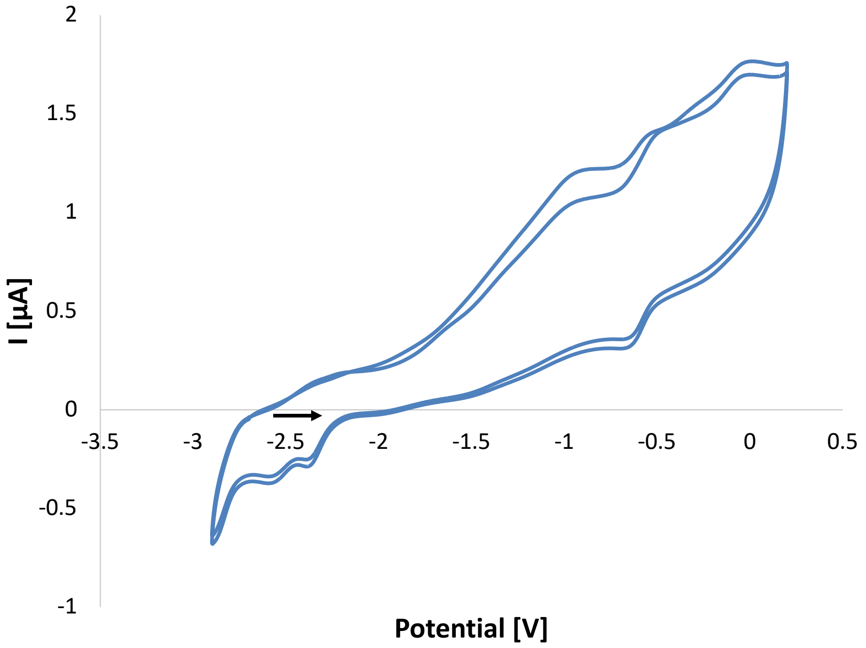

Figure S19. CV of **3-py** (4 mM) in py solution in presence of NBu_4PF_6 0.1 M and excess of 2.2.2-cryptand, using a Pt electrode at a scan rate of 100 mV/s (the arrow indicated the starting potential and the direction).

Appendix chapter 4

NMR spectroscopic data

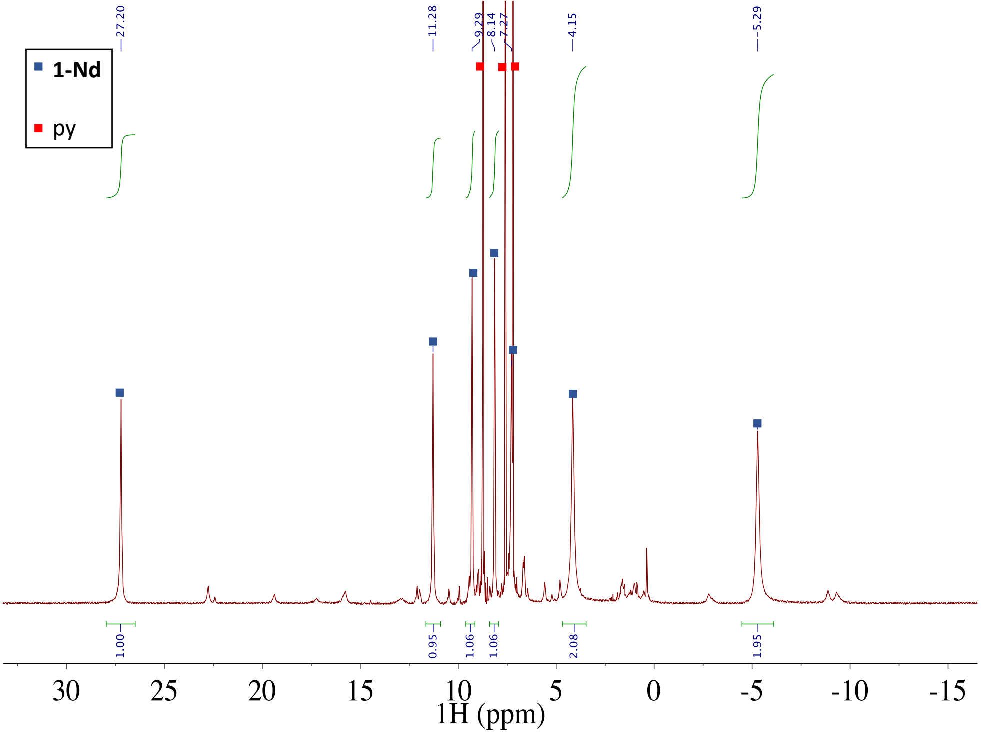

Figure S1. ^{1}H NMR spectrum of in situ synthesized **1-Nd** (400 MHz, py-d5, 298 K).

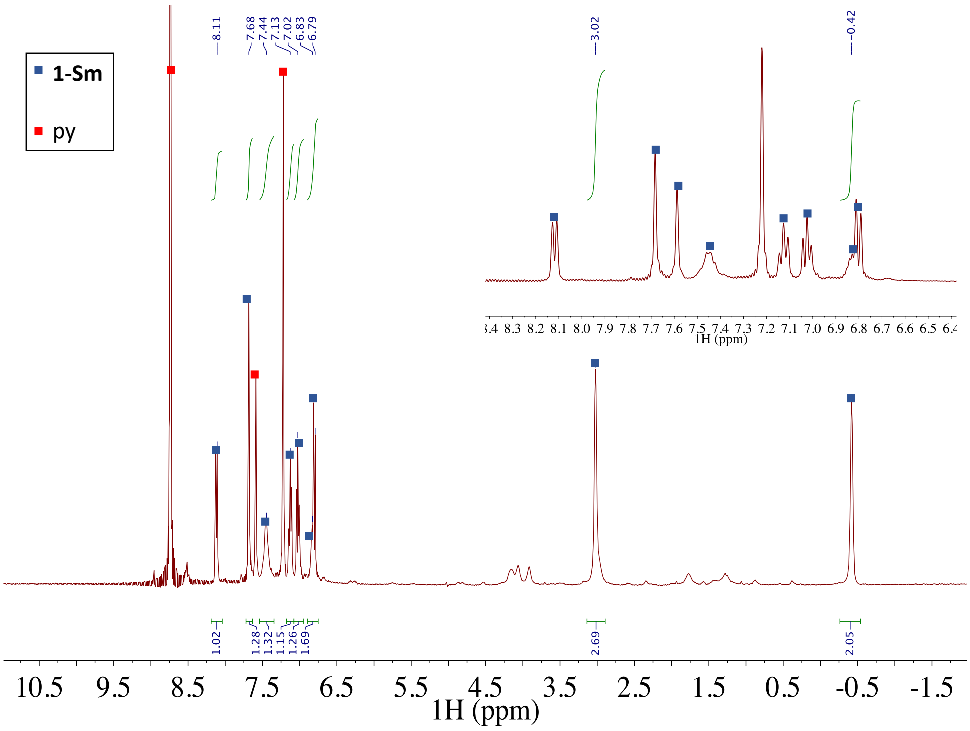

Figure S2. ^{1}H NMR spectrum of in situ synthesized **1-Sm** (400 MHz, py-d5, 298 K).

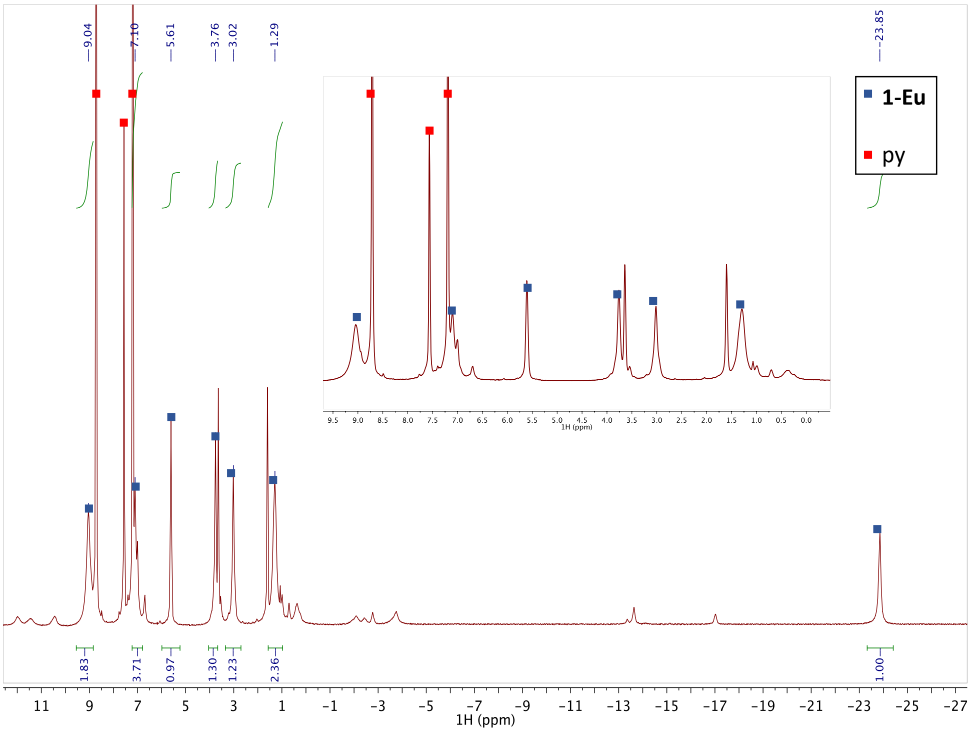

Figure S3. ^{1}H NMR spectrum of in situ synthesized **1-Eu** (400 MHz, pyr-d_5, 298 K).

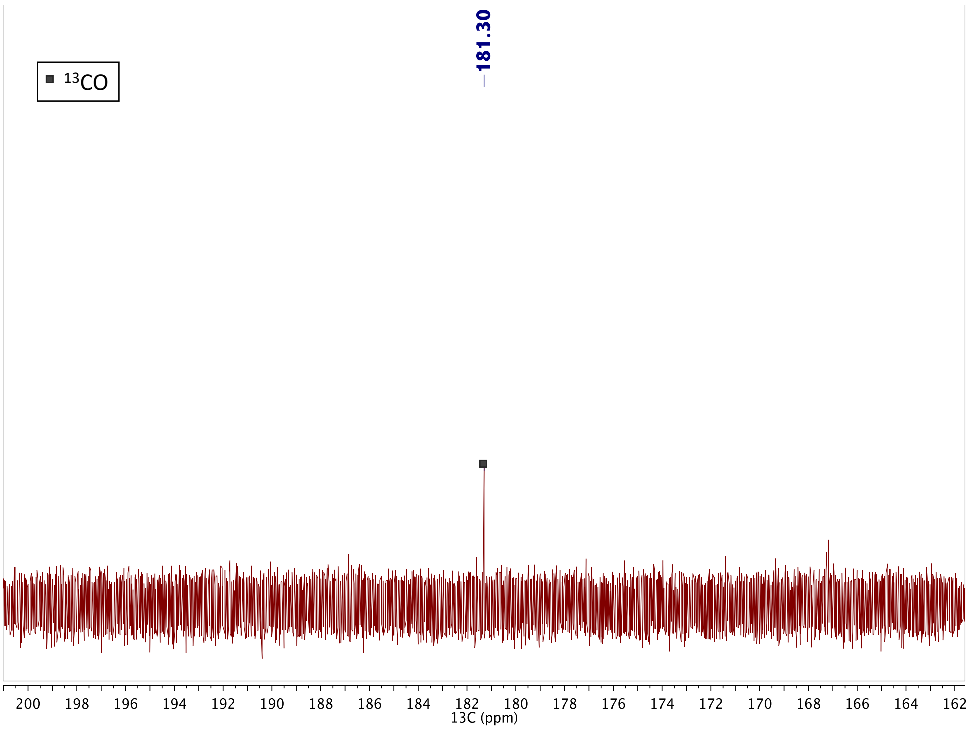

Figure S4 ^{13}C NMR spectrum of the reaction mixture between **4-Sm** and $^{13}CO_2$ (100 MHz, THF-d_8, 298 K).

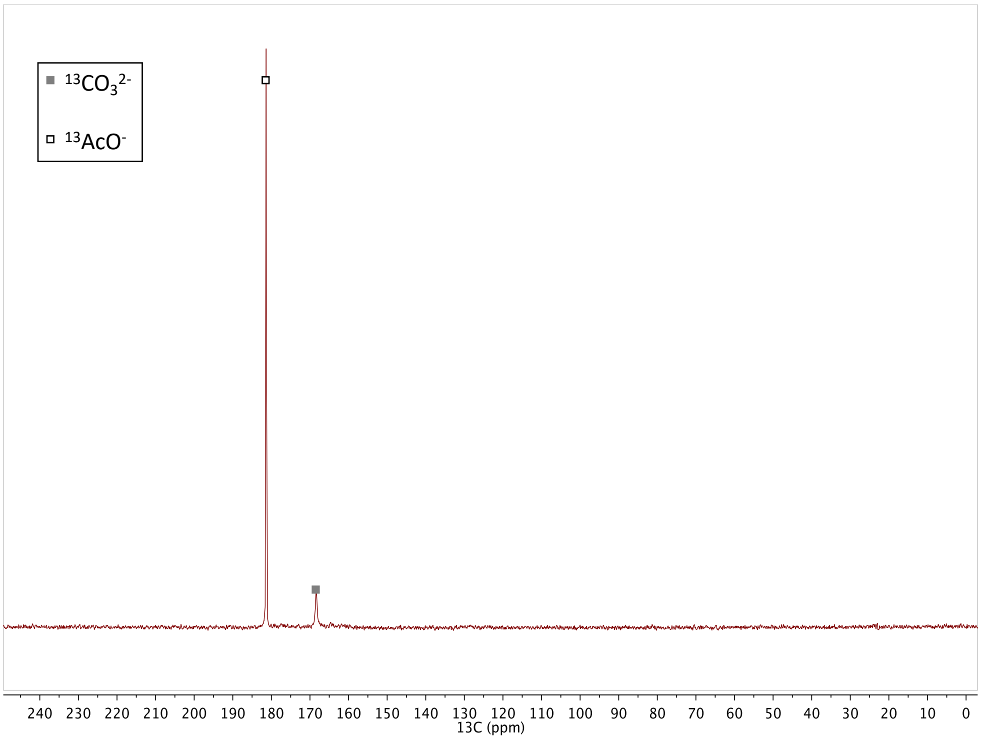

Figure S5 $^{13}C\{^1H\}$ NMR spectrum of the residue obtained removing the solvent from the reaction mixture of **2-Nd** and $^{13}CO_2$ after quenching with basic (pD = 13.6) D_2O (D_2O, 100 MHz, 298 K).

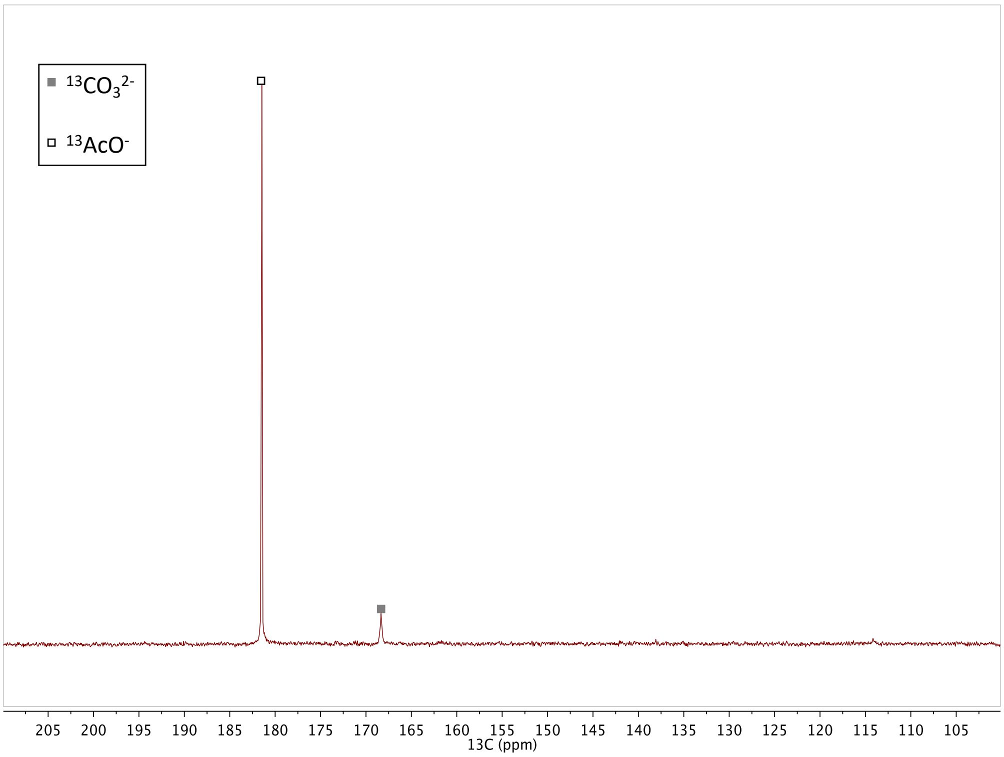

Figure S6. $^{13}C\{^1H\}$ NMR spectrum of the residue obtained removing the solvent from the reaction mixture of **4-Nd** and $^{13}CO_2$ after quenching with basic (pD = 13.6) D_2O (D_2O, 100 MHz, 298 K).

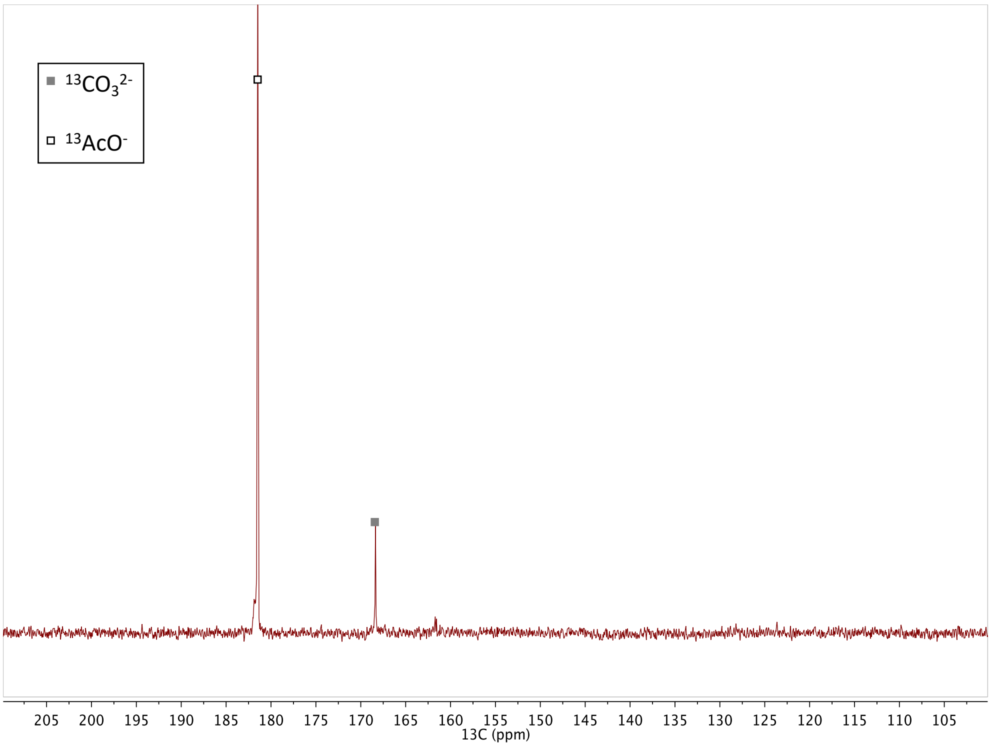

Figure S7. $^{13}C\{^1H\}$ NMR spectrum of the residue obtained removing the solvent from the reaction mixture of **2-Sm** and $^{13}CO_2$ after quenching with basic (pD = 13.6) D_2O (D_2O, 100 MHz, 298 K).

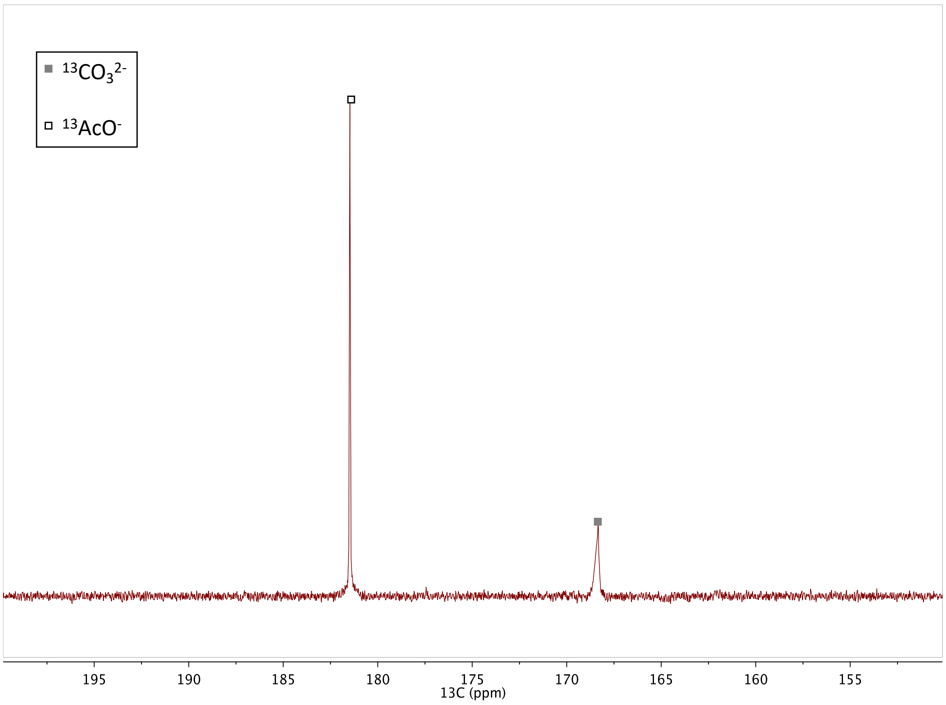

Figure S8. $^{13}C\{^1H\}$ NMR spectrum of the residue obtained removing the solvent from the reaction mixture of **4-Sm** and $^{13}CO_2$ after quenching with basic (pD = 13.6) D_2O (D_2O, 100 MHz, 298 K).

X-ray crystallographic data

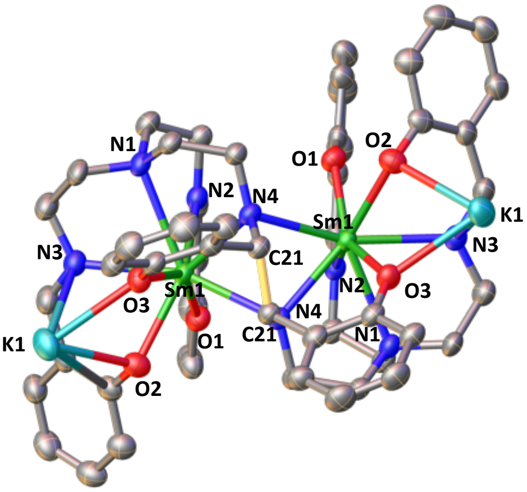
N1
O1
O2
N2
N4
Sm1
K1
N3
C21
N3
O3
Sm1
N2
O3
N4
N1
K1
O1
C21
O2

Figure S9. Molecular structure of complex **2-Sm** (C-C bond between imine highlighted in yellow, 50% probability ellipsoid). Hydrogen atoms were omitted for clarity.

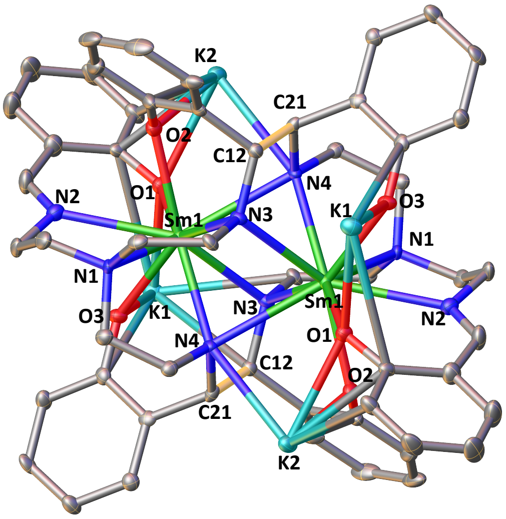
K2
C21
O2
C12
N4
O1
O3
K1
N2
Sm1
N3
N1
N1
O3
K1
N3
Sm1
N2
N4
O1
C12
O2
C21
K2

Figure S10. Molecular structure of complex **4-Sm** (C-C bonds between imine highlighted in yellow, 50% probability ellipsoids). Hydrogen atoms were omitted for clarity.

Table S1. X-ray crystallographic data.

Compound	**2-Nd**	**2-Sm**	**3-Eu**	**4-Nd**	**4-Sm**
Formula	$C_{78}H_{102}K_2N_8Nd_2O_{12}$	$C_{72.48}H_{88.96}K_2N_8O_{10.62}Sm_2$	$C_{66}H_{78}Eu_2K_2N_8O_9$	$C_{86}H_{118}K_4N_8O_{14}Nd_2$	$C_{86}H_{118}K_4N_8O_{14}Sm_2$

Crystal size [mm]	0.210×0.057×0.047	0.50×0.09×0.06	0.47×0.28×0.25	0.22×0.20×0.14	0.19×0.13×0.12
Crystal system	Monoclinic	Monoclinic	Monoclinic	monoclinic	Monoclinic
Space group	*C* 2/*c*	C2/c	I2/a	P21/n	*P*2$_1$/*n*
V [Å^3]	7492.2(6)	7268.8(2)	7096.0(3)	4459.02(15)	4462.4(3)
a [Å]	19.1572(10)	18.9002(3)	16.1474(4)	11.5916(2)	11.5872(5)
b [Å]	19.9660(6)	19.5477(2)	26.3520(7)	17.4426(3)	17.4186(7)
c [Å]	21.4402(9)	21.6120(3)	16.7297(4)	22.1502(4)	22.2099(9)
α [°]	90	90	90	90	90
β [°]	113.990(5)	114.4471(18)	94.589(2)	95.3459(18)	95.457(4)
γ [°]	90	90	90	90	90
Z	4	4	4	4	2
Absorption coefficient [mm-1]	1.549	-	-	-	-
F (000)	3520	-	-	-	-
T [K]	140.00(10)	140.01(10)	140.00(10)	100.01(10)	100.01(10)
Total no. reflexions	53552	25997	7266	70708	55351
Unique reflexions [R(int)]	12961 [0.0544]	7150 [0.0314]	7266 [0.0380]	11477 [0.0371]	8454 [0.0436]
Final R indice [I>2σ(I)]	0.0812	0.0549	0.0549	0.0258	0.0740
Largest diff. peak and hole [eA^{-3}]	2.049 and -1.467	1.612 and -0.791	1.653 and -0.836	0.760 and -0.904	1.421 and -0.982
GOF	1.038	1.031	1.046	1.043	1.023

Appendix chapter 5

NMR Spectroscopic Data

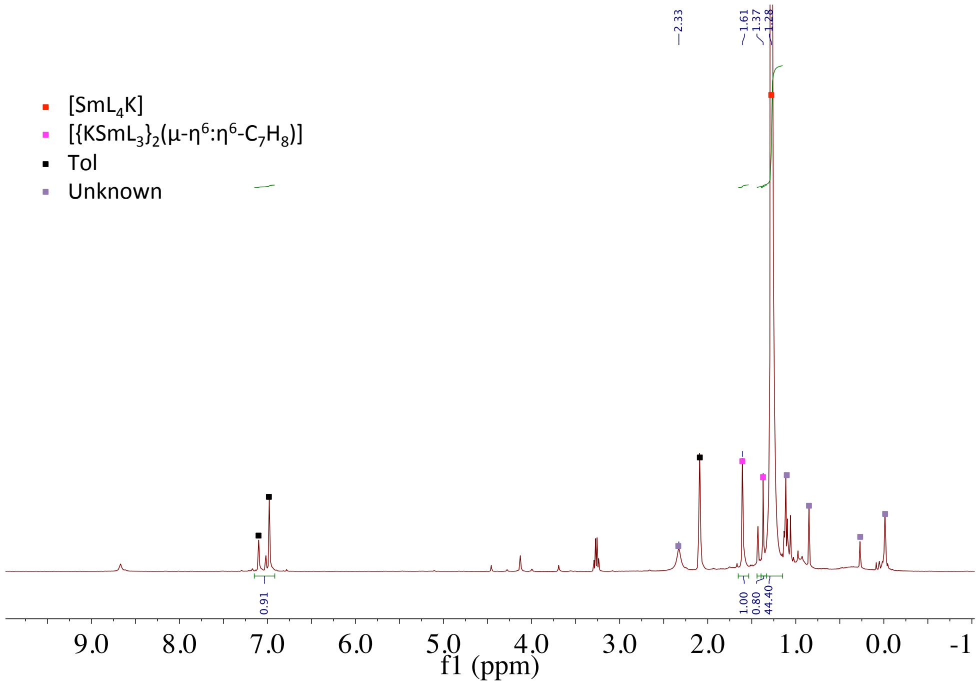

Figure S1. ^{1}H NMR of the reaction mixture of $[\mathrm{SmL_3}]$ and $\mathrm{KC_8}$ in Tol-d8 after 2 days (Tol-d8, 400 MHz, 298 K).

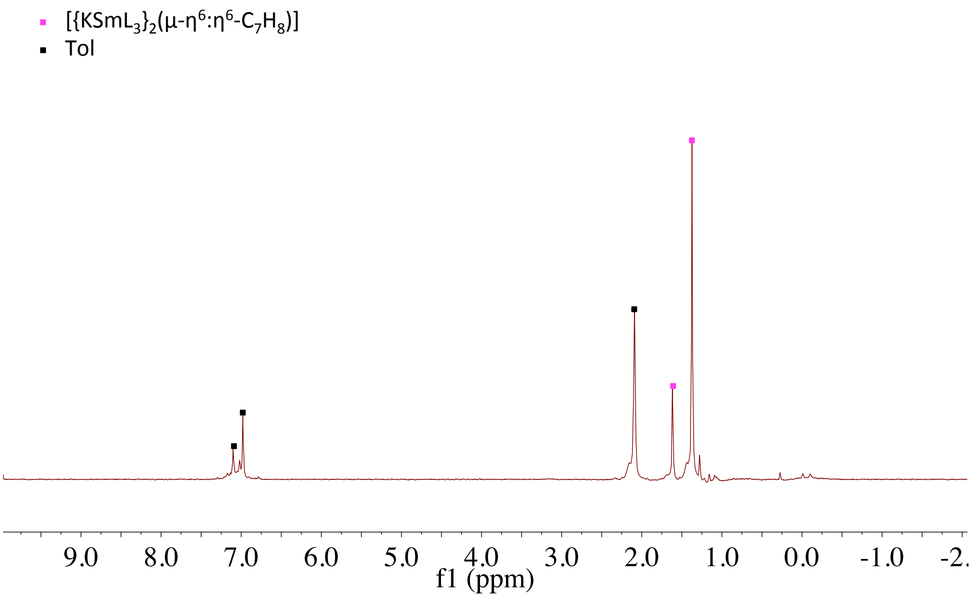

Figure S2. ^{1}H NMR of crystals of 2 immediately after dissolution in Tol-d8 at room temperature (Tol-d8, 400 MHz, 298 K).

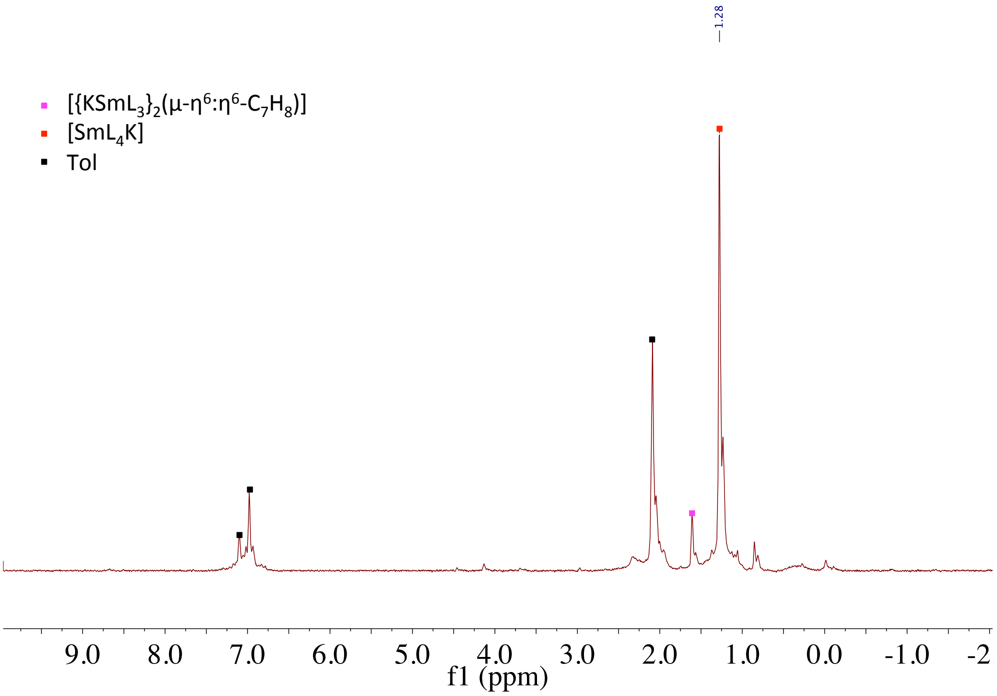

Figure S3. ^{1}H NMR of crystal of 2 three days after the dissolution in Tol-d8 at room temperature (Tol-d8, 400 MHz, 298 K).

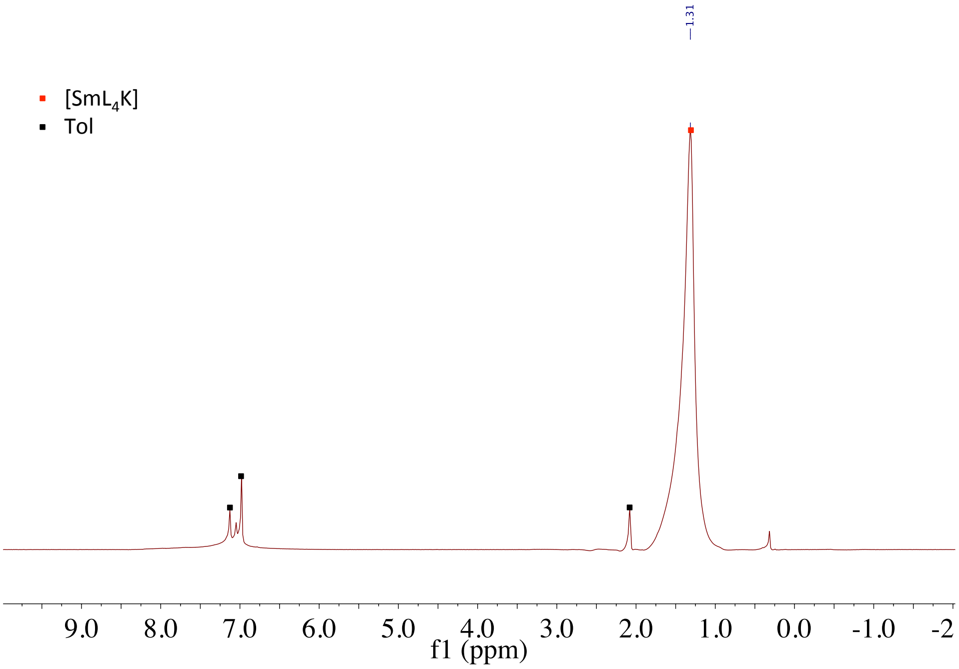

Figure S4. ^{1}H NMR immediately after the dissolution of [SmL_4K_2] in Tol-d8 at -40 °C (Tol-d8, 400 MHz, 233 K).

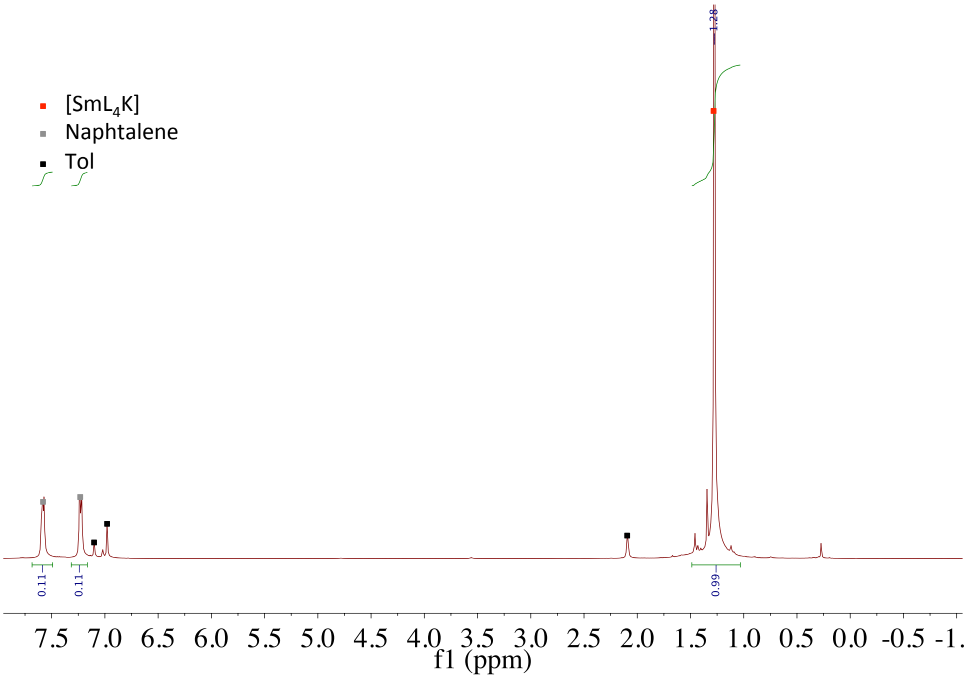

Figure S5. Quantitative integration with respect to naphtalene of [SmL_4K] formed dissolving [SmL_4K_2] in Tol-d8 at room temperature (Tol-d8, 400 MHz, 298 K).

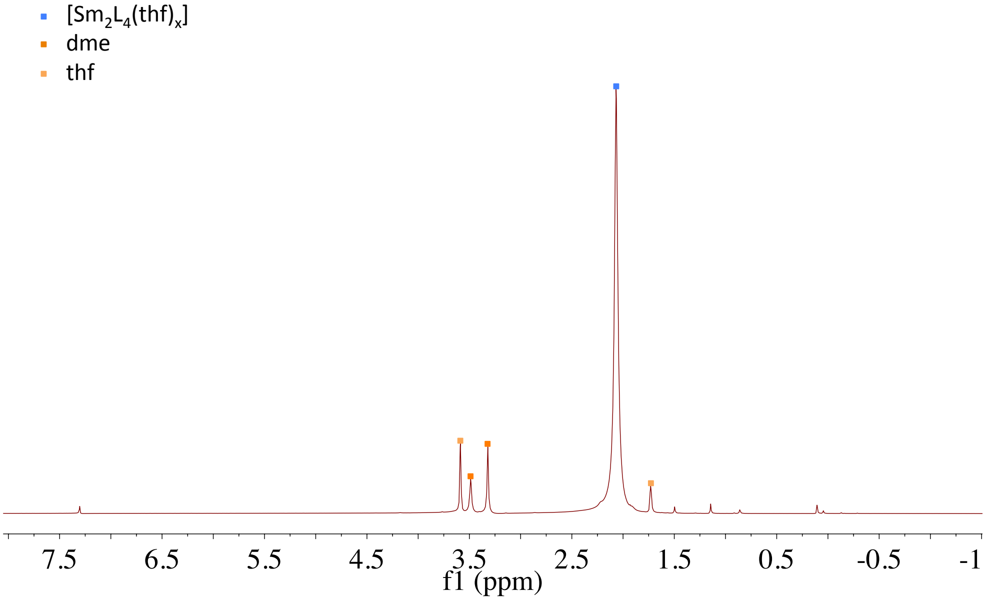

Figure S6. ^{1}H NMR spectrum of **3** in thf-d8 (THF-d8, 400 MHz, 298 K).

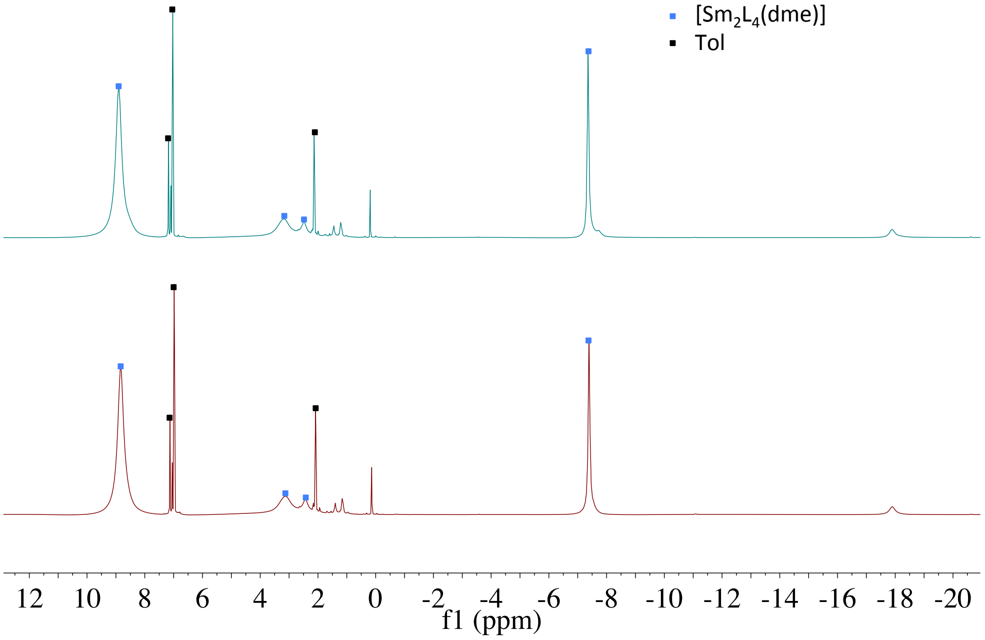

Figure S7. ^{1}H NMR spectrum of a 20 mM solution of 3 (Tol-d8, 400 MHz, 233 K) immediately after the dissolution in Tol-d8 (above) and after 5 days (below).

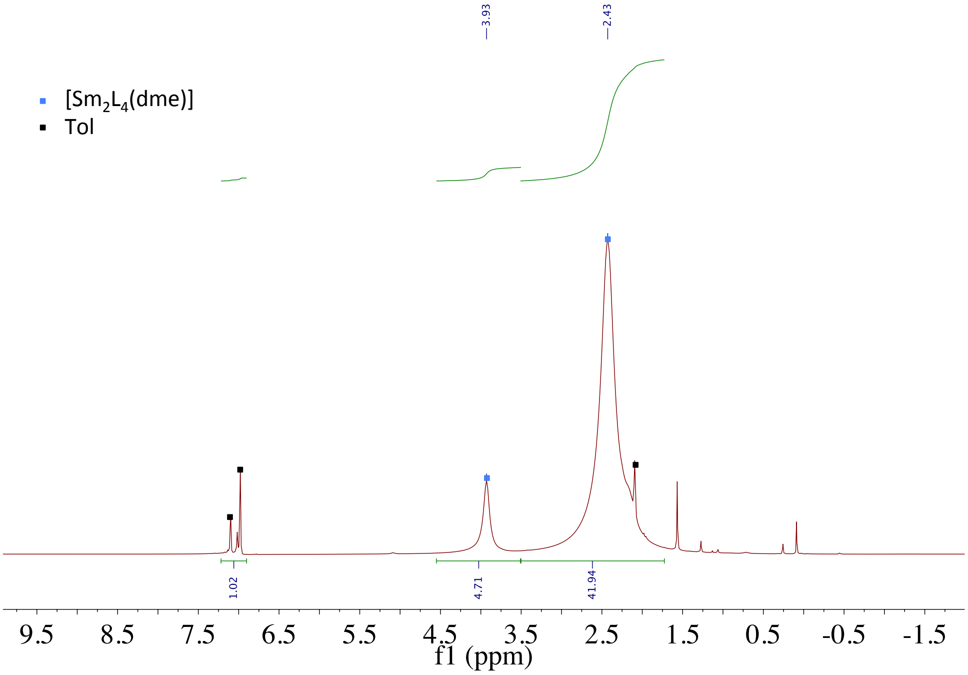

Figure S8. ^{1}H NMR of a 27 mM solution of 3 immediately after dissolution in Tol-d8 (Tol-d8, 400 MHz, 298 K).

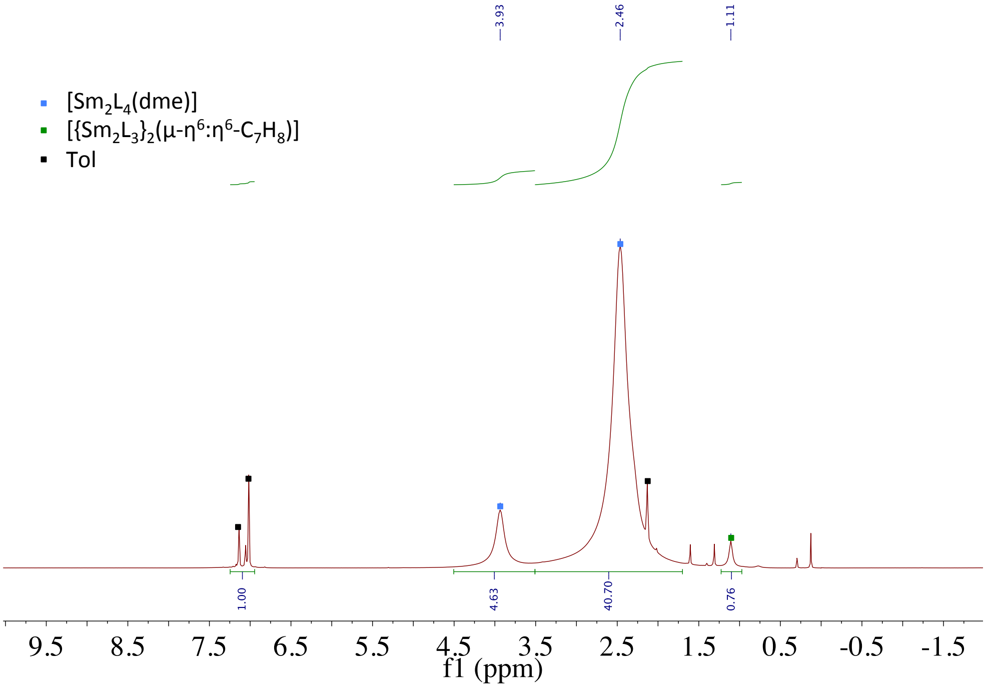

Figure S9. ^{1}H NMR of a 27 mM solution of 3 after one day in Tol-d8 at room temperature (Tol-d8, 400 MHz, 298 K).

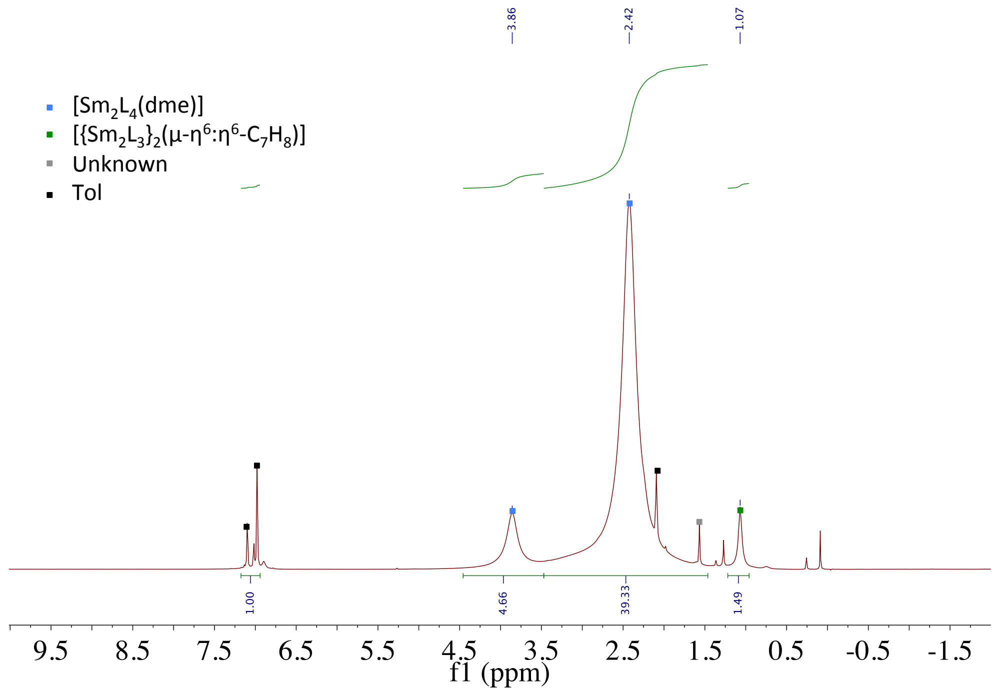

Figure S10. ^{1}H NMR of a 27 mM solution of 3 after two days in Tol-d8 at room temperature (Tol-d8, 400 MHz, 298 K).

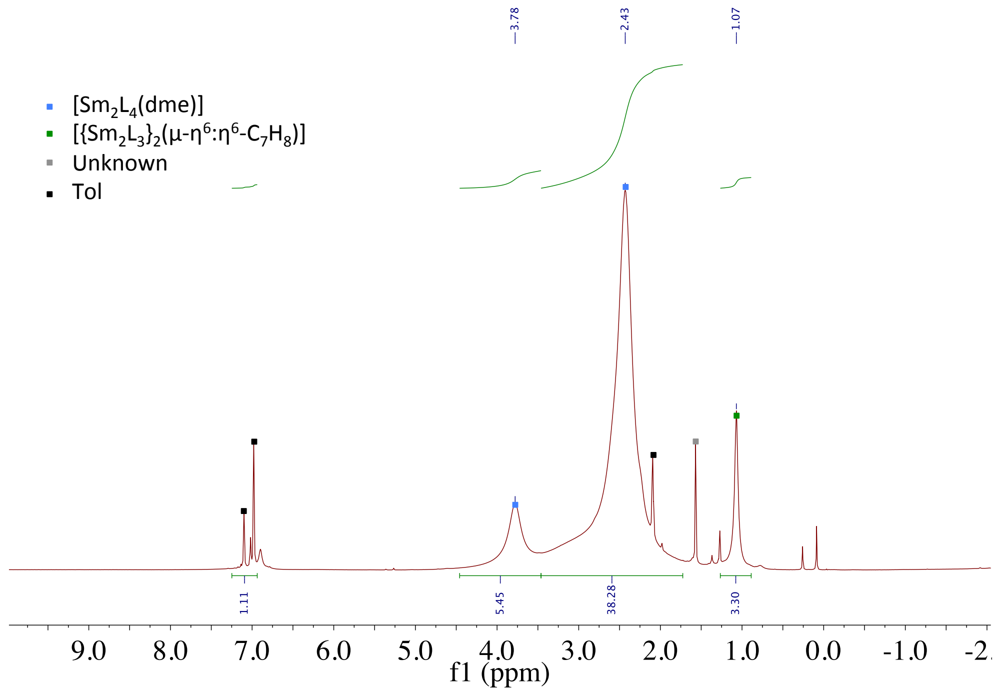

Figure S11. ^{1}H NMR of a 27 mM solution of 3 after six days in Tol-d8 at room temperature (Tol-d8, 400 MHz, 298 K).

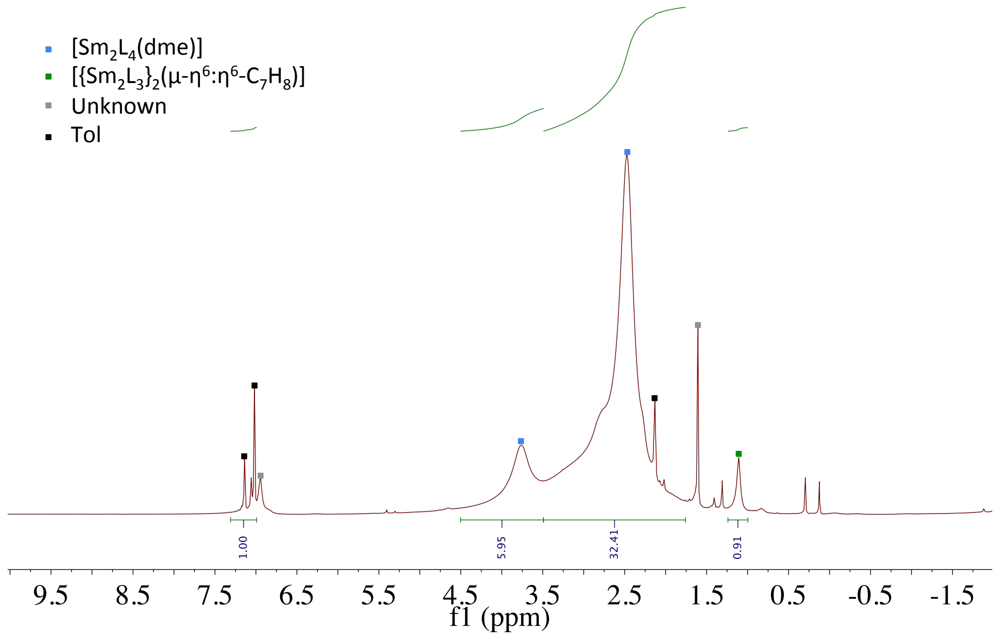

Figure 12. ^{1}H NMR of a 27 mM solution of 3 after nine days in Tol-d8 at room temperature and removal of crystal of 4 that formed in the tube(Tol-d8, 400 MHz, 298 K).

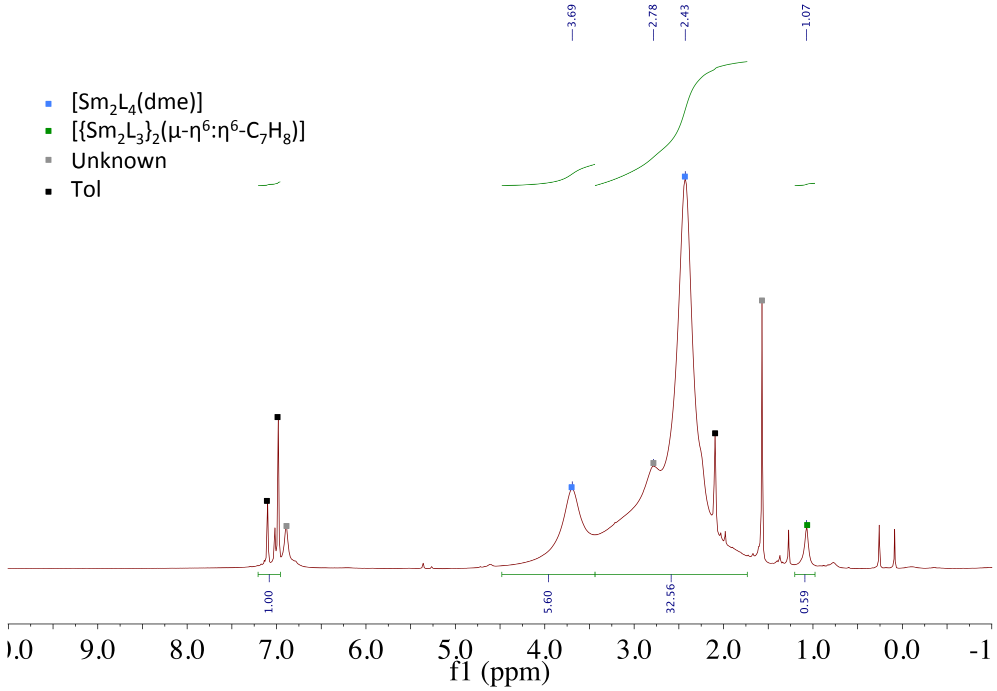

Figure S13. ^{1}H NMR of a 27 mM solution of 3 after twelve days in Tol-d8 at room temperature (crystals of complex 4 have formed in the NMR tube(Tol-d8, 400 MHz, 298 K).

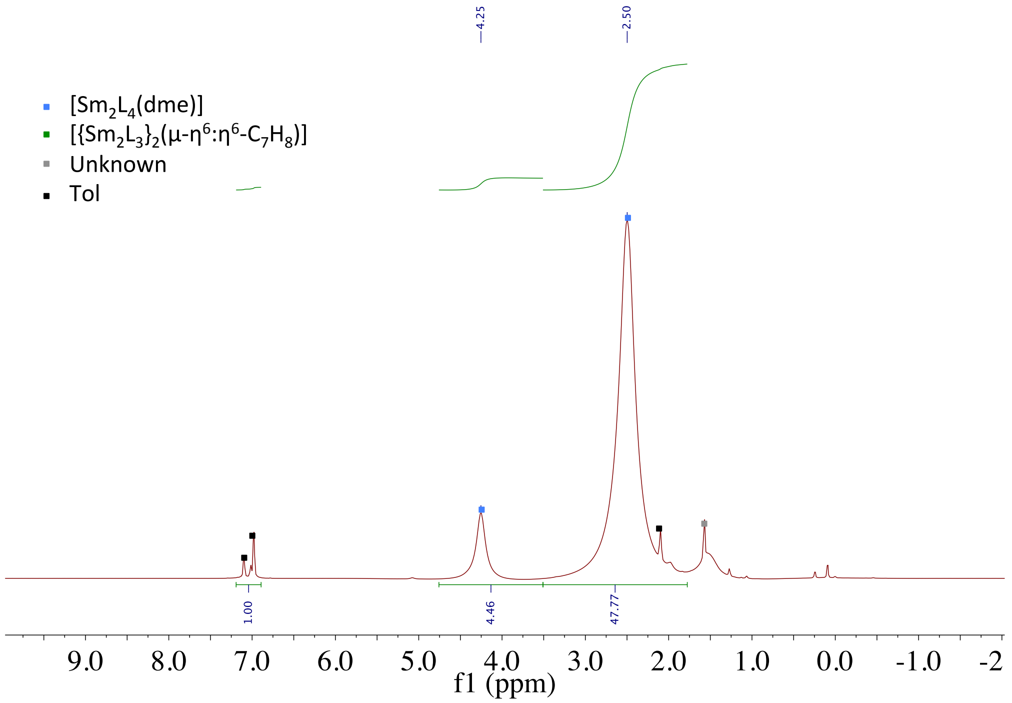

Figure S14.^{1}H NMR of a 69 mM solution of 3 after dissolution in Tol-d8 at room temperature (Tol-d8, 400 MHz, 298 K).

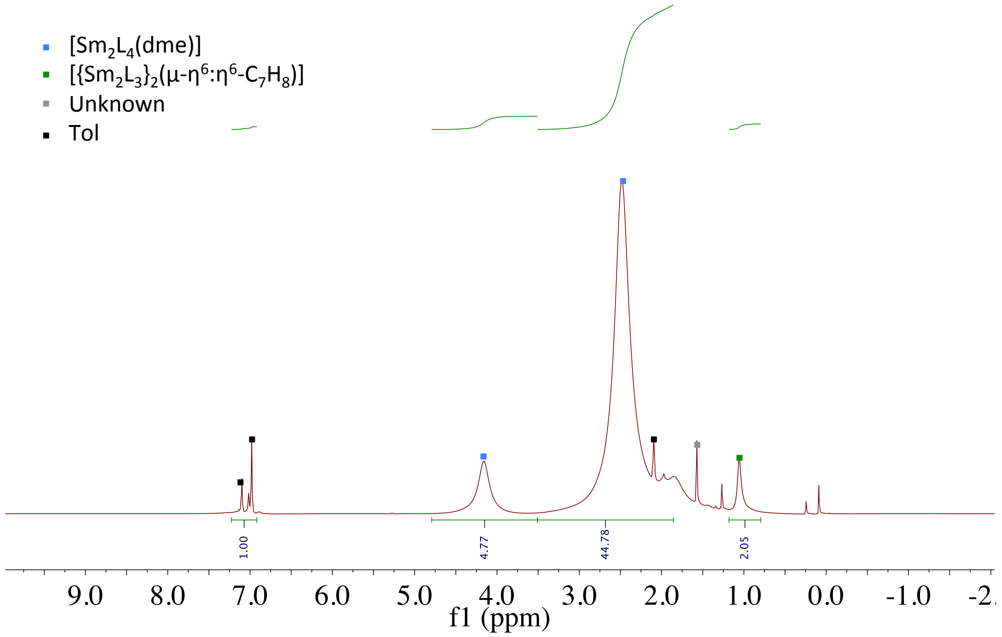

Figure S15. ^{1}H NMR of a 69 mM solution of 3 after one day in Tol-d8 at room temperature (Tol-d8, 400 MHz, 298 K).

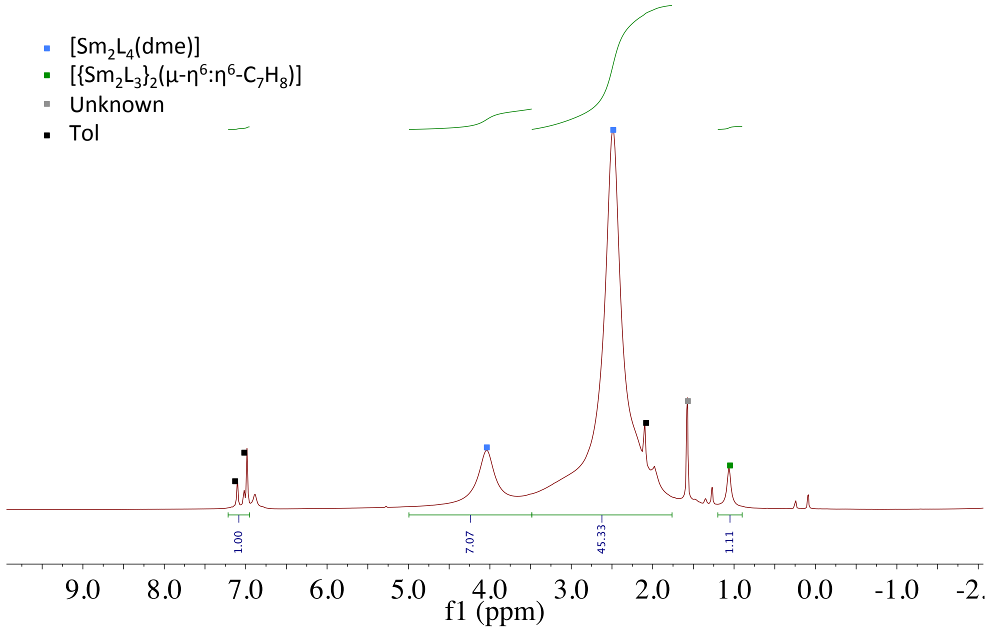

Figure S16. ^{1}H NMR of a 69 mM solution of 3 after three days in Tol-d8 at room temperature (Tol-d8, 400 MHz, 298 K).

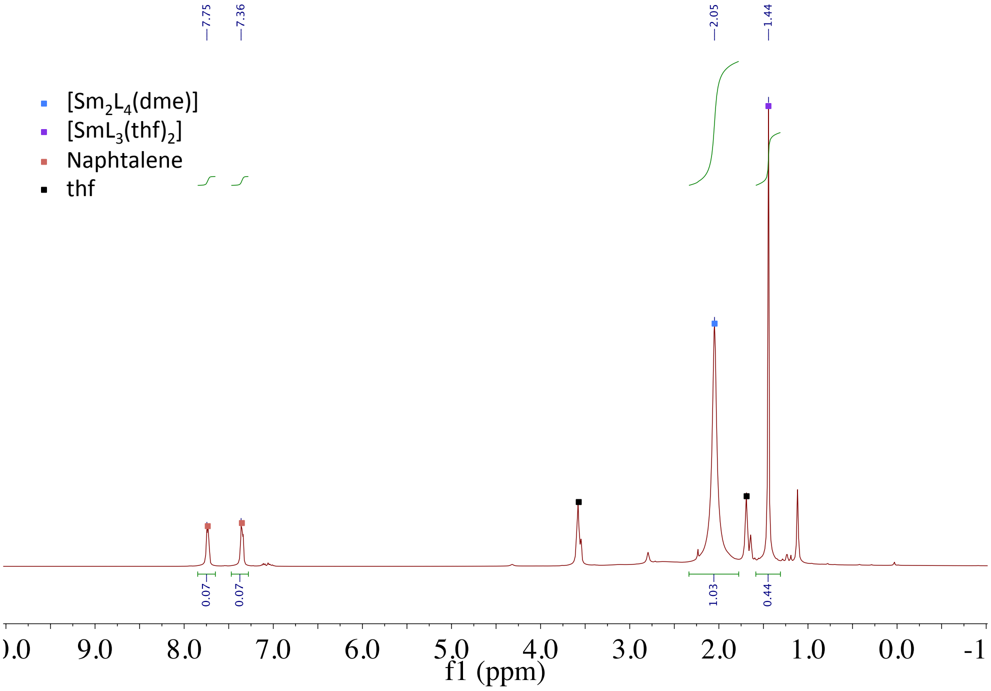

Figure S17. Quantitative integration with respect to naphthalene of the residue from the evaporation of the reaction mixture resulting from leaving a 69 mM solution of 3 for three days in Tol-d8 and after removal of 4 (thf-d8, 400 MHz, 298 K).

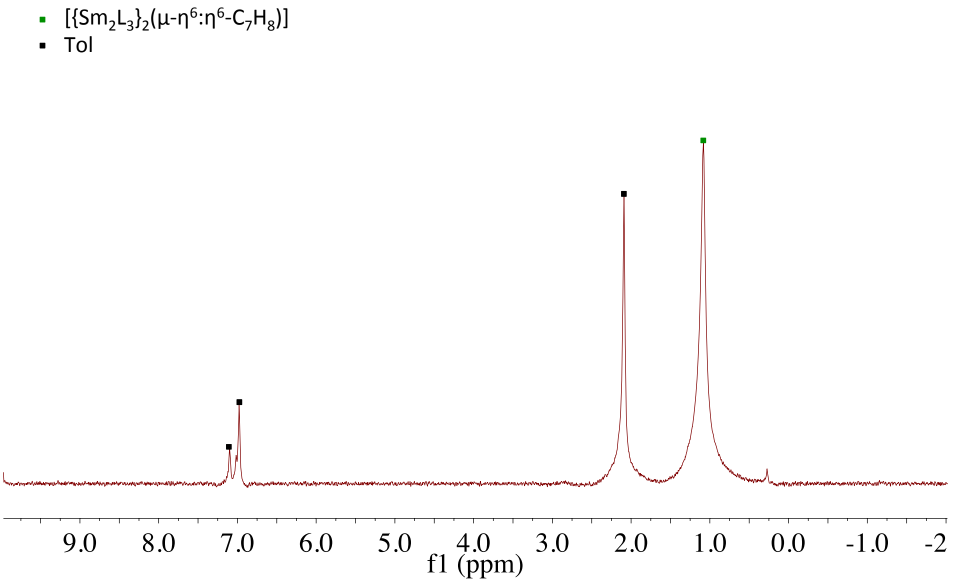

Figure S18. ^{1}H NMR spectrum of 4 in Tol-d8 (Tol-d8, 400 MHz, 298 K).

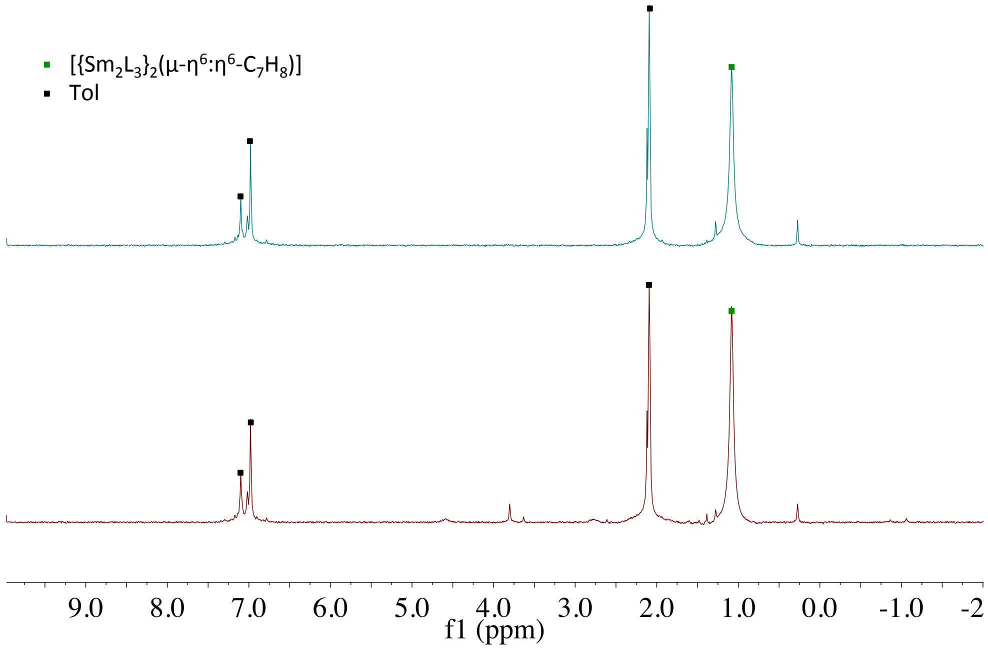

Figure S19. ^{1}H NMR spectrum of 4 in Tol-d8 immediately after the dissolution (above) and after 5 days (below) (Tol-d8, 400 MHz, 298 K).

UV-Vis-NIR Spectra

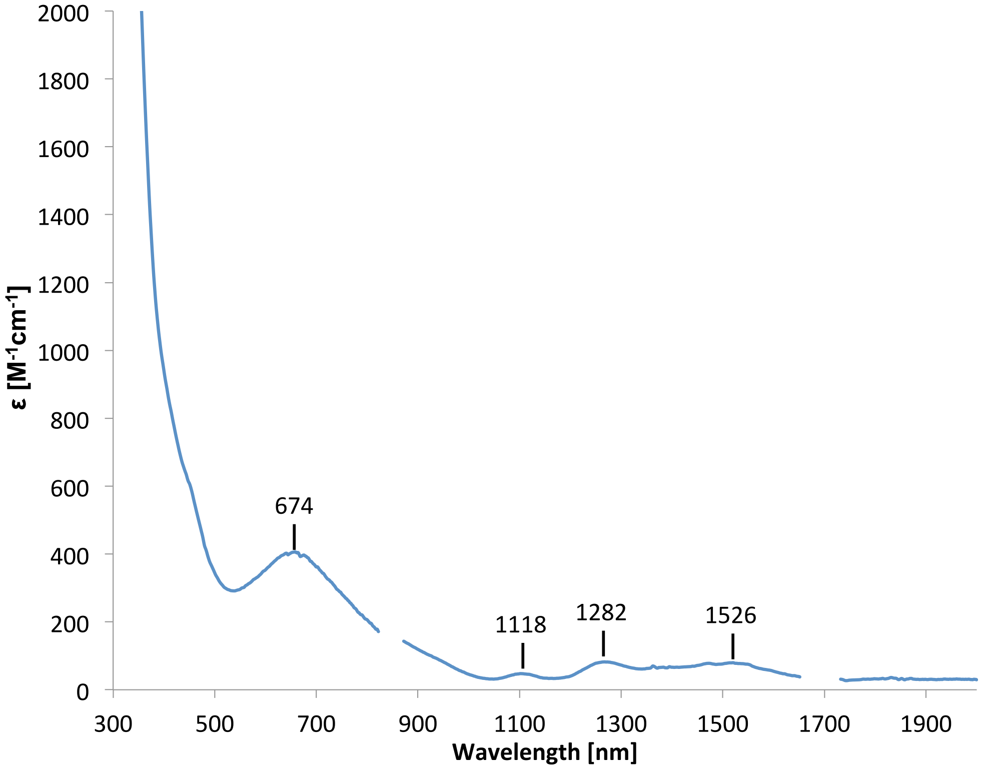

Figure S20. UV-Vis-NIR spectra of a 0.1 mM solution of 2 in toluene.

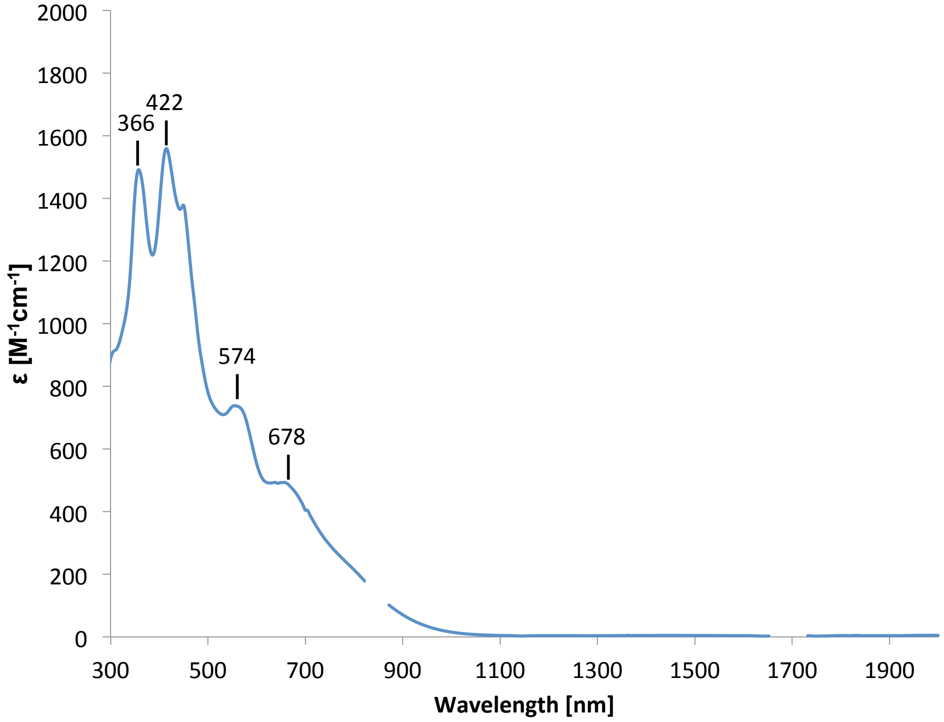

Figure S21. UV-Vis-NIR spectra of a 2 mM solution of 3 in toluene.

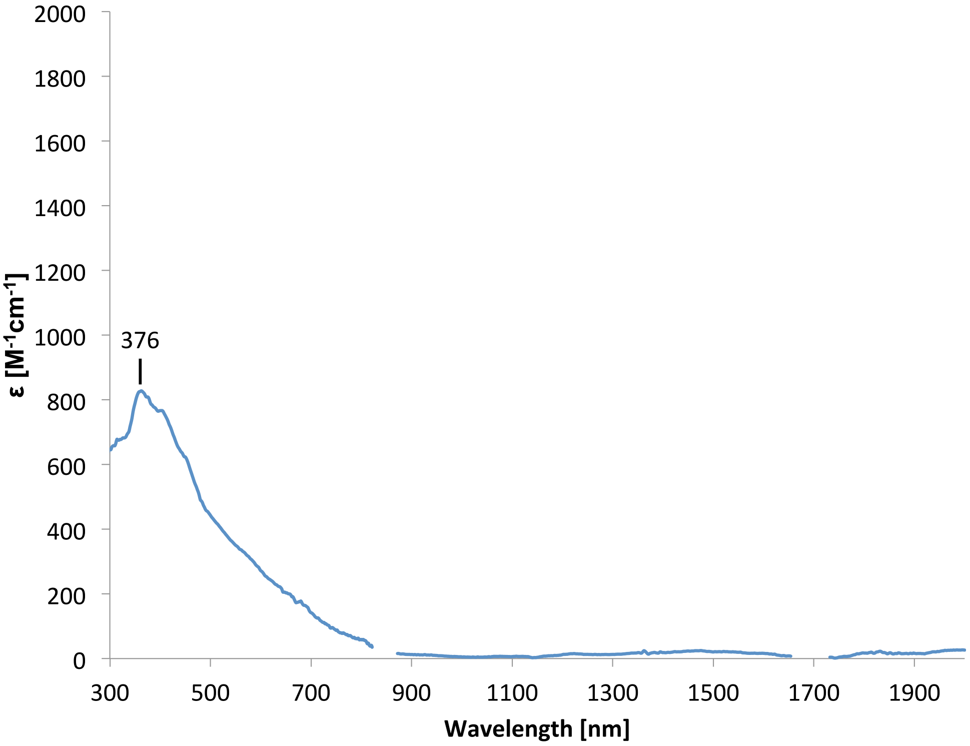

Figure S22. UV-Vis-NIR spectra of a 0.1 mM solution of 4 in toluene.

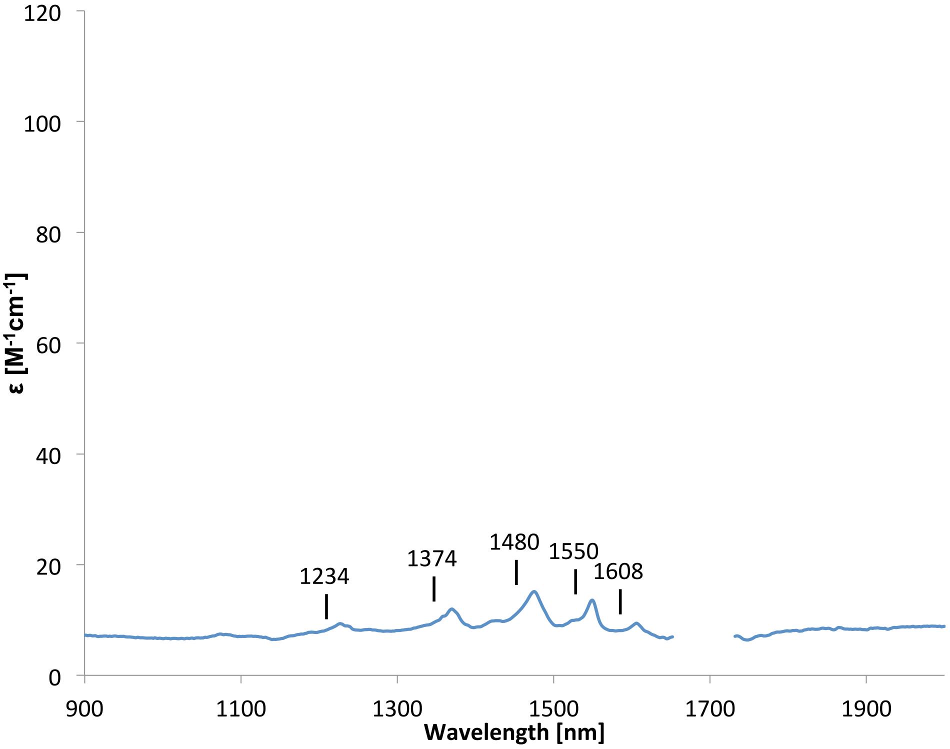

Figure S23. NIR spectrum of a 0.1 mM solution of [SmL_3] in toluene.

X-ray Crystal Structure Determination Details

The X-ray diffraction data of **1** were measured at 120(2) K using Mo *K*α radiation on a Bruker APEX II CCD kappa diffractometer. The dataset was reduced by EvalCCD[1] and then corrected, by modelling an empirical transmission surface as sampled by multiple symmetry-equivalent and/or azimuth rotation-equivalent intensity measurements by real spherical harmonic functions of even order, for absorption.[2]

Bragg-intensities of **2** and **4** were collected at 140(1) K and those of **3** at 90(1) K using Cu K_α radiation. A Rigaku SuperNova dual system diffractometer with an Atlas S2 CCD detector was used for compounds **3** and **4**, and one equipped with an Atlas CCD detector for compound **2**. The datasets were reduced and then corrected for absorption, with the help of a set of faces enclosing the crystals as snugly as possible, with CrysAlis$^{\text{Pro}}$.[3]

The solutions and refinements for the structures were performed by SHELXT[4] and SHELXL-2018[5], respectively, except the structure refinement of **4** that was performed by SHELXL-2017.[5] All non-hydrogen atoms were refined anisotropically using full-matrix least-squares based on $|F|^2$. All hydrogen atoms were placed in geometrically calculated positions and refined using a riding model where each H-atom was assigned a fixed isotropic displacement parameter with a value equal to 1.2 U_{eq} of its parent C-atom (1.5 U_{eq} for the Me groups).

In the structure of **1**, highly disordered solvent molecules were removed with the help of the solvent-masking program in OLEX2.[6] The structure of **2** was refined as a two-component twin with an HKLF 5 file furnished by CrysAlisPro,[3] yielding a BASF parameter of 0.443(3). In the structure of **4**, the contributions of highly disordered solvent molecules were removed from the model by the SQUEEZE algorithm of PLATON.[7]

Table S1. Crystallographic parameters for complexes 1-4.

Compound	$[Sm_2L_5K]$, **1**	$[\{KSmL_3\}(\mu\text{-}\eta^6\text{:}\eta^6\text{-}C_7H_8)]$, **2**	$[Sm_2L_4(DME)]$, **3**	$[\{Sm_4L_6\}(\mu\text{-}\eta^6\text{:}\eta^6\text{-}C_7H_8)]$, **4**
Formula	$C_{60}H_{135}KO_{20}Si_5Sm_2$	$C_{79}H_{169}K_2O_{24}Si_6Sm_2$	$C_{56}H_{128}O_{20}Si_4Sm_2$	$C_{79}H_{170}O_{24}Si_6Sm_4$
Crystal size [mm]	0.217 x 0.135 x 0.080	0.339 x 0.185 x 0.163	0.318 x 0.118 x 0.028	0.311 x 0.223 x 0.143

Crystal system	Triclinic	Triclinic	Hexagonal	Triclinic
Volume [Å^3]	4577.3(8)	2974.4(4)	11617.6(3)	2962.5(3)
a [Å]	13.9095(16)	13.3255(8)	13.49276(16)	13.2055(6)
b [Å]	15.4386(11)	13.4570(8)	13.49276(16)	13.2859(6)
c [Å]	21.897(3)	19.2064(12)	73.6861(7)	19.3107(10)
α [°]	80.979(7)°	80.512(5)	90	81.584(4)
β [°]	87.169(9)°	72.563(6)	90	73.829(4)
γ [°]	80.361(8)°	64.969(6)	120	65.648(4)
Z		1	6	1
Absorption coefficient [mm^{-1}]	1.434	8.981	12.347	15.673
F (000)	1736	1081	4824	1168
T [K]	120(2)	140.00(10)	90.0(3)	140.00(10)
Total no. reflexions	63685	12278	84451	21320
Unique reflexions [R(int)]	20583 [R_{int} = 0.0968]	12278 [R(int)= n/a]	12570 [R_{int} = 0.1104]	11997 [R_{int} = 0.0450]
Final R indices [I>2σ(I)]	R_1 = 0.0692, wR_2 = 0.1303	R_1 = 0.0731, wR_2 = 0.1869	R_1 = 0.0819, wR_2 = 0.1848	R_1 = 0.0536, wR_2 = 0.1396
Largest diff. peak and hole [eA^{-3}]	1.223 and -1.072	2.761 and -1.659	1.509 and -1.436	3.245 and -1.880
GOF	1.015	0.934	1.171	1.028

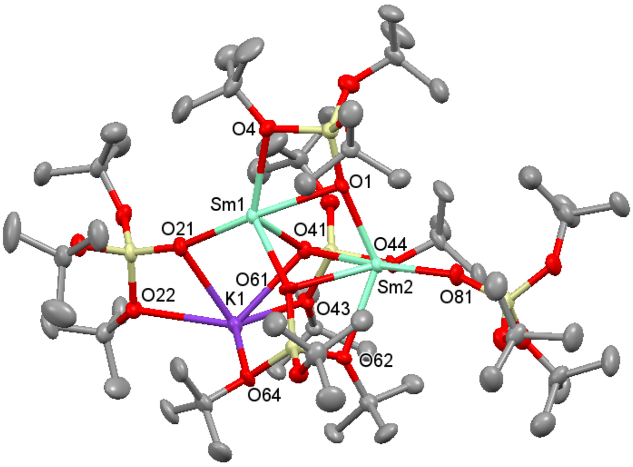

Figure S24. Molecular structure of complex 1 shown with 50% probability thermal ellipsoids. Hydrogen atoms have been omitted for clarity. Selected bond lengths (Å): Sm1–O = 2.381(5)−2.602(5), Sm2–O = 2.356(5)−2.880(5).

Unrestricted DFT calculations with explicit f electrons were carried out for the whole molecule for **2** and **4** with spin state of 13 for **2** and of 25 for **4**. The Gaussian09 program suite was used for performing all the quantum-chemical calculations.[8] As functional we have used the Becke's 3-parameter hybrid one,[9] combined with the non-local correlation functional provided by Perdew/Wang[10] denoted as B3PW91. Two different effective core potentials from Stuttgart-Dresden were used for describing the samarium atoms. The relativistic energy-consistent small-core pseudopotential of the Stuttgart-Köln ECP library was used in combination with its adapted segmented basis set.[11] Samarium atoms were treated with a large- core Stuttgart Dresden relativistic effective core potential (RECP) adapted to the +II oxidation state, and the corresponding optimized basis set augmented by a f polarization function (α=1.000)[12] The aforementioned computational scheme was found previously by our group to give coherent results.[13] For the potassium and silicon atoms the quasi-relativistic energy-adjusted *ab-initio* pseudopotentials were used, along with their corresponding energy-optimized valence basis sets,[14] augmented by a *d* polarization function, for the case of silicon atoms.[15] For all the other atoms, the 6-31G(d,p) basis set was used,[16] In all computations no constrains were imposed on the geometry. Full geometry optimization was performed for each structure using Schlegel's analytical gradient method[17, 18] and the attainment of the energy minimum was verified by calculating the vibrational frequencies that result in absence of imaginary eigenvalues. Natural bond orbital (NBO) analysis[19] was used to analyze electron density.

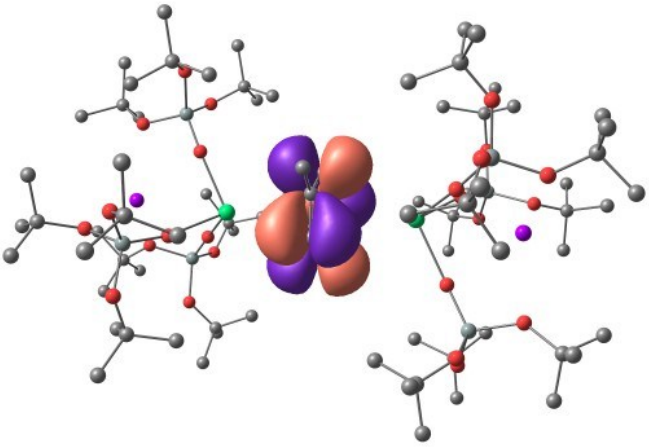

Figure S25: LUMO of complex **2**

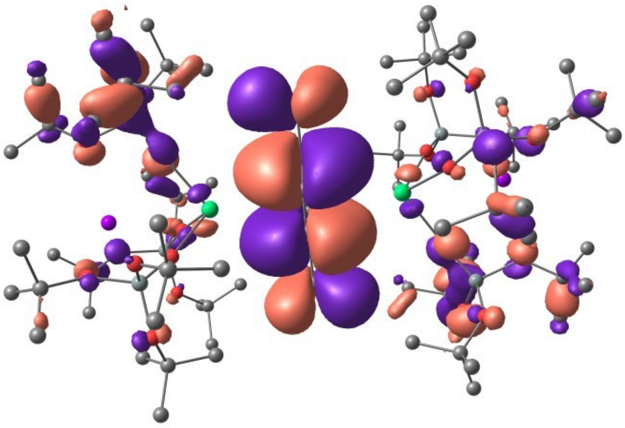

Figure S26: HOMO-42 of complex **2**

References

1 A. J. M. Duisenberg, L. M. J. Kroon-Batenburg, A. M. M. Schreurs, *J. Appl. Crystallogr.,* 2003, **36**, 220-229.

2 R. H. Blessing, *Acta Crystallogr.*, *Sect. A,* 1995, **51**, 33-38.

3 *CrysAlis PRO*. Rigaku Oxford Diffraction 2015.

4 Sheldrick, G. M.; *Acta Crystallogr., Sect. A,* 2015, **71**, 3–8.

5 Sheldrick, G. M., *Acta Crystallogr. C,* 2015, **71**, 3–8.

6 O. V. Dolomanov, L. J. Bourhis, R. J. Gildea, J. A. K. Howard and H. Puschmann; OLEX2: a complete structure solution, refinement and analysis program; *J. Appl. Cryst.,* 2009, **42**, 339-341.

7 *PLATON*, Spek, A. L.; *Acta Crystallogr., Sect. C,* 2015, **71**, 9–18.

8 Gaussian 09, Revision A.02, M. J. Frisch, G. W. Trucks, H. B. Schlegel, G. E. Scuseria, M. A. Robb, J. R. Cheeseman, G. Scalmani, V. Barone, B. Mennucci, G. A. Petersson, H. Nakatsuji, M. Caricato, X. Li, H. P. Hratchian, A. F. Izmaylov, J. Bloino, G. Zheng, J. L. Sonnenberg, M. Hada, M. Ehara, K. Toyota, R. Fukuda, J. Hasegawa, M. Ishida, T. Nakajima, Y. Honda, O. Kitao, H.

Nakai, T. Vreven, J. A. Montgomery, Jr., J. E. Peralta, F. Ogliaro, M. Bearpark, J. J. Heyd, E. Brothers, K. N. Kudin, V. N. Staroverov, R. Kobayashi, J. Normand, K. Raghavachari, A. Rendell, J. C. Burant, S. S. Iyengar, J. Tomasi, M. Cossi, N. Rega, J. M. Millam, M. Klene, J. E. Knox, J. B. Cross, V. Bakken, C. Adamo, J. Jaramillo, R. Gomperts, R. E. Stratmann, O. Yazyev, A. J. Austin, R. Cammi, C. Pomelli, J. W. Ochterski, R. L. Martin, K. Morokuma, V. G. Zakrzewski, G. A. Voth, P. Salvador, J. J. Dannenberg, S. Dapprich, A. D. Daniels, O. Farkas, J. B. Foresman, J. V. Ortiz, J. Cioslowski, D. J. Fox, Gaussian, Inc., Wallingford CT, 2009.

9 A. D. Becke, *J. Chem. Phys*., 1993, **98**, 5648-5652.

10 J. P. Perdew, Y. Wang, *Phys. Rev. B,* 1992, **45**, 13244-13249.

11 a) W. Küchle, M. Dolg, H. Stoll, H. Preuß, *J. Chem. Phys*., 1994, **100**, 7535- 7543; b) X. Y. Cao, M. Dolg, H. Stoll, *J. Chem. Phys*., 2003, **118**, 487-497; c) X. Cao, M. Dolg, *J. Molec. Struct. (Theochem),* 2004, **673**, 203-209.

12 M. Dolg, H. Stoll, A. Savin, H. Preuss, *Theor. Chim. Acta.*, 1989, **75**, 173.

13 a) L. Castro, A. Yahia, L. Maron, *ChemPhysChem,* 2010, **11**, 990-994; b) L. Castro, A. Yahia, L. Maron, *Dalton Trans*., 2010, **39**, 6682-6692; c) B. Kosog, C. E. Kefalidis, F. W. Heinemann, L. Maron, K. Meyer, *J. Am. Chem. Soc*., 2012, **134**, 12792–12797; d) Mougel, V. Camp, C. Pecaut, J. Coperet, C. Maron, L. Kefalidis, C. E. Mazzanti, M. *Angew. Chem. Int. Ed.,* 2012, **51**, 12280-12284.

14 a) Silicon ECP: A. Bergner, M. Dolg, W. Küchle, H. Stoll, H. Preuß, *Mol. Phys.,* 1993, **80**, 1431-1441; b) Potassium ECP: T. Leininger, A. Nicklass, W. Küchle, H. Stoll, M. Dolg, A. Bergner, *Chem. Phys. Lett.,* 1996, **255**, 274-280.

15 A. W. Ehlers, M. Böhme, S. Dapprich, A. Gobbi, A. Höllwarth, V. Jonas, K. F. Köhler, R. Stegmann, A. Veldkamp, G. Frenking, *Chem. Phys. Lett.,* 1993, **208**, 111– 114.

16 a) W. J. Hehre, R. Ditchfield and J. A. Pople, J. Chem. Phys., 1972, **56**, 2257– 2261; b) P. C. Hariharan and J. A. Pople, *Theor. Chim. Acta,* 1973, **28**, 213–222.

17 H. B. Schlegel, *J. Comput. Chem*., 1982, **3**, 214-218.

18 a) C. Gonzalez, H. B. Schlegel, *J. Chem. Phys*., 1989, **90**, 2154-2161; b) C. Gonzalez, H. B. Schlegel, *J. Phys. Chem*., 1990, **94**, 5523-5527.

19 A. E. Reed, L. A. Curtiss, F. Weinhold, *Chem. Rev.*, 1988, **88** (6), 899–926.

Appendix chapter 6

NMR Spectroscopic Data

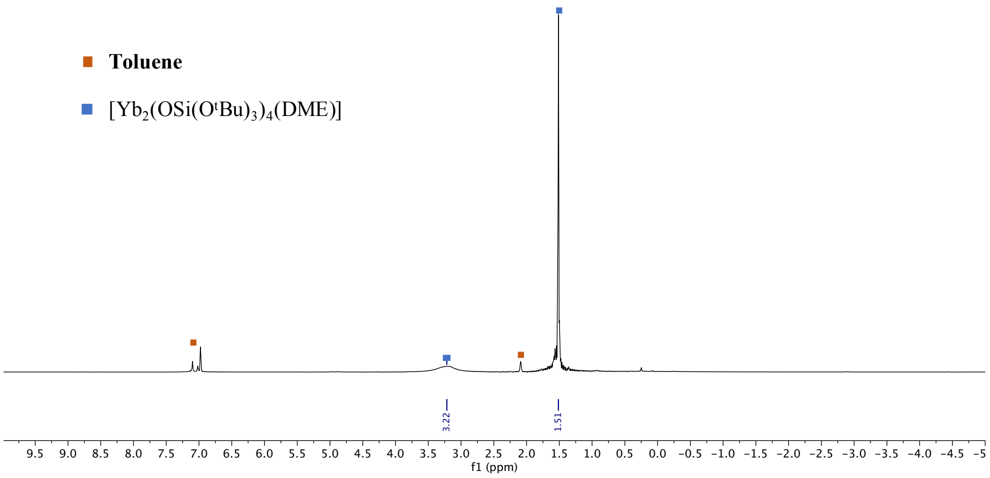

Figure S1: ^{1}H NMR spectrum of [Yb$_2$L$_4$(DME)] (Tol-d8, 400 MHz, 298K).

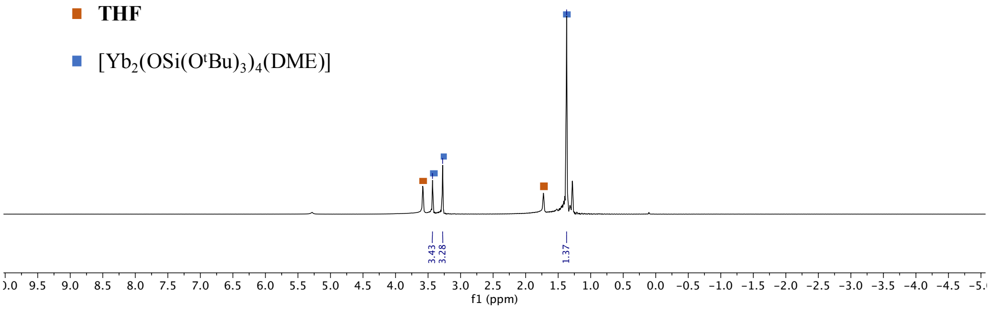

Figure S2: ^{1}H NMR spectrum of [Yb$_2$L$_4$(DME)] (THF-d8, 400 MHz, 298K).

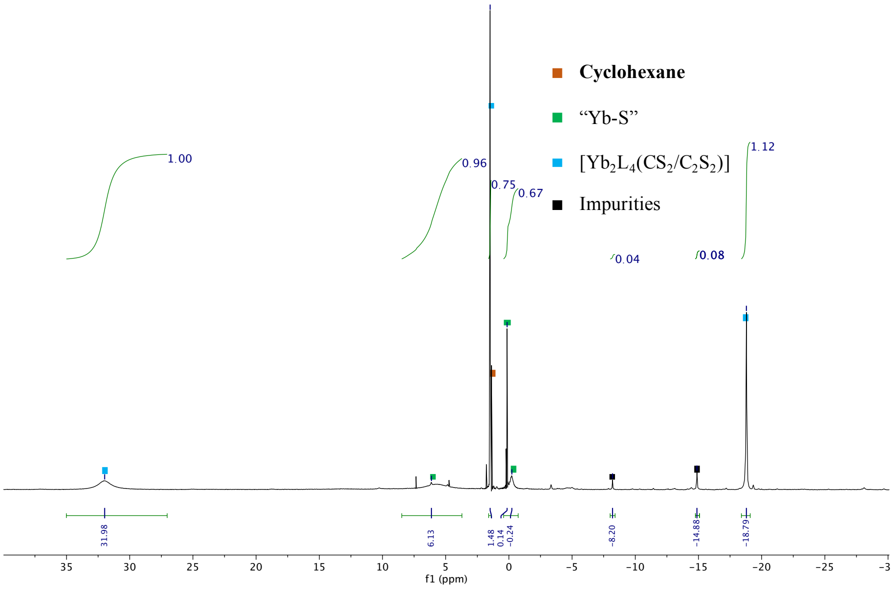

Figure S3: ^{1}H NMR spectrum of the reaction mixture after addition of 1 equivalent $^{13}CS_2$ to a cyclohexane solution of 1 at room temperature (C_6D_{12}, 400 MHz, 298K).

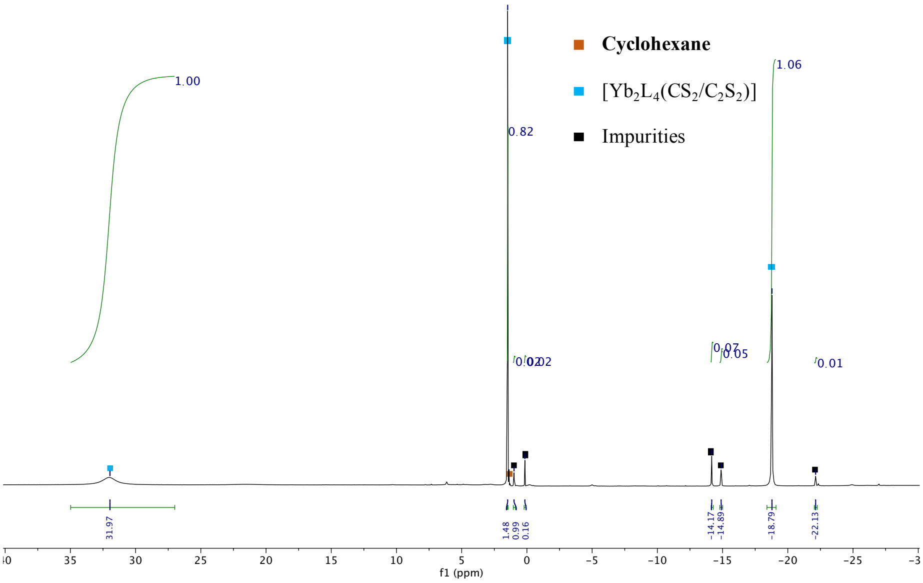

Figure S4: ^{1}H NMR spectrum of 2 / 3 isolated from the reaction mixture after addition of 1 equivalent $^{13}CS_2$ to a cyclohexane solution of 1 at room temperature (C_6D_{12}, 400 MHz, 298K).

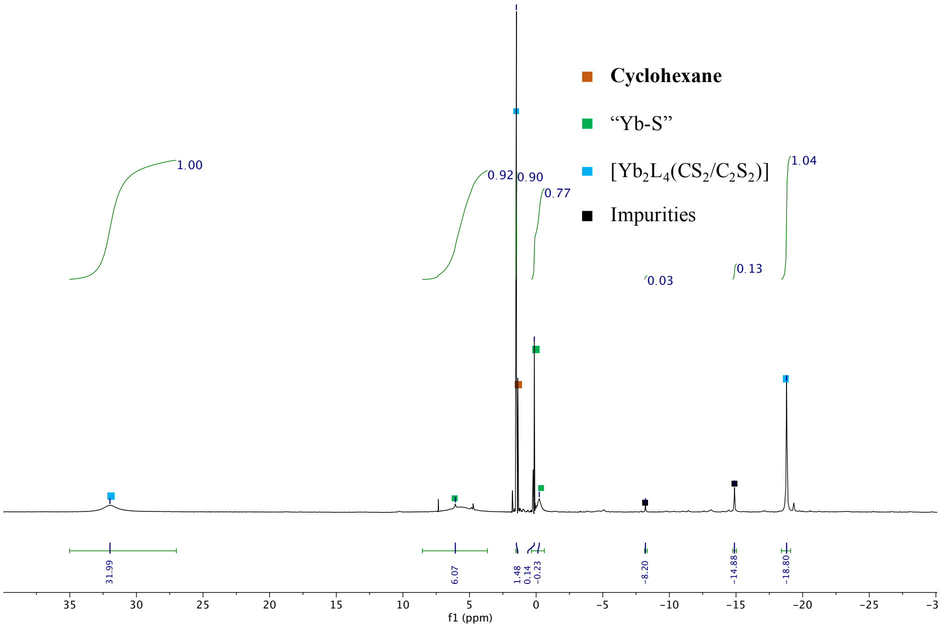

Figure S5: ^{1}H NMR spectrum of the reaction mixture after addition of 2 equivalents $^{13}CS_2$ to a cyclohexane solution of 1 at room temperature (C_6D_{12}, 400 MHz, 298K).

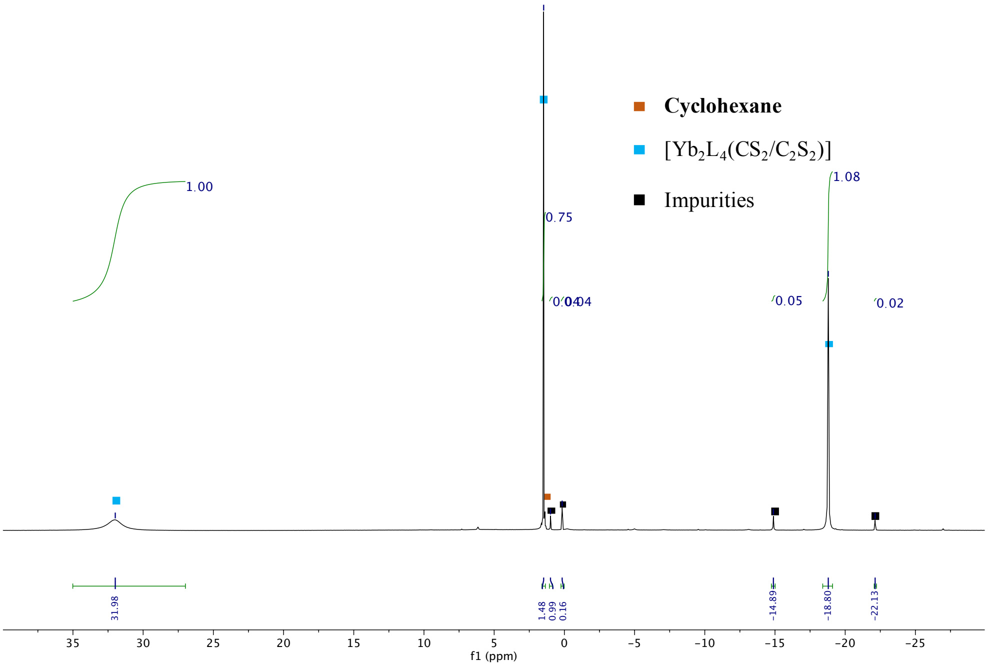

Figure S6: ^{1}H NMR spectrum of 2 / 3 isolated from the reaction mixture after addition of 2 equivalent $^{13}CS_2$ to a cyclohaxane solution of 1 at room temperature (C_6D_{12}, 400 MHz, 298K).

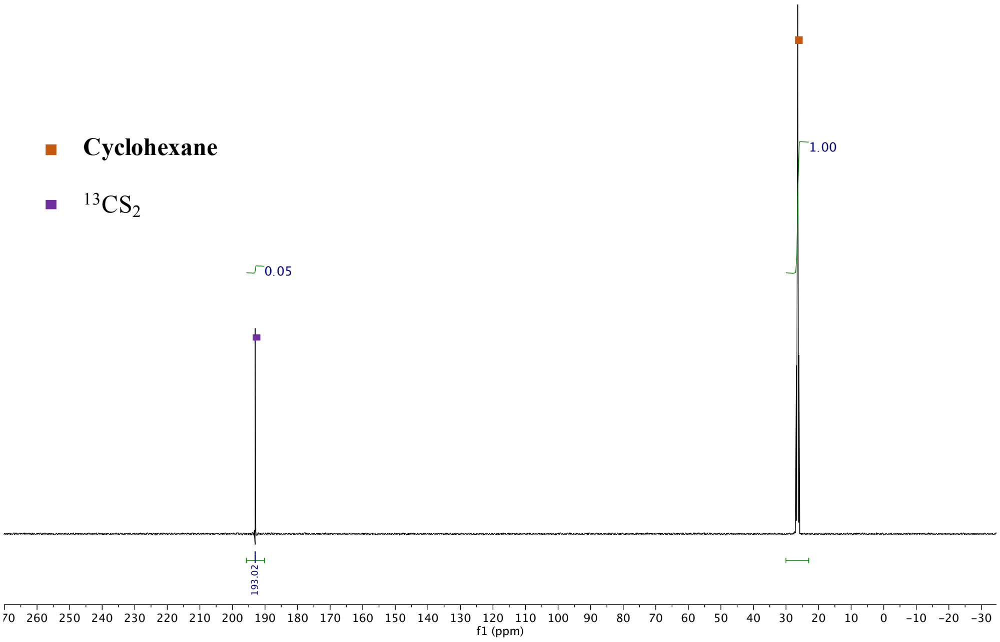

Figure S7: ^{13}C NMR spectrum of the reaction mixture after addition of 1 equivalent $^{13}CS_2$ to a cyclohexane solution of 1 at room temperature (C_6D_{12}, 400 MHz, 298K).

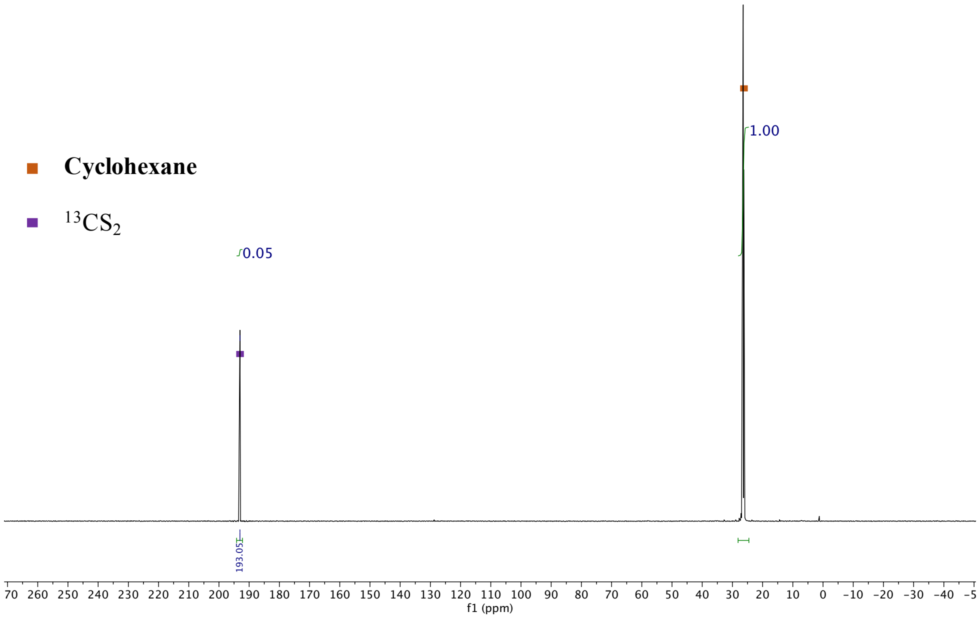

Figure S8: ^{13}C NMR spectrum of the reaction mixture after addition of 2 equivalents $^{13}CS_2$ to a cyclohexane solution of 1 at room temperature (C_6D_{12}, 400 MHz, 298K).

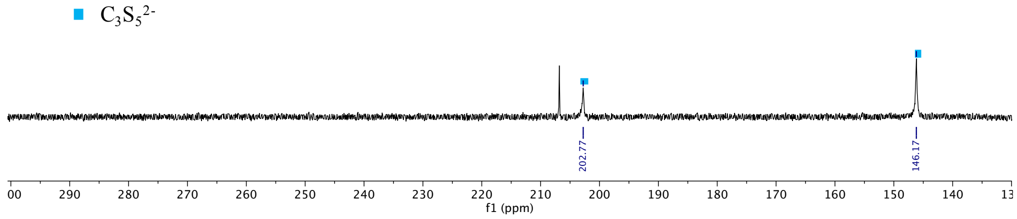

Figure S9: ^{13}C NMR spectrum of 4 (DMSO-d$_6$, 400 MHz, 298K).

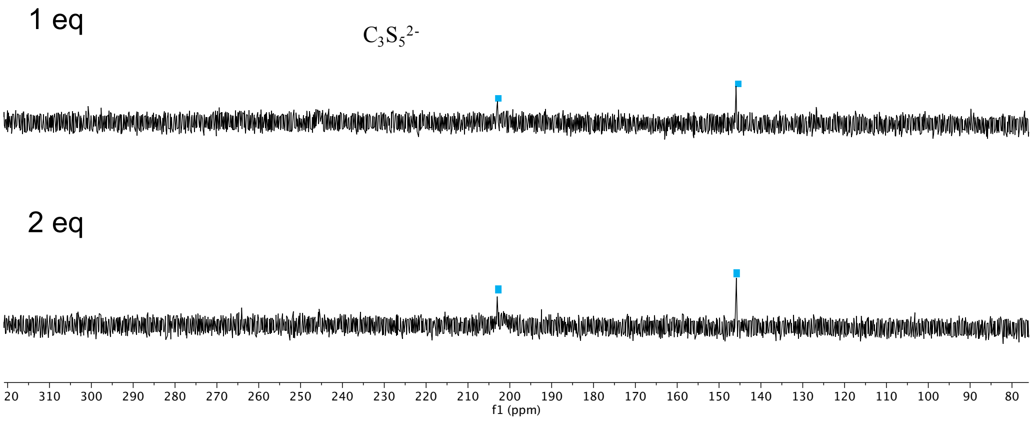

Figure S10: ^{13}C NMR spectrum of the reaction mixture after addition of 1 or 2 equivalents ^{13}CS$_2$ to a cyclohexane solution of 1 at room temperature, removal of the solvent and dissolution in DMSO-d$_6$. (C$_6$D$_{12}$, 400 MHz, 298K).

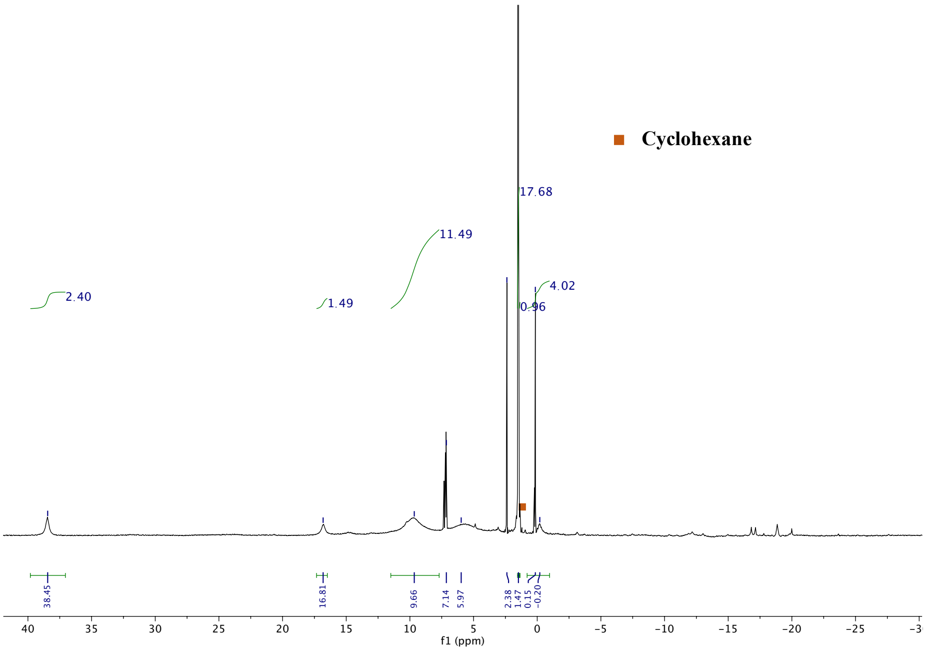

Figure S11: ^{1}H NMR spectrum of the reaction mixture after addition of 1/8 equivalent S$_8$ to a cyclohexane solution of 1 at room temperature (C$_6$D$_{12}$, 400 MHz, 298K).

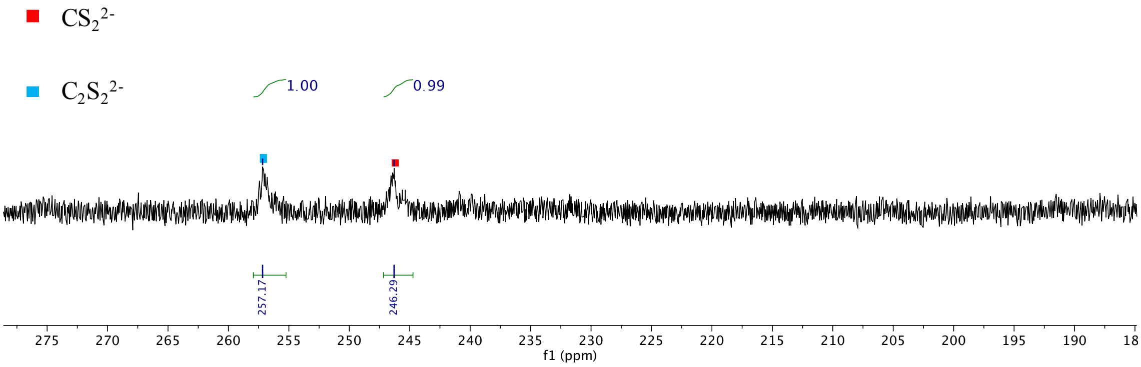

Figure S12: Quantitative ^{13}C NMR spectrum after the removal of the solvent of the reaction mixture after addition of 1 equivalent $^{13}CS_2$ to a cyclohexane solution of 1 at room temperature and addition of 2 equivalents pyHCl (DMSO-d6, 600 MHz, 298K).

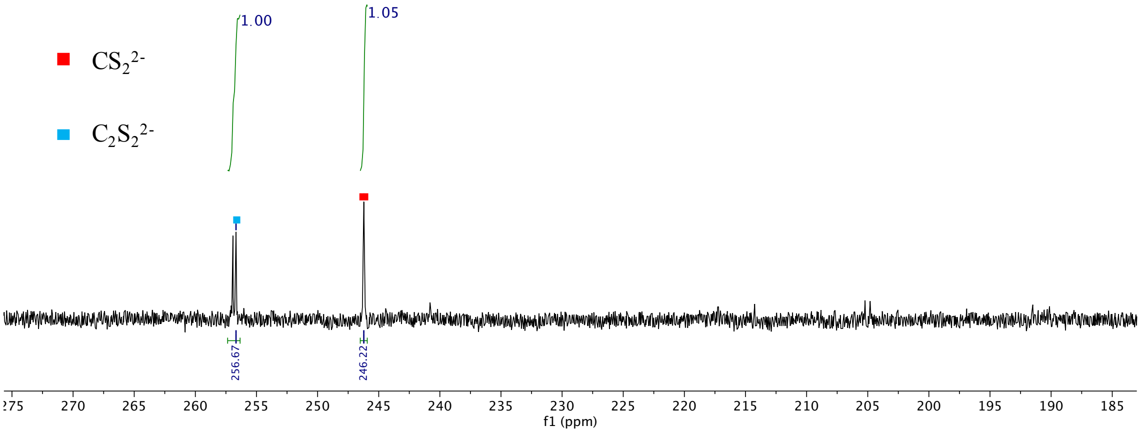

Figure S13: Quantitative ^{13}C NMR spectrum after the removal of the solvent of the reaction mixture after addition of 2 equivalents $^{13}CS_2$ to a cyclohexane solution of 1 at room temperature and addition of 2 equivalents pyHCl (DMSO-d6, 600 MHz, 298K).The presence of two signals for the $C_2S_2^{2-}$ is probably due to the presence of two different isomeric forms.[4]

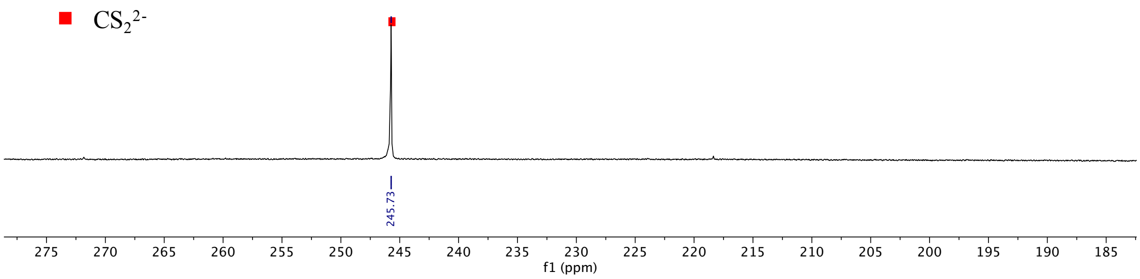

Figure S14: ^{13}C NMR spectrum after addition of 2 equivalents pyHCl to a hexane solution of $[U_2L_6(CS_2)]$ and removal of the solvent (DMSO-d6 600 MHz, 298K).

X-ray Crystals Structure Determination Details

The diffraction data (except compound **2 / 3 (0.24/0.76)**) were measured at low temperature using Cu Ka radiation on a Rigaku SuperNova dual system in combination with Atlas type CCD detector. The data reduction was carried out by *CrysAlis^{Pro}*.[1] The data for crystal structure **2 / 3 (0.24/0.76)** was collected at 100 K using Mo Ka radiation on a Bruker APEX II CCD diffractometer equipped with a kappa geometry goniometer. The dataset was reduced by *EvalCCD*[2] and then corrected for absorption.[3]

The solutions and refinements were performed by SHELXT[4[and SHELXL[5], respectively. The crystal structures were refined using full-matrix least-squares based on F^2 with all non-hydrogen atoms anisotropically defined. Hydrogen atoms were placed in calculated positions by means of the “riding” model. Restraints and constraints were employed during the last stages of refinement of all structures due to the partial disorder. More in details, all **2 / 3** structures display one disordered t-butyl moiety (treated by similarity restraints in order to obtain acceptable geometry and thermal parameters); concerning the CS_2/C_2S_2 disordered anionic ligand, the C-S bond distances and the atomic displacement parameters of the C_2S_2 moiety were restrained to be equal (SADI and SIMU cards). CCDC numbers CCDC 1898685-1898690 for compounds **1** (1898685), **4**, (1898689), **3** (1898686), **crystal 2 / 3 (0.18 / 0.82)**, (1898687), **2 / 3 (0.14 / 0.86)** (1898688), **2 / 3 (0.24 / 0.76)** (1898690) contain the supplementary crystallographic data for this paper. These data can be obtained, free of charge, from The Cambridge Crystallographic Data Centre via www.ccdc.cam.ac.uk/structures.

Table S1: Crystallographic parameters for complexes 1, 4, 2/3 (0.14/0.86).

Compound	**$[Yb_2L_4].n\text{-}C_6H_{14}$, 1**	**$[Yb_2L_4(C_3S_5)]$ $.C_6H_{12}$, 4**	**$[Yb_2L_4(C_2S_2)]$, 2 / $[Yb_2L_4(CS_2)]$, 3**

Ratio	-	**-**	**2/3 (0.14 / 0.86)**
Formula	$C_{54}H_{122}O_{16}Si_4Yb_2$	$C_{57}H_{120}O_{16}S_5Si_4Yb_2$	$C_{49.14}H_{108}O_{16}S_2Si_4Yb_2$
Crystal size [mm]	0.22×0.18×0.12	0.21×0.19×0.10	0.13x0.06x0.04
Crystal system	Triclinic	Monoclinic	Monoclinic
Space group	$P\bar{1}$	$P2_1/c$	$P2_1/c$
V [Å^3]	3644.8(2)	7761.4(4)	6955.33(9)
a [Å]	13.9469(4)	16.2710(4)	27.74553(19)
b [Å]	14.4053(5)	25.2339(7)	13.62376(10)
c [Å]	18.1683(6)	19.1874(5)	18.40448(13)
α [°]	92.280(3)	90	90
β [°]	91.313(3)	99.870(2)	91.2031(7)
γ [°]	91.620(3)	90	90
Z	2	4	4
Absorption coefficient [mm^{-1}]	5.689	2.646	6.501
F(000)	1540	3464	3035
T(K)	100.01(10)	140.00(10)	140.00(10)
Total no. reflections	27361	32193	51649
Unique reflections [R$_{int}$]	14592 [0.0314]	32193 [?]	14360 [0.0232]
Final R$_1$ [I>2 σ(I)]	0.0389	0.0316	0.0319
Largest diff. peak and hole [eA^{-3}]	2.421 and -1.794	2.042 and -1.197	1.812 and -1.035
GOOF	1.038	0.922	1.159

Table S 2: Crystallographic parameters for complexes 2/3 (0.18/0.82), 2/3 (0.24/0.76) and 3.

Compound	**[$Yb_2L_4(C_2S_2)$], 2 / [$Yb_2L_4(CS_2)$], 3**	**[$Yb_2L_4(C_2S_2)$], 2 / [$Yb_2L_4(CS_2)$], 3**	**[$Yb_2L_4(CS_2)$], 3**

Ratio	**2/3 (0.18 / 0.82)**	**2/3 (0.24 / 0.76)**	**-**
Formula	$C_{49.18}H_{108}O_{16}S_2Si_4Yb_2$	$C_{49.24}H_{108}O_{16}S_2Si_4Yb_2$	$C_{49}H_{108}O_{16}S_2Si_4Yb_2$
Crystal size [mm]	0.16×0.04×0.02	0.47×0.26×0.24	0.09×0.04×0.03
Crystal system	Monoclinic	Monoclinic	Monoclinic
Space group	$P2_1/c$	$P2_1/c$	$P2_1/c$
V [Å^3]	6963.66(18)	6990.8(16)	6941.3(11)
a [Å]	27.7601(4)	27.745(3)	27.745(3)
b [Å]	13.6224(2)	13.6746(14)	13.6000(11)
c [Å]	18.4185(3)	18.430(3)	18.3986(19)
α [°]	90	90	90
β [°]	91.1727(14)	91.290(9)	91.054(9)
γ [°]	90	90	90
Z	4	4	4
Absorption coefficient [mm^{-1}]	6.501	2.841	6.521
F(000)	3036	3038	3032
T(K)	140.00(10)	100(2)	140.00(10)
Total no. reflections	28930	103029	29890
Unique reflections [R_{int}]	14134 [0.0282]	20224 [0.0421]	14047 [0.1749]
Final R_1 [I>2 σ(I)]	0.0323	0.0436	0.0843
Largest diff. peak and hole [eA^{-3}]	0.784 and -1.299	3.238 and -1.594	1.458 and -2.968
GOOF	1.044	1.263	0.762

Computational Details

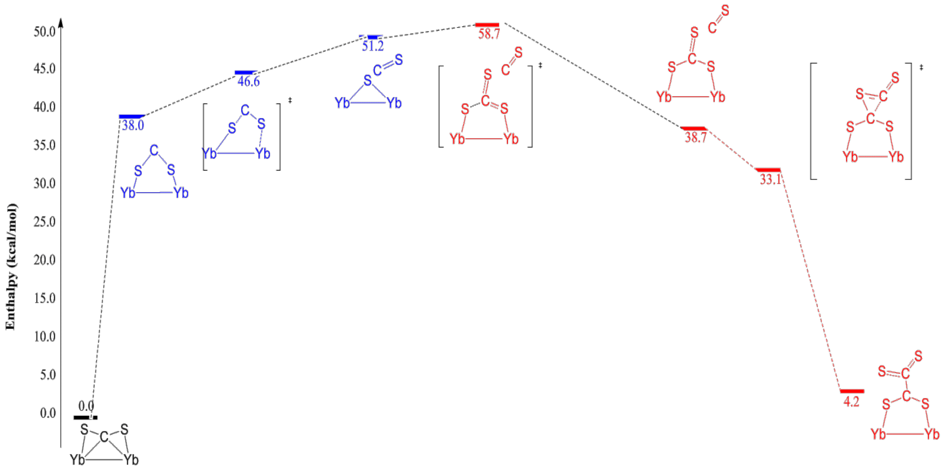

Figure S15. Computed enthalpy profile for the CS bond breaking of CS_2 and the formation of carbonate and oxalate.

Calculations were performed with the GAUSSIAN 09 suite of programs. [6] Density Functional Theory (DFT) was applied by the mean of the B3PW91 hybrid functional.[7] Following our previous work, two kinds of relativistic effective core potential (RECPs) have been used to describe the lanthanide centre: small-core Stuttgart-Dresden RECP[8] (which includes 1*s*, 2*s*, 2*p*, 3*s*, 3*p* and 3*d* electrons) and large-core Stuttgart-Dresden RECP[9] (which includes, in addition, 4*s*, 4*p*, 4*d* and 4*f* electrons), depending on the size of the system. The large-core RECP was chosen according to the formal oxidation state of the lanthanide. The RECPs were used in combination with their optimized valence basis sets supplemented by an f polarization function for the large-core RECP. The Stuttgart-Dresden relativistic effective core potential SDD[10] was employed for silicon centres in association with its valence basis set and a d polarization function, while the 6-31G(d) basis set was used for all other atoms.[11] Geometry optimizations were performed on the whole system and without any symmetry constraints. All stationary points have been identified for the minimum (number of imaginary frequencies, Nimag = 0). The NBO analysis[12] was carried out on the optimized structures using the module included in the Gaussian package and the Chemcraft graphical program was used for the 3D representations of the structures and the orbital plots.[13]

References

1 *CrysAlis*^{Pro}, Rigaku Oxford Diffraction, release 1.171.39.46, 2018.

2 A. J. M. Duisenberg, L. M. J. Kroon-Batenburg, A. M. M. Schreurs, *J. Appl. Crystallogr.* **2003**, *36*, 220-229.

3 R. H. Blessing, *Acta Crystallogr.*, *Sect. A* **1995**, *51*, 33-38.

4 *SHELXT* - Integrated space-group and crystal-structure determination¸ G. M. Sheldrick**,** *Acta Crystallogr.*, *Sect. A* **2015**, *71*, 3-8.

5 *SHELXL* - Crystal structure refinement, G. M. Sheldrick**,** *Acta Crystallogr.*, *Sect. C* **2015**, *71*, 3-8.

6 Frisch, M. J.; Trucks, G. W.; Schlegel, H. B.; Scuseria, G. E.; Robb, M. A.; Cheeseman, J. R.; Montgomery, J. A., Jr.; Vreven, T.; Kudin, K. N.; Burant, J. C.; Millam, J. M.; Iyengar, S. S.; Tomasi, J.; Barone, V.; Mennucci, B.; Cossi, M.; Scalmani, G.; Rega, N.; Petersson, G. A.; Nakatsuji, H.; Hada, M.; Ehara, M.; Toyota, K.; Fukuda, R.; Hasegawa, J.; Ishida, M.; Nakajima, T.; Honda, Y.; Kitao, O.; Nakai, H.; Klene, M.; Li, X.; Knox, J. E.; Hratchian, H. P.; Cross, J. B.; Bakken, V.; Adamo, C.; Jaramillo, J.; Gomperts, R.; Stratmann, R. E.; Yazyev, O.; Austin, A. J.; Cammi, R.; Pomelli, C.; Ochterski, J. W.; Ayala, P. Y.; Morokuma, K.; Voth, G. A.; Salvador, P.; Dannenberg, J. J.; Zakrzewski, V. G.; Dapprich, S.; Daniels, A. D.; Strain, M. C.; Farkas, O.; Malick, D. K.; Rabuck, A. D.; Raghavachari, K.; Foresman, J. B.; Ortiz, J. V.; Cui, Q.; Baboul, A. G.; Clifford, S.; Cioslowski, J.; Stefanov, B. B.; Liu, G.; Liashenko, A.; Piskorz, P.; Komaromi, I.; Martin, R. L.; Fox, D. J.; Keith, T.; Al-Laham, M. A.; Peng, C. Y.; Nanayakkara, A.; Challacombe, M.; Gill, P. M. W.; Johnson, B.; Chen, W.; Wong, M. W.; Gonzalez, C.; Pople, J. A. Gaussian 03, Revision E.01; Gaussian, Inc.: Wallingford, CT, **2004**.

7 Becke, A. D. *J. Chem. Phys.* **1993**, 98, 5648–5662; Perdew, J. P.; Wang, Y. *Phys. Rev. B* **1992**, *45*, 13244–13249.

8 Dolg, M.; Stoll, H.; Preuss, H. *J. Chem. Phys.* **1989**, *90*, 1730–1734; Cao, X.; Dolg, M. *J. Chem. Phys.* **2001**, *115*, 7348–7355.

9 Dolg, M.; Stoll, H.; Savin, A.; Preuss, H. *Theor. Chim. Acta* **1989**, *75*, 173–194; Dolg, M.; Stoll, H.; Preuss, H. *Theor. Chim. Acta* **1993**, *85*, 441–450.

10 Bergner, A.; Dolg, M.; Kuechle, W.; Stoll, H.; Preuss, H. *Mol. Phys.* **1993**, *80*, 1431–1441.

11 W. J. Hehre, R. Ditchfield, J. A. Pople *J. Chem. Phys*. **56,** 2257–2261 (1972); P. C. Hariharan and J. A. Pople *Theor. Chim. Acta* **28**, 213–222 (1973).

12 A. E. Reed, L. A. Curtiss, F. Weinhold, *Chem. Rev.* **88**, 899–926 (1988).

13 G. A. Zhurko, *Home Page: a set of graphical tools for facilitating working with quantum chemistry computations (*http://www.chemcraftprog.com).

Appendix chapter 7

NMR spectroscopic data

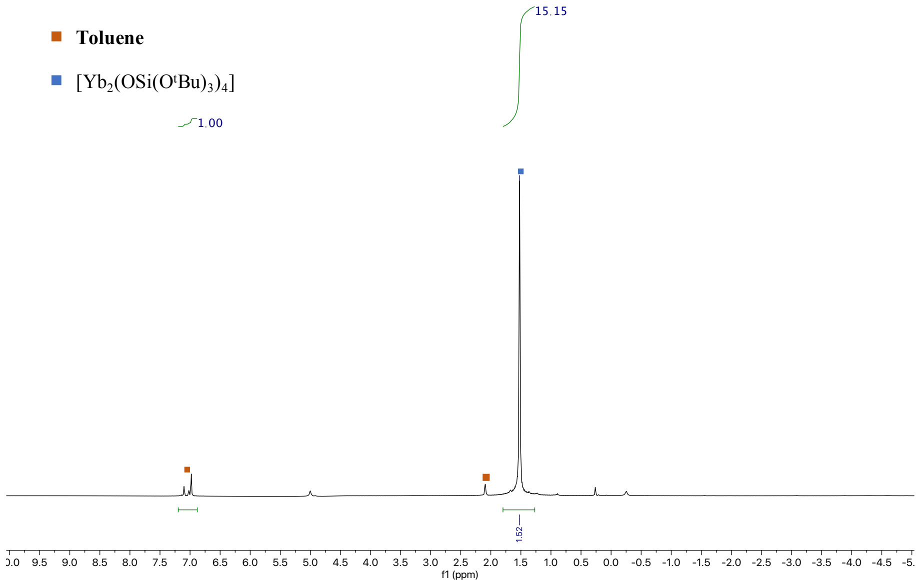

Figure S1. ^{1}H NMR spectrum of **1-Yb** (THF-d8, 400 MHz, 298K) immediately after the dissolution in THF-d8.

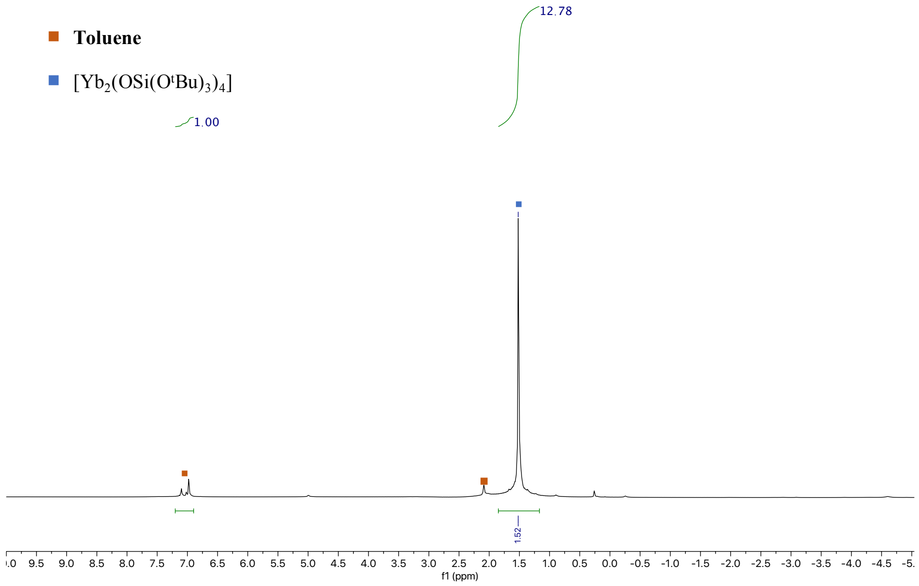

Figure S2. ^{1}H NMR spectrum of **1-Yb** (THF-d8, 400 MHz, 298K) after 5 days at room temperature in THF-d8.

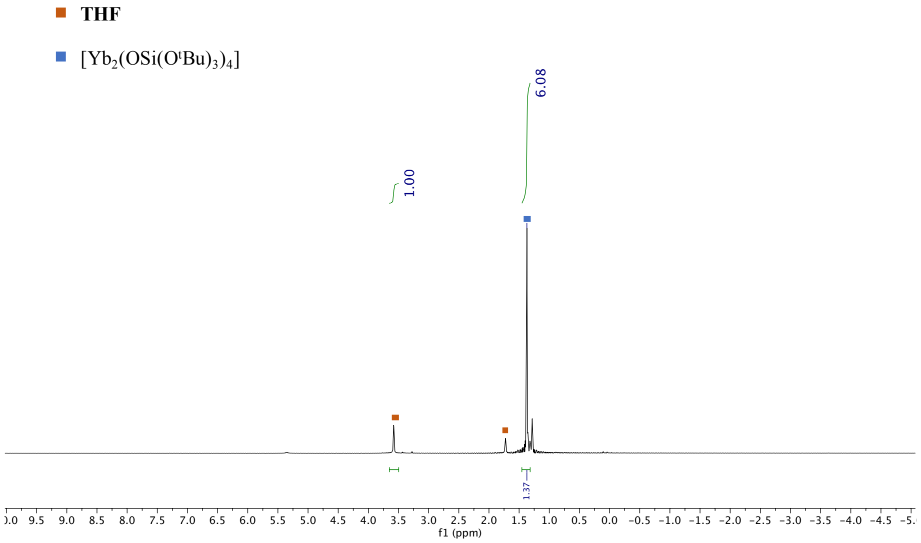

Figure S3. ^{1}H NMR spectrum of **1-Yb** (THF-d8, 400 MHz, 298K) immediately after the dissolution in THF-d8.

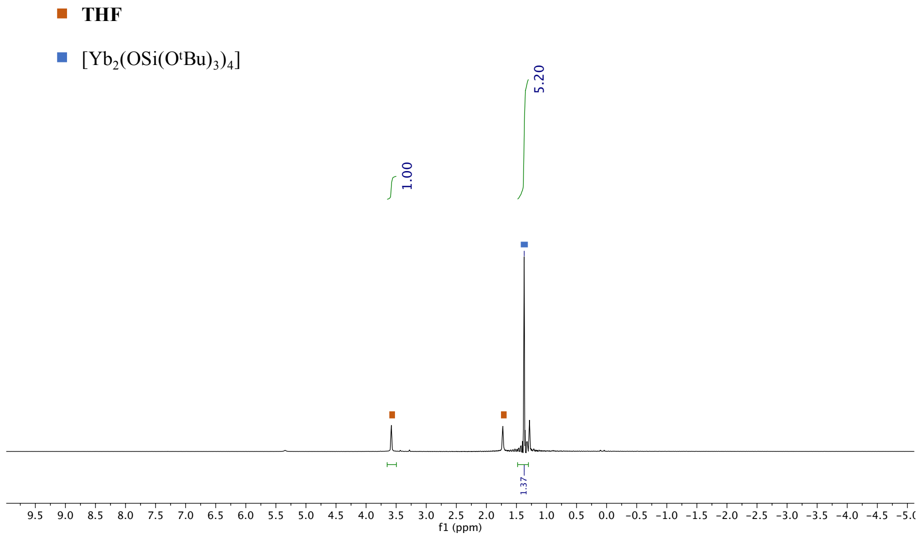

Figure S4. ^{1}H NMR spectrum of **1-Yb** (THF-d8, 400 MHz, 298K) after 5 days at room temperature in THF-d8.

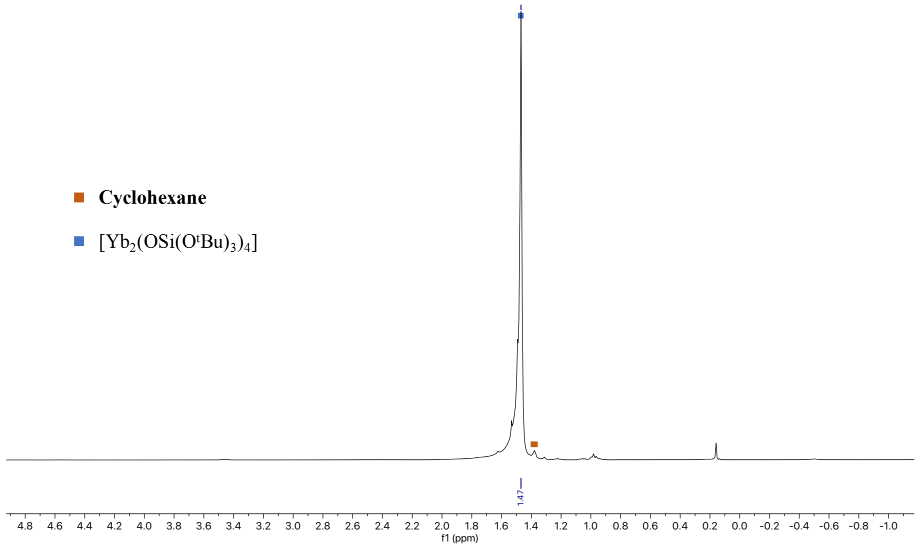

Figure S5. ^{1}H NMR spectrum of **1-Yb** (C_6D_{12}, 400 MHz, 298K).

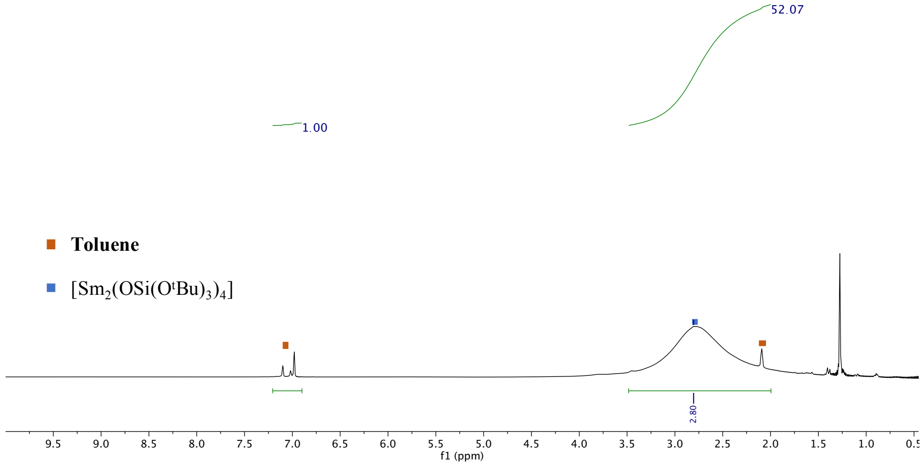

Figure S6. ^{1}H NMR spectrum of **1-Sm** (THF-d8, 400 MHz, 298K) immediately after the dissolution in THF-d8.

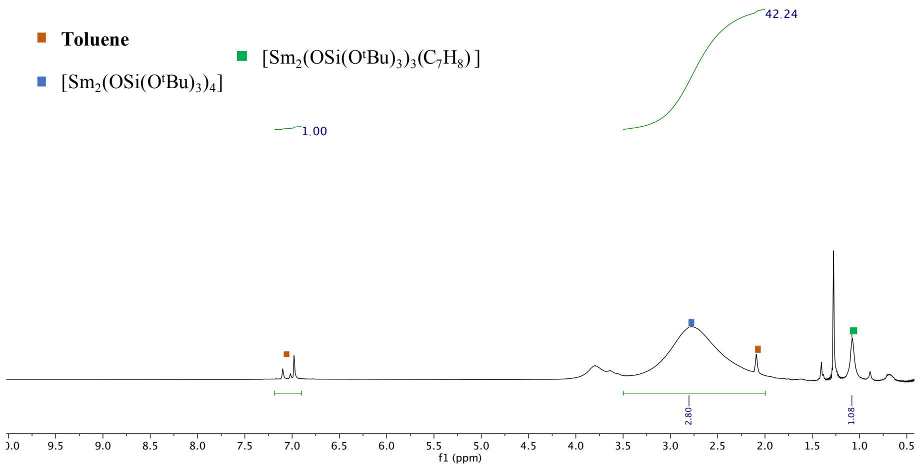

Figure S7. ^{1}H NMR spectrum of **1-Sm** (THF-d8, 400 MHz, 298K) after 5 days at room temperture in THF-d8.

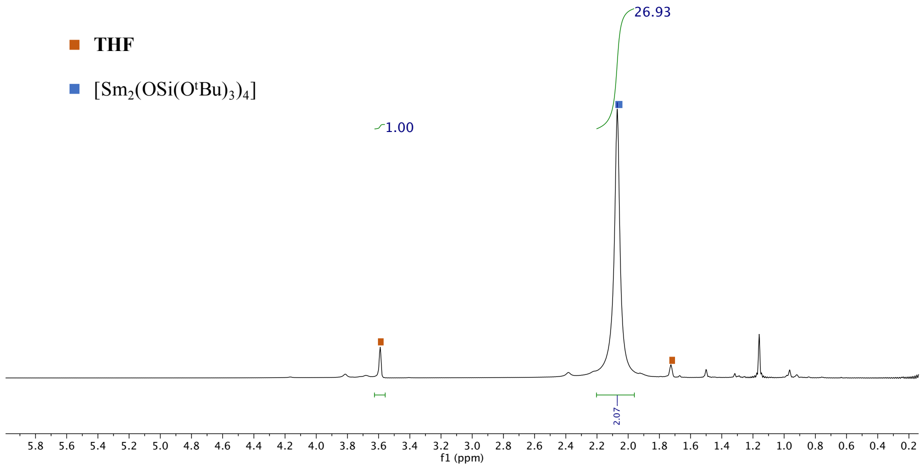

Figure S8. ^{1}H NMR spectrum of **1-Sm** (THF-d8, 400 MHz, 298K) immediately after the dissolution in THF-d8.

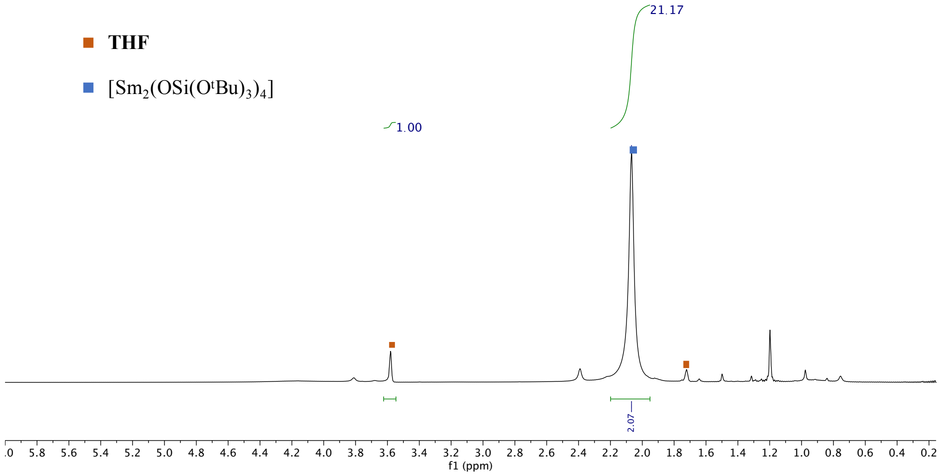

Figure S9. ^{1}H NMR spectrum of **1-Sm** (THF-d8, 400 MHz, 298K) after 5 days at room temperature in THF-d8.

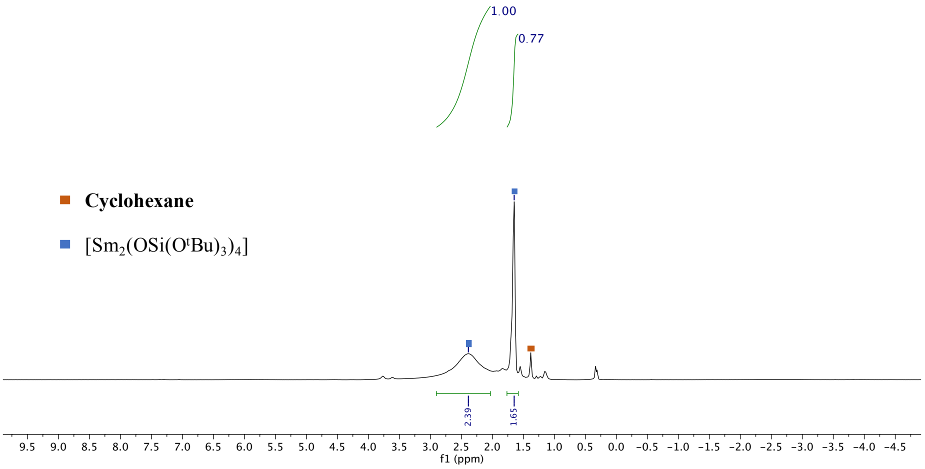

Figure S10. ^{1}H NMR spectrum of **1-Sm** (C_6D_{12}, 400 MHz, 298K).

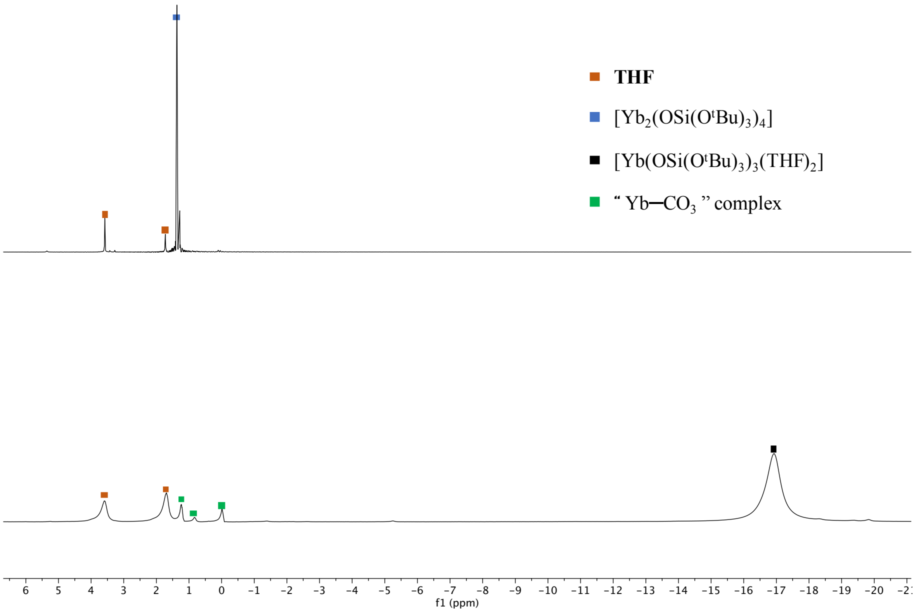

Figure S11. ^{1}H NMR spectrum of the reaction mixture before the addition of 5 equivalents $^{13}CO_2$ to a THF-d8 solution of **1-Yb** at room temperature (above) and 10 days after addition (below) (THF-d8, 400 MHz, 298K).

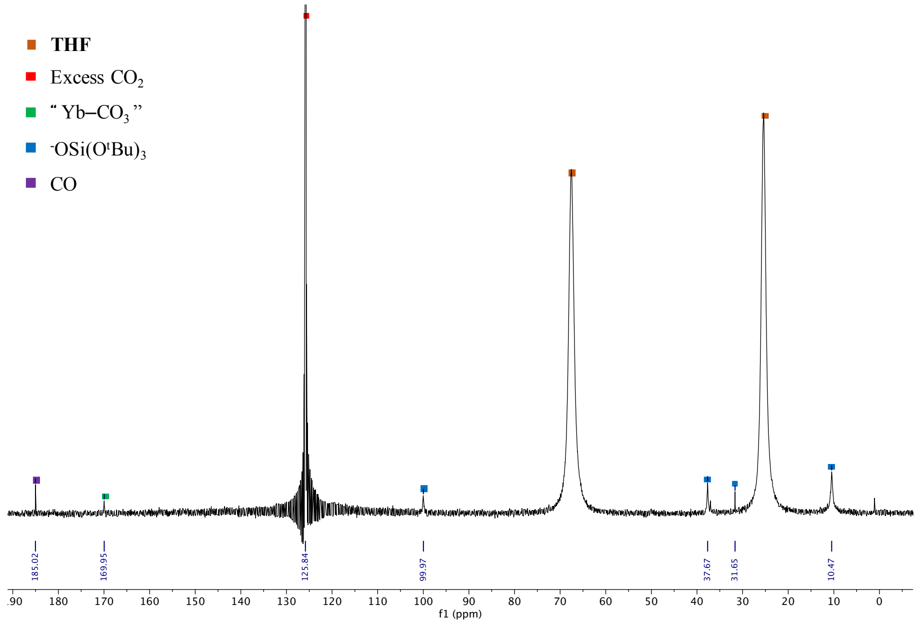

Figure S12. ^{13}C NMR spectrum of the reaction mixture after addition of 5 equivalents ^{13}CO$_2$ to a THF-d8 solution of **1-Yb** at room temperature (THF-d8, 400 MHz, 298K).

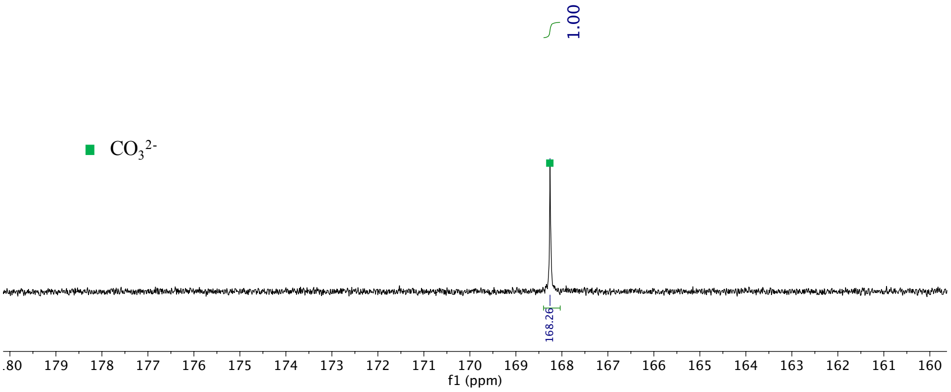

Figure S13. Quantitative ^{13}C NMR spectrum of the reaction mixture after addition of 5 equivalents ^{13}CO$_2$ to a THF-d8 solution of **1-Yb** at room temperature after removal of excess ^{13}CO$_2$ and solvent (D$_2$O, 600 MHz, 298K, pD-13).

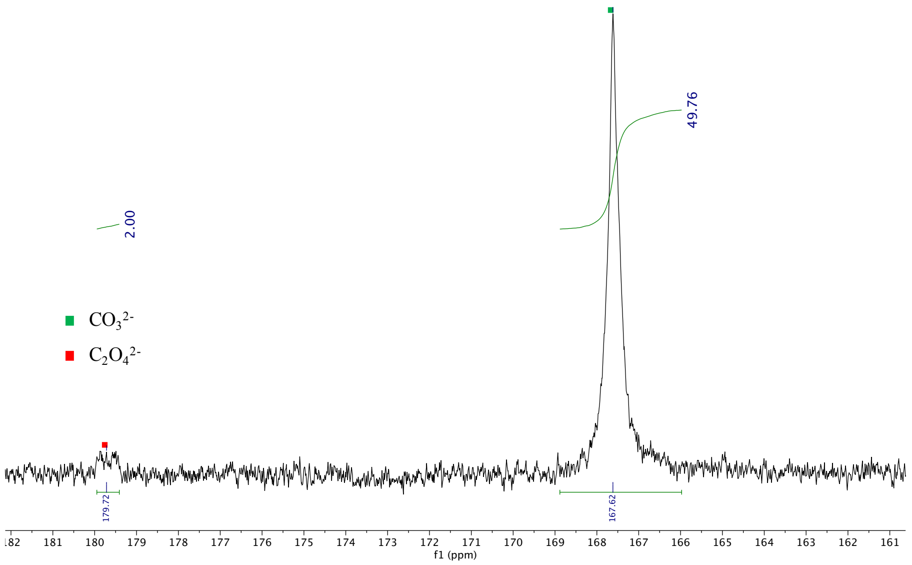

Figure S14. Quantitative ^{13}C NMR spectrum of the reaction mixture after addition of 5 equivalents $^{13}CO_2$ to a C_6D_{12} solution of **1-Yb** at room temperature after removal of excess $^{13}CO_2$ and solvent (D_2O, 600 MHz, 298K, pD-13).

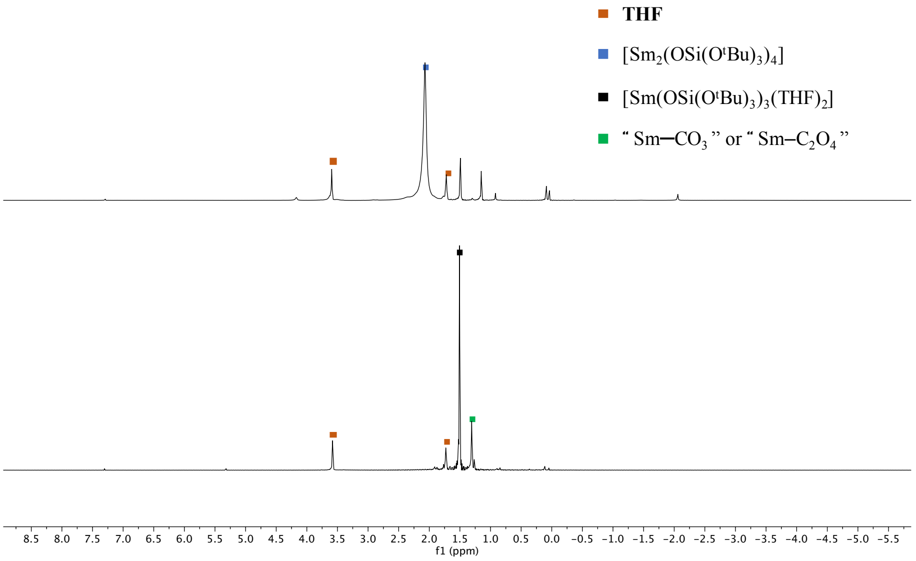

Figure S15. ^{1}H NMR spectrum of the reaction mixture before the addition of 5 equivalents $^{13}CO_2$ to a THF-d8 solution of **1-Sm** at room temperature (above) and 2 days after addition (below) (THF-d8, 400 MHz, 298K).

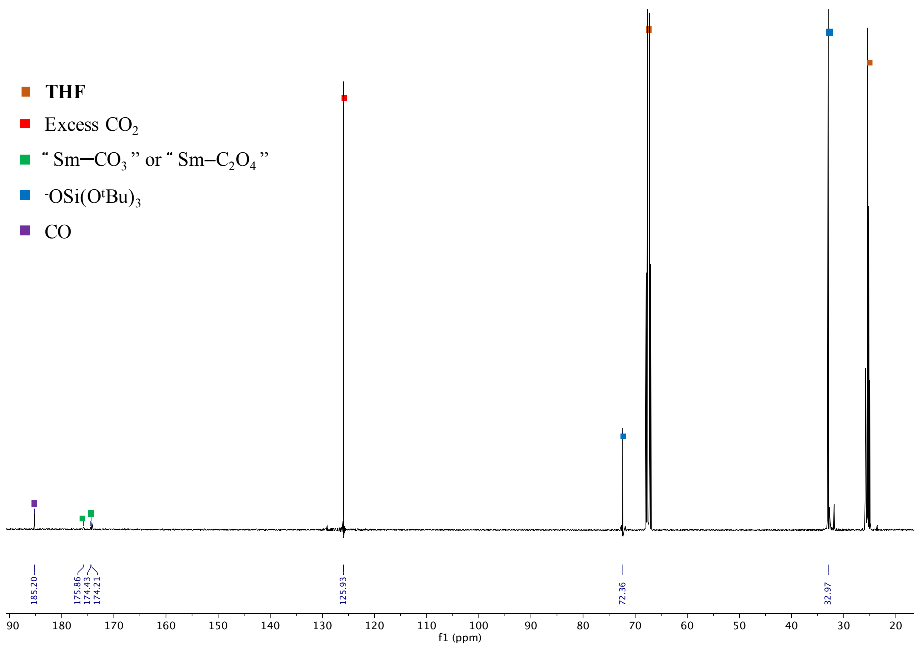

Figure S16. ^{13}C NMR spectrum of the reaction mixture 2 days after addition of 5 equivalents ${}^{13}CO_2$ to a THF-d8 solution of **1-Sm** at room temperature (THF-d8, 400 MHz, 298K).

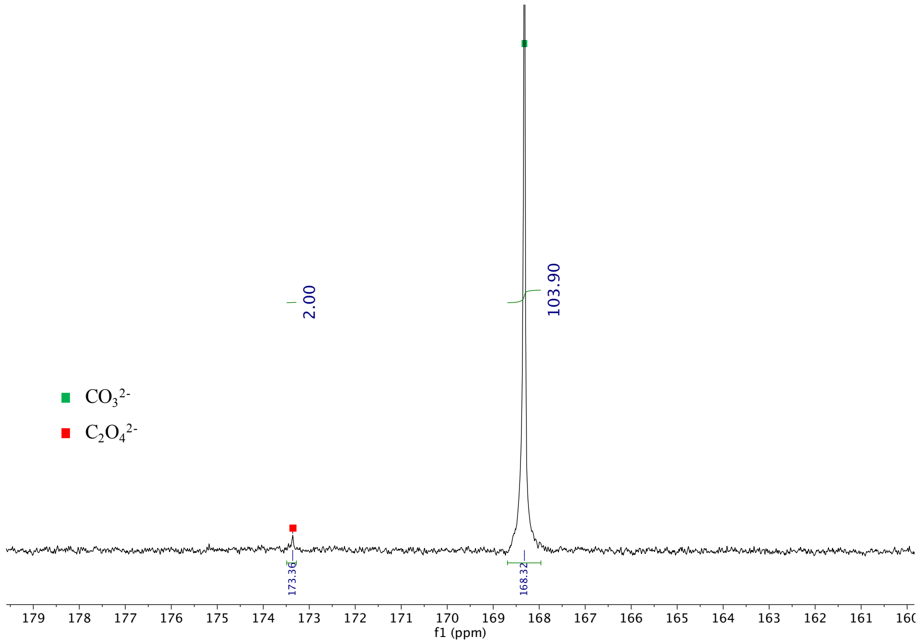

Figure S17. Quantitative ^{13}C NMR spectrum of the reaction mixture after addition of 5 equivalents ${}^{13}CO_2$ to a THF-d8 solution of **1-Sm** at room temperature, after 10 days, after removal of excess ${}^{13}CO_2$ and solvent (D_2O, 600 MHz, 298K, pD-13).

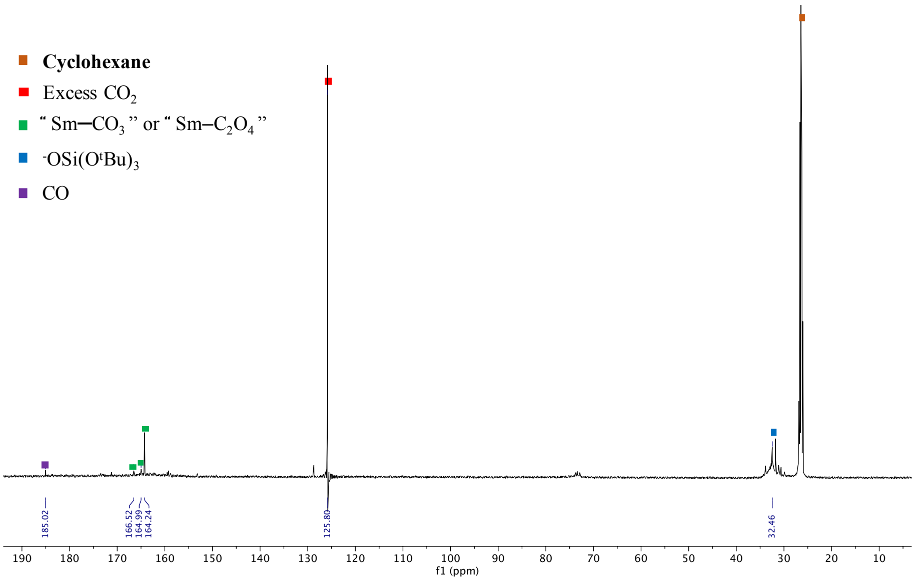

Figure S18. ^{13}C NMR spectrum of the reaction mixture 2 weeks after addition of 5 equivalents $^{13}CO_2$ to a C_6D_{12} solution of **1-Sm** at room temperature (C_6D_{12}, 400 MHz, 298K).

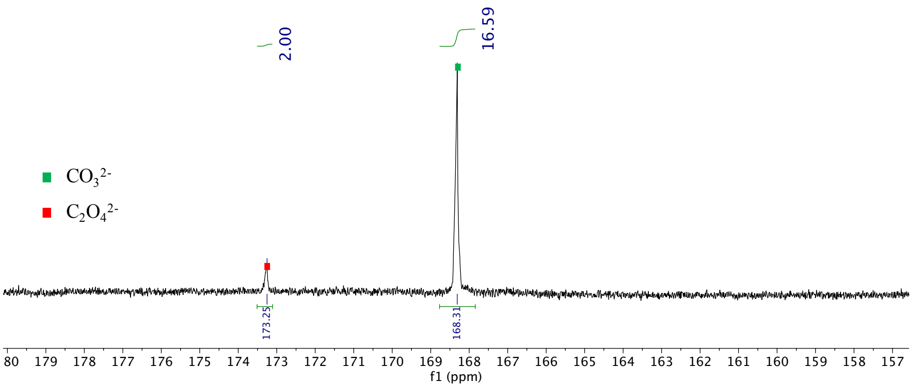

Figure S19. Quantitative ^{13}C NMR spectrum of the reaction mixture after addition of 5 equivalents $^{13}CO_2$ to a C_6D_{12} solution of **1-Sm** at room temperature after removal of excess $^{13}CO_2$ and solvent (D_2O, 600 MHz, 298K, pD-13).

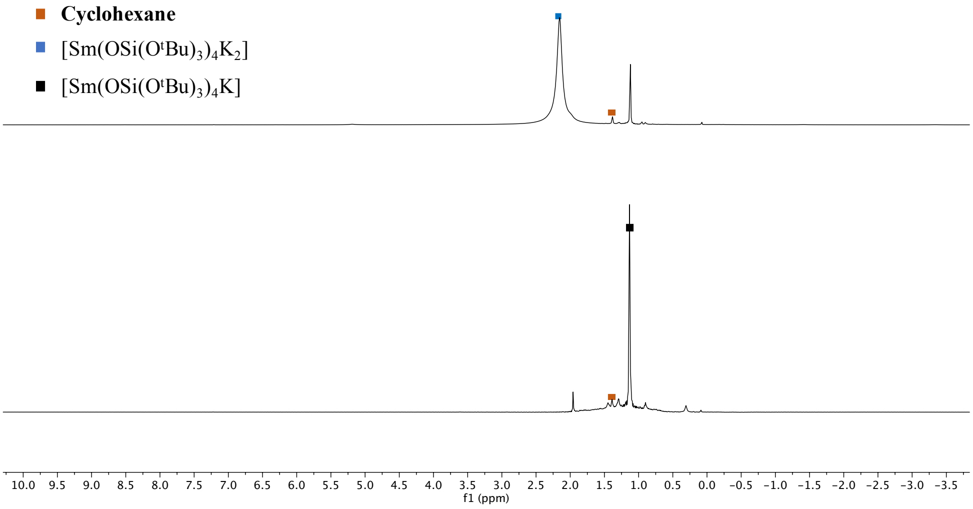

Figure S20. ^{1}H NMR spectrum of the reaction mixture before the addition of 5 equivalents $^{13}CO_2$ to a C_6D_{12} solution of $[SmL_4K_2]$ at room temperature (above) and after addition (below) (C_6D_{12}, 400 MHz, 298K).

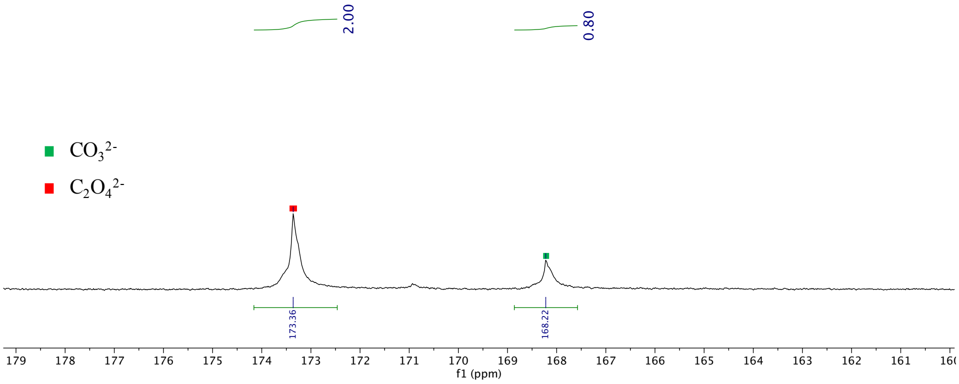

Figure S21. Quantitative ^{13}C NMR spectrum of the reaction mixture after addition of 5 equivalents $^{13}CO_2$ to a C_6D_{12} solution of $[SmL_4K_2]$ at room temperature after removal of excess $^{13}CO_2$ and solvent (D_2O, 600 MHz, 298K, pD-12).

X-ray Crystal Structure Determination Details

Bragg-intensities of **1-Sm, 3** and **4** were collected at low temperature (See Table S1) using Cu$K\alpha$ radiation. A Rigaku SuperNova dual system diffractometer with an Atlas S2 CCD detector was used for compounds **1-Sm** and **4**, and one equipped with an Atlas CCD detector for compound **3**. The datasets were reduced and corrected for absorption, with the help of a set of faces enclosing the crystals as snugly as possible, with CrysAlis$^{\mathrm{Pro}}$.[1]

The X-ray diffraction data of **2** were measured at 120(2) K using Mo$K\alpha$ radiation on a Bruker APEX II CCD kappa diffractometer. The datasets were reduced by EvalCCD[2] and corrected for absorption by modelling an empirical transmission surface as sampled by multiple symmetry-equivalent and/or azimuth rotation-equivalent intensity measurements by real spherical harmonic functions of even order.[3]

The solutions and refinements of the structures were performed by the latest available version of ShelXT[4] and ShelXL.[5] All non-hydrogen atoms were refined anisotropically using full-matrix least-squares based on $|F|^2$, but the hydrogen atoms were placed at calculated positions by means of the "riding" model where each H-atom was assigned a fixed isotropic displacement parameter with a value equal to 1.2 U_{eq} of its parent C-atom (1.5 U_{eq} for the methyl groups). Crystallographic and refinement data are summarized in Table S1. CCDC numbers 1895385-1895388 for compounds **1-Sm** (1895385), **2**, (1895387), **3** (1895386), and **4** (1895388), contain the supplementary crystallographic data for this paper. These data can be obtained, free of charge, from The Cambridge Crystallographic Data Centre via www.ccdc.cam.ac.uk/structures.

In the structure of **3**, a solvent mask was calculated with the help of the solvent-masking program in OLEX2[6] and 55.0 electrons were found in a volume of 483.0 Å^3 in three voids. This is consistent with the presence of one hexane solvent molecule per formula unit which accounts for 50.0 electrons.

In the case of **4**, a calculated solvent mask found 356.0 electrons in a volume of 2524.0 Å^3 in two voids. This is consistent with the presence of two hexane solvent molecules per formula unit which account for 400.0 electrons.

Table S1: Crystallographic parameters for complexes **1**-**4**.

Compound	**[Sm_2L_4] (1-Sm)**	**[Yb_2L_4(μ-OMe)$_2$(DME)$_2$] (2)**	**[$Yb_4L_8(C_2O_4)$] (3)**	**[$Sm_4L_8(CO_3)_2$] (4)**
Formula	$C_{48}H_{108}O_{16}Si_4Sm_2$	$C_{58}H_{134}O_{22}Si_4Yb_2$	$C_{98}H_{216}O_{36}Si_8Yb_4$	$C_{98}H_{216}O_{38}Si_8Sm_4$
Crystal size [mm]	0.38 x 0.29 x 0.25	0.25×0.16×0.07	0.38×0.32×0.28	0.19×0.14×0.07
Crystal system	Triclinic	Triclinic	Triclinic	Monoclinic
Space group	$P\bar{1}$	$P\bar{1}$	$P\bar{1}$	$C2/c$
V [Å^3]	3355.4(4)	2022.8(6)	3600.41(12)	15088.5(16)
a [Å]	12.9099(7)	9.5823(14)	13.1265(2)	34.217(2)
b [Å]	14.0475(9)	14.4327(18)	15.6137(3)	14.6315(7)
c [Å]	20.4106(8)	16.330(3)	18.8708(4)	30.140(2)
α [°]	88.122(4)	64.364(11)	72.6073(17)	90
β [°]	88.122(4)	85.709(14)	80.2421(15)	90.606(6)
γ [°]	65.093(6)	83.694(12)	79.3717(13)	90
Z	2	1	1	4
Absorption coefficient [mm^{-1}]	14.134	2.418	5.768	12.626
F(000)	1408	854	1484	5872
T(K)	100.00(10) K	120(2)	140.01(10)	140.00(10)
Total no. reflections	24633	24632	38077	37370
Unique reflexions [R_{int}]	13518 [0.0548]	7397 [0.0772]	14966 [0.0185]	12866 [0.0919]
Final R_1 [I>2 σ(I)]	0.0661	0.0564	0.0215	0.0729
Largest diff. peak and hole [eA^{-3}]	2.033 and -1.416	0.915 and -0.778	0.596 and -0.796	2.324 and -2.707
GOOF	1.024	1.118	1.049	1.055

Computational details

Calculations were performed with the GAUSSIAN 09 suite of programs.[7] Density Functional Theory (DFT) was applied by the mean of the B3PW91 hybrid functional [8]. Following our previous work, two kinds of relativistic effective core potential (RECPs) have been used to describe the lanthanide centre: small-core Stuttgart-Dresden RECP[9] (which includes 1*s*, 2*s*, 2*p*, 3*s*, 3*p* and 3*d* electrons) and large-core Stuttgart-Dresden RECP[10] (which includes, in addition, 4*s*, 4*p*, 4*d* and 4*f* electrons), depending on the size of the system. The large-core RECP was chosen according to the formal oxidation state of the lanthanide. The RECPs were used in combination with their optimized valence basis sets supplemented by an f polarization function for the large-core RECP. The Stuttgart-Dresden relativistic effective core potential SDD[11] was employed for silicon centres in association with its valence basis set and a d polarization function, while the 6-31G(d) basis set was used for all other atoms.[12] Geometry optimizations were performed on the whole system and without any symmetry constraints. All stationary points have been identified for the minimum (number of imaginary frequencies, Nimag = 0). The NBO analysis[13] was carried out on the optimized structures using the module included in the Gaussian package and the Chemcraft graphical program was used for the 3D representations of the structures and the orbital plots.[14]

References

1 *CrysAlis^{Pro}* Software System, Rigaku Oxford Diffraction, 2015.

2 A. J. M. Duisenberg, L. M. J. Kroon-Batenburg, A. M. M. Schreurs, *J. Appl. Crystallogr.*, 2003, **36**, 220-229.

3 R. H. Blessing, *Acta Cryst.*, 1995, **A51**, 33-38.

4 Sheldrick, G.M., ShelXT-Integrated space-group and crystal-structure determination, *Acta Cryst.*, 2015, **A71**, 3-8.

5 Sheldrick, G.M., Crystal structure refinement with ShelXL, *Acta Cryst.*, 2015, **C71**, 3-8.

6 O.V. Dolomanov, L.J. Bourhis, R.J. Gildea, J.A.K. Howard, H. Puschmann, Olex2: A complete structure solution, refinement and analysis program, *J. Appl. Cryst.*, 2009, **42**, 339-341.

7 Frisch, M. J.; Trucks, G. W.; Schlegel, H. B.; Scuseria, G. E.; Robb, M. A.; Cheeseman, J. R.; Montgomery, J. A., Jr.; Vreven, T.; Kudin, K. N.; Burant, J. C.; Millam, J. M.; Iyengar, S. S.; Tomasi, J.; Barone, V.; Mennucci, B.; Cossi, M.; Scalmani, G.; Rega, N.; Petersson, G. A.; Nakatsuji, H.; Hada, M.; Ehara, M.; Toyota, K.; Fukuda, R.; Hasegawa, J.; Ishida, M.; Nakajima, T.; Honda, Y.; Kitao, O.; Nakai, H.; Klene, M.; Li, X.; Knox, J. E.; Hratchian, H. P.; Cross, J. B.; Bakken, V.; Adamo, C.; Jaramillo, J.; Gomperts, R.; Stratmann, R. E.; Yazyev, O.; Austin, A. J.; Cammi, R.; Pomelli, C.; Ochterski, J. W.; Ayala, P. Y.; Morokuma, K.; Voth, G. A.; Salvador, P.; Dannenberg, J. J.; Zakrzewski, V. G.; Dapprich, S.; Daniels, A. D.; Strain, M. C.; Farkas, O.; Malick, D. K.; Rabuck, A. D.; Raghavachari, K.; Foresman, J. B.; Ortiz, J. V.; Cui, Q.; Baboul, A. G.; Clifford, S.; Cioslowski, J.; Stefanov, B. B.; Liu, G.; Liashenko, A.; Piskorz, P.; Komaromi, I.; Martin, R. L.; Fox, D. J.; Keith, T.; Al-Laham, M. A.; Peng, C. Y.; Nanayakkara, A.; Challacombe, M.; Gill, P. M. W.; Johnson, B.; Chen,

W.; Wong, M. W.; Gonzalez, C.; Pople, J. A. Gaussian 03, Revision E.01; Gaussian, Inc.: Wallingford, CT, **2004**.

8 Becke, A. D. *J. Chem. Phys*. **1993**, 98, 5648–5662; Perdew, J. P.; Wang, Y. *Phys. Rev. B* **1992**, *45*, 13244–13249.

9 Dolg, M.; Stoll, H.; Preuss, H. *J. Chem. Phys.* **1989**, *90*, 1730–1734; Cao, X.; Dolg, M. *J. Chem. Phys.* **2001**, *115*, 7348–7355.

10 Dolg, M.; Stoll, H.; Savin, A.; Preuss, H. *Theor. Chim. Acta* **1989**, *75*, 173–194; Dolg, M.; Stoll, H.; Preuss, H. *Theor. Chim. Acta* **1993**, *85*, 441–450.

11 Bergner, A.; Dolg, M.; Kuechle, W.; Stoll, H.; Preuss, H. *Mol. Phys.* **1993**, *80*, 1431–1441.

12 W. J. Hehre, R. Ditchfield, J. A. Pople *J. Chem. Phys*. **56,** 2257–2261 (1972); P. C. Hariharan and J. A. Pople *Theor. Chim. Acta* **28**, 213–222 (1973).

13 A. E. Reed, L. A. Curtiss, F. Weinhold, *Chem. Rev.* **88**, 899–926 (1988).

14 G. A. Zhurko, *Home Page: a set of graphical tools for facilitating working with quantum chemistry computations (*http://www.chemcraftprog.com).

Appendix chapter 8

Evaluation of water content in DMSO, PhCCH and Cs_2CO_3

The water content in DMSO and PhCCH is easily evaluated using ^1H NMR spectroscopy by integration of the water signal in DMSO-d6. The water signal can be well observed at a concentration of 10 ppm. For the experimental conditions used by us, this corresponds to less than 0.01 equiv of water with respect to the carbonate anion and does not appear to affect the reaction. At a concentration of about 100 ppm (corresponding to 0.1equiv.) the isolated yield is reduced to 80%.

Attention should be payed to the fact that Cs_2CO_3 acts as a drying agent in DMSO so the use of larger amounts of Cs_2CO_3 can prevent reduced yields in not perfectly dried DMSO solvent. The water content in different samples of Cs_2CO_3 dried in different ways was evaluated by elemental analysis conducted under inert atmosphere (Table S1).

Table S1. Evaluation of the water content in commercial Cs_2CO_3. Average values calculated over three measurements.

Entry	Note	Average H % ± σ	Equiv. of water
1	Dried 5 days at 60 °C at 10^{-3} bar	0 ± 0	0
2	Dried one hour at room temperature at 10^{-3} bar	0.1 ± 0.06	0.2 ± 0.1
3	Not dried, stored outside of the glovebox	0.64 ± 0.05	1.1 ± 0.1

NMR spectroscopic data

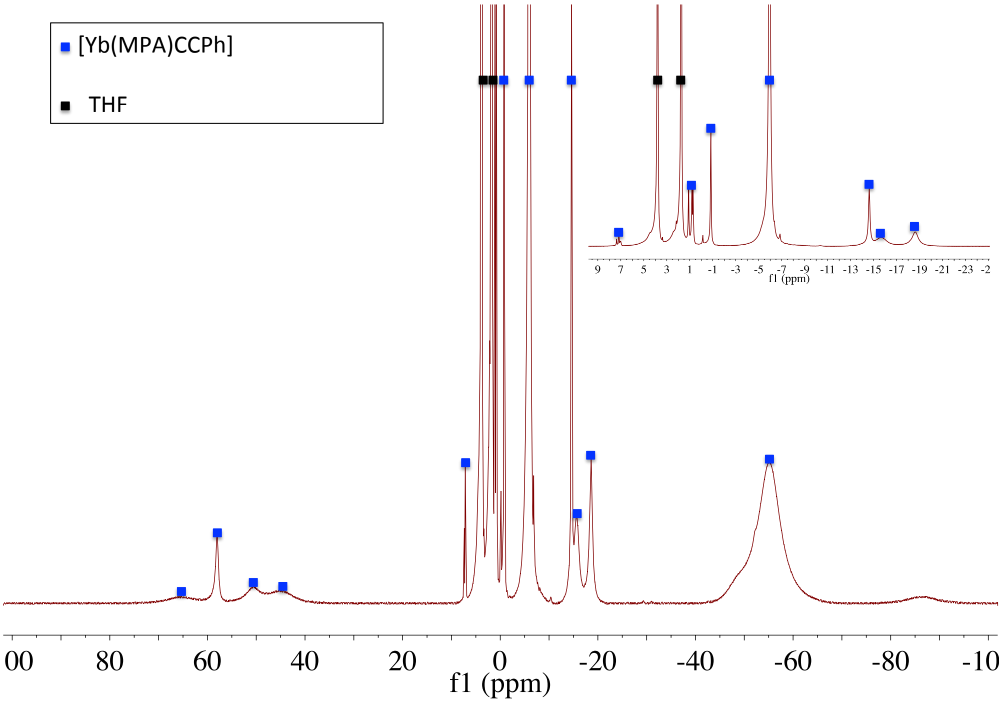

Figure S1. ^{1}H NMR spectrum of the isolated [Yb(MPA)CCPh(THF)] (THF-d8, 400 MHz, 298 K).

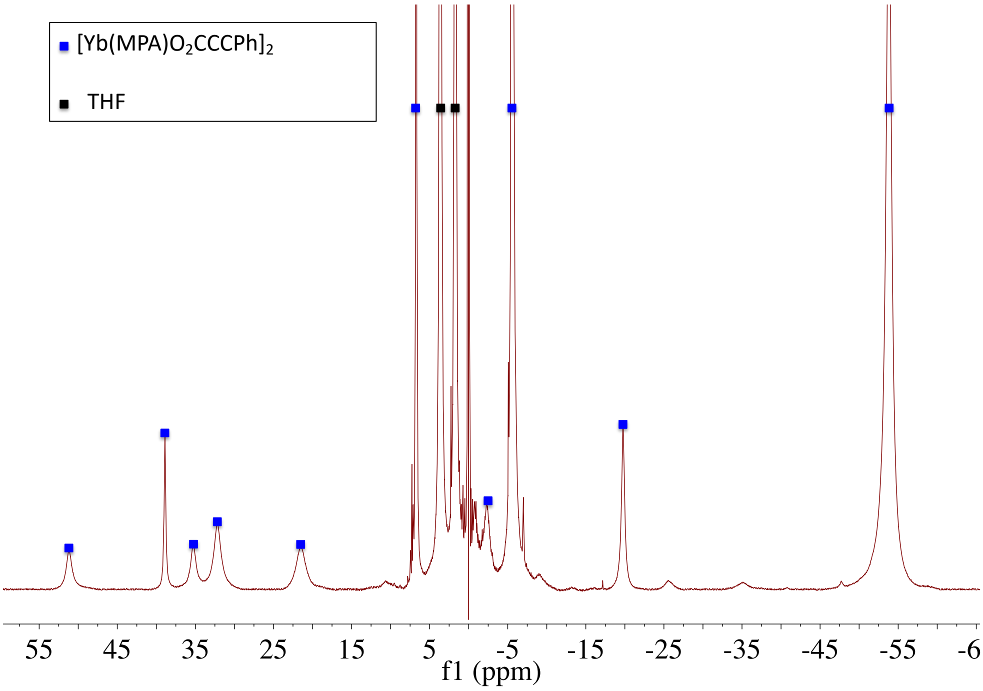

Figure S2. ^{1}H NMR spectrum of the isolated [Yb(MPA)O$_2$CCCPh]$_2$ (THF-d8, 400 MHz, 298 K).

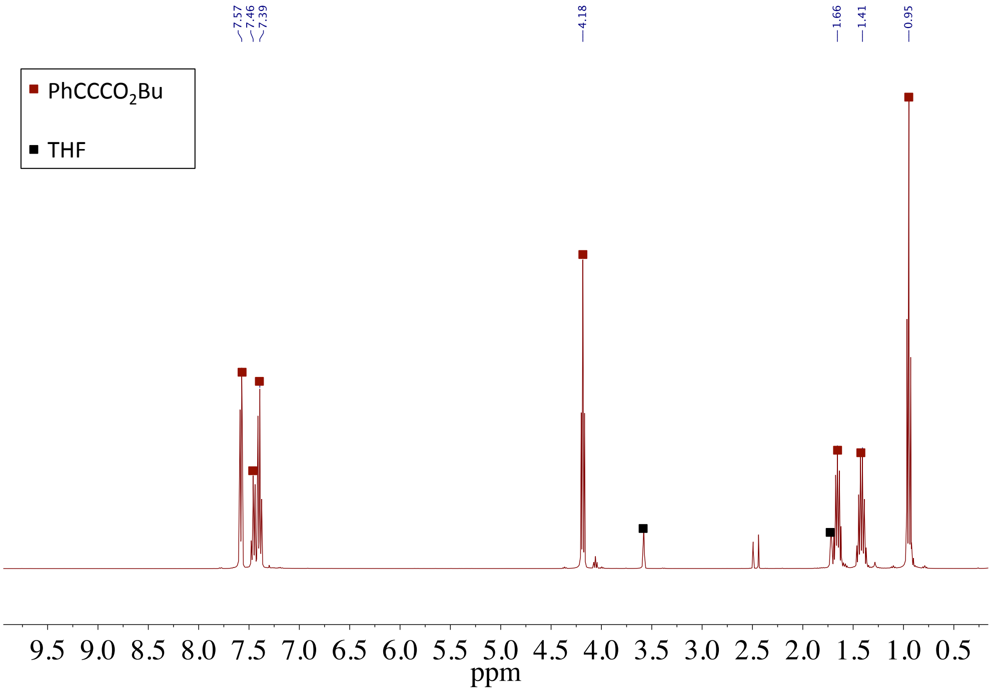

Figure S3. ^{1}H NMR spectrum of the isolated ester PhCCCO$_2$Bu under air (THF-d8, 400 MHz, 298 K).

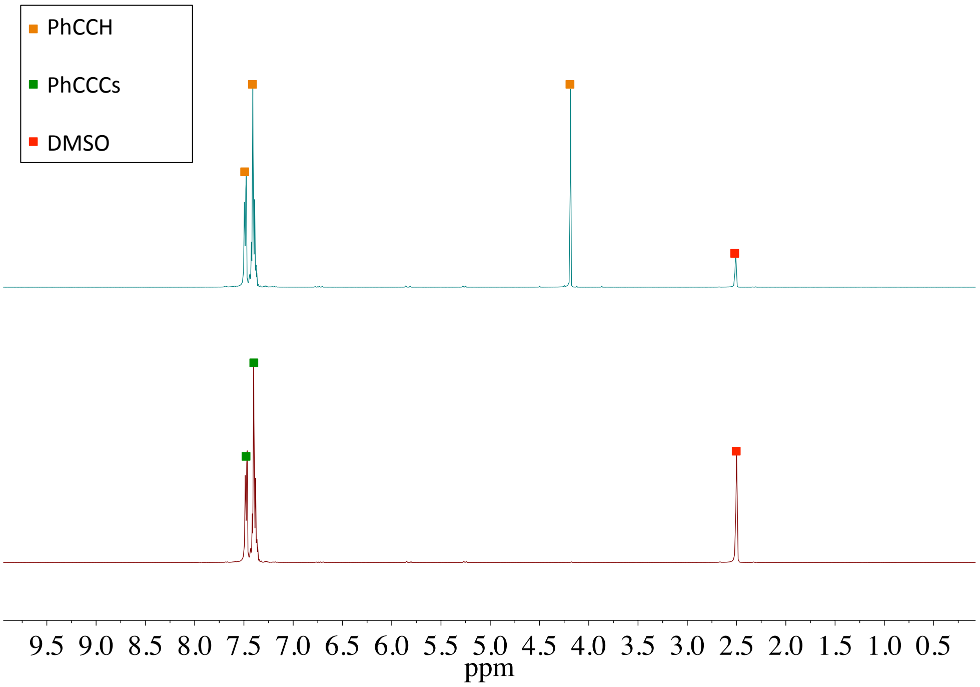

Figure S4. ^{1}H NMR spectra of PhCCH (above) and of the reaction mixture between PhCCH and 1 equiv. Cs$_2$CO$_3$ after one hour at 80 °C under argon (below) (DMSO-d6, 400 MHz, 298 K).

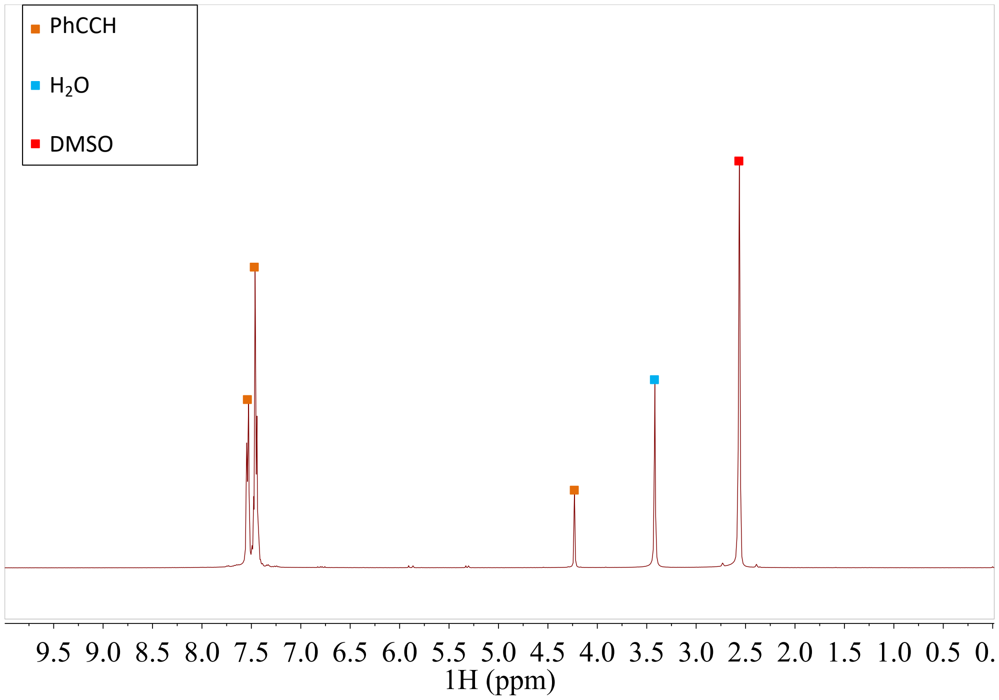

Figure S5 ^{1}H NMR spectra of the reaction mixture between PhCCH and 1 equiv. Cs_2CO_3 in presence of 1 eq of water after one hour at 80 °C under argon (DMSO-d6, 400 MHz, 298 K).

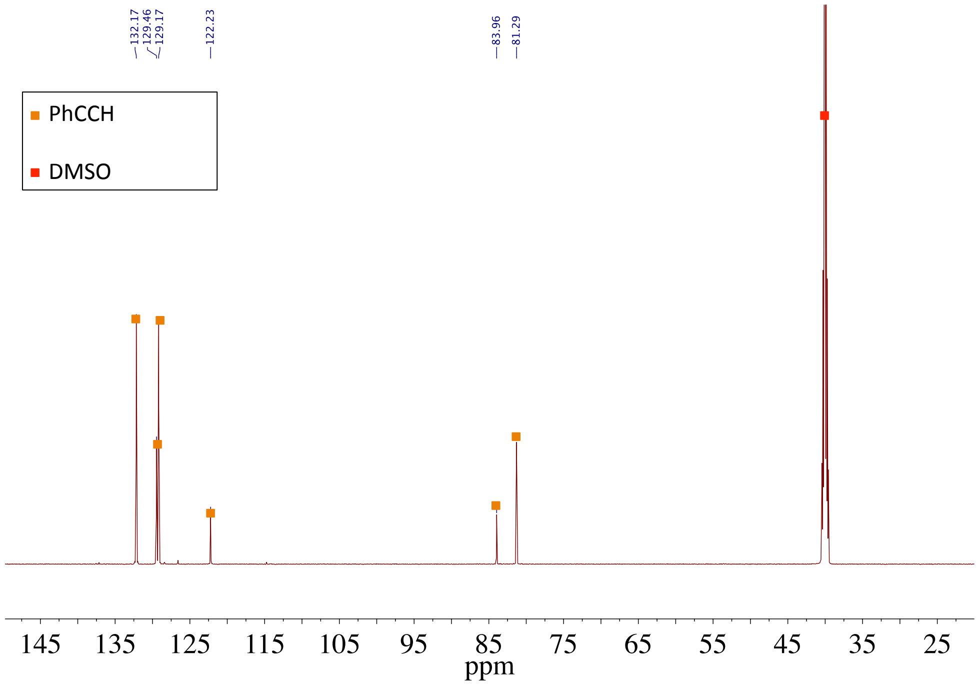

Figure S6. ^{13}C NMR spectrum of PhCCH under argon (DMSO-d6, 800 MHz, 298 K).

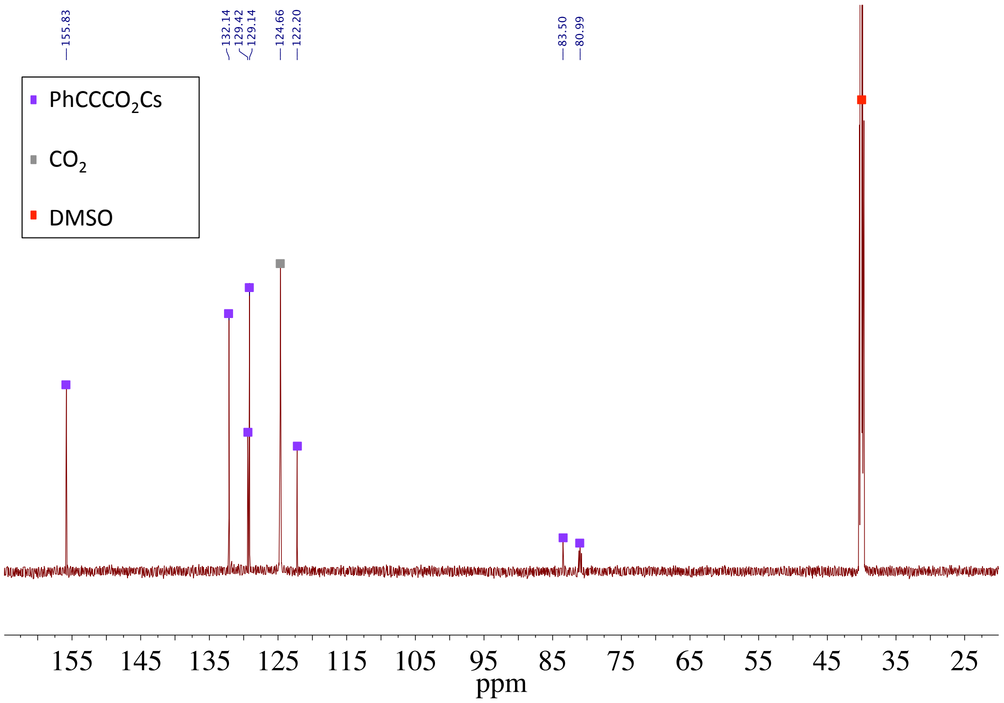

Figure S7. ^{13}C NMR spectrum of the product obtained after addition of $^{13}CO_2$ to the “in situ” deprotonated PhCCCs under $^{13}CO_2$ (DMSO-d6, 800 MHz, 298 K).

Curriculum Vitae

DAVIDE TONIOLO

CHEMIST

CONTACTS

+ 41 775296266 ☎

davide.tonyoh@gmail.com ✉

Ch du Devin 47c, 1012, Lausanne, Switzerland 📍

SOFT SKILLS

Project Management

Practical Skills

Presentation Skills

Leadership

Report and Technical Writing

LANGUEGES

Italian – Mother Tongue

English – Fluent

French – A2 Speaking

ABOUT ME

I am an ambitious, self-motivated and problem driven researcher interested in many fields of chemistry and intrigued by application oriented interdisciplinary research. Having worked in different branches of chemistry and being a fast learner, I enjoy facing complex problems

EDUCATION AND RESEARCH

PhD in chemistry at Ecole Polytechnique Fédéral de Lausanne (EPFL)

Aug 2016 – Aug 2020

Chemistry
Project Title: Activation of small molecules promoted by multimetallic complexes supported by redox active ligands

Internship at University of Cambridge

Mar 2016 – Jul 2016

Project Title: Functionalization of cholesteric liquid crystals based on hydroxypropyl cellulose

Degree at Scuola Normale Superiore di Pisa

Sep 2010 – Dec 2015

Faculty of Science, Chemistry
Final Grade 70/70 cum Laude

Master's degree in chemistry at University of Pisa

Sep 2013 – Dec 2015

Inorganic Chemistry

Project Title: Synthesis and characterization of functionalized magnetic nanoparticles for water depuration
Final grade: 110/110 cum Laude

Tranship at University of Pisa

Jen 2014 – Apr 2014

Project Title: Luminescent solar cells based on perylene

Bachelor’s Degree in chemistry at University of Pisa

Sep 2010 – Sep 2013

Chemistry
Project Title: Analysis of InAs nanowires morphology
Final grade: 110/110 cum Laude

WORK EXPERIENCE

Lab Technician, SELLA FARMACEUTICI

Jun 2009 – Aug 2009

Responsibilities: Quality control of drugs

Lab Technician, CISCATO SPA

Jun 2008 – Sep 2008

Responsibilities: Mechanical tests on steel

SELECTED PUBLICATIONS

- Rory P. Kelly,‡ Davide Toniolo,‡ Farzaneh Fadaei Tirani, Laurent Maron and Marinella Mazzanti, **“A tetranuclear samarium(II) inverse sandwich from direct reduction of toluene by a samarium(II) siloxide”**, *Chem. Comm.,* **2018**, 54, 10268—10271

- Davide Toniolo, Aurélien R. Willauer, Julie Andrez, Yan Yang, Rosario Scopelliti, Laurent Maron and Marinella Mazzanti, **“CS_2 Reductive Coupling to Acetylenedithiolate by a Dinuclear Ytterbium(II) Complex”**, *Chem. Eur. J.*, **2019**, 25, 7831-7834

- Davide Toniolo, Felix D. Bobbink, Paul J. Dyson and Marinella Mazzanti, **“Anhydrous conditions enable the catalyst-free carboxylation of alkynes with CO_2 under mild conditions”**, *Helv. Chim. Acta*, **2020**, *103*, e1900258

- Davide Toniolo, Rosario Scopelliti, Ivica Zivkovic, and Marinella Mazzanti, **“Assembly of high-Spin [Fe_3] clusters by ligand-based multielectron reduction”**, *J. Am. Chem. Soc.*, **2020**, 142, 7301–7305